Hyperspectral imaging application to deoxynivalenol management in wheat

Antoni Femenias Llaneras

Universitat de Lleida

TESIS DOCTORAL

Hyperspectral imaging application to deoxynivalenol management in wheat

Antoni Femenias Llaneras

Memòria presentada per optar al grau de Doctor per la Universitat de Lleida

Programa de Doctorat en Ciència i Tecnologia Agrària i Alimentària

Director/a

Sonia Marín Sillue

Vicente Sanchis Almenar

Tutor/a

Sonia Marín Sillue

2022

The present work is part of the following research projects:

- AGL2017-87755-R project funded by MCIN/ AEI /10.13039/501100011033/ FEDER "A way of making Europe"
- PDC2021-121191-I00 project funded by MCIN/AEI /10.13039/501100011033 and by the European Union Next Generation EU/ PRTR

Predoctoral fellowship

2018-2022 University of Lleida predoctoral grant.

Training and collaborative institutions

June-November 2021: Institute of Analytical and Bioanalytical Chemistry (IABC), University of Ulm, Germany. Research internship.

Lleida, 2018-2022

Author

Antoni Femenias Llaneras

Supervisors

Sonia Marín Sillue

Vicente Sanchis Almenar

Major contributors

Antonio J. Ramos Girona

Ferran Gatius Cortiella

Boris Mizaikoff

Technical contributors

Montserrat Prim Latorre

Acknowledgements/Agraïments/Agradecimientos

Com a cada recerca que acaba amb la producció d'una tesi, no només hi contribueixen investigadors i experts, sinó que inclou l'esforç de totes aquelles persones que t'acompanyen durant aquesta etapa. Per això, a la portada no hi hauria d'haver només el nom de l'investigador, sinó que també hauria d'incloure tots el autors anònims que, imprescindiblement, han contribuït en aquest treball, ja sigui des d'assistència, guia i coratge. Em sento profundament agraït del temps, paciència i energia que m'han entregat per a produir aquest treball. Sense ells no hauria estat possible.

Primer, em complau agrair als meus supervisors, la Sonia, el Vicent i l'Antonio per la seva constància i dedicació en la meva formació i per donar-me l'oportunitat d'unir-me al seu projecte per emprendre la meva carrera com a investigador.

Individually, I would like to thank to my external supervisor, Boris, for giving me the opportunity to join his amazing team when the world was stopped, and convey me his enthusiasm in the spectroscopy field. My adventure in Germany made me grow not only professionally but also personally.

M'agradaria agrair especialment a la nostra assistent de recerca, la Montse, qui m'ha guiat el camí no només amb la ciència sinó també amb la vida. La seva experiència i consells han fet possible aquesta tesi. D'igual manera, agraeixo al Jordi per sempre donar-me una mà (o un braç) en el laboratori sempre que ho he necessitat.

A tots els companys de departament que he tingut el plaer de conèixer durant aquesta etapa. El dia a dia i la convivència han sigut excel·lents, així com també les sortides fora de l'àmbit de treball.

A big thank must go to my lab mates in Ulm, Polina, Patrick and Diellza, for receiving me with open arms in the lab and for their help and cooperation during

my research stay. Also, I must thank to the Norwegian team for the close collaboration during the last year.

Agrair al meu pare, Tomeu, a la meva mare, Maria i al meu germà, Tomeu, el suport que m'han anat donant, no tan sols durant aquesta etapa, sinó durant tota la vida. Sempre han sigut un pilar on recolzar-me en els moments difícils.

The present thesis is based on the following articles:

1. **Femenias, A.**, Gatius, F., Ramos, A. J., Sanchis, V., & Marín, S. (2020). Use of hyperspectral imaging as a tool for *Fusarium* and deoxynivalenol risk management in cereals: A review. Food Control, 108, 106819. https://doi.org/10.1016/j.foodcont.2019.106819
2. **Femenias, A.**, Gatius, F., Ramos, A. J., Sanchis, V., & Marín, S. (2020). Standardisation of near-infrared hyperspectral imaging for quantification and classification of DON contaminated wheat samples. Food Control, 111, 107074. https://doi.org/10.1016/j.foodcont.2019.107074
3. **Femenias, A.**, Gatius, F., Ramos, A. J., Sanchis, V., & Marín, S. (2021). Near-infrared hyperspectral imaging for deoxynivalenol and ergosterol estimation in wheat samples. Food Chemistry, 341(September 2020), 128206. https://doi.org/10.1016/j.foodchem.2020.128206
4. **Femenias, A.**, Belén Bainotti, M., Gatius, F., Ramos, A. J., & Marín, S. (2021). Standardization of near-infrared hyperspectral imaging for wheat single kernel sorting according to deoxynivalenol level. Food Research International, 139 (November 2020), 109925. https://doi.org/10.1016/j.foodres.2020.109925
5. **Femenias, A.**, & Marín, S. (2021). Hyperspectral Imaging. In Electromagnetic Technologies in Food Science (Vol. 46, pp. 363–390). Wiley. https://doi.org/10.1002/9781119759522.ch15
6. **Femenias, A.**, Gatius, F., Ramos, A. J., Teixido-Orries, I., & Marín, S. (2021). Hyperspectral imaging for the classification of individual cereal kernels according to fungal and mycotoxins contamination: A review. *Manuscript submitted.*
7. **Femenias, A.**, Llorens-Serentill, E., Ramos, A. J., Sanchis, V., & Marín, S. (2021). Near-infrared hyperspectral imaging evaluation of *Fusarium* damage and DON in single wheat kernels. *Manuscript submitted.*

8. **Femenias, A.**, Fomina, P., Tafintseva, V., Freitag, S., Shapaval, V., Sulyok, M., Zimmerman, B., Marín, S., Krska, R., Kohler, A., & Mizaikoff, B. (2022). Determination of the best solvent for deoxynivalenol (DON) extraction from the maize for the subsequent Fourier transform infrared spectroscopic analysis with attenuated total reflection (ATR-FTIR) using advanced chemometric methods. *Manuscript in preparation.*

Table of content

List of figures

Figure 15. *Predicted vs. measured plot for PLS calibration set. Optimum number of PC: 17. N = 200.*

Figure 16. *Predicted vs. measured plot for PLS validation set. The optimum number of PC: 12. N = 150.*

Figure 17. *Predicted vs. measured plot of ergosterol PLS regression for 1st derivate spectra. a) Unground wheat data set. Optimum number of PC = 21; N = 135. b) Ground wheat data set. Optimum number of PC = 21; N = 141.*

Figure 18. *Predicted vs. measured plot for the PLS validation set in unground samples. Optimum number of PC = 13. N of validation = 239.*

Figure 19. *Predicted vs. measured plot for PLS validation set in ground samples. Optimum number of PC = 10. N of validation = 243.*

Figure 20. *Schematic representation of the methodology for SK-HSI analysis.*

Figure 21. *Symptomatology and DON effect on spectral profiles depending on kernel position and image acquisition (raw reflectance's). A) Mean spectra of crease-down positioned kernels for each symptomatology category (one image per kernel). B) Mean spectra of crease-up positioned kernels for each symptomatology category (one image per kernel). C) Mean spectra of crease-down positioned kernels for each symptomatology category (one image for the 50 kernels). Categories: A = Asymptomatic (red); M = Mildly-symptomatic (blue); S = Symptomatic (green). D) Mean spectra of crease-down positioned kernels DON level (one image per kernel). E) Mean spectra of crease-up positioned kernels DON level (one image per kernel). F) Mean spectra of crease-down positioned kernels DON level (one image for 50 kernels). DON levels: ≥ 1.25 mg/kg (blue); < 1.25 mg/kg (red).*

Figure 22. *Distribution of DON content and kernel weight in single wheat kernels on the full dataset. A) Total kernel DON frequency and distribution. B) Total kernel weight frequency and distribution.*

Figure 23. *Predicted vs measured plots of cross-validated models. Spectral range: 1000-1650 nm. A) SNV pre-treated model for crease-up kernel position; n =135; optimum PCs = 10. B) 1st derivative pre-treated model for crease-up kernel position; n =137; optimum PCs = 13. C) 1st derivative + SNV pre-treated model for crease-up kernel position; n =135; optimum PCs = 8.*

Figure 24. *PCA scores for visual symptoms screening. A = asymptomatic; M = mildly-symptomatic; S = symptomatic. A) Raw spectra, X-exp: 96%, 4%. B) Multiplicative Scatter Corrected spectra, X-exp:83%, 7%. C) SNV corrected spectra, X-exp: 83%, 7%. D) 1st Derivative spectra, X-exp: 71%, 12%. E) 1st Derivative + SNV corrected spectra, X-exp: 62%, 17%. F) 2nd Derivative spectra, X- exp: 50%, 28%. G) Normalised spectra, X-exp: 99%, 1%.*

Figure. 25. *PCA scores for visual DON screening. B = < 1250 μg/kg kernels; C = ≥ 1250 μg/kg kernels. A) Raw spectra, X-exp: 96%, 4%. B) Multiplicative Scatter Corrected spectra, X-exp:83%, 7%. C) SNV corrected spectra, X-exp: 83%, 7%. D) 1st Derivative spectra, X-exp: 77%, 14%. E) 1st Derivative + SNV corrected spectra, X-exp: 62%, 17%. F) 2nd Derivative spectra, X-exp: 50%, 28%. G) Normalised spectra, X-exp: 99%, 1%.*

Figure 26. *Distribution of DON content and kernel weight in 300 single wheat kernels dataset. (A) Total kernel DON frequency (in number of kernels) and distribution. (B) Total kernel weight frequency (in number of kernels) and distribution.*

Figure 27. *Mean 1st derivated spectral profile of the (A) difference between FDK (red/bold), mildly-damaged (yellow/semi-bold) and healthy kernels (green/light) and (B) DON contaminated above (red/bold) and below (green/light) 1250 μg/kg.*

Figure 28. *PLS regression predicted vs. measured plot for independent set validation. Model A: SNV pre-treated 1000-1600 nm spectra; optimum number of PC = 14. Model B: SNV pre-treated 11 characteristic wavelengths; optimum number of PC = 10.*

Figure 29*. Histogram of DON concentrations of naturally contaminated (NAC) and artificially inoculated (INO) maize samples.*

Figure 30. *PCA score plot for the first two PCs of different solvents (a), (c) water, (b), (d) methanol 70% where colours of labels correspond to (a), (b) inoculation type: inoculated in red and naturally contaminated in blue, (c), (d) fungal strain and inoculation method used (IG:* F. graminearum *in the silk channel; ZC: toothpick inoculation with* F. culmorum*; IV: injection of* F. verticillioides *in the silk channel; ZV: toothpick inoculation with* F. verticillioides *and; NA: natural infection, unknown strains), while labels correspond to DON levels where 0: DON < 1750 μg/kg, 1: DON ≥ 1750 μg/kg obtained by the reference method. The PCA plots (a), (c) and (b), (d) represent the same models, with different colour coding used.*

Figure 31. *SPLS-DA classification results for maize samples into two groups: non-contaminated labelled as (0) DON < 1750 µg/kg and contaminated labelled as (1) DON ≥ 1750 µg/kg (a) in water and (b) methanol 70% extracts. The results are provided as accuracy of cross-validation, the number of latent variables are* $A_{opt} = 11$ *for both models, the number of samples are indicated in parenthesis next to groups' labels 1 and 0.*

Figure 32. *SPLS-DA score plot of different solvents (a) water and (b) methanol 70%. The colour corresponds to inoculation type: inoculated (INO) in red and naturally contaminated (NAC) in blue, and labels represent DON concentration (0: < 1750 µg/kg, 1: ≥1750 µg/kg).*

Figure 33. *SPLS-DA score plot of (a) water and (b) methanol 70% extracts. Colours represent fungal strains and method of inoculation used (IG:* F. graminearum *in the silk channel; ZC: toothpick inoculation with* F. culmorum*; IV: injection of* F. verticillioides *in the silk channel; ZV: toothpick inoculation with* F. verticillioides *and; NA: natural infection, unknown strains) and labels represent DON concentration (0: < 1750 µg/kg, 1: ≥1750 µg/kg).*

Figure 34*. Correlation loading plots using SPLS-DA models' scores for (a) water and (b) methanol 70% showing correlations of the major spectral variables and design parameters such as maize origin, type of inoculation, fungal species and DON levels for the first two LVs. The labels are:* F. graminearum *in the silk channel (IG); toothpick inoculation with* F. culmorum *(ZC); injection of* F. verticillioides *in the silk channel (IV); toothpick inoculation with* F. verticillioides *(ZV); natural infection (NAC), inoculated (INO); Saatbau Linz (SBL); and Cereal Research Center (CRC).*

List of tables

List of abbreviations

15-ADON: 15-acetyl-deoxynivalenol

1stD: First Derivative

3-ADON: 3-acetyl-deoxynivalenol

ABS/BC: Baseline Corrected Absorbance Spectra

AdaBoost: Adaptive Boosting

AFs: Aflatoxins

ANN: Artificial Neural Networks

ATR: Attenuated Total Reflectance

ATR-FTIR: Attenuated Total Reflection – Fourier Transform Infrared

BP-ANN: Backpropagation Artificial Neural Networks

CA: Component Analysis

CARS: Competitive Adaptive Reweighted Sampling

CCD: Charge-Coupled Device

CM: Confusion Matrix

DA: Discriminant Analysis

DAD: Diode Array Detector

DON: Deoxynivalenol

DPI: DON Preliminary Index

ELISA: Enzyme-Linked Immuno-Sorbent Assay

ELM: Extreme Learning Machine

EU: European Union

FBs: Fumonisins

FD: Fluorescent Detector

FDK: *Fusarium*-Damaged Kernel

FHB: Fusarium Head Blight

FI: *Fusarium* Index

FTIR: Fourier Transform Infrared (at the mid-infrared region)

FT-NIR: Fourier Transform Near Infrared

GA: Genetic Algorithm

GC: Gas Chromatography

GC-ECD: Gas Chromatography with Electron Capture Detector

GC-MS: Gas Chromatography – Mass Spectrometry

GLSW: General Least Square Weighting

HgCdTe: Mercury Telluride

HPLC: High-Performance Liquid Chromatography

HPLC-MS: High-Performance Liquid Chromatography – Mass Spectrometry

HSI: Hyperspectral Imaging

HSI-NIR: Hyperspectral Imaging Near Infrared

IAC: Immunoaffinity Columns

IARC: International Agency for Research on Cancer

IR: Infrared

ISSPA: Iterative Selection of Successive Projections Algorithm

JSRC: Joint Sparse Representation-based Classification

K-NN: K-Nearest Neighbors

LC: Liquid Chromatography

LC-MS: Liquid Chromatography – Mass Spectrometry

LC-MS/MS: Liquid Chromatography – Tandem Mass spectrometry

LDA: Linear Discriminant Analysis

LFD: Lateral Flow Device

LMT: Logistic Model Tree

LS: Least-Square

LV: Latent Variable

MAPK: Mitogen-Activated Protein Kinases

MIR: Mid-Infrared

MLP: Multilayer Perceptron

MLR: Multiple Linear Regression

MS: Mass Spectrometry

MSC: Multiplicative Scatter Correction

MSI: Multispectral Imaging

NIR: Near-Infrared

NIRS: Near-Infrared Spectroscopy

NIV: Nivalenol

OTA: Ochratoxin A

OW: Object-Wise

PC: Principal Component

PC-LDA: Principal Component Linear Discriminant Analysis

PCA: Principal Component Analysis

PCR: Principal Component Regression

PLS: Partial Least Squares

PLS-DA: Partial Least Square Discriminant Analysis

PMTDI: Provisional Maximum Tolerable Daily Intake

PW: Pixel-Wise

QDA: Quadratic Discriminant Analysis

qPCR: Quantitative Polymerase Chain Reaction

R^2: Coefficient of Determination

R_c^2: Coefficient of Determination of Calibration

R_P^2: Coefficient of Determination of Prediction

R_{cv}^2: Coefficient of determination of Cross-Validation

R_v^2: Coefficient of determination of Validation

RF: Random Frog

RI: Reflective Index

RMSE: Root Mean Square Error

RMSEC: Root Mean Square Error of Calibration

RMSECV: Root Mean Square Error of Cross-Validation

RMSEP: Root Mean Square Error of Prediction

ROI: Region of Interest

RPD: Ratio of Performance to Deviation

RT-PCR: Reverse-Transcription Polymerase Chain Reaction

SAE: Sparse Autoencoder

SAM: Spectral Angle Mapper

SEC: Standard Error of Calibration

SECV: Standard Error of Cross-Validation

SEP: Standard Error of Prediction

SEPc: Standard Error of Prediction corrected by bias

SIMCA: Soft Independent Modelling by Class Analogy

SK-HSI: Single Kernel – Hyperspectral Imaging

SK-NIR: Single Kernel – Near Infrared

SNV: Standard Normal Variate

SOM: Self-Organizing Map

SPA: Successive Projections Algorithm

SPLS-DA: Sparse Partial Least Square Discriminant Analysis

SVM: Support Vector Machine

SWIR: Short-Wave Infrared

UHPLC: Ultra High-Performance Liquid Chromatography

UHPLC-DAD: Ultra High-Performance Liquid Chromatography – Diode Array Detector

UV: Ultraviolet

UVE: Uninformative Variables Elimination

Vis: Visible

WL: Wavelength

ZEN: Zearalenone

ZnSe: Zinc Selenide

Abstract

Mycotoxins are fungal secondary metabolites that are harmful to human and animal health and reduce economic yield in cereal production. The cereal industry and suppliers require novel technologies to detect their presence before entering the food chain. Traditional analytical techniques for mycotoxins are time-consuming, expensive, destructive and pollutant. Contrarily, spectroscopic applications are rapid, eco-friendly and non-destructive, depending on the technology used. The present work tests the suitability of near-infrared hyperspectral imaging and Fourier transform mid-infrared to detect deoxynivalenol (DON) in two of the most consumed commodities worldwide, wheat and corn.

For the HSI-NIR application, the methodological design started with the standardization of the analytical procedure and sampling parameters before the spectra acquisition. Two samplings were tested depending on the analytical purpose: wheat samples and individual wheat kernels. For sample analysis, bulk and milled wheat samples were scanned under the imaging system, obtaining their NIR spectra. Then, the samples were analysed by HPLC, determining the ergosterol (fungal metabolite not present in plant cells) and DON concentrations as the reference data. Spectral and chromatographic data were modelled using chemometric tools, calibrating predictive models for ergosterol and DON quantification and discrimination models to reject DON contaminated samples over the regulatory limits (1250 μg/kg). For single grain analysis, pixels mean NIR spectra of the kernel were the analytical target. In this instance, grains were categorised as symptomatic, mildly-symptomatic or healthy according to Fusarium Head Blight common damages and analysed by HPLC, obtaining their DON concentration. Predictive models for DON quantification and discrimination models for *Fusarium*-damaged kernels and DON detection (at EU limits) were calibrated as a cereal sorting strategy. Additionally, several solvents,

based on water, methanol, acetonitrile and ethanol, were tested, determining the DON extraction and FTIR analytical power of corn-infected samples.

For HSI-NIR, the standardization started by assessing the method repeatability, the most suitable region of interest selection and the kernel orientation and location effect. The PCA results showed good repeatability between measurements. In addition, the ROI delimitation method selected was by similar pixels selection with Euclidean distance. The results also demonstrated that kernel location had no effect on the measurement and that, although the kernel orientation affected the PCA projection, fungal damage and DON contamination predominated.

HPLC analysis demonstrated the weak correlation between ergosterol and DON (0.61). Consequently, the next step was to calibrate independent predictive models for each compound. PLS regression on ergosterol presented cross-validation performances of R_{cv}^2 of 0.89 and RMSECV of 1.17 mg/kg, while DON predictive ability on an independent validation set was R^2 of 0.61 and RMSEP of 501.4 μg/kg. The classification results showed an accuracy of 85.4% to discriminate samples at EU regulatory limits.

DON prediction results in individual wheat kernels showed better adjustment R^2 of 0.88 but higher RMSEP (6.66 mg/kg) for a DON contamination ranging from LOD to 135.7 mg/kg. Alternatively, the discrimination of *Fusarium*-damaged and DON-contaminated kernels discrimination were more suitable than the predictive models to work at regulatory limits, with an accuracy of 85.8% and 76.9%, respectively.

For FTIR, water and methanol (70%) were selected for the tendency to form clusters for maize samples contaminated above and below the DON EU limit (1750 μg/kg) and their technological applications. SPLS-DA discriminated samples with an accuracy of 86.7% and 90.8% for water and methanol, respectively. In addition, the SPLS-DA score plots displayed a will-defined

separation of samples according to the regulatory limit and revealed the impact of the fungal species on the clustering ability.

The present thesis proves the ability of HSI-NIR to manage fungal and DON contamination in cereals. Although prediction models are insufficient for DON quantification at low concentrations, classification models are accurate enough at regulatory EU thresholds. In addition, the FTIR analysis of water and methanol 70% maize extracts exhibited also high accuracy discriminations. Thus, the general results indicate that both technologies are potent to reject contaminated samples and that HSI-NIR is suitable as a cereal sorting tool.

Resum

Les micotoxines són metabòlits secundaris fúngics causants de malalties en humans i animals i de reduccions del rendiment econòmic en la producció de cereals. La indústria i els proveïdors demanden noves tecnologies per detectar la seva presència abans de la seva entrada en la cadena alimentària. Les tècniques d'anàlisi convencionals per a la detecció de micotoxines són lentes, costoses, destructives i contaminants. No obstant això, les aplicacions espectroscòpiques es caracteritzen per ser ràpides, respectuoses amb el medi ambient i no destructives, depenent de la tecnologia utilitzada. Aquest treball examina l'aptitud de l'anàlisi per imatges hiperespectrals l'infraroig proper i l'espectrofotometria de transformada de Fourier a l'infraroig mitjà per detectar deoxinivalenol (DON) en dos dels cereals més consumits a escala mundial, el blat i el panís.

Per aplicar HSI-NIR, el disseny metodològic passa primer per estandarditzar el procediment analític i els paràmetres de mostreig abans d'adquirir l'espectre. Es van posar a prova dos tipus de mostreigs, segons l'objectiu analític: l'anàlisi de mostra sencera i de grans individuals. Per l'anàlisi de mostra, els grans sencers i mòlts es van posicionar sota del camp de visió del sistema i es van escanejar, obtenint l'espectre infraroig. Es van determinar les concentracions d'ergosterol (metabòlit fúngic absent en les cèl·lules vegetals) i DON mitjançant HPLC com a mètode de referència. Un cop aconseguides les dades espectrals i de referència, es van modelar per quimiometria per a la calibració de models de predicció de DON i models de discriminació per rebutjar mostres per sobre del límit legal (1250 μg/kg). En l'anàlisi de grans individuals, l'espectre NIR corresponent a la mitjana de píxels de cada gra fou la regió analítica d'interès. En aquest cas, els grans es varen categoritzar com a simptomàtics, lleugerament simptomàtics o sans segons els símptomes comuns de la fusariosi de l'espiga, i es varen analitzar per HPLC per determinar la concentració de DON. Un cop adquirides les dades,

es van calibrar models de predicció per quantificar DON i els models de discriminació per detectar grans amb danys per *Fusarium* i DON (segons el límit legal de la UE) com a estratègia per separar grans contaminats. Per altra banda, es varen provar diferents dissolvents, basats en aigua, metanol, acetonitril i etanol per determinar la seva capacitat d'extracció de DON en mostres de panís contaminat, analitzades posteriorment per FTIR.

En el cas de l'HSI-NIR, l'estandardització va passar per identificar la repetibilitat del mètode, l'eina de selecció de la regió d'interès més convenient i l'efecte de la posició i l'orientació dels grans. Els resultats de PCA demostren una bona repetibilitat entre mesures. A més, el mètode seleccionat per a la delimitació de la regió d'interès va ser mitjançant píxels similars amb distància Euclidiana. Els resultats també varen demostrar que la posició del gra dins el camp de visió de l'equip no afecta a la mesura espectre i que, encara que l'orientació del gra té influència sobre la projecció del gra, el dany fúngic i DON predominen per sobre d'aquesta.

L'anàlisi per HPLC va demostrar la baixa correlació entre ergosterol i DON (0,61). A causa d'això, el pròxim pas va ser calibrar models de predicció independents per cada un d'aquests components. Les regressions PLS per ergosterol van presentar un rendiment per validació creuada de R_{cv}^2 de 0,89 i un RMSECV de 1,17 mg/kg, mentre que l'habilitat de predir DON per un conjunt de validació independent va ser de R^2 de 0,61 i un RMSEP de 501,4 μg/kg. L'exactitud en la classificació als límits màxims establerts per la UE va ser del 85,4%.Els models de predicció de DON en grans de blat individuals varen presentar millors ajustaments amb una R^2 de 0,88, encara que l'RMSEP va ser major (6,66 mg/kg), amb una rang de contaminació dels grans des de LOD fins a 135,7 mg/kg. Malgrat això, les discriminacions de grans danyats per *Fusarium* i contaminats amb DON foren més adequades per a l'anàlisi a concentracions properes al límit legal que

els models de predicció, classificant correctament el 85,8% i 76,9% dels grans, respectivament.

En l'anàlisi per FTIR, les extraccions basades amb aigua i metanol 70% es varen seleccionar per la seva tendència en agrupar mostres de panís segons el límit establert en panís (1750 μg/kg) respecte als altres dissolvents i per les seves aplicacions tecnològiques. Els models SPLS-DA discriminaren mostres amb una precisió 86,7% i 90,8% per aigua i metanol (70%), respectivament. A més, els gràfics SPLS-DA mostraren una bona separació de mostres segons el límit legal i un impacte de les espècies fúngiques sobre aquestes agrupacions.

Aquesta tesi demostra l'habilitat de l'HSI-NIR per detectar les contaminacions fúngiques i el DON en cereals. Encara que els models de predicció són insuficients per determinar la quantitat de DON a baixes concentracions, els models de classificació són precisos a límits propers als establerts per la UE. A més, l'anàlisi per FTIR dels extractes d'aigua i metanol (70%) també va presentar alta capacitat de discriminació. D'aquesta manera, els resultats demostren que ambdues tecnologies presenten potencial per rebutjar mostres contaminades i l'HSI-NIR és adequada com a tècnica de separació de grans contaminats.

Resumen

Las micotoxinas son metabolitos secundarios fúngicos causantes de enfermedades en humanos y animales y de reducciones del rendimiento económico en la producción de cereales. La industria y proveedores de cereales demandan nuevas tecnologías para detectar su presencia antes de su entrada en la cadena alimentaria. Las técnicas de análisis convencionales para la detección de micotoxinas son lentas, costosas, destructivas y contaminantes. Sin embargo, las aplicaciones espectroscópicas se caracterizan por ser rápidas, respetuosas con el medio ambiente y no destructivas, dependiendo de la tecnología utilizada. Este trabajo examina la aptitud del análisis por imágenes hiperespectrales en el infrarrojo cercano y la espectrofotometría de transformada de Fourier en el infrarrojo medio para detectar deoxinivalenol (DON) en dos de los cereales más consumidos a nivel mundial, el trigo y el maíz.

Para aplicar HSI-NIR, el diseño metodológico pasa primero por estandarizar el procedimiento analítico y los parámetros de muestreo antes de adquirir el espectro. Se pusieron a prueba dos tipos de muestreos dependiendo del objetivo analítico: el análisis de muestra entero y de granos individuales. Para el análisis de muestra, los granos a granel y molidos se escanearon bajo del campo de visión del sistema, obteniendo el espectro infrarrojo. Después, se determinaron las concentraciones de ergosterol (metabolito fúngico no presente en las células vegetales) y DON mediante HPLC como método de referencia. Además, se modelaron datos espectrales y de referencia por quimiometría para la calibración de modelos de predicción capaces de cuantificar DON y modelos de discriminación para rechazar muestras por encima del límite legal (1250 μg/kg). Para el análisis de granos individuales, el espectro NIR correspondiente a la media de los píxeles de cada grano fue establecido como la región analítica de interés. En este caso, los granos se categorizaron como sintomáticos, ligeramente sintomáticos o sanos según los síntomas comunes de la fusariosis de la espiga y

se analizaron por HPLC para obtener la concentración de DON. Una vez obtenidos ambos datos, se calibraron modelos de predicción de DON y los modelos de discriminación para detectar granos dañados por *Fusarium* y contaminados con DON (usando el límite legal de la UE) como estrategia para separarlos. Por otra parte, se probaron diferentes disolventes basados en agua, metanol, acetonitrilo y etanol para determinar su capacidad para extraer DON en muestras de maíz contaminadas, para su posterior análisis por FTIR.

En el caso del HSI-NIR, la estandarización pasó por identificar la repetibilidad del método, la herramienta de selección de la región de interés más conveniente y el efecto de la posición y la orientación de los granos. Los resultados de PCA muestran una buena repetibilidad entre medidas. Además, el método seleccionado para la delimitación de la región de interés fue mediante píxeles similares con distancia Euclidiana. Los resultados también demostraron que la posición del grano dentro del campo de visión del equipo no afecta a la medida espectro y que, aunque la orientación del grano tiene influencia sobre la proyección en el PCA, el daño fúngico y DON predominan por encima de esta.

El análisis por HPLC demostró la baja correlación entre ergosterol y DON (0,61). Debido a esto, el siguiente paso fue calibrar modelos de predicción independientes para cada uno de estos componentes. Las regresiones PLS por ergosterol presentaron un rendimiento por validación cruzada de R_{cv}^2 de 0,89 y un RMSECV de 1,17 mg/kg, mientras que la habilidad de predecir DON validado con un conjunto de muestras independiente fue de R^2 de 0,61 y un RMSEP de 501,4 μg/kg. La exactitud en la clasificación según los límites máximos establecidos por la UE fue del 85,4%. Los modelos de predicción de DON en granos de trigo individuales presentaron mejores ajustes, con una R^2 de 0,88, aunque el RMSEP fue mayor (6,66 mg/kg) con un rango de contaminación desde LOD hasta 135,7 mg/kg. Sin embargo, las discriminaciones de granos dañados por *Fusarium* y contaminados con DON son más adecuadas para el análisis a

concentraciones cercanas al límite legal, clasificando correctamente el 85,8% y 76,9% de los granos, respectivamente.

En el análisis por FTIR, se seleccionaron las extracciones basadas en agua y metanol (70%) por su mayor tendencia en agrupar muestras de maíz según el límite legal (1750 μg/kg), además de sus aplicaciones tecnológicas. Los modelos SPLS-DA discriminaron muestras con una precisión 86,7% y 90,8% para agua y metanol (70%), respectivamente. Además, los gráficos de SPLS-DA mostraron una buena separación de muestras según el límite legal y un impacto de las especies fúngicas sobre estas agrupaciones.

La presente tesis demuestra la habilidad del HSI-NIR para detectar las contaminaciones fúngicas y contaminaciones por DON en cereales. Aunque los modelos de predicción son insuficientes para determinar la cantidad de DON a bajas concentraciones, los modelos de clasificación son precisos en límites cercanos a los establecidos por la UE. Además, el análisis por FTIR de los extractos de agua y metanol (70%) también presentaron alta capacidad de discriminación. De esta forma, los resultados demuestran el potencial de ambas tecnologías para rechazar muestras contaminadas y la habilidad del sistema HSI-NIR como técnica de separación de granos contaminados.

Chapter 1. Introduction

1.1. *Fusarium* species and pathogenicity

Cereals and their derived products are a considerable part of the daily diet in the worldwide population. Almost 80% of the European cereal production is wheat, maize and barley and more than 60% of the global. Under several environmental conditions, cereal crops are susceptible to mould contamination associated with a negative impact on the quality and safety of the final product. *Fusarium* is a plant pathogen that produces diseases in small grain cereals related to a crop yield reduction. It belongs to a large genus of filamentous fungi, which presents high occurrences in cereal seeds (Uoti, 1975). Although the recent technological advances in mitigation strategies, it remains a problem for cereal producers (Nelson, Dignani, & Anaissie, 1994).

Depending on the host, fungal species cause more acute diseases on the plant. The most widely known fusariosis associated diseases are seed blight, foot rot and head blight in numerous cereals; and stalk, ear rot and seedling blight in maize (Janse & Obradovic, 2015). Soil-habiting fungi can rot the seed before germination or cause seedling blight, in which the fungi infected grains are discoloured and soft. Alternatively, *Fusarium graminearum* predominantly produces head blight, thus is known as Fusarium Head Blight (FHB) or scab. In continuous climate change, the environmental conditions are becoming favourable for *Fusarium* species growth and disease production (Chakraborty & Newton, 2011).

Wheat and barley are the most affected cereals due to fungal growth within the spikelet head, which becomes bleached (Zhang et al., 2013). With favourable conditions, they produce pinkish spores, which are visible on the spikelets. In the late stages, black spheres called perithecia appear on the surface of the affected spikes. At the grain level, the colonization of the fungi during cereal growth stages causes the shrink and wrinkle of the kernel, producing a shrivelled, rough

and pinkish appearance. The adverse effects of FHB include the loss of around 50% of the entire production yield and, in worst cases, 70%; a loss of grain quality caused by the destruction of proteins, cells walls and starch during fungal infection with negative effects on bread and beer fermentation; and an undesirable effect on seed drilling and foot rot during plant growth (Osborne & Stein, 2007; Pirgozliev, Edwards, Hare, & Jenkinson, 2003).

Fusarium species not only have side effects on grain quality, as their secondary metabolism can produce a wide range of toxic compounds, known as mycotoxins, being the trichothecenes one of the most important group. Although many *Fusarium* species are not trichothecene producers (they can be non-pathogenic), the species responsible for FHB predominantly produce toxins from this group. *F. graminearum* species complex, *Fusarium culmorum*, *Fusarium poae*, *Fusarium cerealis*, *Fusarium sibiricum*, *Fusarium langsethiae*, *Fusarium pseudograminearum* and *Fusarium sporitrichioides* contaminate cereals for human and livestock consumption with trichothecenes (Foroud et al., 2019). Despite the efforts to control *Fusarium* species growth and FHB in cereals, such as cultural and biological control, cultivar resistance and chemical control, they remain a concern for farmers, food producers and consumers.

1.2. Trichothecenes

When fungi infect the inflorescence structure of the small grain cereals in favourable environmental conditions, *Fusarium* can produce FHB and penetrate the cell wall after germination. Fungi produce trichothecene toxins excreted from the mycelium, which accumulate on infected tissues and, consequently, on the agricultural product (Sweeney, 1999). Although *Fusarium* is the most studied trichothecene-producer, other genera can also produce them, such as *Myrothecium*, *Spicellum*, *Stachybotrys*, *Cephalosporium*, *Trichoderma*, and *Trichothecium* (Kimura, Tokai, Takahashi-Ando, Ohsato, & Fujimura, 2007).

Trichothecenes are one of the main groups of mycotoxins, which present a structure derived from the 12,13-epoxytrichothec-9-ene ring. The molecular structure within these toxins can differ depending on the functional groups (Kotal, Holadová, Hajšlová, Poustka, & Radová, 1999). The trichothecenes are divided into four groups (A, B, C and D) depending on the producer and the functional groups, although other classifications are reported depending on the number of molecules in the ring, conformation, reactivity, etc. Farmers consider types A and B for their high incidence in commonly cultivated crops, such as wheat, barley, oats and maize. Trichothecenes are amphipathic and small molecules that easily penetrate cell membranes and are rapidly absorbed by intestinal tissues. Their ingestion is related to immunological and haemorrhagic problems, dermatitis, vomiting and feed refusal (McCormick, Stanley, Stover, & Alexander, 2011). Type A is represented by T-2 and HT-2 toxins, being of concern from the extreme acute toxicity perspective, which affects mainly the hematologic and immune systems. On the other hand, deoxynivalenol (DON) and nivalenol (NIV) and their acetylated derivatives: 3-acetyl-deoxynivalenol (3-ADON) and 15-acetyl-deoxynivalenol (15-ADON) constitute the type B group (Rosa et al., 2018). The phytotoxic effects of this group are more severe than in group A, caused by the inhibition of protein synthesis and cellular intake of DON and 3-ADON. In addition, type B trichothecenes are also associated to a reduced feed uptake, nausea and immunosuppression in animals (Foroud et al., 2019). Among the trichothecenes, DON is the toxin found with the highest occurrence worldwide and presents the highest concentrations as a consequence of the extended *Fusarium* infections. Consequently, due to its high incidence and toxic effects, DON is the most studied *Fusarium* toxin.

1.3. Deoxynivalenol

DON also known as vomitoxin, is a mycotoxin produced predominantly by *F. graminearum*, but also by *F. culmorum* and *F. crookwellense* (Bianchini & Bullerman,

2014). From the chemical point of view, DON is a polar and organic chemical, containing three free hydroxyl (-OH) groups responsible for DON toxicity (Sobrova et al., 2010). In addition, DON is very stable under temperatures up to 350 °C. Consequently, it is not reduced in cooking or baking steps. However, some studies reported its reduction in boiling or malting water due to its high solubility into polar substances (Pascari et al., 2019; Vidal, Sanchis, Ramos, & Marín, 2016). Studies reported DON high prevalence in small grain cereals, such as wheat, barley, maize, oats and rye (Mishra, Srivastava, Dewangan, Divakar, & Kumar Rath, 2020; Patriarca & Fernández Pinto, 2017).

Based on toxicological studies, DON can produce acute and chronic effects on human and animal health. In acute exposure doses, DON is related to nausea, vomiting, diarrhoea, abdominal pain and malnutrition (Knutsen et al., 2017). Cellular behaviour is also affected by the alteration of protein synthesis on the ribosomes, producing a ribotoxic effect that phosphorylates mitogen-activated protein kinases (MAPK) and activates genes associated with immune response, chemotaxis, inflammation and apoptosis. Consequently, DON intake is related to intestinal, immune, endocrine and nervous system affectations (Escrivá, Font, & Manyes, 2015). International Agency for Research on Cancer (IARC, 2012) classifies DON as a group 3 carcinogen as there is inadequate evidence in experiments of its carcinogenicity in humans and animals. However, a 2-year bioassay in mice established the Provisional Maximum Tolerable Daily Intake (PMTDI) for DON at 1 μg/kg bw/day (WHO, 2011). Due to the exposure risks of DON, the European Commission (2006a) set maximum levels for DON in foodstuffs, establishing the limit of 1250 μg/kg for unprocessed cereals other than durum wheat, oats and maize; 1750 μg/kg for durum wheat, oats and maize; 750 μg/kg for direct human consumption cereals and pasta; and 500 μg/kg for bread. The cereal products that present contaminations above the regulatory threshold

are rejected from the food chain, producing a negative impact on the economic yield of producers.

1.4. Analytical techniques commonly used for DON in cereals

Food producers in European countries based the majority of DON analyses (55 %) on liquid chromatography (LC) coupled with ultraviolet (UV), fluorescent (FD), or mass spectrometry detectors (MS); the 23 % with Gas Chromatography (GC) coupled with an electron capture detector or with MS; and the 22 % with Enzyme - Linked Immunosorbent Assay (ELISA) (European Food Safety Authority, 2013). High-Performance Liquid Chromatography (HPLC) is a suitable technique for DON detection due to its polarity, which can be dissolved into organic solvents and water. Depending on the detector used, HPLC presents LOD for DON between 14-200 μg/kg and LOQ between 47-380 μg/kg (Ran et al., 2013). Thus, its main advantages are high sensitivity and selectivity and reliable repeatability. On the other hand, Liquid Chromatography–Mass Spectrometry (LC-MS) analysis also presents high sensitivity, accuracy and reliability for DON analysis in cereals. Additionally, this technique offers the highest degree of certainty in analyte identification (Lattanzio, Solfrizzo, & Visconti, 2008). Despite the advantages of LC analysis, they have several throwbacks, as the elevated cost, a significant time-consumption, the sample destruction, a complex cleaning step, and the pollutant chemicals usage. Moreover, Gas Chromatography coupled to Mass Spectrometry (GC-MS) depends on derivatization and has thermal stability problems; while LC-MS has matrix effects that can affect the results, a complex selection of an internal standard, and a limitation caused by the diversity of polarities and ionization capacities of the analyte (Turner, Subrahmanyam, & Piletsky, 2009). ELISAs are kits available for multiple mycotoxins, characterised for their specificity, fast and relatively easy-usage. The most frequent

disadvantages present in ELISA are false positives due to antibodies' cross-reactivity and matrix dependence, and false negatives caused by low sensitivity (Kharayat & Singh, 2018). Consequently, farmers and industry require alternative detection and quantification techniques, substituting expensive laboratory facilities and pollutant chemicals and to analyse mycotoxins in a rapid, non-destructive and eco-friendly way. Thus, advanced methods involving the maximum information possible are required to control rapidly and accurately fungi and associated metabolites in industrial stages. Hyperspectral imaging (HSI) has been considered a promising method to assess the quality and safety of food products. The HSI introduces the spectral recognition of the sample that makes it suitable for heterogeneous foods analysis, presenting solutions to conventional analysis techniques.

1.5. Basis of Near-Infrared Hyperspectral imaging (HSI-NIR)

Near-Infrared Spectroscopy (NIRS) employs the spectral range from 780 to 2500 nm, offering information about the overtones and the combination of the molecular vibrations of the hydrogen bonds (O-H, C-H, N-H and S-H) from the tested object (Cen & He, 2007). When the organic molecules are exposed to NIR frequencies, the vibration of the abovementioned bonds absorbs the spectral energy. Then, the rest of the chemical bonds reflect or transmit the other beams at different infrared (IR) wavelengths and are dispersed and measured by the detector. In solid samples, the spectral bands in the NIR regions are wide and overlapped, so the spectra obtained is characterized by a smooth shape.

Preliminary studies of Dowell, Ram, & Seitz (1999) demonstrated the ability of NIR for DON classification. They observed absorption patterns of DON determined by its functional groups (O-H, C-H and N-H), comprised between the NIR spectral region. The characteristic overtones of each group were (750, 950

and 1400 nm), (1200, 1400 and 1650 nm), and (1050 and 1500 nm) respectively, and the absorption wavelengths were used for DON detection. Several studies proved the feasibility of NIR technologies to detect DON in different cereal commodities and proposed it as an efficient tool to manage contaminations in cereal industry (Caporaso, Whitworth, & Fisk, 2018). However, NIR spectroscopy is a spatially limited technique, especially for heterogeneous samples measurement (Manley, 2014). Consequently, efficient technologies in the spatial characterization of the samples are required.

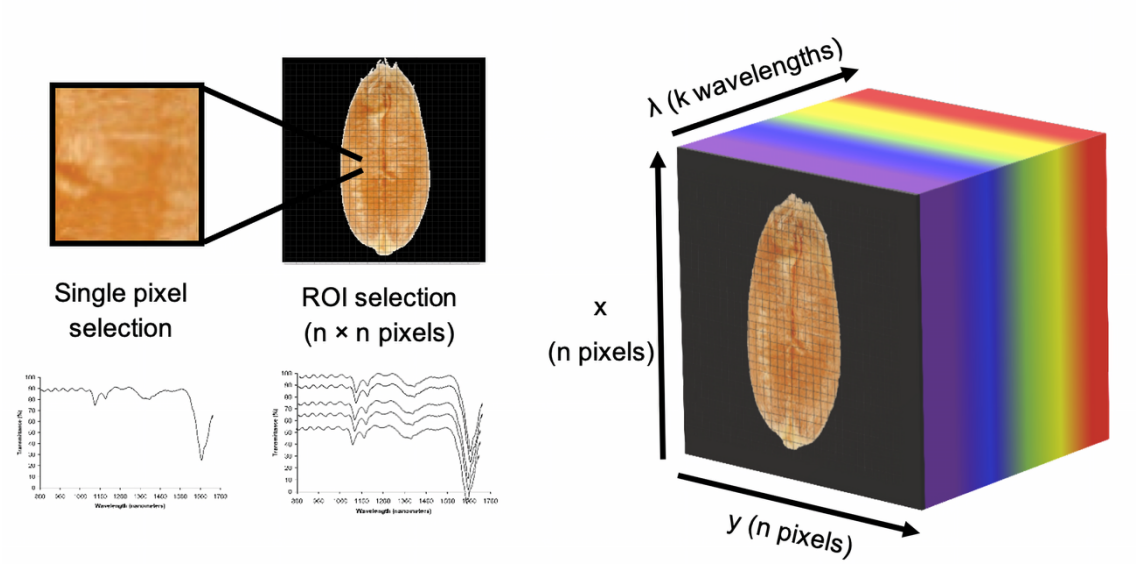

Figure 1. Basis of the hypercube in HSI. Relationship between the spatial resolution (x, y) and the spectral resolution (λ).

HSI is a high-potential technique based on the electromagnetic spectrum collection through the spatial positions of the measured object. Figure 1 shows a schematic representation of the three dimensions captured by the image, two of them corresponding to the spatial location of the pixel, and the third one equivalent to the spectral data acquisition through the NIR wavelength range. In addition, the illustration presents the spectral response for both individual pixels and the whole image. The multiple combinations between the imaging vectors (X, Y), which determine the pixel location in the scanned region, and the spectral information vector for each pixel at different wavelengths create a three-dimensional hypercube containing an elevated amount of information (Dale et

al., 2013). The HSI technique generates a spectral variation map showing many advantages such as a minimum and non-destructive sample manipulation, environmental-friendly, extremely rapid measurements once validated, low-cost analysis and detection of different chemical compounds at specific sample locations (Sendin, Williams, & Manley, 2018).

HSI application in the food industry would imply a diminished loss in production yield associated with a positive economic impact and a more sustainable working system. In addition, it would also include a substitution of the expensive laboratory equipment and qualified personnel. Thus, the application of HSI technology in postharvest and in the industry would offer an alternative to wet chemistry methods. HSI present several advantages beyond other conventional methods of chemical analysis. Imaging-based systems have high analysis speed compared to chromatographic and immunoassay techniques. Consequently, although chromatography has high sensitivity and specificity, HSI is more suitable for routine analysis in cereal-based industries. In addition, the interest in green analysis methods is a concern to develop new approaches in chemical analysis. HSI uses light sources to detect sample features to substitute pollutant reagents for eco-friendly sources (Caporaso et al., 2018). HSI is applied at a laboratory scale to screen quality and safety in individual grains (e.g. protein, starch, moisture, hardness, fungal contamination, mycotoxins, defects, etc.) (Fox & Manley, 2014). Several studies built robust models to manage these parameters to accomplish the established quality and safety standards.

Moreover, cereal sorting after reception would be interesting to remove kernels that do not accomplish the established quality and safety parameters. Some kernels from the batch can present fungal contamination, while others can remain uncontaminated, due to the uneven contamination of ears or spikes in the field (Lu, Saeys, Kim, Peng, & Lu, 2020). For that reason, high contaminations are

found in a minority of the kernels, which can be responsible for a whole batch rejection in the industry based on sampling and analysis protocols (Shahin & Symons, 2012).

1.6. HSI equipment

The most common HSI acquisition method is the push-broom for its online scanning ability line by line while the sample moves. A typical push-broom HSI system incorporates an optical system, an illumination device, a moving unit and a data acquisition instrument. The optical systems include the following three components: a charged coupled device (CCD) camera characterized by semiconductor electronic properties for spectral and spatial detection; a spectrograph, which is considered the key of the optical system, disperses the light into different wavelengths to generate a spectrum for each pixel of the image (ElMasry, Kamruzzaman, Sun, & Allen, 2012); and an objective lens which is coupled to the spectrograph to focus the light beam from the scanned object to

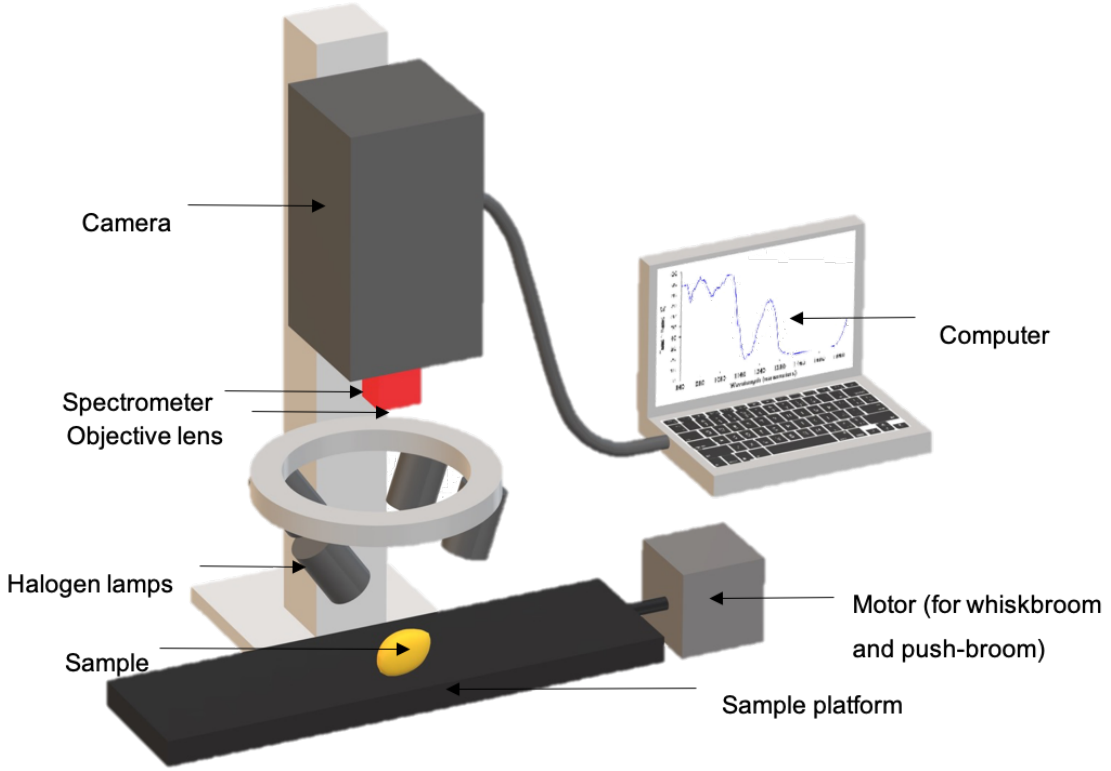

Figure 2. HSI acquisition system.

the detector (camera). The illumination unit produces a homogeneous focus of light, which does not alter the sample (ElMasry & Sun, 2010). The target is scanned line by line by a moving system, which permits the measurement of the entire Region of Interest (ROI) with the optical systems fixed. The translation stage and the motor are the two main components of the moving device, and they control the sample movement speed (Delwiche et al., 2017). Finally, the data acquisition instrument is based on computer processing software, which converts the raw data from the measurements to band image data. Furthermore, it also permits dark and light correction, image improvement, simple mathematical operations and a high volume of data storage as spectral band images (Kim & Chen, 1998). Figure 2 is a schematic representation of a tower push-broom HSI system.

Recent studies have used HSI devices to screen *Fusarium* and DON contamination of cereal kernels. Tekle, Måge, Segtnan, & Bjørnstad (2015) used a SWIR (Short-Wave Infrared) camera coupled to a Mercury Telluride (HgCdTe) detector with a spectral range of 1000-2500 nm. The data obtained were processed by SpectralDAQ software. Barbedo, Tibola, & Lima, (2017) used a XENICS camera combined with a VIS/NIR spectrometer working at wavelengths of 528-1785 nm. The illumination system consisted of a Quartz Tungsten-Halogen Lamp. In recent publications, Ropelewska & Zapotoczny (2018) acquired images with a CCD camera, a VIS/NIR (400-1100 nm) spectrometer and a Fiber Optic Illuminator associated with a supplementary IR lamp (600-1100 nm). Liang et al. (2018) also used a CCD camera but a different spectrometer (ImSpector V10) detecting 400-1000 nm wavelengths. The illumination source was a 150-W halogen lamp. Finally, Alisaac, Behmann, Kuska, Dehne, & Mahlein (2018) used two different cameras (Hyperspectral Camera ImSpector V10 and SWIR-camera) with wavelengths ranging from 400 to 1000 and 1000 to 2500 nm, respectively.

Analytical Spectral Devices PRO-Lamps illuminated the samples, and Spectral Cube Software controlled the spectral measurements of both cameras.

1.6.1. Measurement modes

The three most used methods for hyperspectral images production are push-broom imaging (two-dimension spectral information across the spatial axis line by line), whisk-broom scan (spectrum generation for a single pixel at a time) and staring imaging (spectral plan across the wavelength axis generation). The interaction of the light beam with the measured object can be recorded in different ways. Some measurement modes are more suitable for specific samples depending on the nature of its matrix, as the light has several behaviours depending on the chemical and physical properties (Pasquini, 2003). Light reflection variances, caused by the interaction with the sample, should be recorded and interpreted correctly, correlating them with the changes in chemical composition or physical features of the measured object.

1.6.1.1. Push-broom imaging

A push-broom imaging scanner is a system that obtains spectral measurements for each pixel in a line. The push-broom imager is based on the sample movement in the Y-axis direction, in which the spectrometer records the spectra for each pixel in the X-axis line. This technique displays good relationships between spatial and spectral resolution. Consequently, its main uses are online and in-line measurements (Boldrini, Kessler, Rebnera, & Kessler, 2012).

1.6.1.2. Whisk-broom imaging

A point-scanning method (or whisk-broom method) is an imaging system obtaining spectral measurement pixel by pixel. The hyperspectral image is acquired while the sample or the detector moves in the X and Y axis for a single position spectral acquisition. This mode requires an exhaustive pixel by pixel data collection to obtain high spectral resolutions of the physical and chemical

information of the sample (Qin, 2010). Nevertheless, the method shows low spatial resolutions due to the long times used to measure the sample point by point.

1.6.1.3. Staring Imaging

The staring method is an area scanning technique characterized by the 2-D spatial (x, y) plane acquisition at a single spectral wavelength. The hypercube is constructed collecting of the spatial areas through the spectral domain for a determined number of wavelengths. They can be selected by illuminating the sample at a specific wavelength or by the monochromatic reflection analysis in the detector. In this case, the advantage is that the images obtained have a high spatial resolution, although lower spectral resolutions are obtained (ElMasry & Sun, 2010; Gupta, 2011).

The comparison between the studies using HSI shows that the predominant method used for HSI-NIR is line-by-line scanning (push-broom imaging) at different pixel resolutions (x, y, λ). Barbedo, Tibola, & Fernandes (2015) and Barbedo, Guarienti, & Tibola (2018) used this method to capture a 3D hypercube with a 320 x 800 x 256 dimension. Besides, Delwiche, Kim, & Dong (2011) also acquired a push-broom image, using a different pixel resolution of 320 x 320 x 288. The hypercube dimension depends on the wavelength range, the spectral resolution of the camera, and the field of view (spatial resolution) selected for the image capture.

1.6.2. Object measurement modes

Hyperspectral measurement modes are generally based on reflectance, transmittance or absorbance. The difference between the modes depends on how the light beam reaches the detector after interacting with the sample. The variances in the light due to its interaction with the measured object should be recorded, correlating them with the contamination changes and sample features.

The light radiation of the illumination unit to the sample can be reflected, transmitted or absorbed, so that one of them is measured. Thus, the relationship between incident illumination, fixed at characteristic optical properties, and the released radiation is employed to obtain sample properties information (Pasquini, 2003).

In transmittance mode, the detector is placed on the opposite side of the light source, thus is ideal for transparent samples, as liquids or gases. An additional way to transmittance is the transflectance mode, consisting of the light beam amplification by a mirror to make it pass twice through the sample. Alternatively, diffuse reflectance measurement is used in NIR spectroscopy. The scattering and absorbance of the solid bonds produce changes in the signal intensity. In the interactance mode, the light beam penetrates deeper into the sample because the detector is located distant from the emission position. Consequently, the light beam contains more information about the sample composition. Finally, light absorption is also related to food chemical and biological properties, estimated by the inversed logarithm of the measured reflectance.

1.6.2.1. Reflectance Calibration

When the HSI system works in reflectance mode, the raw data obtained from the measurements are in absolute reflectance. These values require compensation by removing the dark current noise and correcting the white response (Ngadi & Liu, 2010). Thus, a reflectance correction of the original measurements is performed, obtaining the relative reflectance, according to equation 1:

$$I = \frac{I_0 - I_b}{I_w - I_b} \qquad (1)$$

where I_0 is the raw hyperspectral image obtained, I_w is the white reference and I_b is the dark current reference. In practice, the compensation of dark and white is performed by covering the lens with a zero reflectance cap and using a white

fluoropolymer with the highest known reflectance (99%), respectively (Huang, Liu, & Ngadi, 2014).

1.7. Basis and applications of Fourier Transform Infrared Spectroscopy (FTIR)

The light absorption produces energy differences which can be detected, obtaining a chemical profile of the analysed material in the MIR region (2500-25000 nm), which is a reproducible and robust region that can reliably represent minor differences in sample composition (Subramanian & Rodriguez-Saona, 2009). The information obtained includes all the biological information of the sample, permitting the differentiation of the major constituents, such as water, lipids, carbohydrates, etc., in specific and known bands. The 2500-3225 nm region absorbances correspond to the O–H stretching vibrations from hydroxyl groups and the N–H from amides of proteins. Protein features are not only shown in this region but also the 5882-8695 nm (amide I & II) and 7633-8000 nm (amide III) (Barth, 2007). The region of the MIR spectrum between 3225-3571 nm contains the C–H stretching information from the $–CH_3$ and $=CH_2$ groups. Carbohydrates and phosphodiester vibrational signals are present in the 8000-12500 nm region. Finally, a commonly-used MIR region (8333-16666 nm), well-known as the fingerprint region, presents detectable signal differences between samples and remains stable within the same. Consequently, MIR region interpretation is simpler than NIR, although it still requires multivariate analysis for information enhancement and application (Bureau, Cozzolino, & Clark, 2019).

1.7.1. Attenuated Total Reflectance

Attenuated total reflectance (ATR) is one of the most frequently used sampling accessories for IR spectroscopy. Consequently, its application in food analysis using ATR-FTIR spectrometers is interesting for producers to obtain a rapid and accurate analysis. The ATR principle consists of the IR beam movement from a

material with a high reflective index (RI), such as Zinc Selenide (ZnSe) crystal, to a low RI material, such as a sample. Although the light rays do not propagate into the low RI medium, an evanescence field is formed, interacting with the material placed at the surface. When using a critical incident angle, the crystal reflects almost all the incident light, less some of the energy that extends beyond the crystal (0.1-5 μm) in waveform within the sample (Milosevic, 2004). This condition, named total internal reflection, is represented graphically in Figure 3, where the extension of the light energy (evanescent wave) is specified. When this

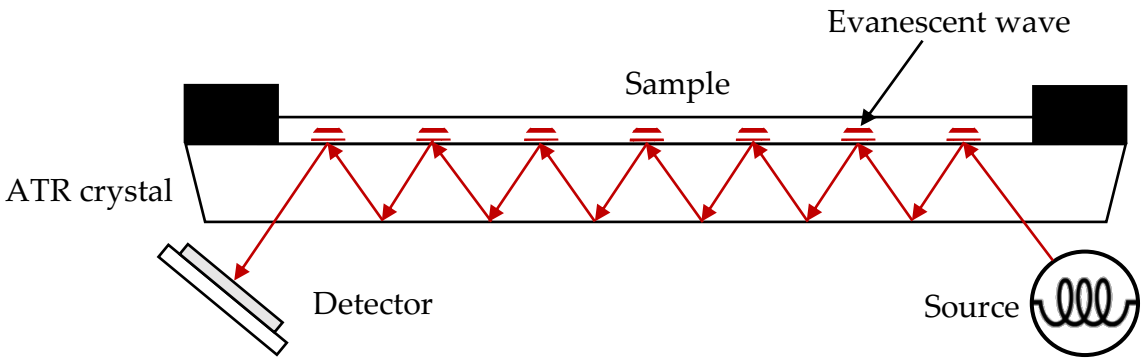

Figure 3. Schematic representation of Attenuated Total Reflection (ATR) sampling technique.

light penetrates the sample, some of the light is absorbed, giving the IR spectrum of the target compounds (Vigano, Ruysschaert, & Goormaghtigh, 2005).

The outgoing IR beam registered by the detector contains the structural and compositional information of the substances in contact with the surface. Accordingly, it gives high reproducible results and the detection of specific compounds variations. It can be used for solid samples, pressing the material against the crystal, liquid samples or the solid residue after liquid evaporation on the ATR crystal. The light does not penetrate deep inside the target material, so the ATR is considered a surface analysis. Consequently, sample preparation should ensure adequate homogenization to obtain accurate results (Ramer & Lendl, 2013; Subramanian & Rodriguez-Saona, 2009).

1.8. Hyperspectral data pre-processing

Pre-processing techniques aim to reduce the data variability to highlight desired spectral characteristics before modelling Frequently used pre-processing techniques in HSI-NIR spectroscopy are classified into two main groups: scatter-correction methods and spectral derivatives. Additional objectives of these approaches are to improve subsequent exploratory analysis, ameliorate linear calibration modes, or improve classification or prediction models (Martens, Nielsen, & Engelsen, 2003). The success of the models depends on the suitable pre-processing technique selection to reduce or maintain model complexity. On the other hand, too strict pre-processings should be avoided because they can hide valuable information from the spectral data.

Scatter correction approaches are designed to solve multiple light scatterings or additive effects which produce non-linearities for the calibration model. The extensively used technique for NIR pre-processing is the Multiplicative Scatter Correction (MSC). When samples are solid or emulsions, multiplicative scattering effects occur due to the deviations in the optical path length. The influence of the vibrations of the neighbour chemical bonds of the sample is responsible for this effect. Coefficients of regression, which describe the dispersion, are obtained from the original spectrum to build a scatter corrected one (Wu et al., 2019). The first step involves the estimation of the correction coefficients that are obtained from a least-square (LS) linear regression against the average optical spectrum from the calibration set, given by the equation 2:

$$y_i = a + b \cdot y_{ref} + e \qquad (2)$$

Where y_i is the previously measured spectrum from the sample; a is the specular effect of the reflection; b are the estimated scatter interferences different for each sample; y_{ref} is a reference spectrum used for the pre-processing of the data set, which usually corresponds to the average spectral information of the calibration

set; and e is the error which contains the chemical information not explained by physical variations.

The second step is the correction of the recorded spectrum using the coefficients obtained previously, following the equation 3:

$$y_{corr} = \frac{y_{ref} - a}{b} = y_{ref} + \frac{e}{b} \quad (3)$$

Where y_{corr} is the corrected spectrum similar to y_{ref} in terms of linear regression. The transformation would give a consistent baseline to the spectra (Rinnan, Berg, & Engelsen, 2009).

The second most applied technique used for scatter correction of NIR is the Standard Normal Variate (SNV) (Equation 4). This pre-processing method has similar benefits to MSC, as it is suitable for removing multiplicative and additive interferences of scattering in the light distance and particle size (Barnes, Dhanoa, & Lister, 1989; Cen & He, 2007). The mean spectrum and the standard deviations are first calculated, and then each point is recalculated, subtracting the mean and dividing by the standard deviation.

$$SNV_i = \frac{(A_i - \bar{A})}{\sqrt{\frac{(A_i - \bar{A})^2}{n-1}}} \quad (4)$$

Where, SNV_i are individual standard normal variations for i wavelengths (corrected value); A_i is reflectance value at i wavelength; $\bar{A}$ is the mean of the A_i reflectance's for all the wavelengths and n is the number of wavelengths from the used range (Caporaso, Whitworth, & Fisk, 2017).

The first and second derivatives are widely applied in analytical spectroscopy for data in which noise is a problem. Such transformations remove both multiplicative and additive effects. The first or second derivative differ in that the first works on the difference between two subsequent spectral points, correcting the baseline, while the second derivative uses the successive spectral

points of the first derivative (1stD), removing both baseline and derivative trends (Tsai & Philpot, 1998).

Moreover, Savitzky-Golay smoothing and differentiation are derivative techniques based on the computation of local polynomial regression to obtain a similar but smoothed function. The advantages of this approach are noise reduction, the smoothing of spectra and a single-step derivative computation with the application of a filter. The difference with other pre-processing techniques is that the initial distribution, relative maxima and minima, and peak width are preserved (Savitzky & Golay, 1964).

Two more pre-processing techniques, such as averaging and normalization, transform data sets into a suitable matrix for subsequent modelling. Averaging reduces the number of variables or objects in the data set, noise and uncertainty measurements. On the other hand, normalization uses the vector scaling (to 1.00 or 100) of the sample set to obtain variables of the same size. This pre-processing is used to compensate variances in analytical measurements, and it is similar to SNV (Esbensen, Guyot, Westad, & Houmoller, 2002).

1.9. Hyperspectral data calibration

Hyperspectral data complexity should be modelled to obtain efficient quantitative and qualitative information. Once the data is pre-processed, multivariate statistical tools are applied to find relationships between the samples and the numerous spectral variables. Figure 4 is a graphical representation of multivariate qualification (projection and classification models) and quantification (regression models) methods used as chemometric tools to deal with *Fusarium* and DON contaminated samples using HSI-NIR (Dale et al., 2012; Kumar, Bansal, Sarma, & Rawal, 2014).

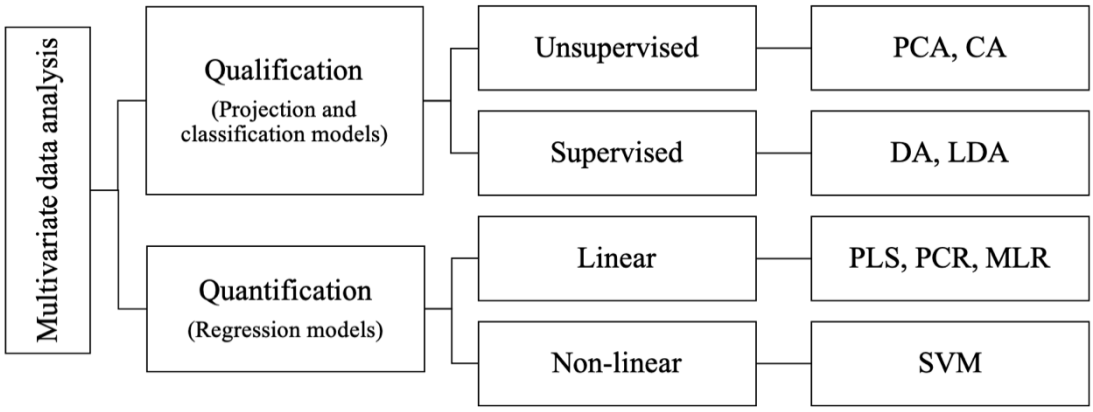

Figure 4. Diagram of the most commonly used multivariate data analysis systems in HSI-NIR.

Principal component analysis (PCA); component analysis (CA); discriminant analysis (DA); linear discriminant analysis (LDA); partial least squares (PLS) regression; principal component regression (PCR); multiple linear regression (MLR); supported vector machines (SVM).

Multivariate qualification methods are applied to reduce a large amount of data to a limited number of variables, called principal components (PC). Principal component analysis (PCA) extracts the most relevant information from the raw data and reduce its dimension by compressing the spectral data into a new group of orthogonal variables. It primarily permits the detection of sample groups used to classify them (Gatius, Lloveras, Ferran, & Puy, 2004). The optimum number of PC should be fixed to build the best projection method. The optimum number is reached when, introducing one more PC, the performance does not improve, so we are increasing the computation time and the complexity of the model without improving the explained variance. Cross-validation methods are useful to determine the optimum number of PC for the best performance of the analysis and are adequate when the data set is reduced (Jiang, Zhu, & Tao, 2010). Supervised classification models can be constructed making class models independently, each one described by a PCA. Unknown samples can be assigned to the known classes to classify them. Several studies of fungal contamination in cereals have used this technique to explain their results (Barbedo et al., 2015;

Serranti, Cesare, & Bonifazi, 2013; Shahin & Symons, 2011). The structure of the PCA model is characterized by equation 5:

$$X = t_1 p_1^T + t_2 p_2^T + \cdots + t_A p_A^T + E_A \qquad (5)$$

Where X are the coordinates expressed over the original X variables; t corresponds to the coordinates of the objects over the PCs; p corresponds to the vectors of the new subspace where the original variables X are projected; E corresponds to the noise characterized by the residuals; and A corresponds to the number of PC used.

Polder, Heijden, Pioneer, Waalwijk, & Young, (2005) used Fuzzy c-means clustering as a statistical method for a prediction model development. Cluster analysis is a method that consists of the categorization of the observations into groups (clusters), in which each one has more similar features than other groups. More specifically, Fuzzy C-means clustering is used to characterize each data point inside the clusters by ranging the observation between 0 and 1 (fuzzy partition). An algorithm is built to discriminate according to the observation group and the other group's differences, minimizing iteratively and obtaining optimal fuzzy partition. Values close to 1 indicate the similarity of the observation with its cluster, and values near 0 indicate less similarity (Bezdek, Ehrlich, & Full, 1984).

An additional extensively used classification method in HSI is discriminant analysis (DA), which aims to find recognition patterns that permit the separation of the observations into classes. The rules obtained should also allow the association of new data into one of these groups, so it belongs to the supervised method's group (requires calibration and validation sets) (Hubert & Van Driessen, 2004). Linear Discriminant Analysis (LDA) is used when de data shows the same covariance matrix. LDA uses a linear combination of features in the multivariate data, dividing observations into two or more groups and maximising the ratio between variances of the compared data points concerning

the group variance (Esteki, Shahsavari, & Simal-Gandara, 2018). This latest method was applied more commonly because of the reduced number of parameters involved in contrast with the unequal covariance matrix structures. Consequently, both procedures have been used for hyperspectral data analysis in *Fusarium* and DON contamination in cereals (Delwiche & Kim, 2000; Delwiche et al., 2011; Delwiche, Kim, & Dong, 2010; Rinnan et al., 2009; Ropelewska & Zapotoczny, 2018; Serranti et al., 2013; Shahin & Symons, 2012, 2011; Singh, Jayas, Paliwal, & White, 2012; Tekle et al., 2015).

Linear and non-linear regression techniques have been used to predict unknown sample concentrations from the spectral data (Westad, Bevilacqua, & Marini, 2013). Regression methods require a calibration set, for which the coefficients of the relationship between concentrations and spectra are calculated; and a validation group, in which these coefficients obtained from the calibration set are checked with a new sample set to give the prediction error (Boldrini et al., 2012). The most commonly used methods in hyperspectral image data analysis are Principal Component Regression (PCR) and Partial Least Squares (PLS) (Caporaso et al., 2018; Viscarra Rossel, 2008).

MLR is the most basic regression method, which can provide successful models for data matrix with few X variables. Thus, for the prediction of simple components, it does not present substantial differences with other regression procedures. However, its application in complex systems (more X than Y variables) gives ineffectiveness because it cannot deal with interferences, noise, errors and collinearity between X variables. For that reason, MLR is not used commonly in HSI-NIR calibration (Balabin, Safieva, & Lomakina, 2007; Fox, Onley-Watson & Osman, 2002).

PCR is a two-step model which involves PCA on the spectral data and a subsequent MLR of the prediction parameters on the scores obtained from the PCA. The regression is performed on the scores with the optimum number of

PCs, which are much less than the number of original X variables, avoiding MLR weaknesses. The scores are orthogonal, so collinearity problems disappear. In addition, the reduction of the number of variables permits solving the model with a lower number of equations (Næs & Martens, 2005).

PCR is used when the target is the X information corresponding to the spectral data because it works with the maximum variance direction of X. However, the HSI-NIR calibration focuses on the Y information about the analyte. PLS focuses the instrumental data on the Y variables to obtain a well-fitted model and lower prediction errors.

PLS is, as PCR, a two-step model, that, instead of projecting on the directions of maximum variance of X, it does on the covariance of X-Y, so it improves the subsequent regression of the dependent variable on these directions. To reach this cooperation, Latent Variables (LV) are computed to model the covariance structure for matrix and dependent variables (Mehmood, Liland, Snipen, & Sæbø, 2012; Westad et al., 2013). PLS algorithms can be applied to a single Y variable (PLS1) or multiple Y variables (PLS2). Both PCR and PLS methods are adequate for wavelength selection, permitting the analysis of the original variables and discerning the significant ones that introduce much information from the irrelevant ones.

Finally, Support Vector Machines (SVM) are frequent in kernel classification approaches due to their applications in recognition and detection. Theoretically, SVM purposes finding an optimal hyperplane surface that divides the maximum of the data points into classes by representing the sample points in the space. The space divides by this hyperplane, consisting of a vector between both groups points. When a new sample is introduced to the model, it will classify it into one group depending on its position previously separated by the hyperplane (Yang, Hong, You, & Cheng, 2015).

1.9.1. Characteristic wavelength selection

Depending on the spectral resolution of the HSI device, the acquired spectral information may include hundreds or even thousands of wavelengths for each sample. Moreover, the management of such a dataset is laborious, and the mathematical computation of the model is time-consuming. In addition, those methods applied to the industry would need simplified and rapid procedures. Consequently, wavelength selection is an important step to reduce irrelevant bands and noise, obtaining fast and reliable analysis. Wavelengths can be localized manually by selecting the highest regression coefficients, which have more influence over the model. Alternatively, also complex algorithms are applied to the optimal band selection. The most common ones are Competitive Adaptive Reweighted Sampling (CARS), Random Frog (RF), Successive Projections Algorithm (SPA), genetic algorithm (GA) and Uninformative Variables Elimination (UVE) (Li et al., 2018; Tang, 2012; Xiaobo, Jiewen, Povey, Holmes, & Hanpin, 2010).

1.10. Model validation and performance

The procedures for calculating a regression model include the reference values and spectral data (usually pre-treated) achievement for the calibration set. A cross-validation procedure or an independent sample set should be introduced, obtaining a realistic prediction error to achieve concentration values as close as possible to the real concentration of the analytes of interest in unknown samples from their spectral data. The previous calibration step involves the reference values and spectra included in the training set, both related with a regression model that has a basic form as shown in the equation 6:

$$Y = b_0 + b_1X_1 + b_2X_2 + \cdots + b_kX_k \qquad (6)$$

Where Y is the unknown variable to be measured; X_i are characteristic wavelengths used for the regression model; b_i are the regression coefficients,

which estimates the unknown parameters; and b_0 is the offset (Givens, De Boever, & Deaville, 2005). During calibration, the spectral values are used to calculate the regression coefficients. Subsequently, a set of new spectral data and the previously obtained regression coefficients are used to predict and measure the unknown variables (Y) in the validation set. The information from the reference method and the spectral data used for calibration and validation should represent the maximum population features.

To adjust the model, the number of PCs to be used should be fixed to explain the variability of the calibration and validation sets efficiently. The criteria used to select the number of PCs to optimize the model is to detect the PC where a break on the curve of the residual variance or a minimum in the prediction error occurs. Other considerations about the analyte should also be considered to obtain a feasible method (Viscarra Rossel, 2008).

The following statistical parameters describe the calibration adjustment: Coefficient of Determination of Calibration (R_C^2), Standard Error of Calibration (SEC), the Root Mean Square Error of Calibration (RMSEC) (Chavez et al., 2013). The closest R_C^2 value to 1 and the closest SEC and RMSEC values to 0 correspond to the best calibration model.

To achieve the internal test and know which model fits the data, cross-validation is a procedure commonly used when it is not possible to have a large number of independent samples from the calibration set. Leave-one-out cross-validation removes a single sample of the training set for each iteration. Otherwise, k-fold cross-validation leaves out an entire data group. They separate into different groups (k), *k-1* used for the calibration training and one remaining group for the test set. The test set group is changed until all samples are tested (Ramírez-Morales, Rivero, Fernández-Blanco, & Pazos, 2016). Thus, the number of LV and the model parameters, such as Root Mean Square Error of Cross-Validation (RMSECV), is evaluated by its internal implementation.

Full cross-validation is considered the most realistic estimation when only one sample set is available, although it will always be more optimistic than the prediction error calculated from a training and a test set. Two sample sets are not always accessible because it requires a large number of samples and, if they are not representative of the population you are working with, the model will not be so realistic. Thus, to build an ideal model, large and representative sets of samples from the calibration and external validation of the model are needed. It improves the model linearity, specificity, and accuracy for future sample concentrations prediction (Levasseur-Garcia, 2018).

Table 1. Performance statistic parameters of the validation set (adapted from Agelet & Hurburgh, 2010; Levasseur-Garcia, 2018).

	Validation set parameters	
R_p^2	Coefficient of determination of prediction	$R_p^2 = \frac{\Sigma\,(\hat{y}_i - \bar{y})^2}{\Sigma\,(y_i - \bar{y})^2}$
d_i	Residual	$d_i = \hat{y}_i - y_i$
Bias	Bias	$Bias = \frac{\Sigma\, d_i}{n}$
SEPc	Standard Error of Prediction (corrected by the bias)	$SEPc = \sqrt{\frac{(d_i - bias)}{n-1}}$
RMSEP	Root Mean Square Error of Prediction	$RMSEP = \sqrt{\frac{\Sigma\,(d_i)^2}{n}}$
RPD	Ratio of Performance to Deviation	$RPD = \frac{Sdev_{ref}}{SEPc}$

$\hat{y}_i$ = ith validation sample predicted value, y_i = ith validation measured values, $\bar{y}$ = mean of the n values (measured or predicted), n = number of samples; $Sdev_{ref}$ = Standard deviation of reference.

Model performance is described by the statistical parameters, that have to be compared to select the most suitable one. Table 1 presents the most used statistic parameters to estimate the statistical performance of the models. The Coefficient of Determination of Prediction (R_p^2) numerically describes the variance between reference and predicted values and the reference values versus the total. The Standard Error of Prediction (SEP) determines the model precision. However, it should be corrected by the bias, which considers the difference between the

expected SEP value and its true value. The Root Mean Square Error of Prediction (RMSEP) determines how accurate is the calibration, and it is closely related to SEP and bias. Finally, the Ratio of Performance to Deviation (RPD) is the ratio between the SEP and the standard deviation of the samples, and it is under discussion for its advantages in NIR calibration. Thus, some publications consider RPD a redundant parameter (Bellon-Maurel, Fernandez-Ahumada, Palagos, Roger, & McBratney, 2010). The optimum model has the R_p^2 closer to 1, and the SEPc (corrected by bias) and the RMSEP closer to 0.

1.11. HSI and DON management in cereal samples

HSI-NIR is not applied only to improve the detection of visible features by sight but also to detect components in a sample not appreciated visually. DON is found commonly in asymptomatic grains, and its detection is more complex than other visible traits. The application of HSI-NIR to DON detection is a novel approach that could solve the heterogeneity problem of the toxin through the sample with the spatial examination capacity (Fox & Manley, 2014). Recent studies based on detection, screening and quantification of DON in cereal samples have been summarised in Table 2 to present the last progresses about the topic.

Tekle et al. (2015) aimed to measure DON content from oat using average NIR spectra by a PLS regression model. They obtained the reference contaminations using GC-MS, and the images were acquired by HSI-NIR at a wavelength range of 1000-2500 nm. Then, they transformed reflectances into absorbances, and SNV was applied to remove the scattering impact and calibrated a PLS model. Using 112 validation images and five PCs to optimize de model, they obtained a R_v^2 of 0.81. On the other hand, they build an alternative PLS-LDA using the ratio of damaged pixels in the kernel. The correlation between predicted and measured DON was 0.79, proving that both were valid for DON prediction.

Barbedo et al. (2015) built an algorithm to assess DON contamination of wheat samples. They used the spectra from the entire image (cereal samples), avoiding the analysis of individual kernels. The authors studied the correlation between the *Fusarium* index (FI) and DON concentrations, obtaining a strong correlation of 0.84. Due to the complexity of DON assessment with visual discrimination, the correlation with FI decreased at low DON levels. Later studies by Barbedo et al. (2017) focused on DON screening and developed a new algorithm. In this case, they obtained DON reference values by ELISA and LC-MS. Two wavelengths (627 and 1411 nm) were selected because they seemed to converge with DON presence. The authors obtained a DON preliminary index (DPI) calculation, based on the kernel reflectance. They were able to classify the samples into the three classes proposed with an accuracy of 72%. In addition, the accuracy increased to 81% when the classes were reduced into two, separated by the UE legal limit (1250 μg/kg). Liang et al. (2018) also used algorithms for DON detection in the Vis/NIR of 400-1000 nm. First, they analysed the entire samples using LC-MS and divided them into three groups. Then, they acquired images from each level of contamination, pre-processing the spectra obtained by SNV and MSC. The authors also selected optimal wavelengths by SPA and RF methods to reduce dimensionality. The best combination between pre-processing and the selected algorithm was the MSC-SPA-SVM, obtaining an accuracy of 100% and 97.72% in the training and the testing set, respectively. A visual representation of the DON contamination using the same model was obtained, which provided information about the toxin levels within the sample.

Table 2. HSI studies for DON management in cereals.

Crop	Number of samples	Wavelength range	Reference of contamination/Type of infection	Spectral pre-processing and characteristic wavelength	Model	Performance	Reference
Oat kernels	Calibration set: 248 kernels; 31 kernels/category; 4 dorsal, 4 ventral Validation set: 112 kernels; 14 kernels/category; 4 dorsal, 4 ventral	HSI-NIR 1000-2500 nm	GC-MS Artificially infected	Positive infection: 1925, 2070, 2140 nm Negative infection: 1400, 1626, 1850 nm SNV	PLSR, PLS-LDA	Calibration R^2 = 0.75 Cross-validation R^2 = 0.71 Correlation PLSR = 0.81 Correlation PLS-LDA = 0.79	(Tekle et al., 2015)
Bulk wheat	25-50 kernels/image 6 hyperspectral images	HIS-Vis/NIR 528-1785 nm	LC-MS Naturally infected	PCA: 1411 nm	FI	Correlation FI/DON = 0.84	(Barbedo et al., 2015)
Bulk wheat	30-50 kernels/image 3 levels of contamination 251 total images Calibration set: 33 images Validation set: 218 images	HSI-Vis/NIR 528-1785 nm	ELISA, LC-MS Naturally infected	Wavelength observation 623, 1411 nm	Confusion matrix, k values	Classification accuracy: 72% in three classes, 81% in two classes (EU limit)	(Barbedo et al., 2017)
Bulk wheat	70 kernels/image 60 images/level of contamination Calibration set: 44 images Validation set: 16 images	HSI-Vis/NIR 400-1000 nm	LC-MS/MS Naturally infected	SNV, MSC 14, 12, 7, 14 wavelengths for each pre-processing method	SVM, PLS-DA	Classification accuracy: 100% in training set; 97.92% in testing set	(Liang et al., 2018)

FI = *Fusarium* index, PLS-DA = partial least squares regression – discriminant analysis, PLSR = partial least squares regression, SVM = support vector machine.

1.12. HSI as a cereal sorting tool

Generally, mono or dichromatic cameras have been used for fungal inspection purposes. High-power LED pulses have been applied as inspection systems, measuring samples reflectance. Although kernel classifications are achieved, spatial characterization of the grain is not possible, so the image is processed as a whole, not selecting its regions of interest. Consequently, the imaging system needs a measurement analysis for the whole field of view, making it impossible to use a spectrum from a specific area, like a kernel (Delwiche, 2008, 2009). Thus, massive and rapid classification systems are needed to achieve discriminations of tonnes of grain in a few hours (Fox & Manley, 2014).

The first approaches of optical cereal sorting started in the Single Kernel-NIR (SK-NIR) spectroscopy, focused on the automatic classification of grain. McMullin, Mizaikoff, & Krska (2015) reached this aim by providing a wheat kernels discernment according to DON contamination at a limit of 60 mg/kg in 96% of the cases. Moreover, they obtained positive and negative fungal infection discrimination in corn kernels with an efficacy of 96% and 98%, respectively

Other rapid cereal sorting methods have also been tested to reduce mould damage and DON contamination. The rejections of contaminated kernels during freefalling along a steeply inclined surface were interesting for their rapid discrimination (Delwiche, 2006, 2007). Although the studies reached good results, they were in laboratory-controlled conditions, so further reports are needed to improve fungi and DON sorting in wheat. Moreover, recent studies also obtained good in-line results for AFB1, with 99% of the samples accepted below 10 μg/kg with a laser-based system (Liu et al., 2019).

HSI has been proposed as a routine grain inspection tool in food industries. Its ability to 'see' all over the kernels and across them to detect fissures or insect damage has driven this instrument to be promising to detect real-time *Fusarium*

damage and mycotoxins. Asymptomatic kernels hinder visual evaluation, making their detection for fungal contamination more complex than for symptomatic. HSI-NIR can evaluate fungal growth and spatially ubicate its presence on a single kernel. Moreover, although *Fusarium* produces DON, both contaminations are not proportional. Asymptomatic samples with high DON concentrations can be fungal-free. For that reason, a precise technique with the ability to chemically inspect and sort contaminated cereals is needed (Tatzer, Wolf, & Panner, 2005). A typical Single Kernel-Hyperspectral Imaging (SK-HSI) analysis flowchart is represented in the Figure 5.

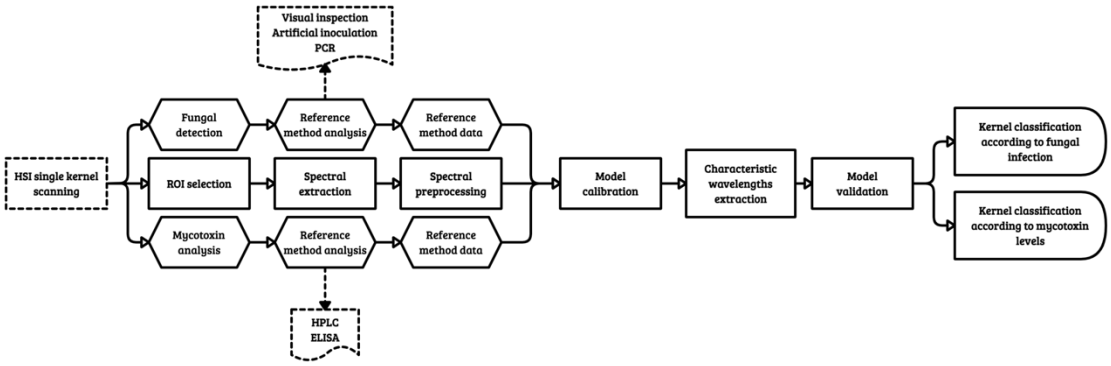

Figure 5. Flowchart of the most common SK-HSI analysis process of cereals for fungal and mycotoxin contamination

Industrial reception of grain is a critical step in which HSI-NIR applications would be interesting to substitute classical analysis methods. Still, the heterogeneity of the batches often presents troubles in the representativeness of the samples to be analysed. Moreover, HSI-NIR would overcome this heterogeneity by rapid kernel or pixel spectra evaluation (Gruna, Vieth, Michelsburg, & Puente-León, 2010). In short, HSI is an encouraging analysis technique for fungal damage and mycotoxin analysis due to the spatial dimension introduced and its fast scanning capacity.

1.13. SK-HSI classification according to fungal contamination

Fungal contamination is responsible for the quality and yield reduction of cereal crops. Fungal growth produces several changes on cereal kernels structure that can be visualized as weight loss, shrivelling, discolouration, etc. Several authors proposed visible (Vis) (400-700 nm) and near-infrared (NIR) (780-2500 nm) regions of the electromagnetic spectrum for fungal detection in single cereal kernels. Therefore, they also proposed classification models for kernel sorting according to fungal species or the symptomatology caused on the grain. The classification accuracies describe model performances, which assess the correctly classified percentage of the kernels (Xing et al., 2019).

In this section, the studies focused on single kernels as the ROI for fungal infection assessment are reviewed and compiled in Table 2. Numerous studies focused on single wheat kernels in the last years. The two most studied fungi in grain sorting publications are *Aspergillus* and *Fusarium* genera for their associated impact on grain quality and health effects. The studies of Zhang, Paliwal, Jayas, & White (2007) and Singh et al. (2012) discriminated between non-contaminated kernels and fungal infected kernels by *Penicillium* spp., *Aspergillus niger*, and *Aspergillus glaucus* in the NIR region. Previous to the HSI analysis, the kernels were artificially contaminated with fungal spores and incubated for growth. This reference method ensured fungal growth but, depending on the inoculation method, it could cause differences from the inoculation naturally found in the field. Although they used different chemometric tools to calibrate the models, both studies obtained positive results above 87% of correctly classified grains. Alternatively, Alisaac et al. (2019) represented their results as differences in the spectral signature of the scanned kernels instead of evaluating the percentage of correct classification. This study used the differences in several spectral regions

to correlate them with artificial fungal presence and DON. Despite the obtained good correlations, spectral characterization in the NIR region is complex due to the peak overlapping, especially in high-frequencies (low wavelengths).

The alternative to fungal inoculation is assessing the visual changes produced during fungal growth. Kernels can be inspected visually to determine the damage caused by *Fusarium* infection, categorizing the kernels as FDK according to their weight loss, shrivelling and discolouration. Despite the simplicity of this method, it is less reliable than chemical or biological techniques due to the subjectivity of the inspector. Several authors used LDA as a classification tool for FDK (Delwiche, Rodriguez, Rausch & Graybosch, 2019 and Shahin & Symons, 2011). They presented high-accurate results between 92 and 100% of correctly classified kernels. Despite the high accuracies, the visual inspection categorization of kernels does not consider the fungal contaminations not visually detectable, introducing some deviations. There are some alternatives to identify fungi by visual inspection, e.g. automatized kernel categorization, fungal isolation, fungal DNA quantification, among others. Ropelewska & Zapotoczny (2018) study additionally classified wheat kernels as healthy or infected with *Fusarium* species in the Vis and NIR region using visual inspection as reference method. However, they used further chemometric analyses to LDA, such as Bayes, K-Star, Rules PART and Decision Tree classifiers, obtaining classification accuracies between 78 and 100%.

Delwiche & Kim (2000) used a spectral range of 430-860 nm obtaining classifications accuracies of 86.8 and 98.4% in two different wheat varieties. Moreover, Delwiche et al. (2010) combined two pairs of wavelengths in the spectral range of 1000-1700 nm (1199, 1474 nm and 1315, 1474 nm), obtaining an LDA classification accuracy of 82.5% in high visual contrast kernels. A year later, Delwiche et al. (2011) repeated the experiment at similar conditions but adding a

Vis camera (400-1000 nm) and different wavelength pairs (502/678 nm) and (1198/1498 nm), achieving a better LDA classification accuracy (95%).

Chemometric alternatives to LDA were also used, as PLS-DA, applied in the study of Serranti, Cesare, & Bonifazi (2012) and Delwiche et al. (2019) for wheat kernels sorting according to the damage caused by fungal infection. The first study obtained accurate classifications with a percentage of correctness above 94%. Likewise, Delwiche et al. (2019) classified with an overall accuracy of 97.3% and an optimized model with four LV of 96.8%. Finally, Barbedo et al. (2015) classified wheat grains according to fungal damage using the FI, which measures the probability of wheat kernels to develop FHB. The FI based algorithm obtained a classification accuracy of 91%. Generally, the studies aiming at wheat kernels sorting according to fungal infection presented good results. However, the researchers based their models on low-precision reference data. Consequently, they require field fungal infections and improved reference methods to apply their classifications to the food industry. Polder et al. (2005) also used the HSI-NIR for wheat analysis, but they employed PLS regression for *Fusarium* quantitative analysis in single kernels. The reference values were fungal DNA concentration obtained with Taqman Real-Time PCR (RT-PCR). The spectra were pre-processed by normalization and second polynomial order SG-smoothing. The regression model permitted a well-defined identification for *Fusarium* DNA in concentrations above 6000 pg and the concentration prediction of higher than 100 pg with an R^2 of 0.8. Although the correlation between the *Fusarium* DNA and the spectra was acceptable, further investigations are needed to improve fungal and DON concentration predictions.

Table 3. Single-kernel HSI studies for the classification of fungal infection in cereals.

Cereal	Fungi	Spectral range Nº of LV used	Pre-processing technique	Reference method	Training/test set Total kernels	Classification model and accuracy (%)	References
Wheat	FDK (Natural contamination)	430-860 nm	-	Visual inspection	Cross-validation 32 scabby kernels 32 control kernels	Increasing 5 bands from 458-844 nm LDA (83-98%)	(Delwiche & Kim, 2000)
	A. niger, *A. glaucus* and *Penicillium spp.* (Inoculated)	900-1700 nm 20 LV	Normalization PCA transformation	Artificial inoculation	400/140 kernels for each mould specie 2160 total kernels	SVM (> 87.2%)	(Zhang et al., 2007)
	F. verticillioides (Inoculated)	960–1662 nm and 1000–2498 nm	MSC SNV	Fungal artificial inoculation	15 kernels (5 infected, 5 asymptomatic, 5 control)	Fuzzy c-means clustering (94.4-97.7%)	(Williams et al., 2010)
	FDK (Natural contamination)	400-1700 nm 4 LV	-	Visual inspection	~480 kernels	LDA (95%)	(Delwiche et al., 2011)
	FDK (Natural contamination)	400-1000 nm 6 LV	Normalization Extremes removal	Visual inspection	400/400 (200 healthy and 200 FDK) 800 total kernels	LDA (92%)	(Shahin & Symons, 2011)
	FDK (Natural contamination)	1000-1700 nm 4 LV	GLS Weighting	Visual inspection	40/30 70 total kernels	PLS-DA (94.4-99.2%)	(Serranti et al., 2012)
	Penicillium spp., A. glaucus, and A. niger (Inoculated)	700-1100 nm 13 LV	-	Artificial inoculation	240/60 300 total kernels (Independent)	LDA, QDA, Mahalanobis (94-98.3%)	(Singh et al., 2012)
	FDK (Inoculated)	528-1785 nm 1 LV	Normalization	Visual inspection	50-100/700-750 803 total kernels	Fusarium index (91%)	(Barbedo et al., 2015)
	F. graminearum (Natural contamination)	600-1100 nm 3 LV	-	Visual inspection	120 total kernels (Cross-validated)	LDA, K Star, PART, LMT (78-100%)	(Ropelewska & Zapotoczny, 2018)
	FDK (Natural contamination)	938-1654 nm 2-7 LV	Mean centring SNV	Visual inspection	556/20820 21376 total kernels	LDA, PLS-DA (> 92%)	(Delwiche et al., 2019)
	F. culmorum and F. poae (Inoculated)	400-2500 nm (Whole range)	-	qPCR	No calibrations performed	Spectral signature (-)	(Alisaac et al., 2019)
Maize	*A. flavus*, *A. parasiticus* and *A. niger* (Inoculated)	400–1000 nm 3 WL	-	Artificial inoculation	No validation performed	PCA-DA (-)	(Del Fiore et al., 2010)
	A. flavus (Inoculated)	400-700 nm 2 LV	-	Artificial inoculation	243/249 247/245 492 total kernels	Maximum likelihood: >80% Binary encoding: >87%	(Yao et al., 2013)
	A. flavus, *A. niger and A. ochraceus* (Natural contamination)	900-1700 nm 8-10 LV	-	Fungal isolation	595/297 892 total kernels	PW-PCA-SVM (100%)	(Chu et al., 2020)
	F. verticillioides and F. graminearum (Inoculated)	1000-2100 nm 4 LV	SNV Mean-centring	Fungal isolation	2/13 isolates 15 total isolates	PCA (-) PLS-DA (88-100%)	(da Conceição et al., 2021)
Rice	*A. oryzae* (Inoculated)	400-1000 nm 10 LV	-	Artificial inoculation Electron microscopy	119/91 kernels 210 total kernels	SOM (-)	(Siripatrawan & Makino, 2015)
	Villosiclava virens (Inoculated)	874-1734nm Regions selection	Extremes removal	Artificial inoculation PCR	Different sets 1720 total kernels	PLS-DA (98.4%) SVM (98%) ELM (99.2%)	(Wu et al., 2020)
Barley	*A. glaucus* and *Penicillium spp.* (Inoculated)	400-2500 nm 3 LV	-	Artificial inoculation	240/60 300 total kernels	Linear, Quadratic and Mahalanobis discriminant analysis (> 94%)	(Senthilkumar et al., 2016)

ELM = Extreme Learning Machine; JSRC = Joint Sparse Representation based Classification; PW = Pixel-wise; SOM = Self-Organizing Map; SPA = Successive Projection Algorithm; SVM = Support Vector Machines; FDK = Fusarium-damaged kernel, iPLS-DA = interval partial least squares – discriminant analysis, LDA = Linear discriminant analysis, LMT = decision tree classifier, ND = not defined, PART = rules classifier, PCA = Principal component analysis, QDA = quadratic discriminant analysis, SND = sound.

Although wheat is the most investigated cereal, other grains have been tested to assess the fungal infection at the single-kernel level. Maize is the second most investigated cereal, mainly for *Aspergillus* infection assessment. Del Fiore et al. (2010) and Yao et al. (2013) used similar spectral regions to differentiate among previously inoculated *Aspergillus* species, such as *Aspergillus flavus*, *Aspergillus parasiticus*, and *Aspergillus niger*. The first study used PCA to discriminate the species in the Vis-NIR region at different infection stages after artificial inoculation. Yao et al. (2013) used only the Vis spectra to build two classification models. Alternatively, they calibrated an LDA model, for which weak results were obtained (44.2%). By a confusion matrix (CM), the previous results improved, with a percentage of accuracy of 74.7%. Naturally contaminated kernels with *A. flavus*, *A. ochraceus*, and *A. niger* were analysed in the NIR region by Chu, Wang, Ni, Li, & Li (2020). In this study, they built a complex algorithm composed of pixel-wise (PW), PCA, and SVM, obtaining a classification of 100%.

Da Conceição et al. (2021) analysed two *Fusarium* species infection (*Fusarium verticillioides* and *F. graminearum*) in maize kernels by HSI after their artificial inoculation. They pre-processed the NIR spectra with SNV and mean-centring, calibrating a PLS-DA model with a perfect discrimination accuracy. Alternatively, Williams, Manley, Fox, & Geladi (2010) proved the discrimination power of HSI-NIR of *Fusarium*-infected corn with different pre-processing techniques (MSC, SNV and non-processed). Selecting the wavelengths 1960 nm and 2100 nm for infected and 1450 nm, 2300 nm and 2350 nm for non-infected kernels, a classification accuracy between 94.0-97.7%, a coefficient of determination (R^2) of 0.73 and 0.86 for each camera, and an RMSEP of 0.23 was reached. The best classification conditions were applying an MSC step in infected kernels spectra.

Maize analysis by HSI should offer advantages compared to cereals with smaller kernel sizes, like wheat and rice. Size is directly related to the light penetration

in diffuse reflection or transmittance modes. Maize permits deeper penetration of incident radiation and, thus, enhanced information is obtained for the inner part of the kernels. For small kernel analysis, surface information has more influence on the overall data. In addition, it is not possible to compare cereal types due to different light incidence angles and shadowing effects. Some studies evaluated rice by HSI. They analysed artificially inoculated *Aspergillus oryzae* rice by Vis-NIR HSI, prior to electronic microscopic examination. The authors also built an unsupervised Self-Organizing Map (SOM) to visually assess the different fungal levels of contamination (Siripatrawan & Makino, 2015). The study of Senthilkumar, Jayas, White, Fields, & Gräfenhan (2016) evaluated barley kernels according to previously inoculated *A. glaucus* and *Penicillium* spp. in the Vis-NIR region. They used different DA (linear, quadratic, and Mahalanobis) for which the classification accuracy of barley kernels was greater than 94%.

Finally, other studies evaluating fungal infection in individual kernels other than cereals were also reviewed. Legumes, which have a similar shape as cereal kernels, could be handled using HSI analysis. The study of Karuppiah et al. (2016) evaluated the fungal infection in different pulses, including chickpeas, green peas, lentils, pinto beans and kidney beans. They evaluated inoculated legumes by an HSI-NIR analysis by Quadratic Discriminant Analysis (QDA) and LDA modelling. The results were similar for both models, despite LDA achieving slightly better classifications (98-100%). Finally, fungal contamination in peanuts was also studied, calibrating algorithms based on Joint Sparse Representation based Classification (JSRC) and SVM for individual peanut kernels discrimination. The accuracies ranged from 96.8-99.2% in JSRC models and 90.5-97.6% depending on the threshold and the peanut variety.

Taken together, the overall results in SK-HSI reviewed studies are positive, achieving classification accuracies above 90% in most cases. The results are promising to implement HSI technologies in the food industry aiming at cereal

sorting according to fungal infections. Although the authors obtained high accuracies, further studies are required, including bigger data sets and independent model validations for routine analysis. In addition, calibrations should be on naturally contaminated kernels to build robust algorithms to predict and discriminate typical fungal contamination found in the field. However, despite the results obtained, further studies with more precise reference methods and natural contamination are also required to assess the usefulness of their application in industrial sorting processes.

Artificial fungal inoculation offers some advantages, as controlled growing conditions and selected strains. However, the changes produced on cereals differ from the naturally infected, which experience contamination with more than one fungal strain and at variable contamination levels. Consequently, artificial inoculation may be considered a suitable approach for laboratory-controlled preliminary studies, despite further investigations on independent and naturally-infected kernels should be performed. Moreover, the comparison of studies with different infection types is complex and has to be considered in further sections. The infection type is collected in the Table 3 for the most relevant studies using HSI-NIR for fungal infection detection.

Almost all the studies reviewed attempted the optimal LV selection. The number of wavelengths selected is variable, and it goes from 1 to 20 LV, using different selection strategies. Although the LV selection does not improve model performance in all the studies, it offers a reduction in data dimension, reducing computational time in online sorting strategies, in which the contaminated kernels removal has to be in situ. The characterization of the selected wavelengths is also fundamental to correlate the changes produced by fungi on cereals with the spectral profile obtained. Optimal selection is an essential point for sorting purposes. Although the presented results discriminate kernels accurately, future additional work on this item is required.

1.13.1. Optical changes produced by fungal growth

Fungal metabolism produces physical and chemical changes in cereals. Physical features of kernels include structural changes (kernel size, kernel shape and shrivelling) and colour changes (discolouration and pinkish colour). On the other hand, noticeable chemical changes produced by fungi are inherent to their growth, such as protein, starch, lipid and water composition. The spectral changes correspond to the differences in matrix composition. Thus, these optical variations can monitor fungal growth and point out to mycotoxin production in cereal products. In addition, long-wavelength regions are more suitable for the quantification of minor components in food matrices, as they require a shorter optical path length and penetration depth.

The structural changes and chemical decompositions affect the different spectral regions on the NIR window. Kernel size differences produce baseline offset, as the thicker kernels would have a deeper penetration of the light, and the absorbance would be higher (Chu et al., 2020). Otherwise, kernel infections produce reflectance changes in cereal kernels at the late Vis spectral region (628-706 nm) (Su et al., 2021). Dowell et al. (1999) correlated the differences caused by fungal infection in protein and starch content with 1400 nm region for its use as indirect detection of DON in cereals. Nevertheless, Peiris, Pumphrey, & Dowell (2009) studied NIR absorption related to fungal damage and DON. First, they identified the NIR changes produced by shrink and brightness in FDK, which is a known difference due to fungal infection. The spectral differences were in the 1425-1450 nm region, where FDK kernels showed a shifted peak at 1445 nm, while for the sound the difference was at 1430 nm. Liang et al. (2020) attributed the changes produced around 1190-1212 nm (2nd overtone of C–H stretching vibration) to starch and fat content that are some of the principal storage compounds. In addition, the region between 1733-1778 nm (1st overtone C–H) changed according to amylose content, a majority component of the starch. The

authors also attributed higher radiations (1935-1952 nm) to the combinations of stretching and bending of water molecules.

Protein changes in NIR spectra were in the 1446-1502 nm region, corresponding to the 1st overtone of N–H. Otherwise, N–H stretching related to $CONH_2$ in maize proteins was related to absorbance deviations in the 1520 nm region reported by Chu et al. (2020). In addition, variations in functional groups of oils and fatty acids caused by fungal infection were in the 1666-1818 nm region. Phenolic content produced by vegetal products also experienced a difference between damaged and healthy kernels, presenting intensity alterations in 1415-1512 nm.

1.14. SK-HSI classification according to mycotoxins contamination

NIR differences due to mycotoxins are complex due to their low concentrations. However, Peiris et al. (2009) identified the spectral characteristics for pure DON solution in acetonitrile and FDK. The authors recognised two NIR regions that differ with DON concentration, corresponding to 1390-1440 nm and 1880-1950 nm regions. Two characteristic peaks inside these regions correlated with DON 1st overtone in 1414 nm for O–H bonds and 1906 nm for -C=O and R–OH. *Fusarium* damage related with DON in the NIR region, where the most noticeable alterations were detected in 1204, 1365 and 1700 nm, associated with 1st overtone alterations in C–H groups in reserve compounds of grains (carbohydrate, lipids and proteins).

Fungal infection is frequently associated with mycotoxin production, inherent to fungal secondary metabolism. Mycotoxin contamination of cereals is associated with harmful health effects in humans and animals. Consequently, food safety authorities (European Commission, 2006a) established maximum mycotoxin limits in cereal products. According to their potential health risk, the regulated mycotoxins are aflatoxins (AFs), ochratoxin A (OTA), patulin, deoxynivalenol

(DON), zearalenone (ZEN), and fumonisins (FBs). Mycotoxin detection with HSI in cereal products is challenging because they do not produce visual changes in kernels, their low levels (low ppm or ppb) in samples regarding other majority substances, and their heterogeneous distribution in a batch. Notwithstanding the detection difficulties, several authors applied the HSI potential to discriminate the highly-contaminated kernels in a cereal batch (Table 4). DON contamination in wheat and AFs in maize are the most studied for HSI mycotoxin assessment.

Several authors classified contaminated wheat kernels according to DON levels. Liang et al. (2020) used a complex computational model based on the combination of MSC, GA and Sparse Autoencoder (SAE), which separated contaminated kernels above and below 1 mg/kg of DON with an accuracy of 100%. In addition, the study of Senthilkumar, Jayas, White, Fields, & Gräfenhan (2017) studied OTA contamination in wheat kernels for five different thresholds between 54-700 μg/kg. The DA performed (linear, quadratic and Mahalanobis) reached classifications above 98% of precision.

The legal limit for the sum of AFs in maize subjected to physical treatments before sorting is 10 μg/kg (European Commission, 2006b). Thus, the classification of individual kernels according to AFs contamination is not allowed. However, AFs in individual maize kernels were investigated in two similar studies from the same authors, with two limits established in 20 and 100 μg/kg (Yao et al., 2010). Although both analyses included the Vis spectrum, they used different discrimination tools and reference methods. The results ranged between 84-87% and 86-91% for 20 and 100 μg/kg threshold, respectively. On the other hand, other authors worked on the NIR range (1000-2500 nm) with the same purpose. First, Wang, Lawrence et al. (2015) classified extreme (very high or very low) contaminated kernels with better precision between the 10-100 μg/kg range. Nevertheless, the overall result was 86.3% using the Spectral Angle Mapper (SAM) classifier. Then, Chu, Wang, Yoon, Ni, & Heitschmidt (2017) validated a

SVM classifier in 3 classes (< 20, 20-100, and > 100 μg/kg) with a precision of 82.5%.

Some authors also analysed different mycotoxins by HSI in individual barley kernels. Barley grain sorting according to OTA, which legal limit is 5 mg/kg, was first studied by Senthilkumar et al. (2016). However, they established a 140 μg/kg threshold before calibrating several discriminant models (linear, quadratic and Mahalanobis). The accuracy reached 100% in the differentiation of OTA contaminated and non-contaminated kernels. Unlike OTA analysis, DON was also evaluated by Vis-NIR HSI, using complex wavelength selection tools based on CARS and Iterative Selection of Successive Projections Algorithm (ISSPA) (Su et al., 2021). They fixed five different thresholds (1.25, 3, 5, and 10 mg/kg), and the PLS-DA accuracy improved as the limit increased (79.2, 90.9, 91.7, and 95.8 %, respectively).

Tekle et al. (2015) investigated DON infection in oat kernels in the NIR region (1000-2500 nm). They obtained a positive correlation of 0.8 by PLS analysis between the spectra from oat and the reference values obtained by GC-MS. In addition, they identified DON, based on LDA, for the visual representation of infected regions within the wheat kernels. Finally, single peanut kernels were analysed using similar processes to the used for cereal sorting by HSI (Zhongzhi & Limiao, 2018). AFs sorters were evaluated based on different chemometric and artificial intelligence tools (Random forest, SVM, K-NN and Backpropagation Artificial Neural Networks -BP-ANN-) using a Savitzky-Golay modified spectrum. Models performance for a 20 μg/kg threshold were 89.4, 62.2, 88.1, and 80.9%, respectively. Thus, the studies demonstrated the single kernel sorting potential of HSI according to toxic substances.

1.15. Applications of FTIR in cereal quality and safety

NIR spectroscopy has been used extensively for food analysis purposes compared to FTIR. However, FTIR application to food analysis has increased recently due to its suitability in numerous applications. In recent studies, FTIR has been used to quantify nutritional compounds and other molecules in food, characterize the structure of food molecules, determine the quality and safety of raw products and detect food adulteration (Badhan, Wang, & McAllister, 2017; Cavin et al., 2016; Fernández & Agosin, 2007; Patz, Blieke, Ristow, & Dietrich, 2004; Rodríguez, Rolandelli, & Buera, 2019).

Although several studies focused on food products analysis, such as fruits, vegetables, wine, etc., FTIR analysis of cereals increased in the last decades for quality and safety control. Hell et al. (2016) developed multivariate calibrations with ATR-FTIR for wheat bran compositional parameters, including water, protein, ash, starch, soluble and insoluble dietary fibres, and lipids. They compared the results with FT-NIR and, even FTIR presented better accuracy for protein content prediction, NIR results seemed to be more robust. Shi & Yu (2017) followed the same objective, but only for protein and moisture content in wheat. They determined that the best spectral pre-treatment for crude protein prediction in the characteristic wavelength region selected (5714-9090 nm) was SNV with an R^2 of 0.90. The results do not match with the ones in the previous study because the MIR prediction performance is lower than the NIR (R^2 of 0.97). FTIR moisture prediction presents a weaker adjustment (R^2 of 0.72) than for protein content, using the combination of 1^{st}D and SNV. In both studies, the FT-NIR prediction showed higher performances than FTIR. They agree that more appropriate pre-treatments and chemometric tools are required to improve ATR-FTIR results. In addition, Kim, Himmelsbach, & Kays (2007) focused on other compositional parameters detection in cereals by ATR-FTIR. They measured the *trans* fatty acids from cereal-derivate products (snacks, cookies, breakfast cereals, etc.), pressing

the ground samples on the ATR crystal. Although they did not extract the oil from the products, they obtained accurate performance parameters for the PLS models, with an R^2 of 0.89-0.92 for the validation results. The fingerprint range selection 6666-1111 nm presented similar results to the full-range, representing the trans double bonds at the 10351 nm band included in the region. The studies did not focus only on the compositional analysis to determine the cereal quality but also on the baking quality of wheat flour (Chen, Ye, & Zhao, 2017). Combining determined bands from NIR and MIR region, they obtained correlations above 0.94 for all the analysed quality parameters (water absorption, dough development time, dough stability, and degree of softening), improving the performance of both regions analyses separately.

The food industry demands the rapid identification of cereal varieties. The FTIR application to identify cereal species has been recently investigated (Porker, Zerner, & Cozzolino, 2017; Suchowilska, Kandler, Wiwart, & Krska, 2012). Suchowilska et al. (2012) used FTIR spectroscopy and PCA to determine the differences of four wheat species by PCA. However, Porker et al. (2017) used additional chemometric tools (PLS-DA, LDA and Soft independent modelling by class analogy -SIMCA-) to discriminate barley malt varieties. PLS-DA presented classification accuracies between 91-100% for eight different barley varieties. The fingerprint region showed the differences between cereal varieties, discriminated by the cereal matrix composition. These results showed the initial suitability of MIR spectra to classify or identify cereal varieties with potential application in breeding programmes.

The high prevalence of fungal-related contaminations in cereal products has yielded many studies on the feasibility of FTIR to control those infections. *Fusarium* is one of the most studied species using this technology. Kos, Lohninger, & Krska (2001, 2002, 2003) measured the corn ergosterol content to indirectly detect fungal contamination with ATR-FTIR, pressing the ground

sample against a diamond crystal. The first two studies showed high classification accuracies for a cut-off of 8.23 mg/kg (analysed by HPLC), with 75% and 100% of correctly-classified samples, respectively. In their last work, they used Gas Chromatography with Electron Capture Detector (GC-ECD) as the reference method and the accuracy improved for low levels (0.88 mg/kg), although they reduced the sample set (n = 14). In addition, they built a PLS model, which permitted ergosterol content prediction with a R of 0.77 and an RMSECV of 0.66 mg/kg. Peiris, Bockus, & Dowell (2012) attempted the same objective but for wheat. They did not use chemometric tools to model the MIR spectral information, correlating visual fungal contamination signs with five spectral bands. The results suggested that ATR-MIR is suitable for fungal contamination detection in cereals.

The same authors (Kos et al., 2002 & 2003) not only classified samples according to ergosterol but also to DON. In their first study using 52 samples, PCA classified correctly more than 75% of the samples with a DON level higher than 0.13 mg/kg from the blank ones. Alternatively, they increased the classification to 100% in distinguishing 14 naturally-contaminated corn with higher levels than 0.31 mg/kg. Abramović, Jajić, Abramović, & Jurić (2007) used a similar sample amount (17) to predict and classify DON-contaminated samples. The selected spectral information was 5665–5917 nm range for PLS and two spectral bands (5737 and 5851 nm) for Multiple Linear Regression (MLR) models. PLS validation presented a high correlation of 0.92 and an RMSEP of 1.64 mg/kg. The results for MLR had lower RMSEP (1.48 mg/kg) and equal correlation (0.92) for a model calibrated using the ratio between 5851/5737 nm. In addition, a cluster analysis attempted to discern three blank samples from samples with a DON concentration range of 2.51-5.55 mg/kg, obtaining an inappropriate classification for one of the three blank samples.

Further studies focused on the classification of DON levels in cereals. The fingerprint spectral region was used to classify DON-contaminated corn samples in Kos et al. (2016) study. The spectra were obtained from ground and sieved artificially infected samples, pressed against a diamond crystal before ATR-FTIR analysis. Several pre-treatments were applied, such as baseline correction, mean-centring, normalisation and 1stD. PCA models could classify correctly 79% of the 110 samples used, establishing the threshold at the European Union (EU) limit (1750 μg/kg). Sieger et al. (2017) followed the same strategy but used a portable laser-based spectrometer and the 5494-6410 nm region. Although they used a reduced sample set (24), they demonstrated an accurate PCA discrimination of samples contaminated above 1250 μg/kg from uncontaminated ones. Öner et al. (2019) also used the fingerprint region to discriminate 183 corn samples on the regulatory limits (1250 μg/kg). They used several sophisticated classification models (Adaptive Boosting -AdaBoost-, Multilayer Perceptron -MLP-, Random Forests, and SVM). All the models obtained accurate classifications, despite the MLP showed the better performances classifying correctly 91% of the contaminated samples and 94% of uncontaminated. Finally, De Girolamo et al. (2019) also used an FTIR spectrometer applied to DON detection on wheat bran. They used 0.5 g of ground sample pressed on an ATR accessory, consisting of two crystals, one diamond attached to a ZnSe. The spectral range used was 2500-28571 nm (not selecting any variable) and was pre-processed by correcting the baseline and applying SNV and MSC transformations. The PLS-DA and Principal Component Linear Discriminant Analysis (PC-LDA) models classified 86% and 87% of the 94 samples used with a cut-off established at 400 μg/kg. Studies results suggest that FTIR is a suitable technique to detect cereal fungal and mycotoxins contamination at regulatory levels with minimum sample preparation. Consequently, the approach is adequate for rapid and routine analysis for cereal producers and traders as an alternative to complex chromatography and immuno-based methods.

Table 4. FTIR studies for *Fusarium* and DON management in cereals.

Product	Contaminant	Range	Pre-treatment	Reference method	Sample set	Model performance	References
Maize	Ergosterol (*F. graminearum* artificial inoculation)	15384-2500 nm	1stD	HPLC-DAD	52	PCA: > 75% accuracy for levels > 8.23 mg/kg	(Kos et al., 2002)
Maize	Ergosterol (*F. graminearum* artificial inoculation)	15384-2500 nm	Normalisation 1stD	GC- ECD	14	PCA: 100% accuracy for levels > 0.88 mg/kg PLS: R 0.77; RMSECV 0.66 mg/kg	(Kos et al., 2003)
Wheat	*F. graminearum* (Artificial inoculation)	26315-2500 nm	SG 2ndD	Visual inspection	145-150	Differences in bands: 9661, 8620, 8312, 7616, and 7272 nm	(Peiris et al., 2012)
Maize	DON (Artificial fungal inoculation)	15384-2500 nm	1stD	HPLC-DAD	52	PCA: > 75% accuracy for levels > 0.13 mg/kg	(Kos et al., 2002)
Maize	DON (Natural infection)	15384-2500 nm	Normalisation	GC- ECD	14	PCA: 100% accuracy for levels > 0.31 mg/kg PLS: R 0.81; RMSECV 0.49 mg/kg	(Kos et al., 2003)
Wheat	DON (Artificial fungal inoculation)	15384-2500 nm 5851/5737 nm	-	HPLC-DAD	17	PLS: R 0.92; RMSEP 1.64 mg/kg MLR: R 0.92; RMSEP 1.48 mg/kg	(Abramović et al., 2007)
Maize	DON (Artificial fungal inoculation)	12500-5555 nm	Baseline, mean-centring, normalisation, 1stD	LC/MS-MS	110	PCA: 79 % accuracy (cut-off 1750 µg/kg)	(Kos et al., 2016)
Maize	DON (Artificial/natural infection)	6410-5494 nm	Averaging, smoothing	LC/MS-MS	24	PCA discrimination (cut-off 1250 µg/kg)	(Sieger et al., 2017)
Maize	DON (Artificial/natural infection)	12500-5555 nm	Baseline, averaging, de-trending, normalisation	LC/MS-MS	183	MLP: 91% (contaminated) 94% (non-contaminated) samples accuracy (cut-of 1250 µg/kg)	(Öner et al., 2019)
Wheat bran	DON (Natural infection)	28571-2500 nm	SNV, baseline, MSC	HPLC-DAD	94	PLS-DA: 86% (cut-off 400 µg/kg) PC-LDA: 87% (cut-off 400 µg/kg)	(De Girolamo et al., 2019)

1.16. References

Abramović, B., Jajić, I., Abramović, B., Ćosić, J., & Jurić, V. (2007). Detection of deoxynivalenol in wheat by fourier transform infrared spectroscopy. *Acta Chimica Slovenica*, 54, 859–867.

Agelet, L. E., & Hurburgh, C. R. (2010). A tutorial on near infrared spectroscopy and its calibration. *Critical Reviews in Analytical Chemistry*, *40*, 246–260.

Alisaac, E., Behmann, J., Kuska, M. T., Dehne, H.-W., & Mahlein, A. K. (2018). Hyperspectral quantification of wheat resistance to Fusarium head blight: comparison of two *Fusarium* species. *European Journal of Plant Pathology*, *152*, 869–884.

Alisaac, E., Behmann, J., Rathgeb, A., Karlovsky, P., Dehne, H. W., & Mahlein, A. K. (2019). Assessment of *Fusarium* infection and mycotoxin contamination of wheat kernels and flour using hyperspectral imaging. *Toxins*, *11*, 1–18.

Badhan, A., Wang, Y., & McAllister, T. A. (2017). Analysis of complex carbohydrate composition in plant cell wall using Fourier transformed mid-infrared spectroscopy (FT-IR). *Methods in Molecular Biology*, *1588*, 209-214.

Balabin, R. M., Safieva, R. Z., & Lomakina, E. I. (2007). Comparison of linear and nonlinear calibration models based on near infrared (NIR) spectroscopy data for gasoline properties prediction. *Chemometrics and Intelligent Laboratory Systems*, *88*, 183–188.

Barbedo, J. G. A., Guarienti, E. M., & Tibola, C. S. (2018). Detection of sprout damage in wheat kernels using NIR hyperspectral imaging. *Biosystems Engineering*, *175*, 124–132.

Barbedo, J. G. A., Tibola, C. S., & Fernandes, J. M. C. (2015). Detecting Fusarium head blight in wheat kernels using hyperspectral imaging. *Biosystems Engineering*, *131*, 65–76.

Barbedo, J. G. A., Tibola, C. S., & Lima, M. I. P. (2017). Deoxynivalenol screening in wheat kernels using hyperspectral imaging. *Biosystems Engineering*, *155*, 24–32.

Barnes, R. J., Dhanoa, M. S., & Lister, S. J. (1989). Standard normal variate transformation and de-trending of near-infrared diffuse reflectance spectra. *Applied Spectroscopy*, *43*, 772–777.

Barth, A. (2007). Infrared spectroscopy of proteins. *Biochimica et Biophysica Acta - Bioenergetics*, *1767*, 1073–1101.

Bellon-Maurel, V., Fernandez-Ahumada, E., Palagos, B., Roger, J. M., & McBratney, A. (2010). Critical review of chemometric indicators commonly used for assessing the quality of the prediction of soil attributes by NIR spectroscopy. *TrAC - Trends in Analytical ChemistryTrends in Analytical Chemistry*, *29*, 1073–1081.

Bezdek, J. C., Ehrlich, R., & Full, W. (1984). FCM: The fuzzy c-means clustering algorithm. *Computers & Geosciences*, *10*, 191–203.

Bianchini, A., & Bullerman, L. B. (2014). Mycotoxins: Classification. *Encyclopedia of Food Microbiology: Second Edition*, *2*, 854–861.

Boldrini, B., Kessler, W., Rebnera, K., & Kessler, R. W. (2012). Hyperspectral imaging: A review of best practice, performance and pitfalls for in-line and on-line applications. *Journal of Near Infrared Spectroscopy*, *20*, 483–508.

Bureau, S., Cozzolino, D., & Clark, C. J. (2019). Contributions of Fourier-transform mid infrared (FT-MIR) spectroscopy to the study of fruit and vegetables: A review. *Postharvest Biology and Technology*, *148*, 1–14.

Caporaso, N., Whitworth, M. B., & Fisk, I. D. (2017). Application of calibrations to hyperspectral images of food grains: example for wheat falling number. *Journal of Spectral Imaging*, *6*, 1–15.

Caporaso, N., Whitworth, M. B., & Fisk, I. D. (2018). Near-Infrared spectroscopy and hyperspectral imaging for non-destructive quality assessment of cereal grains. *Applied Spectroscopy Reviews*, *53*, 667–687.

Cavin, C., Cottenet, G., Blancpain, C., Bessaire, T., Frank, N., & Zbinden, P. (2016). Food adulteration: From vulnerability assessment to new analytical solutions. *Chimia*, *70*, 329–333.

Cen, H., & He, Y. (2007). Theory and application of near infrared reflectance spectroscopy in determination of food quality. *Trends in Food Science and Technology*, *18*, 72–83.

Chakraborty, S., & Newton, A. C. (2011). Climate change, plant diseases and food security: An overview. *Plant Pathology*, *60*, 2–14.

Chavez, P. F., De Bleye, C., Sacré, P.-Y., Rozet, E., Hubert, P., & Ziemons, E. (2013). Validation methodologies of near infrared spectroscopy methods in pharmaceutical applications. *European Pharmaceutical Review*, *18*, 3–6.

Chen, J., Ye, F., & Zhao, G. (2017). Rapid determination of farinograph parameters of wheat flour using data fusion and a forward interval variable selection algorithm. *Analytical Methods*, *9*, 6341–6348.

Chu, X., Wang, W., Ni, X., Li, C., & Li, Y. (2020). Classifying maize kernels naturally infected by fungi using near-infrared hyperspectral imaging. *Infrared Physics and Technology*, *105*, 103242.

Chu, X., Wang, W., Yoon, S. C., Ni, X., & Heitschmidt, G. W. (2017). Detection of aflatoxin B1 (AFB1) in individual maize kernels using short wave infrared (SWIR) hyperspectral imaging. *Biosystems Engineering*, *157*, 13–23.

Da Conceição, R. R. P., Simeone, M. L. F., Queiroz, V. A. V., de Medeiros, E. P., de Araújo, J. B., Coutinho, W. M., … de Resende Stoianoff, M. A. (2021). Application of near-infrared hyperspectral (NIR) images combined with multivariate image analysis in the differentiation of two mycotoxicogenic

Fusarium species associated with maize. *Food Chemistry*, *344*, 128615.

Dale, L. M., Thewis, A., Boudry, C., Rotar, I., Dardenne, P., Baeten, V., & Pierna, J. A. F. (2013). Hyperspectral imaging applications in agriculture and agro-food product quality and safety control: A review. *Applied Spectroscopy Reviews*, *48*, 142–159.

Dale, L. M., Thewis, A., Rotar, I., Pierna, J. A. F., Boudry, C., Vidican, R. M., & Baeten, V. (2012). Chemometric Tools for NIRS and NIR Hyperspectral Imaging. *Bulletin UASVM Agriculture*, *69*, 70–76.

De Girolamo, A., Cervellieri, S., Cortese, M., Porricelli, A. C. R., Pascale, M., Longobardi, F., … Lippolis, V. (2019). Fourier transform near-infrared and mid-infrared spectroscopy as efficient tools for rapid screening of deoxynivalenol contamination in wheat bran. *Journal of the Science of Food and Agriculture*, *99*, 1946–1953.

Del Fiore, A., Reverberi, M., Ricelli, A., Pinzari, F., Serranti, S., Fabbri, A. A., … Fanelli, C. (2010). Early detection of toxigenic fungi on maize by hyperspectral imaging analysis. *International Journal of Food Microbiology*, *144*, 64–71.

Delwiche, S. R. (2006). Improvements in optical sorting of mold-damaged wheat. *Optics for Natural Resources, Agriculture, and Foods*, *6381*, 1–8.

Delwiche, S. R. (2007). Optical characterization of free-falling mold-damaged wheat kernels. *Optics for Natural Resources, Agriculture, and Foods II*, *6761*, 67610G.

Delwiche, S. R. (2008). High-speed bichromatic inspection of wheat kernels for mold and color class using high-power pulsed LEDs. *Sensing and Instrumentation for Food Quality and Safety*, *2*, 103–110.

Delwiche, S. R., & Kim, M. S. (2000). Hyperspectral imaging for detection of scab in wheat. *Biological Quality and Precision Agriculture II*, *4203*, 13–20.

Delwiche, S. R., Kim, M. S., & Dong, Y. (2010). Damage and quality assessment in wheat by NIR hyperspectral imaging. *Sensing for Agriculture and Food Quality and Safety II*, *7676*, 1–8.

Delwiche, S. R., Kim, M. S., & Dong, Y. (2011). *Fusarium* damage assessment in wheat kernels by Vis/NIR hyperspectral imaging. *Sensing and Instrumentation for Food Quality and Safety*, *5*, 63–71.

Delwiche, S. R., Qin, J., Chao, K., Chan, D., Cho, B., & Kim, M. (2017). Line-scan hyperspectral imaging techniques for food safety and quality applications. *Applied Sciences*, *7*, 125.

Delwiche, S. R., Rodriguez, I. T., Rausch, S. R., & Graybosch, R. A. (2019). Estimating percentages of *Fusarium*-damaged kernels in hard wheat by near-infrared hyperspectral imaging. *Journal of Cereal Science*, *87*, 18–24.

Dowell, F. E., Ram, M. S., & Seitz, L. M. (1999). Predicting scab, vomitoxin, and ergosterol in single wheat kernels using near-infrared spectroscopy. *Cereal Chemistry*, *76*, 573–576.

ElMasry, G., Kamruzzaman, M., Sun, D., & Allen, P. (2012). Principles and applications of hyperspectral imaging in quality evaluation of agro-food products: a review. *Critical Reviews in Food Science and Nutrition*, *52*, 999–1023.

ElMasry, G., & Sun, D. W. (2010). Principles of hyperspectral imaging technology. *Hyperspectral Imaging for Food Quality Analysis and Control*, 3–43.

Esbensen, K. H., Guyot, D., Westad, F., & Houmoller, L. P. (2002). *Multivariate data analysis-in practice: an introduction to multivariate data analysis and experimental design*. CAMO.

Escrivá, L., Font, G., & Manyes, L. (2015). In vivo toxicity studies of *Fusarium* mycotoxins in the last decade: A review. *Food and Chemical Toxicology*, *78*, 185–206.

Esteki, M., Shahsavari, Z., & Simal-Gandara, J. (2018). Use of spectroscopic methods in combination with linear discriminant analysis for authentication of food products. *Food Control*, *91*, 100–112.

European Commission. (2006a). Commission Regulation (EC) Nº 1881/2006 of 19 December 2006. Setting maximum levels for certain contaminants in foodstuffs. *Official Journal of the European Communities*, *364*, 5–24.

European Commission. (2006b). Commission regulation (EC) Nº 401/2006 of 23 February 2006. Laying down the methods of sampling and analysis for the official control of the levels of mycotoxins in foodstuffs. *Official Journal of the European Union*, *70*, 12–34.

European Food Safety Authority. (2013). Deoxynivalenol in food and feed: occurrence and exposure. *EFSA Journal*, *11*, 3379.

Fernández, K., & Agosin, E. (2007). Quantitative analysis of red wine tannins using Fourier-Transform Mid-Infrared spectrometry. *Journal of Agricultural and Food Chemistry*, *55*, 7294–7300.

Foroud, N. A., Baines, D., Gagkaeva, T. Y., Thakor, N., Badea, A., Steiner, B., … Bürstmayr, H. (2019). Trichothecenes in cereal grains - An update. *Toxins*, *11*, 634.

Fox, G., & Manley, M. (2014). Applications of single kernel conventional and hyperspectral imaging near infrared spectroscopy in cereals. *Journal of the Science of Food and Agriculture*, *94*, 174–179.

Fox, G., Onley-Watson, K., & Osman, A. (2002). Multiple linear regression calibrations for barley and malt protein based on the spectra of hordein. *Journal of the Institute of Brewing*, *108*, 155–159.

Gatius, F., Lloveras, J., Ferran, J., & Puy, J. (2004). Prediction of crude protein and classification of the growth stage of wheat plant samples from NIR spectra. *Journal of Agricultural Science*, *142*, 517–524.

Givens, D. I., De Boever, J. L., & Deaville, E. R. (2005). The principles, practices and some future applications of near infrared spectroscopy for predicting the nutritive value of foods for animals and humans. *Nutrition Research Reviews*, *10*, 83.

Gruna, R., Vieth, K. U., Michelsburg, M., & Puente-León, F. (2010). Hyperspectral imaging - from laboratory to in-line food sorting. *International Workshop on Image Analysis in Agriculture, 2*, 79–90.

Gupta, N. (2011). Development of staring hyperspectral imagers. *Applied Imagery Pattern Recognition Workshop*, 1–8.

Hell, J., Prückler, M., Danner, L., Henniges, U., Apprich, S., Rosenau, T., … Böhmdorfer, S. (2016). A comparison between near-infrared (NIR) and mid-infrared (ATR-FTIR) spectroscopy for the multivariate determination of compositional properties in wheat bran samples. *Food Control*, *60*, 365–369.

Huang, H., Liu, L., & Ngadi, M. O. (2014). Recent developments in hyperspectral imaging for assessment of food quality and safety. *Sensors (Switzerland)*, *14*, 7248–7276.

Hubert, M., & Van Driessen, K. (2004). Fast and robust discriminant analysis. *Computational Statistics and Data Analysis*, *45*, 301–320.

International Agency for Research on Cancer (IARC). (2012). Mycotoxins and human health. *IARC Scientific Publications*, *158*, 87–104.

Janse, J. D., & Obradovic, A. (2015). Società Italiana di Patologia Vegetale (SIPaV). *Journal of Plant Pathology*, *80*, 85–103.

Jiang, L., Zhu, B., & Tao, Y. (2010). Hyperspectral image classification methods. *Hyperspectral Imaging for Food Quality Analysis and Control*, 79–98.

Karuppiah, K., Senthilkumar, T., Jayas, D. S., & White, N. D. G. (2016). Detection of fungal infection in five different pulses using near-infrared hyperspectral

imaging. *Journal of Stored Products Research*, *65*, 13–18.

Kharayat, B. S., & Singh, Y. (2018). *Mycotoxins in Foods: Mycotoxicoses, Detection, and Management*. *Microbial Contamination and Food Degradation*, 395-421.

Kim, Y., Himmelsbach, D. S., & Kays, S. E. (2007). ATR-Fourier Transform Mid-Infrared Spectroscopy for determination of trans fatty acids in ground cereal products without oil extraction. *Journal of Agricultural and Food Chemistry*, *55*, 4327–4333.

Kimura, M., Tokai, T., Takahashi-Ando, N., Ohsato, S., & Fujimura, M. (2007). Molecular and genetic studies of *Fusarium* trichothecene biosynthesis: Pathways, genes, and evolution. *Bioscience, Biotechnology and Biochemistry*, *71*, 2105–2123.

Knutsen, H. K., Alexander, J., Barregård, L., Bignami, M., Brüschweiler, B., Ceccatelli, S., … Edler, L. (2017). Risks to human and animal health related to the presence of deoxynivalenol and its acetylated and modified forms in food and feed. *EFSA Journal*, *15*, 4718.

Kos, G., Lohninger, H., & Krska, R. (2001). Using mid-infrared Fourier-Transform-Spectroscopy with attenuated total reflection (FT-IR/ATR) as a tool for the determination of *Fusarium graminearum* on maize. *Mycotoxin Research*, *17*, 102–106.

Kos, G., Lohninger, H., & Krska, R. (2002). Fourier transform mid-infrared spectroscopy with attenuated total reflection (FT-IR/ATR) as a tool for the detection of *Fusarium* fungi on maize. *Vibrational Spectroscopy*, *29*, 115–119.

Kos, G., Lohninger, H., & Krska, R. (2003). Development of a method for the determination of *Fusarium* fungi on corn using Mid-Infrared spectroscopy with Attenuated Total Reflection and chemometrics. *Analytical Chemistry*, *75*, 1211–1217.

Kos, G., Sieger, M., McMullin, D., Zahradnik, C., Sulyok, M., Öner, T., … Krska,

R. (2016). A novel chemometric classification for FTIR spectra of mycotoxin-contaminated maize and peanuts at regulatory limits. *Food Additives and Contaminants - Part A Chemistry, Analysis, Control, Exposure and Risk Assessment*, *33*, 1596–1607.

Kotal, F., Holadová, K., Hajšlová, J., Poustka, J., & Radová, Z. (1999). Determination of trichothecenes in cereals. *Journal of Chromatography A*, *830*(1), 219–225.

Kumar, N., Bansal, A., Sarma, G. S., & Rawal, R. K. (2014). Chemometrics tools used in analytical chemistry: an overview. *Talanta*, *123*, 186–199.

Lattanzio, V. M. T., Solfrizzo, M., & Visconti, A. (2008). Determination of trichothecenes in cereals and cereal-based products by liquid chromatography–tandem mass spectrometry. *Food Additives & Contaminants: Part A*, *25*, 320–330.

Levasseur-Garcia, C. (2018). Updated overview of infrared spectroscopy methods for detecting mycotoxins on cereals (corn, wheat, and barley). *Toxins*, *10*, 38.

Li, X., Li, R., Wang, M., Liu, Y., Zhang, B., & Zhou, J. (2018). Hyperspectral imaging and their applications in the nondestructive quality assessment of fruits and vegetables. *Hyperspectral Imaging in Agriculture, Food and Environment*, 27-63.

Liang, K., Huang, J., He, R., Wang, Q., Chai, Y., & Shen, M. (2020). Comparison of Vis-NIR and SWIR hyperspectral imaging for the non-destructive detection of DON levels in Fusarium head blight wheat kernels and wheat flour. *Infrared Physics & Technology*, *106*, 103281.

Liang, K., Liu, Q. X., Xu, J. H., Wang, Y. Q., Okinda, C. S., & Shena, M. X. (2018). Determination and visualization of different levels of deoxynivalenol in bulk wheat kernels by hyperspectral imaging. *Journal of Applied Spectroscopy*, *85*,

953–961.

Liu, J. J., Cai, Z., Liao, Y., Zhao, L., Moulin, J., & Hartmann, C. (2019). Validation of a laser based in-line aflatoxin sorting technology in Spanish type raw peanut in factory-scale production conditions. *Journal of Food Safety*, *39*, 1–11.

Lu, Y., Saeys, W., Kim, M., Peng, Y., & Lu, R. (2020). Hyperspectral imaging technology for quality and safety evaluation of horticultural products: A review and celebration of the past 20-year progress. *Postharvest Biology and Technology*, *170*, 111318.

Manley, M. (2014). Near-infrared spectroscopy and hyperspectral imaging: Non-destructive analysis of biological materials. *Chemical Society Reviews*, *43*, 8200–8214.

Martens, H., Nielsen, J. P., & Engelsen, S. B. (2003). Light scattering and light absorbance separated by extended multiplicative signal correction. Application to near-infrared transmission analysis of powder mixtures. *Analytical Chemistry*, *75*, 394–404.

McCormick, S. P., Stanley, A. M., Stover, N. A., & Alexander, N. J. (2011). Trichothecenes: From simple to complex mycotoxins. *Toxins*, *3*, 802–814.

McMullin, D., Mizaikoff, B., & Krska, R. (2015). Advancements in IR spectroscopic approaches for the determination of fungal derived contaminations in food crops. *Analytical and Bioanalytical Chemistry*, *407*, 653–660.

Mehmood, T., Liland, K. H., Snipen, L., & Sæbø, S. (2012). A review of variable selection methods in Partial Least Squares Regression. *Chemometrics and Intelligent Laboratory Systems*, *118*, 62–69.

Milosevic, M. (2004). Internal Reflection and ATR Spectroscopy. *Applied Spectroscopy Reviews*, *39*, 365–384.

Mishra, S., Srivastava, S., Dewangan, J., Divakar, A., & Kumar Rath, S. (2020). Global occurrence of deoxynivalenol in food commodities and exposure risk assessment in humans in the last decade: a survey. *Critical Reviews in Food Science and Nutrition*, *60*, 1346–1374.

Næs, T., & Martens, H. (2005). Principal component regression in NIR analysis: viewpoints, background details and selection of components. *Journal of Chemometrics*, *2*, 155–167.

Nelson, P. E., Dignani, M. C., & Anaissie, E. J. (1994). Taxonomy, biology, and clinical aspects of *Fusarium* species. *Clinical Microbiology Reviews*, *7*, 479–504.

Ngadi, M. O., & Liu, L. (2010). Hyperspectral Image Processing Techniques. In *Hyperspectral Imaging for Food Quality Analysis and Control*, 99–127.

Öner, T., Thiam, P., Kos, G., Krska, R., Schwenker, F., & Mizaikoff, B. (2019). Machine learning algorithms for the automated classification of contaminated maize at regulatory limits via infrared attenuated total reflection spectroscopy. *World Mycotoxin Journal*, *12*, 113–122.

Osborne, L. E., & Stein, J. M. (2007). Epidemiology of Fusarium head blight on small-grain cereals. *International Journal of Food Microbiology*, *119*, 103–108.

Pascari, X., Rodriguez-Carrasco, Y., Juan, C., Mañes, J., Marin, S., Ramos, A. J., & Sanchis, V. (2019). Transfer of *Fusarium* mycotoxins from malt to boiled wort. *Food Chemistry*, *278*, 700–710.

Pasquini, C. (2003). Near infrared spectroscopy: Fundamentals, practical aspects and analytical applications. *Journal of the Brazilian Chemical Society*, *14*, 198–219.

Patriarca, A., & Fernández Pinto, V. (2017). Prevalence of mycotoxins in foods and decontamination. *Current Opinion in Food Science*, *14*, 50–60.

Patz, C. D., Blieke, A., Ristow, R., & Dietrich, H. (2004). Application of FT-MIR

spectrometry in wine analysis. *Analytica Chimica Acta*, *513*, 81–89.

Peiris, K. H. S., Pumphrey, M. O., & Dowell, F. E. (2009). NIR Absorbance characteristics of deoxynivalenol and of sound and *Fusarium*-damaged wheat kernels. *Journal of Near Infrared Spectroscopy*, *17*, 213–221.

Peiris, K. H. S., Bockus, W. W., & Dowell, F. E. (2012). Infrared Spectral Properties of Germ, Pericarp, and Endosperm Sections of Sound Wheat Kernels and Those Damaged by *Fusarium graminearum*. *Applied Spectroscopy*, *66*, 1053–1060.

Pirgozliev, S. R., Edwards, S. G., Hare, M. C., & Jenkinson, P. (2003). Strategies for the control of Fusarium head blight in cereals. *European Journal of Plant Pathology*, *109*, 731–742.

Polder, G., Van Der Heijden, G. W. A. M., Waalwijk, C., & Young, I. T. (2005). Detection of *Fusarium* in single wheat kernels using spectral imaging. *Seed Science and Technology*, *33*, 655–668.

Porker, K., Zerner, M., & Cozzolino, D. (2017). Classification and authentication of barley (*Hordeum vulgare*) malt varieties: combining Attenuated Total Reflectance Mid-infrared spectroscopy with chemometrics. *Food Analytical Methods*, *10*, 675–682.

Qi, X., Jiang, J., Cui, X., & Yuan, D. (2019). Identification of fungi-contaminated peanuts using hyperspectral imaging technology and joint sparse representation model. *Journal of Food Science and Technology*, *56*, 3195–3204.

Qin, J. (2010). Hyperspectral Imaging Instruments. *Hyperspectral Imaging for Food Quality Analysis and Control*, 129–172.

Ramer, G., & Lendl, B. (2013). Attenuated Total Reflection Fourier Transform Infrared Spectroscopy. *Encyclopedia of Analytical Chemistry*.

Ramírez-Morales, I., Rivero, D., Fernández-Blanco, E., & Pazos, A. (2016).

Optimization of NIR calibration models for multiple processes in the sugar industry. *Chemometrics and Intelligent Laboratory Systems*, *159*, 45–57.

Ran, R., Wang, C., Han, Z., Wu, A., Zhang, D., & Shi, J. (2013). Determination of deoxynivalenol (DON) and its derivatives: Current status of analytical methods. *Food Control*, *34*, 138–148.

Rinnan, Å., Berg, F. van den, & Engelsen, S. B. (2009). Review of the most common pre-processing techniques for near-infrared spectra. *TrAC - Trends in Analytical Chemistry*, *28*, 1201–1222.

Rodríguez, S. D., Rolandelli, G., & Buera, M. P. (2019). Detection of quinoa flour adulteration by means of FT-MIR spectroscopy combined with chemometric methods. *Food Chemistry*, *274*, 392–401.

Ropelewska, E., & Zapotoczny, P. (2018). Classification of *Fusarium*-infected and healthy wheat kernels based on features from hyperspectral images and flatbed scanner images: a comparative analysis. *European Food Research and Technology*, *244*, 1453–1462.

Rosa, E., Arraché, S., Ramos, M., Fontes, V., Garda, J., & Badiale-furlong, E. (2018). Trichothecenes in wheat : Methodology, occurrence and human exposure risk, *82*, 129–137.

Savitzky, A., & Golay, M. J. E. (1964). Smoothing and differentiation of data by simplified least squares procedures. *Analytical Chemistry*, *36*, 1627–1639.

Sendin, K., Williams, P. J., & Manley, M. (2018). Near infrared hyperspectral imaging in quality and safety evaluation of cereals. *Critical Reviews in Food Science and Nutrition*, *58*, 575–590.

Senthilkumar, T., Jayas, D. S., White, N. D. G., Fields, P. G., & Gräfenhan, T. (2017). Detection of ochratoxin A contamination in stored wheat using near-infrared hyperspectral imaging. *Infrared Physics and Technology*, *81*, 228–235.

Senthilkumar, T., Jayas, D. S., White, N. D. G., Fields, P. G., & Gräfenhan, T. (2016). Detection of fungal infection and Ochratoxin A contamination in stored barley using near-infrared hyperspectral imaging. *Biosystems Engineering*, *147*, 162–173.

Serranti, S., Cesare, D., & Bonifazi, G. (2012). Hyperspectral-imaging-based techniques applied to wheat kernels characterization. *Sensing for Agriculture and Food Quality and Safety IV*, *8369*, 83690T.

Serranti, S., Cesare, D., & Bonifazi, G. (2013). The development of a hyperspectral imaging method for the detection of *Fusarium*-damaged, yellow berry and vitreous Italian durum wheat kernels. *Biosystems Engineering*, *115*, 20–30.

Shahin, M. A., & Symons, S. J. (2011). Detection of *Fusarium* damaged kernels in Canada Western Red Spring wheat using visible/near-infrared hyperspectral imaging and principal component analysis. *Computers and Electronics in Agriculture*, *75*, 107–112.

Shahin, M. A., & Symons, S. J. (2012). Detection of *Fusarium* damage in Canadian wheat using visible/near-infrared hyperspectral imaging. *Journal of Food Measurement & Characterization*, *6*, 3–11.

Shi, H., & Yu, P. (2017). Comparison of grating-based near-infrared (NIR) and Fourier transform mid-infrared (ATR-FT/MIR) spectroscopy based on spectral preprocessing and wavelength selection for the determination of crude protein and moisture content in wheat. *Food Control*, *82*, 57–65.

Sieger, M., Kos, G., Sulyok, M., Godejohann, M., Krska, R., & Mizaikoff, B. (2017). Portable infrared laser spectroscopy for on-site mycotoxin analysis. *Scientific Reports*, *7*, 44028.

Singh, C. B., Jayas, D. S., Paliwal, J., & White, N. D. G. (2012). Fungal damage detection in wheat using short-wave near-infrared hyperspectral and digital colour imaging. *International Journal of Food Properties*, *15*, 11–24.

Siripatrawan, U., & Makino, Y. (2015). Monitoring fungal growth on brown rice grains using rapid and non-destructive hyperspectral imaging. *International Journal of Food Microbiology*, *199*, 93–100.

Sobrova, P., Adam, V., Vasatkova, A., Beklova, M., Zeman, L., & Kizek, R. (2010). Deoxynivalenol and its toxicity. *Interdisciplinary Toxicology*, *3*, 94–99.

Su, W. H., Yang, C., Dong, Y., Johnson, R., Page, R., Szinyei, T., … Steffenson, B. J. (2021). Hyperspectral imaging and improved feature variable selection for automated determination of deoxynivalenol in various genetic lines of barley kernels for resistance screening. *Food Chemistry*, *343*, 128507.

Subramanian, A., & Rodriguez-Saona, L. (2009). Fourier Transform Infrared (FTIR) Spectroscopy. *Infrared Spectroscopy for Food Quality Analysis and Control*, 145–178.

Suchowilska, E., Kandler, W., Wiwart, M., & Krska, R. (2012). Fourier transform infrared - Attenuated total reflection for wheat grain. *International Agrophysics*, *26*, 207–210.

Sweeney, M. (1999). Molecular biology of mycotoxin biosynthesis. *FEMS Microbiology Letters*, *175*, 149–163.

Tang, H. (2012). Optimal wavelength selection algorithm of non-spherical particle size distribution based on the light extinction data. *Thermal Science*, *16*, 1353–1357.

Tatzer, P., Wolf, M., & Panner, T. (2005). Industrial application for inline material sorting using hyperspectral imaging in the NIR range. *Real-Time Imaging*, *11*, 99–107.

Tekle, S., Mage, I., Segtnan, V. H., & Bjornstad, A. (2015). Near-infrared hyperspectral imaging of *Fusarium*-damaged oats (*Avena sativa L.*). *Cereal Chemistry*, *92*, 73–80.

Tsai, F., & Philpot, W. (1998). Derivative analysis of hyperspectral data. *Remote Sensing of Environment*, *66*, 41–51.

Turner, N. W., Subrahmanyam, S., & Piletsky, S. A. (2009). Analytical methods for determination of mycotoxins: A review. *Analytica Chimica Acta*, *632*, 168–180.

Uoti, J. (1975). Occurrence and Pathogenicity of *Fusarium* Species in Cereals in Finland. *EPPO Bulletin*, *5*(4), 419–424. https://doi.org/10.1111/j.1365-2338.1975.tb02492.x

Vidal, A., Sanchis, V., Ramos, A. J., & Marín, S. (2016). The fate of deoxynivalenol through wheat processing to food products. *Current Opinion in Food Science*, *11*, 34–39.

Vigano, C., Ruysschaert, J. M., & Goormaghtigh, E. (2005). Sensor applications of attenuated total reflection infrared spectroscopy. *Talanta*, *65*, 1132–1142.

Viscarra Rossel, R. A. (2008). ParLeS: Software for chemometric analysis of spectroscopic data. *Chemometrics and Intelligent Laboratory Systems*, *90*, 72–83.

Wang, W., Lawrence, K. C., Ni, X., Yoon, S., Heitschmidt, G. W., & Feldner, P. (2015). Near-infrared hyperspectral imaging for detecting Aflatoxin B1 of maize kernels, *51*, 347–355.

Westad, F., Bevilacqua, M., & Marini, F. (2013). Regression. *Diagnostic Histopathology*, *28*, 127–170.

WHO. (2011). *Safety evaluation of certain contaminants in food*. *FAO food and nutrition paper*, 82, 778.

Williams, P., Manley, M., Fox, G., & Geladi, P. (2010). Indirect detection of *Fusarium verticillioides* in maize (*Zea mays L.*) kernels by near Infrared hyperspectral Imaging. *Journal of Near Infrared Spectroscopy*, *18*, 49–58.

Wu, Y., Peng, S., Xie, Q., Han, Q., Zhang, G., & Sun, H. (2019). An improved

weighted multiplicative scatter correction algorithm with the use of variable selection: application to near-infrared spectra. *Chemometrics and Intelligent Laboratory Systems*, *185*, 114–121.

Xiaobo, Z., Jiewen, Z., Povey, M. J. W., Holmes, M., & Hanpin, M. (2010). Variables selection methods in near-infrared spectroscopy. *Analytica Chimica Acta*, *667*, 14–32.

Xing, F., Yao, H., Liu, Y., Dai, X., Brown, R. L., & Bhatnagar, D. (2019). Recent developments and applications of hyperspectral imaging for rapid detection of mycotoxins and mycotoxigenic fungi in food products. *Critical Reviews in Food Science and Nutrition*, *59*, 173–180.

Yang, I. C., Delwiche, S. R., Chen, S., & Lo, Y.-M. M. (2009). Enhancement of Fusarium head blight detection in free-falling wheat kernels using a bichromatic pulsed LED design. *Optical Engineering*, *48*, 023602.

Yang, X., Hong, H., You, Z., & Cheng, F. (2015). Spectral and image integrated analysis of hyperspectral data for waxy corn seed variety classification. *Sensors (Switzerland)*, *15*, 15578–15594.

Yao, H., Hruska, Z., Kincaid, R., Brown, R., Cleveland, T., & Bhatnagar, D. (2010). Correlation and classification of single kernel fluorescence hyperspectral data with aflatoxin concentration in corn kernels inoculated with *Aspergillus flavus* spores. *Food Additives and Contaminants - Part A Chemistry, Analysis, Control, Exposure and Risk Assessment*, *27*, 701–709.

Yao, H., Hruska, Z., Kincaid, R., Brown, R. L., Bhatnagar, D., & Cleveland, T. E. (2013). Detecting maize inoculated with toxigenic and atoxigenic fungal strains with fluorescence hyperspectral imagery. *Biosystems Engineering*, *115*, 125–135.

Zhang, H., Paliwal, J., Jayas, D. S., & White, N. D. G. (2007). Classification of fungal infected wheat kernels using near-infrared reflectance hyperspectral

imaging and support vector machine. *Transactions of the ASABE*, *50*, 1779–1785.

Zhang, J. B., Wang, J. H., Gong, A. D., Chen, F. F., Song, B., Li, X., … Liao, Y. C. (2013). Natural occurrence of Fusarium head blight, mycotoxins and mycotoxin-producing isolates of *Fusarium* in commercial fields of wheat in Hubei. *Plant Pathology*, *62*, 92–102.

Zhongzhi, H., & Limiao, D. (2018). Application driven key wavelengths mining method for aflatoxin detection using hyperspectral data. *Computers and Electronics in Agriculture*, *153*, 248–255.

Chapter 2. Objectives

The present thesis general objective was to manage *Fusarium* and deoxynivalenol (DON) contamination in wheat using novel technologies based on spectroscopic techniques. We focused our attention on HSI-NIR and FTIR technologies.

The study was divided into diverse sub-sections to achieve the main objective:

- Standardization of HSI-NIR to analyse wheat entire samples and calibration of prediction and discrimination models to detect fungal presence and DON (Chapter 4 and 5).
- Standardization of HSI-NIR to analyse wheat individual kernels and calibration of prediction and discrimination models to detect *Fusarium* damaged kernels (FDK) and DON (Chapter 6 and 7).
- Determination of the most suitable solvent to extract maize samples compounds for the subsequent analysis of DON by FTIR (Chapter 8).

Chapter 3. Global methodology

3.1. Experimental design

The global methodology of the study was divided into two main parts: (i) calibrating predictive and discrimination models for fungal infection and DON quantification and classification in wheat samples with HSI-NIR; (ii) calibrating discrimination models for fungal damage identification and quantification and classification models to discern wheat kernels according to DON levels (Figure 6). Both studies were performed after the standardization of the HSI-NIR, obtaining the optimal lighting, scanning, ROI selection and pre-processing for

Figure 6. Global methodology design.

subsequent models calibration. Additional work (iii), determining the most suitable solvent for DON extraction from maize for the subsequent FTIR analysis, was also included in the experimental design (Figure 7).

3.2. HSI-NIR analysis

Before modelling HSI data, imaging parameters were set, ensuring a subsequent quality analysis. The Pika NIR-320 camera, assembled in RESONON Inc. (Bozeman, MA, USA), was placed 220 mm above the sampling stage and the illumination unit 70 mm. The spectral resolution was 4.9 nm (164 spectral bands from 895 to 1731 nm), with 320-pixel spatial resolution. The camera height chosen had an exploring area of 90 mm vertically. The horizontal dimension corresponded to the selected scanning bands (pixel lines) from the software, which can be extended or reduced depending on the sample size. The framerate was established at 520 fps, and the exposure time was determined before each analysis, avoiding saturated pixels on the images. Also, black and white images were captured before samples scanning. The settings and the scans were adjusted and processed using Spectronon PRO software benchtop.

3.2.1. Wheat bulk samples analysis

A total of 270 naturally contaminated wheat samples were supplied by a feed-producing agricultural cooperative, during 2018–2019. Bulk sample analysis was performed first for the standardization of the HSI system, using 7 g of wheat for each sample and then for fungal infection and DON models, using 14 g and dividing the sample into two equal parts for each reference analysis, respectively. Briefly, the scans were performed in triplicate, mixing the kernels between each one to ensure the maximum sample representation possible. Similar pixel reflectances were selected by Euclidian distance, removing the background. The mean spectra of all the grains composing the sample were exported and considered the ROI for the subsequent spectral processing.

3.2.2. Single wheat kernel analysis

In total, 50 kernels for the standardization and 300 for model calibration were used, selecting them from DON contaminated samples. In single kernel analysis, the ROI changed, providing the mean spectra from the pixels of a wheat grain. The scans were also performed by triplicate, ensuring the adequate selection of the region delimiting the kernel. The 50 wheat kernels were scanned for both positions (crease-up and crease-down) to determine the influence of the different parts on the spectral analysis. The kernel position influence was also tested. The mean raw spectrum and 1stD spectral data for each grain were exported to an excel file, using the Spectronon PRO software for the subsequent spectral processing.

3.2.3. Reference method analysis

3.2.3.1. Visual inspection

The kernels used for the experimental study were manually selected and divided into three levels (symptomatic, mildly-symptomatic and asymptomatic) according to visual symptoms of fungal infection. Discoloured, shrivelled and wrinkled kernels were considered symptomatic (S). Kernels with part of these symptoms were categorized as mildly symptomatic (M), and kernels with no visible signs as asymptomatic (A). The kernels were selected trying to cover, as wide as possible, all the damage visual features. Consequently, the percentage of kernels with symptoms visually perceived in our sample set was higher than in the original sample.

3.2.3.2. Ergosterol HPLC analysis

Concisely, 7 g of previously ground wheat was extracted with a solid-liquid phase extraction, using 40 mL of methanol and 10 mL of hexane. The solution needed 2 g of KOH for a better extraction. Temperature and stirring were applied to the solution, placing it into a bath at 55–60 °C for 20 min. Then, ergosterol was

extracted with three liquid-liquid phase extractions, adding 2 mL of bi-distilled water (to cool the solution) and 2 mL of hexane. The upper layer corresponding to 6 mL of the hexane phase was recovered and evaporated with a low nitrogen steam at 40 °C. The resuspension of the extract in 1 mL of methanol was injected into the analytical system, quantifying ergosterol concentrations, consisting of an HPLC coupled with a UV/Vis detector set at 282 nm with a LOD of 0.5 mg/kg.

3.2.3.3. DON HPLC analysis of wheat

For wheat samples, 7 g of the cereal were ground with a solid-liquid phase extraction, using Milli-Q water. The mixtures were stirred for 10 min and then centrifuged at 1780 × g. 5 mL of the filtered supernatant were passed through IAC, retaining DON and obtaining pure extracts in methanol. These were evaporated and resuspended into the mobile phase before injecting them into the analytical system, which consisted of an Ultra-High-Performance Liquid Chromatography coupled to a DAD detector (UHPLC-DAD) with a LOD of 50 μg/kg.

For single kernel analysis, the grains were ground with a mortar and pestle and mixed with 0.3 mL of Milli-Q water and vortexed for 10 min. The supernatant was obtained by centrifugation before filtering it. The extract was directly injected into the same analytical system used for wheat samples.

3.2.4. Statistical analysis

The results obtained are in the international system units. The spectral and reference data was imported to Office Excel 2016 software to handle spectral data obtained from the Spectronon Pro software. The Excel files were imported to The Unscrambler 7.6 and JMP PRO 14 software for data processing, employing the first for spectral pre-processing and predictive models calibration and the second for classification models calibration. The prediction models performance was

determined using the parameters RMSEP, R^2, RPD, and slope, and the classification models by the percentage of accuracy in the discrimination.

3.3. FTIR analysis

The extractions were done on naturally-contaminated and inoculated with *F. graminearum*, *F. verticillioides* or *F. culmorum* ground samples. First, DON was extracted from samples, using four different solvents: Water (100), Methanol:Water (70:30), Acetonitrile:Water (70:30), and Ethanol:Water (70:30). Two new solvents (Methanol:Water (30:70) and Methanol (100)) were tested, after evaluating the performance of the methanol-water mixtures, following the same extraction procedure as for the previously solvents used. DON was extracted from 200 mg of powder, using 0.8 mL of all the previously solvents

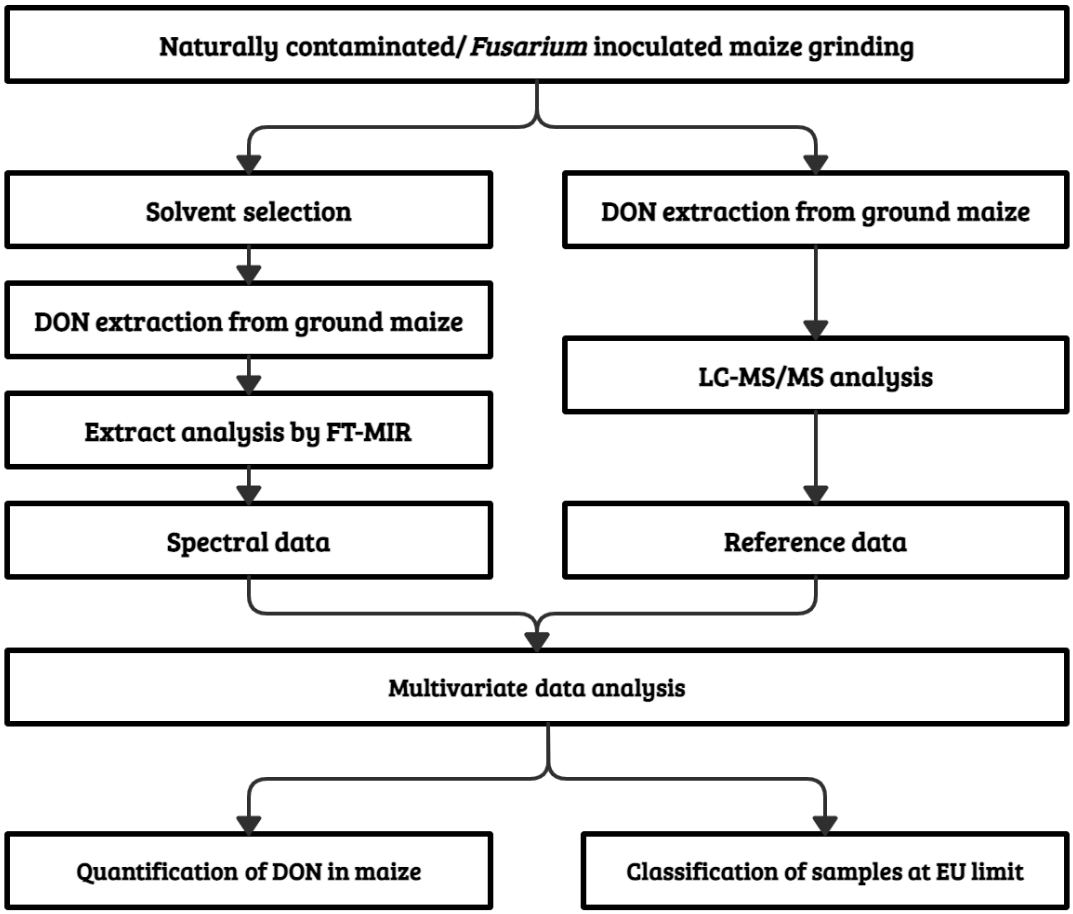

Figure 7. Methodology design for FTIR trials.

selected. The solid-liquid mixtures were shaken for 30 minutes at 70 rpm and then centrifugated twice for 2 minutes at 5800 rpm, obtaining the liquid phase in each step.

The spectroscopic equipment used was an FTIR spectrometer ALPHA II with the platinum ATR unit equipped with the one reflection – diamond crystal as an ATR element. The spectrometer was controlled by Opus 8.1. software, setting the scans at 2 cm^{-1} resolution and the MIR region between 2500-25000 nm. An aliquot of each extraction solution (10 µl) was poured on the ATR crystal, covering it completely for the spectroscopic analysis. Enough time was allowed for solvents to evaporate before analysing. Once the solvent reached the complete evaporation, the thin film formed on the ATR crystal containing the extracted compounds was analysed three times by FTIR spectroscopy, cleaning the crystal with isopropanol between samples and registering subsequent backgrounds to avoid atmospheric effects.

3.3.1. Reference method analysis (LC-MS/MS)

The reference method used for DON analysis was LC-MS/MS with a QTrap 550 LC-MS/MS System equipped with TurboIonSpray electrospray ionization (ESI) source and 1290 Series HPLC Systems. Before, 5 g of homogenized samples were extracted with 20 ml of extraction solvent (acetonitrile/water/acetic acid 79:20:1, v/v/v), shaking the mixture for 90 min. The extracts were injected after a 1 + 1 (v/v) dilution using dilution extraction solvent. The LODs for DON were 1.2 µg/kg.

3.3.2. Statistical analysis

An unsupervised analysis was done by PCA to determine the different patterns in clustering formation depending on the solvent used. Once determined the most suitable solvents, supervised models based on cross-validated Sparse Partial Least Squares – Discriminant Analysis (SPLS-DA) were calibrated to

determine the classification power of FTIR according to the DON regulatory standard in maize (1750 μg/kg). Additionally, SPLS-DA scores were projected to determine the influence of the type of inoculation and fungal species used on the classification accuracy. Also, correlation plots were represented to associate the high influence spectral variables on the model with the matrix compound variations during fungal infection and DON production.

Chapter 4. Standardisation of near-infrared hyperspectral imaging for quantification and classification of DON contaminated wheat samples

Antoni Femenias, Ferran Gatius, Antonio J. Ramos, Vicente Sanchis, & Sonia Marín

Food Control 111 (2020) 107074

4.1. Abstract

HSI-NIR is considered a promising technique able to replace time-consuming, costly and destructive classic methods to predict and classify DON contaminated wheat kernels or samples by their concentration and level of contamination, respectively. The main objective of the present study was to standardise the HSI-NIR image acquisition method in naturally contaminated whole wheat kernels to obtain a high accuracy method to quantify and classify samples according to DON levels. Wheat samples were analysed by HPLC as the reference method, determining their DON levels. Hyperspectral images of single kernels and entire wheat samples were obtained, processing the spectra by the multivariate analysis software. The initial work revealed that HSI-NIR could overcome kernel orientation, position and pixel selection. The subsequent developed PLS prediction achieved an RMSEP of 405 μg/kg and 1174 μg/kg for a cross-validated model and an independent set validated model, respectively. Moreover, the classification accuracy obtained by LDA was 62.7% for two categories depending on the UE maximum level (1250 μg/kg). Although the results are not accurate enough for DON quantification and sample classification, they can be considered a starting point for further improved protocols for DON management.

Keywords: Hyperspectral imaging; Deoxynivalenol; Near infrared; Cereal sorting: Contamination prediction.

4.2. Introduction

DON is a *Fusarium* produced mycotoxin causing increasing concern due to its prevalence in wheat. European diet relies on wheat derivatives consumption, increasing the exposure to DON significantly (Cano-Sancho et al., 2011). There is a highly seasonal variation in *Fusarium* mycotoxins in wheat. Thus, the agronomic factors should be considered to minimise *Fusarium* mycotoxin levels in harvested cereals. *F. graminearum*, a major DON producer, invades the spikelets, causing kernel damage in the form of shrivelling appearance, loss of weight, and discolouration that results in a white or pink appearance (Delwiche et al., 2010). Although different preharvest strategies have been used, minimizing DON presence in wheat, the problem remains (Edwards & Jennings, 2018). Moreover, DON is not removed during food processing steps (Vidal et al., 2016). Consequently, monitoring wheat batches is a key point before entering the food chain to avoid highly contaminated batches.

Several laboratory methods are available to detect and measure DON in cereal grains, including HPLC, MS, and ELISA. However, these methods are not suitable for rapid detection at the entry in food industries. At the moment, companies that monitor entering batches use lateral flow devices (LFD) to rapidly screen, although they have limited accuracy. To date, there exists a high interest to apply spectroscopic techniques to identify DON contaminated samples. Spectroscopic detection techniques are already widely used in food and feed industries to determine organic compounds, like proteins, moisture, starch and pigments. The relatively low concentration range for DON makes it very challenging for NIR quantitative analysis.

As an alternative to measurement of DON, some NIR studies have relied on the positive, though the imperfect correlation between the visual appearance of *Fusarium* damage and DON (Delwiche et al., 2010). For the NIR region, the spectral absorption near 1200 nm, attributed to ergosterol, was used in spectral

recognition of *Fusarium* damage (Delwiche et al., 2011). In particular, FT-NIR and FTIR spectroscopy have been used to detect DON in 30 g (De Girolamo, Cervellieri, Visconti, & Pascale, 2014) and 25 g (Dvořáček, Prohasková, Chrpová, & Štočková, 2012) of wheat. It has allowed the classification of samples according to their level of contamination, although some studies used artificially-inoculated cereals, and, in some cases, milling procedures before spectroscopic measurements. The technology is based on interferometry, opposing the grating-based ones and producing better resolution and throughput.

HSI combined with spectroscopy represents a new non-destructive methodology. Its advantage is that it provides spectral information at each spatial pixel on a sample, thus ensuring higher analytical potential (Cen, Lu, Zhu, & Mendoza, 2016). The most common HSI methods use diffraction gratings based on the online acquisition of spectra. The push-broom method is the most widely spread within the market of HSI cameras. It consists of an online spatial line (x) and the entire lambda range acquisition. Only the 'y' dimension scanning should be performed over time. Studies applying HSI-NIR technology have been reviewed, detecting quality parameters in cereals (Caporaso et al., 2018), assessing *Fusarium* and DON in wheat kernels (Femenias, Gatius, Ramos, Sanchis, & Marín, 2020a) and detecting mycotoxins and mycotoxigenic fungi in food products (Xing et al., 2019).

HSI-NIR has been proposed by some authors to assess the FDK percentage and DON presence at given levels. Delwiche et al. (2010, 2011) studies used visual inspection as a reference method to classify 60-kernels samples by LDA according to FHB presence. Moreover, Shahin & Symons (2011, 2012) and Delwiche et al. (2019) also aimed to classify a high number of FDK by LDA and Partial Least Squares-Discriminant Analysis (PLS-DA). All these authors reduced the dimensionality of the data by characteristic wavelengths selection for FDK analysis. However, the symptomatology of kernels cannot be directly related to

DON presence because asymptomatic grains can contain DON and vice versa (Barbedo et al., 2015). The correlation between DON concentrations and *Fusarium* is higher for elevated DON levels than for low concentrations. Thus, some error is inevitable because, at low DON concentrations, typical *Fusarium* damage symptoms are not visually detectable. Moreover, at high DON contaminations, the correlation is higher, and, consequently, a higher percentage of damaged kernels can be observed (Beyer, Klix, & Verreet, 2007). Therefore, the HSI-NIR technique has been proposed to overcome visual symptoms disassociations with DON contamination.

Moreover, Barbedo et al. (2017) used a CM to classify DON contaminated kernels into three groups: below 500 μg/kg, between 500 and 1250 μg/kg and above 1250 μg/kg (legal EU limit); and Liang et al. (2018) developed a complex method based on SVM and PLS-DA to classify at three DON levels with mean values of < 250, 1162 and 2665 μg/kg.

The present article focuses on HSI-NIR methodology standardisation for wheat kernel scanning to have a precise method to screen samples for DON presence. Once standardised, it uses the protocol for DON levels quantification through PLS regression. Moreover, 150 naturally contaminated samples were scanned and classified according to the maximum limit in the EU (1250 μg/kg).

4.3. Materials and methods

4.3.1. Determination of DON concentration in wheat samples by Ultra-High-Performance Liquid Chromatography (UHPLC)

4.3.1.1. Reagents and chemicals

Water was obtained from a Milli-Q® SP Reagent system (Millipore Corp., Brussels, Belgium). Methanol and acetonitrile (HPLC grade) were purchased from Scharlab (Sentmenat, Spain). Mycotoxin standards of DON were bought to Romer Labs

(Tulln, Austria). Immunoaffinity columns (IAC) for DON (DONPREP®) were acquired from R-Biopharm (Rhone LTD Glasgow, UK).

4.3.1.2. Preparation of DON solutions

DON concentration in the stock solution was checked by UV spectroscopy, according to AOAC Official Methods of Analysis, Chapter 49 (AOAC, 2005), obtaining a concentration of the stock solution of 791 µg/mL. A 9.55 µg/mL DON standard was obtained, storing it at 4 °C. Calibration curves, prepared by diluting known volumes of the stock solution with the mobile phase, were used for DON quantification.

4.3.1.3. DON extraction in wheat

A total of 150 wheat samples, supplied by a feed producing agricultural cooperative from Lleida province, were used in the study. They were taken within its quality control programme from each incoming truck. The cooperative sent a subsample (200-500 g) from each homogenized sample to our laboratory.

DON was extracted from wheat samples with specific IAC (DONPREP®), following the manufacturer's instructions. The mycotoxin extraction followed a slightly modified version of the methodology used by Vidal, Sanchis, Ramos, & Marín (2018). Briefly, five grams of wheat previously ground with an IKA® A11 Basic mill (Darmstadt, Germany) were mixed with 30 mL of MiliQ water in a 250 mL Erlenmeyer flask, followed by 10 min stirring. Then, samples were 10 min centrifuged at 1780×g, the supernatant was filtered through a 9 cm diameter glass microfiber paper filter (Whatman™ GF/A, Maidstone, UK), and 5 mL of the filtrate passed through the IAC. The washed column with 10 mL of bi-distilled water was eluted with 3 mL of methanol HPLC grade (the first 1.5 mL performing back-flushing), recovering DON from the samples. The elution solvent was evaporated under a low nitrogen steam at 40 °C and resuspended in the mobile phase (acetonitrile:methanol:water, 5:5:90, v/v/v). Every resuspended extract was filtered through a nylon filter (0.4µm) before being injected into the UHPLC-DAD system.

4.3.1.4. UHPLC system

DON was quantified using an Agilent Technologies 1260 Infinity UHPLC system (California, USA) coupled with an Agilent 1260 Infinity II Diode Array Detector (DAD). The device used a Gemini® C18 column from Phenomenex 150×4.6 mm (California, USA) with a particle size of 5 μm and a pore size of 110 Å. The absorption wavelength for DON was 220 nm. The mobile phase was composed of methanol:acetonitrile:water (5:5:90, v/v/v) and set at a flow rate of 1 mL/min. The column temperature was 40 °C, the injection volume was 50 μL, and the total run time was 15 min for mycotoxin analyses. The performance of the quantification method of DON in wheat was published by Vidal et al. (2018), considering the limit of detection (LOD) to be three times the signal of the blank (50 μg/kg).

4.3.2. HSI-NIR experimental work

4.3.2.1. Instrumentation and data acquisition by HSI-NIR

A push-broom HSI system, composed of a Pika NIR-320 camera assembled in RESONON Inc. (Bozeman, MA, USA), was used. The device consists of an InGaAs sensor line scan camera with a 320×256-pixel resolution, a 30×30 μm pixel size, and a 14-bit resolution A/D spectrograph (Goldeye G-008 SWIR TEC1, Allied Vision Technologies GmbH, Germany). The spectral resolution is 4.9 nm (164 spectral bands from 895 to 1700 nm), with 320 pixels of spatial resolution and a frame rate of 520 fps. The objective lens has 25 mm of focal length (F/1.4 SWIR, 0.9-1.7 μm, 21mm image format, c-mount) and is positioned 220 mm above the image surface. The illumination unit was composed of a four halogen lamps lighting system with Lambertian filters fixed on an adjustable tower that is turned on at least 20 min before the image acquisition. The illumination system was supplied by Samplexpower® power converter (SEC-1223CE, Burnaby, BC, V5A 0C6, Canada), which provides a highly regulated output DC voltage of 13.8 Volts at 23 Amps with an AC input of 230 Volts, 50 Hz. Finally, a motorized linear

translation stage of 600 mm was also used, which permitted the scan of the entire sample having the optical systems fixed.

The software Spectronon PRO controlled the Resonon's benchtop for image processing. The intensity readings of each test sample data array were transformed automatically to reflectance by dividing the dark current-subtracted intensity by the dark current-subtracted white standard at each of the corresponding wavelengths (1). A dark current intensity image was collected before samples' scanning, removing the dark noise by covering the camera lens. Likewise, the intensity from a 99% reflectance standard, made of PTFE (Spectralon™, SRT-99-120, Labsphere, North Sutton, NH, USA) to correct illumination effects, was collected immediately after the dark image. Both images were applied subsequently to correct sample intensities.

$$I = \frac{I_0 - I_b}{I_w - I_b} \qquad (1)$$

where I_0 is the raw hyperspectral image obtained, I_w is the white reference and I_b is the dark current reference. Apart from the dark and absolute reflectance response, the pixel illumination saturation also was adjusted using the camera controls. The framerate and the integration time were fixed, avoiding saturated pixels on the image.

The work was divided into three parts, first establishing the pixel selection methodology, the kernel location and the repeatability. The results were obtained by acquiring images of 30 individual kernels (from uncontaminated samples), placed crease-down in a template as shown in Figure 8a. The mean spectrum was recorded individually for each grain. In the second part, kernel orientation and data pre-processing were evaluated, acquiring images of 30 individual kernels (from both contaminated and uncontaminated samples) placed crease-down in a template (Figure 8a).

The mean spectrum also was obtained individually for each grain. In the third part, for bulk sample analysis, approximately 7 g of wheat kernels were scanned without any specific template, as in Figure 8b, and the mean spectra were recorded from the entire images. In all parts, a black tray was used as background, reducing the noise on the scan and obtaining an accurate pixel selection. Images adjusted to 350 bands for the horizontal axis and approximately 90 mm for the vertical. The pixels were selected by collecting the mean reflectance's of similar spectrum pixels by Euclidian distance that is best adjusted to the ROI to remove the background signal. Mean spectra for each kernel and entire samples were recorded as a text file, exporting them later to the spectral analysis software.

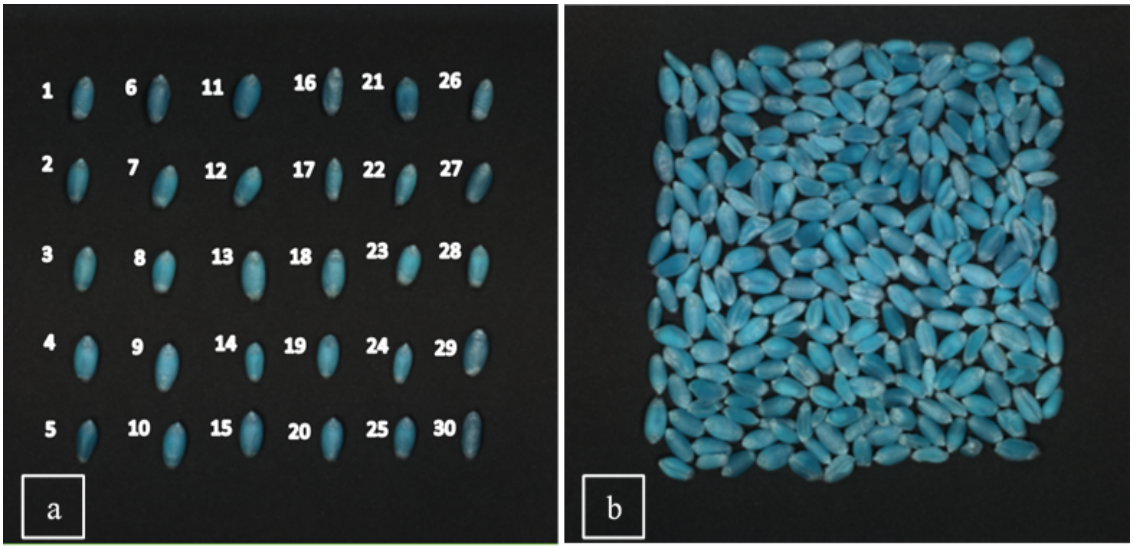

Figure 8. a) Hyperspectral image of 30 wheat kernels in crease-down orientation. b) Hyperspectral image of 7 g of wheat (approximately 200 kernels).

4.3.2.2. Hyperspectral data processing for preliminary work

Spectral data were processed using The Unscrambler software (version 7.6 SR1, CAMO, Oslo, Norway, 2001). For preliminary work, mean spectra from uncontaminated samples were projected by PCA without pre-processing the spectra. The purpose of PCA was to identify the variations between different sampling conditions by highlighting valuable information from the spectral data. First, the

same sample was selected in two modes, comparing by PCA the differences between the selection mode between restrictive (avoiding any pixels from the background) or permissive (extending the selection to all kernel pixels including some from the background). Second, PCA was also used to determine the influence of the kernel position on the scanning tray. For position effect evaluation, 30 crease-down kernels were located on different locations for each of the three images captured, as shown in Figure 9. Finally, the repeatability of the image acquisition was also evaluated by PCA, scanning 5 samples in 3 consecutive days (different calibrations of the equipment).

Figure 9. Evaluation of the differences between kernel position on the scanning tray.

4.3.2.3. Hyperspectral data processing for tests with DON-contaminated and uncontaminated samples

The spectral profile of the mean raw spectra of kernels from non-contaminated (<LOD), mildly-contaminated (1605.9 µg/kg) and highly contaminated (2682.8 µg/kg) samples was determined by a line plot representation of the reflectance spectra. Spectral pre-processing algorithms were evaluated, determining the best-fitted pre-treatment for the raw data obtained. First, the transformation of the reflectance data to absorbance spectra was introduced, using the spectroscopic transformation tool from The Unscrambler software. Second, baseline correction, which subtracted the lowest value from all the remaining values in the spectrum, was applied to both reflectance and absorbance spectra. Third, the algorithms were obtained by pre-processing both spectra with SNV. PCA was used to evaluate the best pre-treatment.

In addition, the kernel axis (crease up and down) orientation effect was determined by capturing images of both orientations of each kernel rotating on themselves. The differences in their spectra were estimated for DON contaminated and non-contaminated samples projecting PCA with the most suitable pre-treatment applied. The DON-effect and kernel orientation were compared by PCA, using grains from contaminated samples with 2190, 2682.8 and 2882 μg/kg paired in each case with grains from samples with DON concentrations below the LOD.

Moreover, kernels from DON-contaminated and uncontaminated samples were classified depending on the symptoms caused by *Fusarium* infection by a visual inspection (e.g. discolouration, wrinkles, wilting and dwarfing). Visually sound kernels were round, large and brownish. Contaminated and uncontaminated samples were scanned, pre-processing the resulting spectra with the best pre-treatment. The pre-processed spectra were modelled by PCA, evaluating the relationship between symptomatology and DON contamination.

4.3.3. Hyperspectral data processing for quantification and classification of bulk DON contaminated samples

Firstly, the within-sample repeatability was assessed by sampling for three times approximately 7 g of grain from the same, evaluating different kernels from the same sample. Grains arising from four samples considered contaminated (2681 μg/kg and 1770 μg/kg), mildly-contaminated (660 μg/kg), and uncontaminated (<LOD) were scanned in triplicate so that a total of 36 images and 12 mean spectra were acquired. The kernels were together in the image, finding some of them overlapped. The spectral processing was applied to the formerly selected spectral pre-treatment, followed by a PCA model.

The prediction model was built recording pixel mean reflectances of 7 g of wheat from 74 samples, covering the DON concentration range from <LOD to 2660.0 μg/kg as explanatory variables and DON concentration obtained by UHPLC as the

dependent variable. A total of 222 images were scanned (74 samples in triplicate), using them to develop a cross-validated model. The same samples were divided into two sets, the first with kernels arising from 24 samples (72 images) for the calibration set and the second with grains from 50 samples (150 images) for the validation set, shaking them between scans to distribute the kernels randomly to obtain major representativeness of the spectra. The spectral data came from the mean of all the pixels spectrum of a scanned grain. The triplicates were independently introduced (a total of 222 observations) in the multivariate analysis tool (The Unscrambler 7.6 SR1). A baseline correction offset (subtracting the minimum value to the entire spectrum) was applied to the absorbances obtained from reflectances transformation. PLS were constructed and refined to simplify the complexity, calibrating two prediction models. The first regression model used full cross-validation, which presented the best RMSECV as possible. The second one used the two sample sets to obtain the prediction performance with the RMSEP. The calibration set presented 22 from 220 spectra considered outliers for the cross-validated model, and the test set only three outliers. The criteria followed for outlier detection was to represent the influence plot and reject those spectra with higher leverage and residual Y-variance, removing less than 10% of the original data. The criteria used to select the number of PCs to optimize the models (for cross-validation and test set) was the PC number where the first minimum on the curve of the Root Mean Square Error (RMSE) occurs. Validation accuracy was determined using the performance parameters: slope, correlation, R^2, RMSEP and SEP.

The classification model was developed with the data in the validation set of the preceding PLS model, corresponding to 150 images from 50 samples at different concentrations. The scans were distributed into two groups, covering the broader range of concentrations possible. The JMP PRO 14.1.0 (SAS Institute Inc., 2018) software analysed the data by multivariate statistics. LDA modelled two or more classes, first by a dimensionality reduction step and a second classification stage. The limit established for the two classes separation was the EU legal limit for

DON (1250 μg/kg). From the 75 images used for the calibration and the 75 for the validation set, 47 corresponded to kernels arising from samples below 1250 μg/kg of DON (B) and 28 to grains from samples above the legal limit (C). The accuracies results were the percentage (%) of correctly classified images from the total (75).

4.4. Results

4.4.1. Preliminary work with uncontaminated samples

4.4.1.1. Image pre-processing: Kernel pixels' selection

The selection tool of the software was used for the segmentation of the kernels from the background, based on the similar spectra to the chosen pixel. The selection tool does not ensure that the same pixels are selected because it depends on the pixel chosen. Still, the recorded reflectances were quite similar when the pixels from the same kernel were selected twice, using 25 grains arising from the same sample placed crease-down and captured in a single image. The score plot of the PCA model showed that the differences among kernels were much broader than the error caused by the selection tool (Annexe, Figure 1).

Moreover, a score plot of the PCA model for the reflectance spectra of the previously used 25 kernels was obtained, selecting twice the ROI for each grain (the first spectra limited to the pixels located within the kernel and the second one including the whole kernel area and, consequently, some background). The differences among grains were broader than those due to the selection method, but still, the difference was considerable (Annexe, Figure 2). Consequently, the narrow selection was selected for the following steps.

4.4.1.2. Kernel location on the scanning tray

The PCA projection, obtained from the three images of 30 kernels crease-down placed on different locations on the plate (as explained in methodology), did not present considerable differences among the three repetitions of the same kernel, as is shown in the score plot in Figure 10. It means that radiation reached kernels equally regardless of their location on the tray and was reflected and measured similarly.

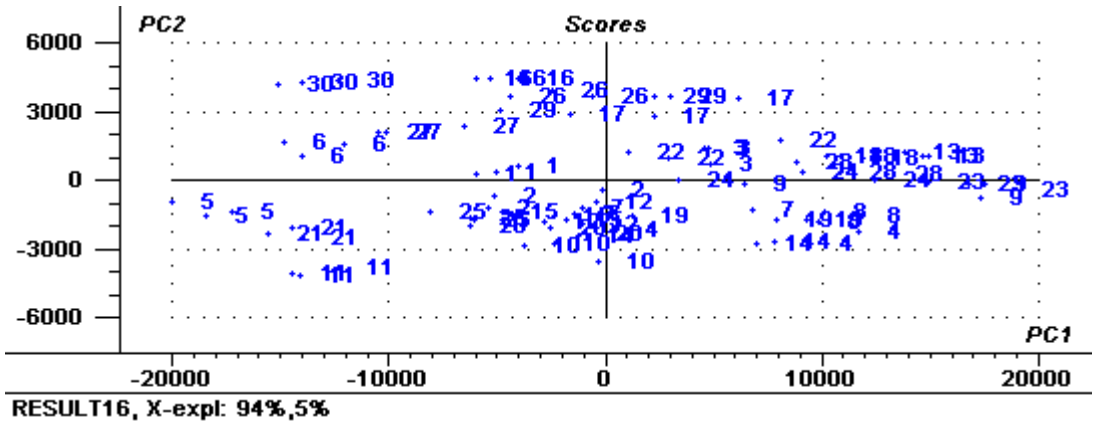

Figure 10. PCA score plot of the 3 different scans of the same kernels placed in different positions on the tray. X-expl: 94%, 5%. N=90.

4.4.1.3. Repeatability of image acquisition

A PCA model showed the differences among sample scans for three different days. The possible variances caused by time intervals between analyses were checked by analysing five samples. Although projections between days presented differences, they did not present day-grouping, explaining that time did not influence group formation. In addition, the plot showed a grouping for the repeated samples, each one represented with the same colour for the three scores (Annexe, Figure 3).

4.4.2. Tests on DON-contaminated and uncontaminated samples

4.4.2.1. Spectral profiles of different DON levels

Figure 11 shows three spectra corresponding to different levels of contamination of 30 kernels placed crease-down on the scanning area. In general, uncontaminated samples showed higher reflectance, however, this point was not confirmed for different samples, thus it was concluded that some kind of data pre-processing was required. In Figure 11, the 1200 nm and 1480 nm absorption bands are indicated as they have been related to ergosterol and chitin, respectively (Delwiche et al., 2011, 2019). However, the observed differences were not clear at these wavelengths.

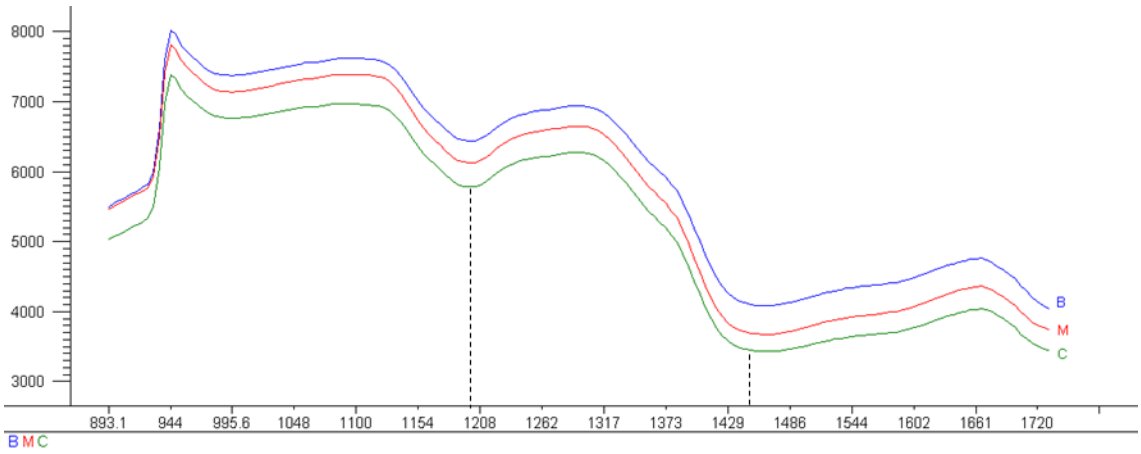

Figure 11. Mean spectra profile of 30 crease-down kernel samples at three DON concentrations. B = <LOD; M = 1605.9 µg/kg; C = 2682.8 µg/kg.

4.4.2.2. Kernel orientation (crease-down or crease-up)

Kernels reflectances were compared by rotating grains on themselves to obtain crease-down and crease-up images for a DON-free and a DON-contaminated sample. Figure 4 (Annexe) shows the projections for 30 kernels of a non-contaminated sample in the upper part and a contaminated sample in lower part. The dashed line ellipse is the group that represents the majority of the crease-up kernels. Besides, the continuous line ellipse includes the crease-down grains. PC1 explained most of the kernels differences (93% of the variability), while the

impact of the different orientations appeared in the PC2, explaining less than 7% of the spectral variance.

4.4.2.3. Spectral data pre-treatment determination

A PCA analysis compared the different spectral pre-treatments applied to the raw data (reflectance spectra) in the ability of HSI-NIR to discriminate DON-contaminated kernels from those under the LOD (Annexe, Figure 5 and 6). The PCA score plot corresponded to crease down and crease up kernels scan, respectively. Continuous line ellipses represent the projection area in the score plot for grains contaminated with 1719.8 μg/kg, while dashed-lines ellipses correspond to the <LOD kernels. The ellipses showed kernels clusters for each contamination level. In some cases, they were overlapped, appearing some samples in the middle of two groups. The results showed that transformation to absorbance plus baseline correction was the best choice for grains in the crease-down and crease-up positions placed in the scanning area.

4.4.2.4. Kernel orientation and discrimination of DON contaminated kernels

Figure 12 shows the comparison of contaminated (C) and non-contaminated (B) kernels placed crease-down (D) or crease-up (V) during the scan. The following results obtained using the absorbance spectra pre-treated with a baseline correction were categorized as the most appropriate adjustment to highlight DON contamination. Each number corresponds to the evaluation of four different samples, three contaminated with DON and one under the LOD. Result 1A depicts 60 wheat kernels arising from a batch with a DON concentration of 2682.8 μg/kg; result 2A from a sample with 2190.0 μg/kg of DON and finally; result in 3A plots the same number of kernels from a batch with 2660.0 μg/kg. Group B kernels came from samples with concentrations below the LOD. The results showed that, while separation of grains due to DON-contamination

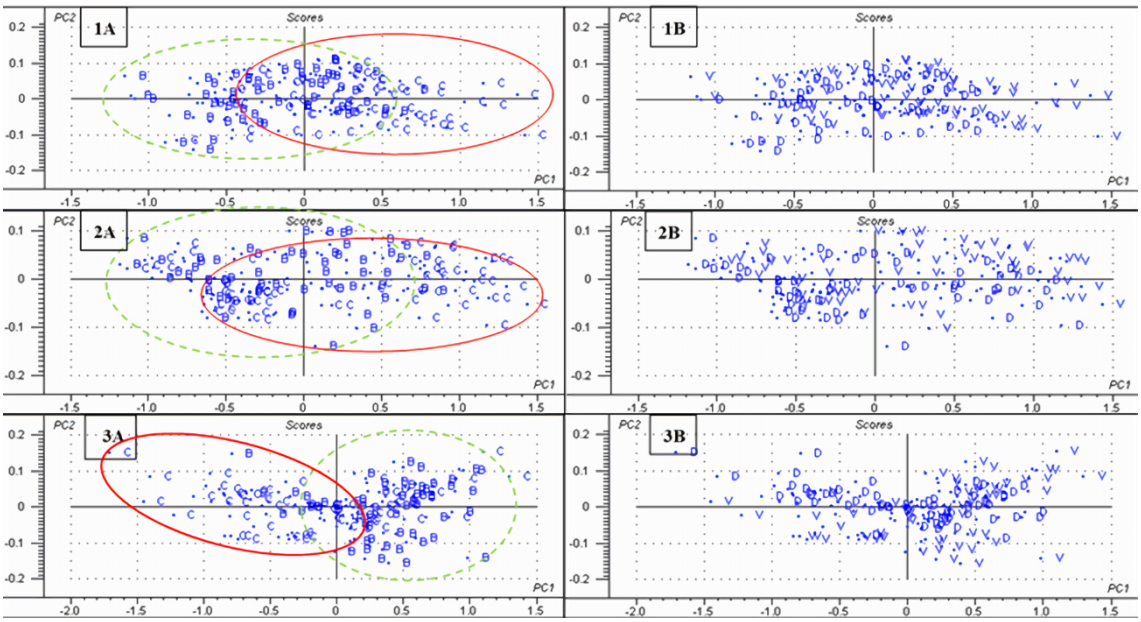

Figure 12. Evaluation of the influence of the kernel position on the ability of HSI-NIR to discriminate between DON-contaminated and <LOD kernels. Result 1 = X-expl: 97%; 1%. Result 2 = X-expl: 99%; 1%. Result 3 = X-expl: 98%; 1%. N = 120.

occurs in the PC1 (A figures), no relation exists with the grain orientation (B figures). Thus, it concludes that grains could be placed in the scanning area oriented randomly.

4.4.2.5. Visual symptoms and contaminated kernels detection

A PCA score plot of the combination of two features, DON contamination and kernel symptoms, is presented in Figure 13. It shows kernel symptoms influence (discolouration, wrinkles and wilting) in the discrimination of kernels with and without DON. Contaminated samples contained more symptomatic grains than non-contaminated ones. Four different groups: contaminated and symptomatic (CS), contaminated and asymptomatic (CA), non-contaminated and symptomatic (BS) and non-contaminated and asymptomatic (BA), showed that the separation along PC1 (97% of explained variance) is due to the difference among symptomatic contaminated kernels from uncontaminated ones (either symptomatic or not). We remind that, in this study, no confirmation of the DON-contamination at kernel level exists, so some of the kernels classified as

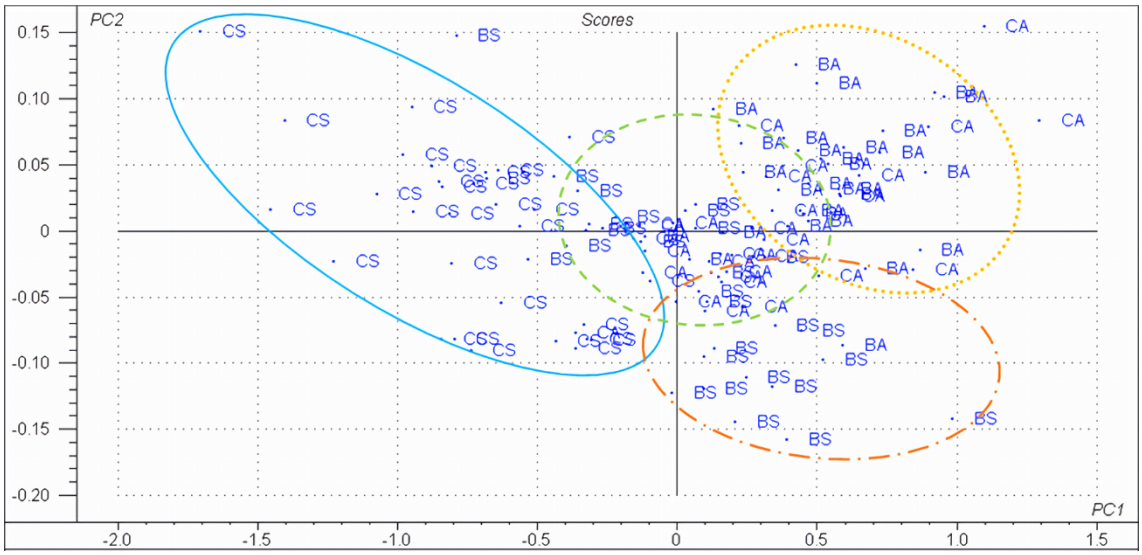

Figure 13. Evaluation of the influence of the kernel symptomatology on the ability of HSI-NIR to discriminate between DON-contaminated and <LOD kernels. CS = Contaminated/Symptomatic; CA = Contaminated/Asymptomatic; BS = Non-contaminated/Symptomatic; BA = Non-contaminated/Asymptomatic. Xexpl: 97%, 1%.

contaminated could be uncontaminated and vice-versa. In conclusion, the symptoms of *Fusarium* damage are the basis for the discrimination, as it was expected. Thus, the discrimination success is directly affected by the correlation between *Fusarium*-DON.

4.4.3. Quantification and classification models for bulk samples

4.4.3.1. Repeatability within samples

The different subsamples (7 g) arising from the same bulk sample showed some differences (Figure 14). PC1 accounted for 100% of spectral data variability, where subsamples <LOD were projected separately on the left from those contaminated with 660 µg/kg placed in the middle, and those with levels between 1770 and 2881 µg/kg overlapped on the right, which is quite expectable considering the heterogeneous distribution of mycotoxins in cereal commodities.

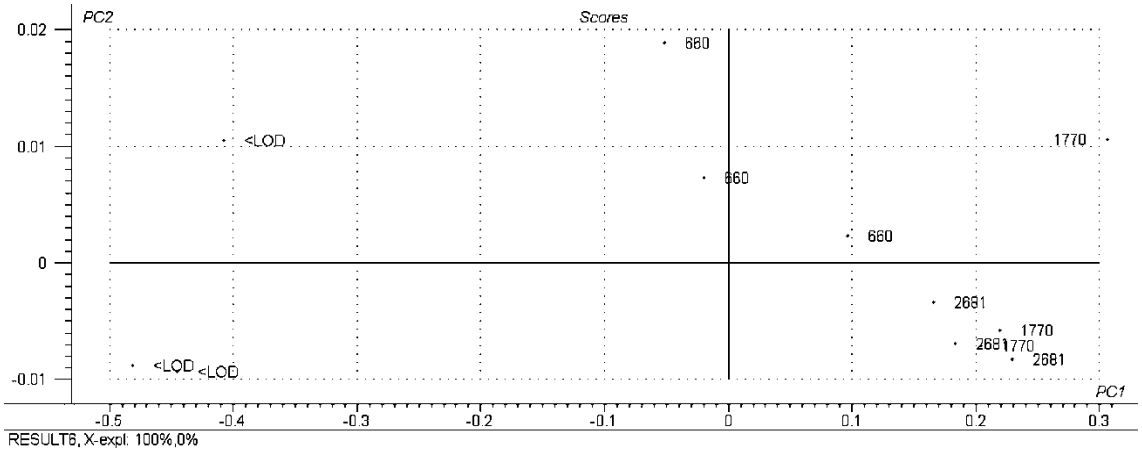

Figure 14. PCA score plot for four bulk samples subsampled three times and scanned (7 g) in triplicate (Mean of triplicated scans are presented). Baseline corrected absorbance spectra. X-expl: 100%, 0%. N=12.

4.4.3.2. Calibration of a PLS regression model and validation

The model used 200 images (from 74 samples scanned in triplicate, less the outliers) to calibrate the PLS model. The model included contaminated cereals between <LOD and 2660 μg/kg, including the legal UE limit (1250 μg/kg). Figure 15 represents the predicted versus measured values plot in which the line corresponds to the regression line of prediction obtained from spectral data (by full cross-validation). Figure 15 also shows the statistic parameters of the validation (obtained by full cross-validation) of the model. The coefficient of determination of cross-validation (R_{cv}^2)

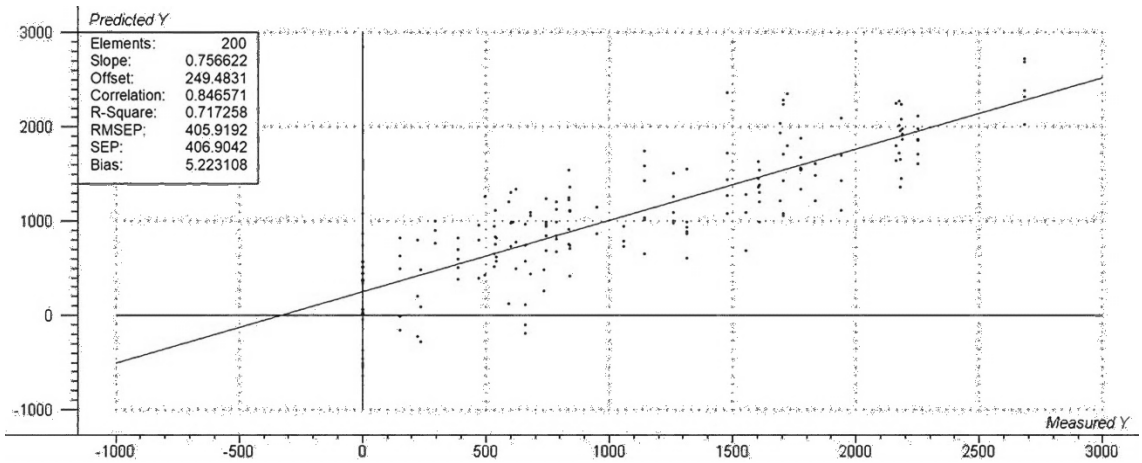

Figure 15. Predicted vs. measured plot for PLS calibration set. Optimum number of PC: 17. N = 200.

was 0.72, the offset 249.48 μg/kg, the RMSECV 405.9 μg/kg, and the slope 0.76. The optimum number of PC used for the best adjustment of the regression was 17.

The same samples were evaluated by dividing the images into 72 for the calibration set (24 in triplicate) and an independent test set of 150 (50 scanned in triplicate). The concentration range used for model testing was the same for the cross-validated model. In this case, the statistic parameters obtained by the model based on the test set spectra were a R_p^2 of 0.27 an offset of 883.4 μg/kg, an RMSEP of 1174.4 μg/kg and a slope of 0.77, which suggested that the prediction of DON concentrations for individual bulk samples was not possible under the conditions tested in this work (Figure 16).

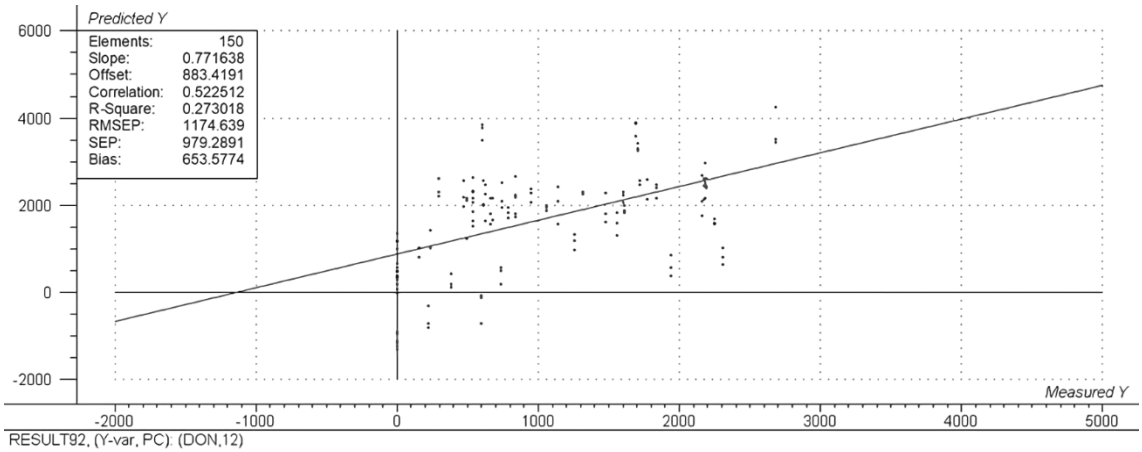

Figure 16. Predicted vs. measured plot for PLS validation set. The optimum number of PC: 12. N = 150.

4.4.3.3. Classification model

A total of 150 images divided into two sets of 75 (training and validation) were used to calibrate an LDA classification model. Each set was composed of 47 corresponding to the B group (grain arising from samples contaminated by DON below 1250 μg/kg) and 28 images corresponding to group C (above 1250 μg/kg). Table 5 shows the number of correct and misclassified samples for both sets by LDA. The percentage of samples correctly classified was 73.4% (55/75) for the training set and 62.7% (47/75) for the validation set. Half of the incorrectly-

classified (19%) were fail-dangerous, meaning that were contaminated over the legal limit but predicted to be under the limit.

Table 5. LDA accuracies for training and validation sets.

Training set				**Validation set**			
	Predicted		Accuracy (%)		Predicted		Accuracy (%)
Groups	B	C		Groups	B	C	
B	33	14	73.4	B	33	14	62.7
C	6	22		C	14	14	

B = low-contaminated group of samples (< 1250 μg/kg); C = contaminated group of samples (≥ 1250 μg/kg). Grey cells indicate the number of correctly-classified samples. White cells indicate the number of miss-classified samples.

4.5. Discussion

In the present work, an HSI-NIR system was standardized for wheat sample images acquisition and to detect DON from naturally-contaminated bulk samples. In summary, for the setup, the results affirmed that good repeatability was expected for intraday and for repeated scannings of the same object (even with mixing up of the kernels), as the position in the scanning area and orientation of the grains had a low impact on the mean reflectance. FT-NIR has also been used to screen bulk samples. Published studies used high DON levels, much above those considered as safe, except for De Girolamo, Lippolis, Nordkvist, & Visconti (2009) and De Girolamo et al. (2014) worked in naturally contaminated samples (ground samples) with a DON range of 50-2600 μg/kg and <50-16,000 μg/kg, the last one so far to the present study. In comparison with De Girolamo et al. (2009), our study achieved a slope of 0.85 for the cross-validated model, slightly better than the 0.83 obtained by the abovementioned author. Otherwise, the R^2 obtained was lower (0.72) than achieved in previous studies (0.82). In addition, the RMSECV obtained in this study was better (405.9 μg/kg) in comparison with the error obtained in the previous one

(516 μg/kg). However, in the present study, 17 LV were required, which resulted in a complex model compared to the two abovementioned studies (4). Our independent validation set model presented poorer results for the model adjustment, obtaining a correlation of 0.52 compared to the 0.79 achieved by both studies. In addition, in our work, the R^2 value was 0.27, lower than 0.63 from both compared studies. However, our RMSEP achieved for the validation set (1174.6 μg/kg) is comparable to the lower error (868.0 μg/kg) obtained by De Girolamo et al. (2009) and the higher (1977.0 μg/kg) achieved by De Girolamo et al. (2014), needing only 8 LV.

Our R^2 described a weak adjustment, but we obtained a significance level for the analysis of variance lower than 0.05 in the predicted vs observed values. Thus, we can affirm that a linear relationship between both measures exists and that the difference between the real and the obtained values is not due to random error. However, our SEP (979.3 μg/kg) was extensively lower than that of the validated model of Peiris, Dong, Bockus & Dowell (2013) by FT-NIR in bulk grain samples, which was 2400 μg/kg. The difference in the errors of prediction between studies could be due to the broader range of concentrations used in previous studies (<50-3000 μg/kg; <50-16000 μg/kg and <40-17400 μg/kg, respectively). At broader concentration ranges, higher RMSEPs are obtained, caused by the higher standard deviations in the extremes of the distribution than in the centre. For that reason, the complete comparison of the results obtained in all these studies should include similar contamination ranges.

As in our study, De Girolamo et al. (2014, 2009) also classified samples by LDA, in the first work applying a cut-off of 300 μg/kg, in which the classification accuracy was 69% and in the second work fixing a similar cut-off as in our study (1200 μg/kg), for which the accuracy was 90%. Our poorer accuracies could be due to the low number of samples (150) compared to previous studies (394 and 464) and their concentration range. In addition, unlike preceding works using FT-NIR, we applied HSI-NIR directly in whole kernel samples, avoiding a previous grinding step. Once

refined, it can be a rapid and cost-effective alternative to chemical analysis for cereal screening batches according to DON contamination. It explains the fitting difficulty due to the complex heterogeneity presented in whole samples compared to previously ground ones.

Barbedo et al. (2017) published the first report using DON concentration as reference and HSI-NIR. Their initial experimental results revealed that direct estimation of DON content using HSI was currently unfeasible but also indicated that an indirect analysis exploiting the correlation between *Fusarium* damage and DON content may be accurate enough to improve the process of DON screening in the production chain. The wheat batches were discriminated between two or three categories, obtaining 81 and 72% of accuracies, respectively. They worked with 251 naturally contaminated samples, from which 152 presented DON levels above 1250 μg/kg, well above our values. However, they analysed by ELISA and LC the same grains as in the HSI-NIR system (after capturing images), this point may be the difference for their better performance and confirms that the variability of the different subsamples taken from the laboratory sample for analysis is an issue (as it is for chemical analysis). Future studies would require enlarging the sample size and determining their optimum dimension. Barbedo et al. (2017) used 30-50 kernels analysing the scanned sample by ELISA/LC to assess more accurately the HSI-NIR performance. Our study presented differences in sampling conditions for the qualitative analysis, in which each image contained approximately 200 kernels (7 g). In addition, for kernel segmentation from the tray and the dark background, Barbedo et al. (2015, 2017) operated on the 647 nm band to obtain the best contrast. Instead, we used background segmentation based on the selection of similar pixels.

In our study, wavelengths were not selected for the classification and regression models, working with the whole range, as this was just a starting point. Interestingly, Barbedo et al. (2017) subtracted the reflectance at 623 nm from that

at 1411 nm band and worked with just one explanatory variable in the developed models. We observed that, for healthy kernels, these two bands did not differ much, diverging only when DON was present. In our case, the results did not differ when subtracting the lower weigh wavelengths, so we decided to maintain the whole NIR region. Other authors working on NIR spectrometry and *Fusarium*-damaged wheat have related changes at 1420 nm to reduced water content (Barbedo et al., 2015), at 1200 nm to ergosterol levels (Dowell et al., 1999), and at 1480 nm to chitin levels (Delwiche et al., 2011). A change near 1450 nm corresponded to the differences in moisture contents (Sundaram, Mani, Kandala, & Holser, 2015). Figure 11 showed two local minimums at 1200 nm and 1450 nm that could be associated with ergosterol produced from fungal cells and to the reduced water content in shrivelled kernels.

Recently, Liang et al. (2018) published the second research on DON detection in bulk wheat kernels by HSI, but at 400-1000nm, thus results are not comparable. However, a peak appeared in 960 nm as in our reflectance raw spectra. They used naturally contaminated grains (250-5000 μg/kg). They placed 70 overlapping wheat kernels in the scanning area, and, as in our study, they recorded the mean spectra. The number of scanned grains was reduced compared to our study, examining approximately 200 kernels in triplicate. After an exhaustive search of the best pre-processing method for the data, as well as for the selection of a discrete number of wavelengths (7 to 14), they achieved a 100% classification (<250, 1162, 2655 μg/kg mean levels in each class) accuracy for the training set and 97.92% for the testing set. They used for each group 44 images to calibrate the model and 16 to validate it. Instead, we used 47 images to calibrate and 28 to obtain the accuracy for each classification group.

The remaining studies on HSI used visual appearance or FDK as a reference variable and used the mean spectra for individual kernels. In the present work, we obtained discrimination between symptomatic and asymptomatic grains by the HSI-NIR system, projecting the data in PCA plots (Figure 13). The use of FDK to estimate DON levels was investigated by Paul, Lipps, & Madden (2005), with a

correlation of 0.73. The PCA scores presented two well-defined groups, one on the left (contaminated and symptomatic) and one on the right (uncontaminated and asymptomatic). These groups corresponded to the positive 0.73 correlation, in which *Fusarium* have produced kernel damage and DON on the kernel. Otherwise, grains with a low correlation between DON and symptomatology were represented in the middle of the score plot, corresponding to the region where both features converged and cannot be distinguished.

As stated before, HSI-NIR analysis can discriminate between FDK and healthy grains and indirectly between DON contaminated and uncontaminated kernels, as both DON and symptomatology show a positive correlation. To deeply evaluate damage by the HSI-NIR, some studies, using a similar spectral range (900-1750 nm) to ours, have been compared (Polder et al., 2005). They worked with 96 artificially contaminated kernels, and they also performed a quantification with HSI-NIR, but in this case, the reference values corresponded to *Fusarium* DNA quantification, using TaqMan RT-PCR. A PLS model was built considering the spectra of complete grains, different from our mean data of the whole sample selection, leading to Q^2 levels of 0.42 (0.80 for highly contaminated grains). Although similar Q^2 values were obtained from the 1250/1050 nm reflectance ratio, it is complex to compare the prediction performances due to the differences in the methodology.

LDA classification methods were also used in previous works by Delwiche et al. (2010, 2011), but they were applied to FHB in samples instead of DON contamination, although they had the information on DON. As in our preliminary studies, they worked on the mean spectra of crease-down positioned kernels. However, they selected 1199, 1474, 1315 nm, and 1998 nm and 1486 nm (local minima or maxima), respectively, as wavelengths required to separate kernels of healthy appearance from FDK in LDA. Both studies results presented correct classifications for high contrast in damage kernels but not for low contrast

ones. This fact agrees with Figure 13, in which the influence of the kernel symptomatology has more weight than DON contamination, although a correlation between both variables exists according to literature. However, Delwiche et al. (2010, 2011) used high DON contaminated samples (2900 to 13500 μg/kg), in which *Fusarium* symptoms are expected. We agree with their study that low DON-contaminated cereals were not distinguishable for their visual *Fusarium* symptoms in a high percentage of the kernels (Barbedo et al., 2015). Thus, spectral pre-treatments, algorithms construction, wavelength selections or more precise calibrations are needed to highlight DON influence above fungal damage on the NIR spectra.

Multivariate methods were applied by Shahin & Symons (2011) work, in which PCA scores extracted six characteristic wavelengths by the loading plot to develop an LDA. Thus, Shahin & Symons (2012) used PLS to select the best wavelength combination (494, 578, 639, 678 nm) by regression coefficients which provided higher accuracies for PLS-DA analysis. By contrast, we used a one-step LDA, which assumes that the within-group covariance matrices are equal. High accuracies were achieved in both studies (92% and 90%, respectively), although their purpose was to classify between FDK and sound kernels and not between DON contaminated and uncontaminated samples. Additionally, individual kernel spectra collection was used, unlike sample mean selection achieved in our study.

The results of Barbedo et al. (2015) compared with our results (Figure 13) regarding the symptomatology of FDK. A correlation of 84% was achieved between DON contamination and visual assessment, distinguishing kernels according to symptomatology and DON contamination. Although correlations between DON/FI for low toxin contamination were accurate, symptoms were absent or too low to be visually assessed. Consequently, future studies are required to quantify DON and discriminate contamination independently from

imprecise visual evaluation. As in our work, they arranged random kernel orientation. Nevertheless, DON reference concentrations were obtained from kernels previously analysed by HSI, not from grains arising from the same sample, as in our case. Thus, their results would be more precise, as the sample heterogeneity can produce discordance between DON concentration in kernels achieved by the reference method and concentration in grains scanned.

The high cost of NIR cameras may be a limiting factor in commercially viable applications development, and developing multispectral cameras may be more feasible than using hyperspectral ones. Moreover, the massive spectral variables and high dimensional data require more processing time than other imaging systems. In addition, large amounts of data noise and redundant information exist in high-dimensional data, which reduce the prediction accuracy of the HSI data model (ElMasry et al., 2012). Although the present work used the whole spectra, wavelength selection would be a future option to improve model performances. As described above, some authors chose a discrete number of wavelengths based on local minima or maxima spectra, and their differences related to visually damaged grains (Barbedo et al., 2018; Delwiche et al., 2010), other used PLS coefficients (Tekle et al., 2015) or more complex techniques (Delwiche et al., 2019; Liang et al., 2018). In the NIR region, the lower wavelength region demonstrated closer similarity between sound and FDK reflectance for most wavelength pairs (Delwiche et al., 2011). The present work obtained high-influence regression coefficients by local minima or maxima selection in 955, 1287, 1403, 1455, 1528, 1671 and 1714 nm. The wavelength selection, especially for the 1403 nm band, is discussed by Peiris et al. (2009), that observed DON absorptions in the 1408 nm band. Previous studies highlight the importance, among others, of 950 nm (absorption from O-H) and 1400 nm (absorption from C-H) bands, which is related to scab effects on protein and starch and consequently the indirect detection of DON (Dowell et al., 1999). Moreover, a

study by Delwiche & Gaines (2005) focused on the single wavelength sorting for *Fusarium*-damaged wheat stated that the best accuracy was between 1450-1460 nm. Some of these bands coincide with ours (955, 1403 and 1455 nm) and present positive or negative coefficients of regression.

On the other hand, besides contaminated samples detection, this technique may have a high potential for cereal grain selection, detecting contaminated single kernels. Preliminary trials showed that single-grains from DON-contaminated samples could be separated from the grains arising from non-contaminated, regardless of kernel location in the scanning area and kernel orientation (either crease-down or crease-up). In this work, DON levels were not known for every single kernel of the scanned sample. Consequently, there is still room for improvement if grain selection was the aim. Similarly, a recent work (Delwiche et al., 2019) proposed HSI-NIR sorting of FDK. They scanned about 200 grains randomly positioned for each sample, using 5 samples for model training and 82 for model testing. The reflectance of each grain was averaged, obtaining the mean reflectance within the kernel. PLS-DA models were used to establish the limits of model accuracy and to evaluate LDA models employing a much smaller number of wavelengths. From the 5 samples, 278 sound and 278 damaged kernels were used. They selected 1100, 1197, 1308, and 1394 nm, with accuracies over 95% in the classification of the test kernels. Although it is still little studied, if sorting of grains by *Fusarium* damage/DON could be feasible, food safety management systems would not have to trust only the analytical screening for wheat batches admission, not able to deal with sampling variability. HSI-NIR sorting implementation would be a critical control measure that. In addition, improving food and feed safety would be more sustainable, as only contaminated kernels and not whole batches would be diverted to other uses or for destruction.

4.6. Conclusions

Rapid and non-destructive methods are required to quantify and discriminate DON, which would be interesting for mycotoxin management in cereals. The results obtained in the present work stated that HSI-NIR is a powerful technique for DON screening, as the preliminary outcomes confirmed the potential of this technique. The most significant parameters which can disturb DON discrimination have been evaluated, obtaining interesting results. Moreover, the quantitative and qualitative analyses do not present high accuracies for naturally contaminated samples, but they are a starting point for further processing improvements and calibration techniques. Future studies will be required to improve the HSI-NIR technique, as high-influence wavelength selection, reference method improvements or single kernel quantification. In addition, new methodologies to overcome sample heterogeneity are necessary to obtain high accurate classification and low prediction error results. Notwithstanding those hitches, the initial results are encouraging, and propose the HSI-NIR as a prospective system for DON quantification and kernel sorting for DON reduction.

4.7. Acknowledgements

The authors are grateful to the University of Lleida (predoctoral grant), and to the Spanish Ministry of Science, Innovation and Universities (Project AGL2017-87755-R) for funding this work.

4.8. References

AOAC. (2005). Official Methods of Analysis. *Official Methods of Ananlysis of AOAC International*, *18*, 20877–22417.

Barbedo, J. G. A., Guarienti, E. M., & Tibola, C. S. (2018). Detection of sprout damage in wheat kernels using NIR hyperspectral imaging. *Biosystems Engineering*, *175*, 124–132.

Barbedo, J. G. A., Tibola, C. S., & Fernandes, J. M. C. (2015). Detecting Fusarium head blight in wheat kernels using hyperspectral imaging. *Biosystems Engineering*, *131*, 65–76.

Barbedo, J. G. A., Tibola, C. S., & Lima, M. I. P. (2017). Deoxynivalenol screening in wheat kernels using hyperspectral imaging. *Biosystems Engineering*, *155*, 24–32.

Beyer, M., Klix, M. B., & Verreet, J. A. (2007). Estimating mycotoxin contents of *Fusarium*-damaged winter wheat kernels. *International Journal of Food Microbiology*, *119*, 153–158.

Cano-Sancho, G., Valle-Algarra, F. M., Jiménez, M., Burdaspal, P., Legarda, T. M., Ramos, A. J., … Marín, S. (2011). Presence of trichothecenes and co-occurrence in cereal-based food from Catalonia (Spain). *Food Control*, *22*, 490–495.

Caporaso, N., Whitworth, M. B., & Fisk, I. D. (2018). Near-Infrared spectroscopy and hyperspectral imaging for non-destructive quality assessment of cereal grains. *Applied Spectroscopy Reviews*, *53*, 667–687.

Cen, H., Lu, R., Zhu, Q., & Mendoza, F. (2016). Nondestructive detection of chilling injury in cucumber fruit using hyperspectral imaging with feature selection and supervised classification. *Postharvest Biology and Technology*, *111*, 352–361.

De Girolamo, A., Cervellieri, S., Visconti, A., & Pascale, M. (2014). Rapid analysis of deoxynivalenol in durum wheat by FT-NIR spectroscopy. *Toxins*, *6*, 3129–3143.

De Girolamo, A., Lippolis, V., Nordkvist, E., & Visconti, A. (2009). Rapid and non-invasive analysis of deoxynivalenol in durum and common wheat by Fourier-Transform Near Infrared (FT-NIR) spectroscopy. *Food Additives & Contaminants: Part A*, *26*, 907–917.

Delwiche, S. R., & Gaines, C. S. (2005). Wavelength selection for monochromatic and bichromatic sorting of Fursarium-damaged wheat. *Applied Engineering in Agriculture*, *21*, 681–688.

Delwiche, S. R., Kim, M. S., & Dong, Y. (2010). Damage and quality assessment in wheat by NIR hyperspectral imaging. *Sensing for Agriculture and Food Quality and Safety II*, *7676*, 1–8.

Delwiche, S. R., Kim, M. S., & Dong, Y. (2011). *Fusarium* damage assessment in wheat kernels by Vis/NIR hyperspectral imaging. *Sensing and Instrumentation for Food Quality and Safety*, *5*, 63–71.

Delwiche, S. R., Rodriguez, I. T., Rausch, S. R., & Graybosch, R. A. (2019). Estimating percentages of *Fusarium*-damaged kernels in hard wheat by near-infrared hyperspectral imaging. *Journal of Cereal Science*, *87*, 18–24.

Dowell, F. E., Ram, M. S., & Seitz, L. M. (1999). Predicting scab, vomitoxin, and ergosterol in single wheat kernels using near-infrared spectroscopy. *Cereal Chemistry*, *76*, 573–576.

Dvořáček, V., Prohasková, A., Chrpová, J., & Štočková, L. (2012). Near infrared spectroscopy for deoxynivalenol content estimation in intact wheat grain. *Plant, Soil and Environment*, *58*, 196–203.

Edwards, S. G., & Jennings, P. (2018). Impact of agronomic factors on *Fusarium* mycotoxins in harvested wheat. *Food Additives & Contaminants: Part A*, *35*, 2443–2454.

Elmasry, G., Kamruzzaman, M., Sun, D., & Allen, P. (2012). Principles and applications of hyperspectral imaging in quality evaluation of agro-food products: a review. *Critical Reviews in Food Science and Nutrition*, *52*, 999–1023.

Femenias, A., Gatius, F., Ramos, A. J., Sanchis, V., & Marín, S. (2020a). Use of hyperspectral imaging as a tool for *Fusarium* and deoxynivalenol risk management in cereals : A review. *Food Control*, *108*, 106819.

Liang, K., Liu, Q. X., Xu, J. H., Wang, Y. Q., Okinda, C. S., & Shena, M. X. (2018). Determination and visualization of different levels of deoxynivalenol in bulk wheat kernels by hyperspectral imaging. *Journal of Applied Spectroscopy*, *85*, 953–961.

Paul, P. A., Lipps, P. E., & Madden, L. V. (2005). Relationship between visual estimates of Fusarium Head Blight intensity and deoxynivalenol accumulation in harvested wheat grain: A meta-analysis. *Phytopathology*, *95*, 1225–1236.

Peiris, K. H. S., Pumphrey, M. O., & Dowell, F. E. (2009). NIR Absorbance characteristics of deoxynivalenol and of sound and *Fusarium*-damaged wheat kernels. *Journal of Near Infrared Spectroscopy*, *17*, 213–221.

Peiris, K. H. S., Y. Dong, W. W. Bockus, & F. E. Dowell. (2013). Estimation of bulk deoxynivalenol and moisture content of wheat grain samples by FT-NIR spectroscopy. *Kansas City, Missouri, July 21 - July 24, 2013*, *American Society of Agricultural and Biological Engineers*, 131593402.

Polder, G., Van Der Heijden, G. W. A. M., Waalwijk, C., & Young, I. T. (2005). Detection of *Fusarium* in single wheat kernels using spectral imaging. *Seed Science and Technology*, *33*, 655–668.

Shahin, M. A., & Symons, S. J. (2011). Detection of *Fusarium* damaged kernels in Canada Western Red Spring wheat using visible/near-infrared hyperspectral imaging and principal component analysis. *Computers and Electronics in Agriculture*, *75*, 107–112.

Shahin, M. A., & Symons, S. J. (2012). Detection of *Fusarium* damage in Canadian wheat using visible/near-infrared hyperspectral imaging. *Journal of Food Measurement & Characterization*, *6*, 3–11.

Sundaram, J., Mani, S., Kandala, C. V. K., & Holser, R. A. (2015). Application of NIR reflectance spectroscopy on rapid determination of moisture content of wood pellets. *American Journal of Analytical Chemistry*, *06*, 923–932.

Tekle, S., Mage, I., Segtnan, V. H., & Bjornstad, A. (2015). Near-infrared hyperspectral imaging of *Fusarium*-damaged oats (*Avena sativa L.*). *Cereal Chemistry*, *92*, 73–80.

Vidal, A., Sanchis, V., Ramos, A. J., & Marín, S. (2016). The fate of deoxynivalenol through wheat processing to food products. *Current Opinion in Food Science*, *11*, 34–39.

Vidal, A., Sanchis, V., Ramos, A. J., & Marín, S. (2018). Stability of DON and DON-3-glucoside during baking as affected by the presence of food additives. *Food Additives and Contaminants - Part A Chemistry, Analysis, Control, Exposure and Risk Assessment*, *35*, 529–537.

Williams, P. J., Geladi, P., Britz, T. J., & Manley, M. (2012). Near-infrared (NIR) hyperspectral imaging and multivariate image analysis to study growth characteristics and differences between species and strains of members of the genus *Fusarium*. *Analytical and Bioanalytical Chemistry*, *404*, 1759–1769.

Xing, F., Yao, H., Liu, Y., Dai, X., Brown, R. L., & Bhatnagar, D. (2019). Recent developments and applications of hyperspectral imaging for rapid detection of mycotoxins and mycotoxigenic fungi in food products. *Critical Reviews in Food Science and Nutrition*, *59*, 173–180.

Chapter 5. Near-infrared hyperspectral imaging for deoxynivalenol and ergosterol estimation in wheat samples

Antoni Femenias, Ferran Gatius, Antonio J. Ramos, Vicente Sanchis, Sonia Marín

Food Chemistry 341 (2021) 128206

5.1. Abstract

The present study aimed to evaluate the use of HSI-NIR spectroscopy to assess the presence of DON and ergosterol in wheat samples through prediction and classification models. To reach the objective, the first set of bulk samples was scanned by HSI-NIR and divided into two subsamples, analysing one for ergosterol and the other for DON by HPLC. The method was repeated for a second set with more samples to build prediction and classification models. All the spectra were pre-treated and statistically processed by PLS and LDA. The prediction models presented an RMSEP of 1.17 mg/kg and 501 μg/kg for ergosterol and DON, respectively. Classification achieved an encouraging accuracy of 85.4% for an independent validation set of samples. The results confirm that HSI-NIR may be a suitable technique for ergosterol quantification and DON classification of samples according to the EU legal limit for DON.

Keywords: Hyperspectral imaging; Deoxynivalenol; Ergosterol; Near-infrared; Cereal analysis.

5.2. Introduction

Fusarium is a plant pathogen that is extensively present in wheat and produces diseases that result in loss of harvest yield, decreased crop quality and decreased economic value. One of the most important diseases caused by these fungi is FHB, which affects spikes causing shrivelling, weight loss and discolouration of kernels (Beyer, Pogoda, Ronellen, Hoffmann, & Udelhoven, 2010). Moreover, under suitable environmental temperature, water activity, pH and nutrient availability conditions, *Fusarium* produces DON, consisting of a mycotoxin with harmful effects on human and animal health. Ineffective approaches for DON reduction in preharvested wheat and its resistance to food processing methods make DON a high prevalence toxin in the food chain (Pestka, 2010). In addition to DON contamination, fungal spoilage results in dry matter loss and reduction of nutritional value. For these reasons, efficient strategies to discern between contaminated and sound, toxin-free wheat batches before food chain entry are needed.

Well-known strategies such as HPLC and ELISA have been used for DON detection and quantification in cereal grains. However, time consumption is one of the most remarkable shortcomings of these techniques. Consequently, companies demand rapid approaches to detect and measure DON, monitoring grains before entry into the food industry, such as LFD. At the moment, spectroscopic techniques are promising not only for the rapid analysis power but also because they are environmental-friendly, cost-effective and non-destructive. NIRs has been used to determine the major components present in food, such as protein, moisture, structural carbohydrates and fats (Caporaso et al., 2018; Pandey, Srivastava, & Mishra, 2018). The application of this technique to minority pollutants, such as DON, has been investigated by many authors. Some studies have also evaluated the influence of ergosterol by measurement of NIR spectra for its determination and prediction concerning *Fusarium* growth and

damage (Dowell et al., 1999; Mancinelli, Costantini, & Rossi, 2014). Ergosterol is a predominant chemical component of the fungi cell membrane. At the same time, it is a minor or absent component in most plants and, consequently, indicates the presence of fungal growth in cereal products (Seitz, 1979).

HSI is a novel approach that presents advantages over conventional NIR devices. Its main advantage is the spectral information acquisition from every image pixel. Thus, it is a high-performance analytical device, especially for heterogeneous samples. The most appropriate spectrometry technology for grain evaluation is diffuse reflectance, which can partially penetrate the object to show its physical and chemical characteristics (Fox & Manley, 2014). In addition, push-broom imaging is the most widely used technique for HSI recording. This measurement involves scanning through the 'y' axis to record NIR spectra for each pixel in the 'x' dimension over all the measured wavelength range (Boldrini et al., 2012).

Several studies tested HSI spectroscopy for *Fusarium* damage assessment. Most of them used visual inspection as a reference for HSI calibration, using kernel symptoms to build classification models (Delwiche et al., 2011; Ropelewska & Zapotoczny, 2018; Serranti et al., 2013). Otherwise, ergosterol has not been used for HSI calibration yet. However, as ergosterol is considered an indicator of fungal growth (Magan, 1993), some authors used this chemical compound to estimate fungal damage in cereals (Börjesson, Stenberg, & Schnürer, 2007; Delwiche et al., 2011; Dowell et al., 1999). In addition, the influence of ergosterol for the spectra measured near the 1200 nm band has been studied (Delwiche et al., 2011; Delwiche et al., 2019; Femenias, Gatius, Ramos, Sanchis, & Marín, 2020b). Consequently, an ergosterol calibration for a rapid determination of fungal growth would improve visual inspection, which is an imprecise and qualitative method.

Likewise, HSI-NIR has been used to detect and quantify DON in wheat. Barbedo et al. (2015) focused on the correlation between the visual symptoms and DON concentration by a FI determination in which they demonstrated that visual symptoms do not correlate with DON contamination. A subsequent study (Barbedo et al., 2017) aimed to classify wheat samples into two (above or under the EU limit, 1250 μg/kg) and three groups (< 500 μg/kg; 500-1250 μg/kg; > 1250 μg/kg) using a CM. In this report, DPI was employed, obtaining notable classification accuracies of above 70%, although prediction models were not used due to their low correlation (0.54) with the DON concentration. Moreover, Liang et al. (2018) also classified wheat samples according to the DON mean concentrations into three groups (< 250 μg/kg; 1162 μg/kg; 2665 μg/kg) using a high complexity model by the combination of SVM and PLS-DA. Recently, published studies determined a positive correlation between the spectral signatures of wheat kernels and wheat flour and fungal DNA and DON content (Alisaac et al., 2019).

The first aim of this study was to determine ergosterol by HSI-NIR as an indicator of fungal presence to assess grain quality, nutritional value and yield loss. Second, by using a considerable number of samples compared to other studies with similar purposes, DON quantification and classification of wheat samples according to the established EU limit was carried out by HSI-NIR analysis. PLS and LDA were used as multivariate statistical techniques to reach these objectives (Esbensen, Swarbrick, Westad, Whitcombe, & Anderson, 2018). In this study, a first approximation of the potential of HSI-NIR, assessing the spatial distribution of the variables, was not achieved. Instead, mean spectra of the image comparing the performance with other techniques recording single spectra, like FT-NIR, etc., were used.

5.3. Materials and methods

5.3.1. Wheat samples

A feed-producing agricultural cooperative supplied a total of 270 wheat samples during 2018 and 2019. The origin of the samples was the plain area of Lleida province. Samples passed within its quality control programme from each incoming truck. The moisture content, protein, fat, and ash levels were determined from the whole homogenized sample, sending a subsample (200-500 g) to our laboratory.

5.3.2. HSI-NIR experimental work: instrumentation and data acquisition

A push-broom HSI system, composed of a Pika NIR-320 camera assembled by RESONON Inc. (Bozeman, MA, USA), was used. The device consists of an InGaAs sensor line scan camera with a 320×256-pixel resolution, 30×30 μm pixel size, and 14-bit resolution A/D spectrograph (Goldeye G-008 SWIR TEC1, Allied Vision Technologies GmbH, Germany). The spectral resolution was 4.9 nm (164 spectral bands from 895 nm to 1700 nm), with a spatial resolution of 320 pixels and a frame rate of 520 fps. The objective lens had a focal length of 25 mm (F/1.4 SWIR, 0.9-1.7 μm, 21 mm image format, c-mount) positioned 220 mm above the image surface. The illumination unit was composed of a four halogen lamp lighting system with Lambertian filters fixed onto an adjustable tower that was turned on at least 20 min before image acquisition. The illumination system, supplied by a Samplexpower® power converter (SEC-1223CE, Burnaby, BC, V5A 0C6, Canada), provided a highly regulated output DC voltage of 13.8 Volts at 23 Amps with an AC input of 230 Volts, 50 Hz. Finally, a motorized linear translation stage with a range of 600 mm was also used, which permitted scanning of the entire sample with the optical systems remaining in a fixed position.

The software Spectronon PRO controlled Resonon's benchtop for image processing. The raw reflectance readings for each test sample data array were corrected by dividing the dark current-subtracted reflectance by the dark current subtracted white standard reflectance at each of the corresponding wavelengths (1). A dark current intensity image, collected before sample scanning, removed the dark noise by covering the camera lens. Likewise, the intensity from a 99% white reflectance standard, made of polytetrafluoroethylene (Spectralon™, SRT-99-120, Labsphere, North Sutton, NH, USA), was used to correct the illumination effects immediately after the dark image. The two images corrected the subsequent sample intensities, set by equation 1.

$$I = \frac{I_0 - I_b}{I_w - I_b} \qquad (1)$$

where I_0 is the raw hyperspectral image obtained, I_w is the white reference and I_b is the dark current reference. Apart from the dark and absolute reflectance response adjustment, the pixel illumination saturation was corrected using the camera controls. The framerate and integration time values were determined, ensuring that no pixel on the image was saturated.

The work had two trials: in the first, 14 g of wheat kernels from each sample were scanned, not following any specific template. The bulk sample mean spectrum was recorded, repeating this process in triplicate and shaking between each scanning to obtain a change in the kernel orientation of the entire sample and representative spectra for its characteristics. The subsamples were ground after the spectra record by an IKA® A11 Basic mill (Darmstadt, Germany). Ground wheat obtained in each subsample (14 g) was scanned, following the same procedure for the whole kernels. After these two steps, each sample was divided into two equal parts of 7 g; one for ergosterol extraction and the other for DON extraction. The second trial was also divided into two steps: In the first, 14 g bulk wheat kernels were scanned in triplicate, grinding the subsamples as in the first

trial and scanning the resulting product three times. This step used the entire 14 g of kernels to extract DON.

In all cases, the black tray reduced the background noise in the image, obtaining an accurate pixel selection. Images had 350 bands for the horizontal axis and approximately 90 mm for the vertical. Pixels were selected from the mean reflectance values of similar spectrum pixels by Euclidian distance, corresponding to the best adjusted to the ROI to remove the background signal. Mean spectra for entire samples were recorded as a text file, exporting the data to the software to analyse the spectra.

5.3.3. Determination of ergosterol and DON concentration in wheat samples by UHPLC

5.3.3.1. Reagents and chemicals

The Milli-Q® SP Reagent water system obtained from Millipore Corp. (Brussels, Belgium) provided the water. Methanol and acetonitrile (HPLC grade) were from Scharlab (Sentmenat, Spain). DON standards were from Romer Labs (Tulln, Austria) and IAC (DONPREP®) from R-Biopharm (Rhone LTD Glasgow, UK). Potassium hydroxide was obtained from VWR Prolabo (Geldenaaksebaan, Leuven) and n-hexane from VWR BDM Prolabo (Fontenay-sous-Bois, France). Finally, ergosterol was purchased from Sigma (St. Louis, Mo).

5.3.3.2. Preparation of ergosterol solutions

Standard solutions were prepared by dissolving 20 mg of ergosterol in 10 mL of solvent (dicloromethane:isopropanol, 99:1, v/v). Then, 3 mL of the solution were evaporated using a nitrogen steam at 40 °C. The resulting product was resuspended in methanol (HPLC grade), and the calibration curves were prepared by diluting appropriately known volumes of the stock solution in methanol.

5.3.3.3. Preparation of DON solutions

The DON concentration in the stock solution was checked by UV spectroscopy, according to the AOAC Official Methods of Analysis, Chapter 49 (AOAC, 2005), obtaining a concentration of 1336 μg/mL for the stock solution. Standard solutions of DON were prepared in methanol at a concentration of 10 μg/mL and stored at 4 °C. Calibration curves were prepared, diluting appropriately known volumes of the stock solution with the mobile phase.

5.3.3.4. Ergosterol extraction in wheat

Concisely, 7 g of previously ground wheat were mixed by an IKA® A11 Basic mill (Darmstadt, Germany) with 40 mL of methanol and 10 mL of hexane. The mix was stirred for 30 min at 112×g and filtered through a sieve of filter paper. Then, 20 mL of the solution was transferred to a tube, adding 2 g of KOH. Next, it was shaken with a magnetic stirrer, placing the mixture into a bath at 55-60 °C for 20 min. The ergosterol was extracted with 2 mL of bi-distilled water to cool the solution and 2 mL of hexane. Then, it was stirred to enable a liquid-liquid extraction and recover the upper layer corresponding to the hexane phase. Two additional liquid-liquid extraction steps with 2 mL of hexane were performed, recovering a final extract volume from the three extractions of 6 mL. This volume evaporated with a low nitrogen steam at 40 °C. The dried samples were resuspended into 1 mL of methanol (HPLC grade) before being injected into the UHPLC-DAD system.

5.3.3.5. DON extraction in wheat

As stated before, the same samples used for spectral analysis were analyzed to determine the mycotoxin content. DON was extracted using specific IAC columns (DONPREP®) and following the manufacturer's instructions. The mycotoxin extraction followed a slightly modified version of the methodology used by Vidal et al. (2018). Briefly, 7 g or 14 g, for the first and the second trial,

respectively, of sample previously ground with an IKA® A11 Basic mill (Darmstadt, Germany) was mixed with 42 mL and 78 mL, correspondingly, of Milli-Q water in a 250 mL Erlenmeyer flask, followed by 10 min of stirring. Then, samples were centrifuged for 10 min at 1780×g, obtaining the supernatant filtered through 9 cm diameter glass microfiber filter paper (Whatman™ GF/A, Maidstone, UK), and, then, 5 mL of the filtrate passed through the IAC column. The columns were washed with 10 mL of bi-distilled water, eluting the toxins with 3 mL of HPLC-grade methanol (the first 1.5 mL performing back-flushing). Samples were evaporated under a low nitrogen steam at 40 °C and resuspended in the mobile phase (methanol:acetonitrile:water, 5:5:90, v/v/v). Every resuspended extract was filtered through a nylon filter (0.4 μm) before being injected into the UHPLC-DAD system.

5.3.3.6. HPLC system for ergosterol analysis

The HPLC equipment consisted of an HPLC Waters 2695 system, with a Waters Spherisorb 5 μm ODS2 and a 4.6 × 250 mm analytical column coupled with a Waters 2487 UV/Vis dual λ absorbance detector set at 282 nm. For each sample analysis, the mobile phase was methanol (HPLC grade) at 1 mL min-1, the injection volume was 100 mL, and the total run time was 18 min. The ergosterol standard was purchased from Sigma (St. Louis, Mo) for calibration solutions preparation, obtaining a curve with R^2 0.99. The limit of detection (LOD) for ergosterol in wheat was 0.5 mg/kg.

5.3.3.7. UHPLC system for DON analysis

DON was determined using an Agilent Technologies 1260 Infinity UHPLC system (California, USA) coupled with an Agilent 1260 Infinity II DAD. A Gemini® C18 column from Phenomenex 150×4.6 mm (California, USA) with a particle size of 5 μm and a pore size of 110 Å was ensembled to the device. The absorption wavelength was 220 nm. The mobile phase was composed of methanol:acetonitrile:water (5:5:90, v/v/v) and set at a flow rate of 1 mL min-1.

For the mycotoxin analyses, the column temperature was 40 °C, the injection volume was 50 μL, and the total run time was 15 min. The performance of this method to quantify DON in wheat has been previously published in Vidal et al. (2018), in which the LOD was three times the signal of the blank (50 μg/kg).

5.3.4. Prediction and classification modelling for bulk ergosterol and DON determination

First, the spectral data were obtained from 50 samples of 14, recording the mean reflectance (167 wavelengths) and using them as explanatory variables. The cross-validated model included 150 images for unground samples and 150 images (50 samples in triplicate in both cases) for ground samples. The samples were achieved in triplicate, shaking the samples between scans to randomly distribute the unground kernels or ground meal to obtain the major representativeness of the sample. The 14 g from each sample were divided into two subsamples of 7 g each, one used for ergosterol and the other for DON analysis. The ergosterol concentration ranged from 1.9 mg/kg to 18.7 mg/kg and the DON contamination range included samples from < LOD to 2660.0 μg/kg. These results were obtained by HPLC and categorized as the dependent variables.

Second, the prediction model used 165 samples of 14g and included a DON concentration range of <LOD - 2660.0 μg/kg. Mean reflectances (167 wavelengths) were the explanatory variables, and the DON concentrations obtained by UHPLC were the dependent variables. A cross-validated model, developed using 495 images (165 samples in triplicate), had two sample sets divided randomly (some kernels were switched from one to the other to obtain similar distributions), in which kernels arising from 83 samples were scanned (249 images) for the calibration set, and grains from 82 samples were scanned (246 images) for the validation set.

The mean spectra correspond to the pixel spectra obtained for all the scanned kernels. Triplicate spectra were treated independently by the statistical software, introducing 495 observations in the multivariate analysis tool (The Unscrambler 7.6 SR1 software by CAMO AS, Oslo, Norway, 2001). First, the reflectances were transformed to absorbances and then baseline corrected. Alternatively, the 1stD was also applied. One PLS model was calibrated for each pre-processing, refining variables and outliers to simplify the model. Models were validated in two ways: by full cross-validation, obtaining the lowest RMSECV possible; and dividing the sample sets to determine the prediction performance with the RMSEP. Some spectra, considered outliers, were removed for all the models. The criterion followed for outlier detection was to represent the influence plot and reject those spectra with higher residual Y-variance, which described the mismatch between the sample and the model. The samples with high leverage and low residual Y-variance were considered extreme samples and maintained in the model. High-leverage and residual Y-variance samples were rejected from the model, as they were considered out of adjustment and influencing the model. Less than 10% of the spectra were removed from the original data. The criterion used to select the number of PCs to optimize the models (for cross-validation and test set) was the PC number where the first minimum on the curve of the RMSE occurs. The performance parameters (slope, correlation, R^2, RMSEP and SEP) gave the validation accuracy.

The 495 images spectra from 165 samples were introduced, as well as for the PLS models, to the classification models. A first classification was calibrated, cross-validating the model to obtain its accuracy. Then, the images were distributed into two sets, each of them covering the broadest range of concentrations possible for an independent validated model. Statistical analysis was performed with JMP PRO 14.1.0 (SAS Institute Inc., 2018) software using a LDA model to characterize two or more classes, first by a dimensionality reduction step, and then, a second

classification stage. The limit established to separate the two classes was the EU legal limit for DON (1250 μg/kg). From the 249 images used for the calibration and the 246 used for the validation set, 411 images corresponded to kernels arising from samples with a DON concentration of below 1250 μg/kg and 84 to grains obtained from samples above the legal limit. Accuracies were the percentage (%) of correctly classified images from the total (495).

5.4. Results

5.4.1. Ergosterol distribution in wheat samples

The mean concentration for the 50 samples was 6.13 mg/kg, with a standard deviation of 3.64 mg/kg. The samples showed a concentration range from < 0.5 mg/kg to 18.65 mg/kg. Finally, the coefficient of variation (CV) was 59.33%. Figure 7 (annexe) represents the distribution frequency for the ergosterol concentration in the whole data set. The highest frequencies were obtained for medium-low concentrations (from 2 mg/kg to 12 mg/kg), finding a data asymmetry distributed under the mean.

Table 6. Performance parameters of ergosterol predictive models.

Sample	Pre-treatment	Slope	RMSEP (mg/kg)	R^2	Number of PC
Whole samples	Raw spectra	0.88	1.35	0.85	20
	ABS/BC	0.85	1.35	0.82	18
	1^{st}D	0.92	1.17	0.89	21
Ground samples	Raw spectra	0.62	2.15	0.57	10
	ABS/BC	0.60	2.24	0.53	11
	1^{st}D	0.84	1.57	0.77	23

ABS/BC = Baseline-corrected absorbance spectra; PC = Principal Components; RMSEP = Root Mean Square Error of Prediction; R^2 = Coefficient of Determination.

5.4.2. Ergosterol quantification for ground and unground wheat samples obtained through HSI-NIR spectroscopy

PLS regression between Y (ergosterol HPLC results) and X variables (HSI-NIR results) was calibrated for whole and ground samples, cross-validating the models because they used just 150 images. Table 6 show performance results for the raw spectra and both spectral pre-treatments.

The application of the 1stD to the raw spectra appeared to be the best pre-treatment for unground wheat samples, obtaining the lowest RMSEP (1.17 mg/kg) and the highest slope and R^2 (0.92 and 0.89, respectively) (Figure 17). However, the model needed too many PC (21) to adjust. In addition, 14 outliers were removed, debugging the models and improving the adjustment.

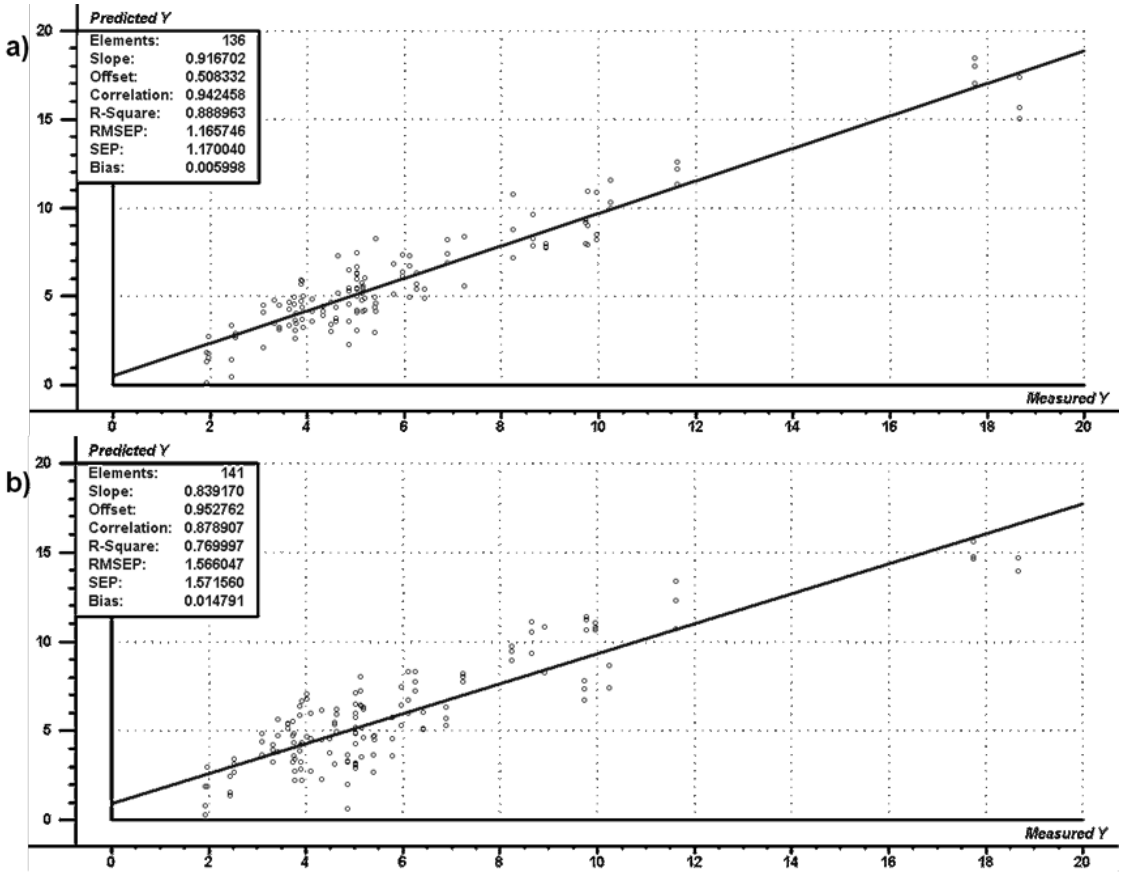

Figure 17. Predicted vs. measured plot of ergosterol PLS regression for 1st derivate spectra. a) Unground wheat data set. Optimum number of PC = 21; N = 135. b) Ground wheat data set. Optimum number of PC = 21; N = 141.

In the case of ground samples, 9 samples were outliers. Table 6 presents the results obtained for the three applied pre-treatments. The best-fitted model was the one built on the 1stD spectra, which had the lowest RMSEP (1.57 mg/kg) and the highest slope and R^2 compared to the obtained with other pre-treatments (0.84 and 0.77, respectively) (Figure 17). Nevertheless, the number of PC used in this model wsa also high (23), so the model presented more complexity.

5.4.3. DON variability in wheat samples

Figure 8 (annexe) shows the distribution of DON concentration in the samples used in the present study for DON quantification and classification trials. The statistical parameters of the calibration and the validation sets are shown independently, with mean DON concentrations of 497.7 μg/kg and 467.1 μg/kg, respectively. Both values are considered low-contaminated due to the high frequency of samples above the LOD. The highest DON concentrations were 3537.0 μg/kg and 2628.5 μg/kg for the calibration and validation sample set, respectively.

Figure 8 (annexe) also represents the frequency of the reference DON content. The frequency histogram shows the number of samples in each category. A high sample density was represented in the medium-low contaminated area followed a non-Gaussian distribution, in which most of the DON contents were under the mean. This fact was expected, due to the heterogeneity between batches, in which fungal production of DON can depend on environmental factors, such as moisture, temperature or harvest season. The samples were divided between two sets, covering the broadest range possible and with similar frequencies for all contamination levels in the calibration and validation sets.

5.4.4. Quantification of DON in unground samples by HSI-NIR PLS regression

The models were based on the 495 images (from 165 samples in triplicate) to calibrate the model, introducing different spectral pre-treatments to determine the best-fitted model with the lowest error of prediction possible. Apart from the raw data, spectra were transformed to absorbances and baseline-corrected (ABS/BC), and first derivated (1^{st}D). The models were verified by cross-validation and independent validation (dividing the samples into two groups, one of 83 to calibrate and another of 82 to validate), assembling a total of six models for each data set. For both validations, the models used the same sample set. Table 7 presents their parameters.

Table 7. Performance parameters of DON predictive models for unground samples.

Bulk samples	Validation	Slope	RMSEP (μg/kg)	R^2	Number of PC
Raw spectra	Cross-validation	0.67	252.70	0.62	18
ABS/BC	Cross-validation	0.59	503.76	0.55	20
1^{st}D	Cross-validation	0.76	354.28	0.73	16
Raw spectra	Test set validation	0.56	540.19	0.56	15
ABS/BC	Test set validation	0.58	561.04	0.52	14
1^{st}D	Test set validation	0.59	501.36	0.61	13

ABS/BC = Baseline-corrected absorbance spectra; 1^{st}D = 1^{st} derivative; PC = Principal Components; RMSEP = Root Mean Square Error of Prediction; R^2 = Coefficient of Determination.

From the original 495 images, a total of 23 (4.64%) were removed, considered as outliers. Figure 18 shows the predicted versus measured plot and the performance parameters obtained for the independent validation of the best-

fitted model. The trend line corresponds to the prediction regression line obtained for model validation. The slope was 0.59, the offset 13.03 μg/kg, the correlation 0.81, the coefficient of determination of validation (R_v^2) 0.61, and the RMSEP 501.36 μg/kg. The optimum number of PCs used to fit the model was 13. From the spectral range used (895–1731 nm), two characteristic wavelengths contributed substantially, explaining the DON variance within the model. These spectral bands showed a maximum at 1220 nm and a minimum at 1380 nm, showing regression coefficients with higher positive and negative weights than the rest of the wavelengths. Thus, both bands contributed significantly to the DON prediction.

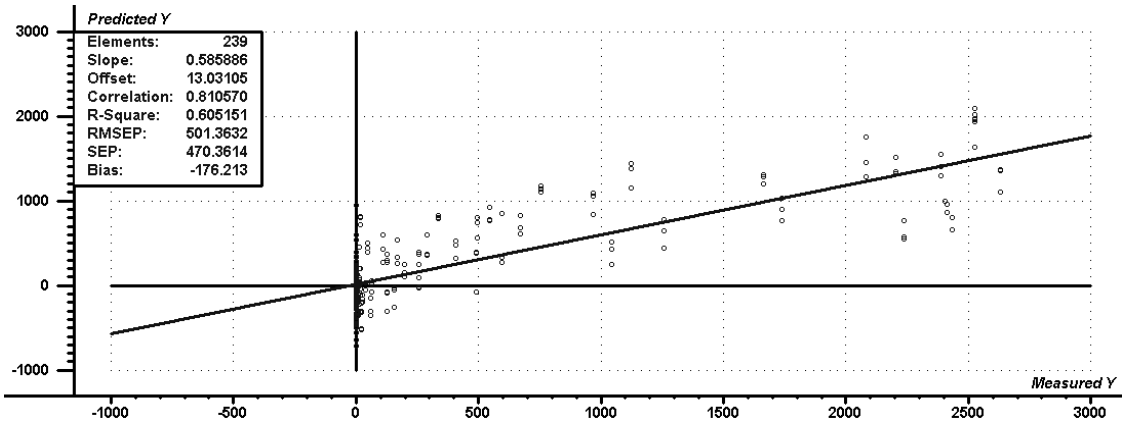

Figure 18. Predicted vs. measured plot for the PLS validation set in unground samples. Optimum number of PC = 13. N of validation = 239.

5.4.5. Classification of unground samples according to DON concentration by LDA

The 495 mean spectra obtained from unground wheat, used to calibrate the models, were introduced to the JMP Pro statistics software for an LDA classification. Two models, one validated by cross-validation and the other dividing samples into training and validation sets, were calibrated. The classification threshold was the actual maximum EU limit (1250 μg/kg) for unprocessed cereals.

Table 8. LDA accuracies for training and validation sets in unground samples.

		Training set				Validation set		
		Predicted		Accuracy		Predicted		Accuracy
Raw spectra	Groups	B	C	86.35	Groups	B	C	82.52
	B	170	34		B	172	35	
	C	0	45		C	8	31	
ABS/BC	Groups	B	C	86.35	Groups	B	C	83.33
	B	172	32		B	174	33	
	C	2	43		C	8	31	
1stD	Groups	B	C	97.99	Groups	B	C	82.93
	B	199	5		B	170	37	
	C	0	45		C	5	34	

B = low-contaminated group of samples (< 1250 μg/kg); C = contaminated group of samples (≥ 1250 μg/kg). Grey cells indicate the number of correctly classified samples. White cells indicate the number of miss-classified samples.

Table 1 (Annexe) shows the results obtained for the cross-validated models for unground samples. The 1stD spectra had higher classification accuracies for LDA, classifying correctly 95.66% of the samples. Only 24 samples were incorrectly classified, being the best model for sample classification according to the DON level for a single dataset. Otherwise, the classification accuracies validated independently were similar for the three pre-treatments (Table 8). Despite the similar results, the best accuracy was for the 1stD pre-treatment, in which 82.93% of the samples were classified correctly. Despite the similarity of the validation accuracies of the different pre-treatments, 1stD model was selected for its accuracy in the training set (97.99), providing robustness to the model. The samples with DON levels below the EU limit incorrectly classified as highly contaminated should be considered. It may be due to the high number of samples below the 1250 μg/kg limit (411) compared to the ones above the threshold in both calibration and validation sets.

5.4.6. Quantification of DON in ground samples by HSI-NIR PLS regression

The predictive model for ground wheat used the same samples as previous models. As for unground sample analysis, the same spectral pre-treatments were applied to the raw data and validated in two ways, building six models. Table 9 includes the results obtained for all the models. The ones with the best performance were for data transformed with the 1stD, which showed a low RMSEP and a high R^2. The independent set validated model is represented by the measured versus predicted plot in Figure 19.

Table 9. Performance parameters of DON predictive models for ground samples.

Bulk samples	Validation	Slope	RMSEP (μg/kg)	R^2	Number of PC
Raw spectra	Cross-validation	0.72	483.28	0.62	13
ABS/BC	Cross-validation	0.73	438.94	0.70	16
1stD	Cross-validation	0.72	403.29	0.69	16
Raw spectra	Test set validation	0.55	578.68	0.49	7
ABS/BC	Test set validation	0.71	588.21	0.48	13
1st D	Test set validation	0.55	518.95	0.59	10

ABS/BC = Baseline-corrected absorbance spectra; 1stD = 1st derivative; PC = Principal Components; RMSEP = Root Mean Square Error of Prediction; R^2 = Coefficient of Determination.

First, from the original 495 images used for the cross-validated model, 24 (4.84%) were discarded, considered as outliers. These 471 samples were used to both calibrate and validate the model. The most remarkable performance parameters were a slope of 0.72, an offset of 108.57 μg/kg, a correlation of 0.83, a R_{cv}^2 of 0.69 and an RMSEP of 403.29 μg/kg. The model needed 16 PCs to be correctly fitted.

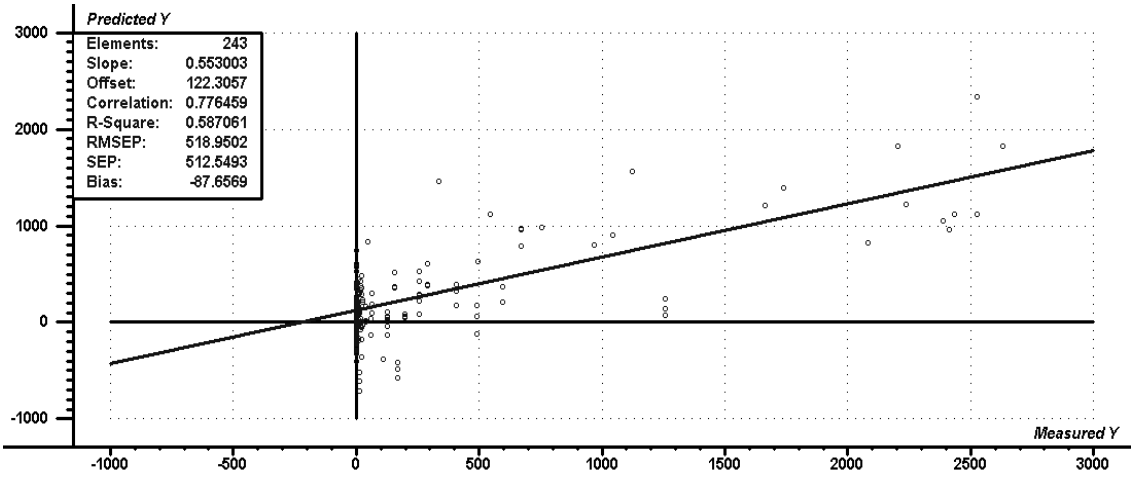

Figure 19. Predicted vs. measured plot for PLS validation set in ground samples. Optimum number of PC = 10. N of validation = 243.

Likewise, the same pre-treatments were applied to the spectra, obtained from ground samples and divided into calibration and a test set. Only 5 (1.98%) outliers were discarded from the calibration data, considering them abnormal compared with the rest. The regression parameters were a slope of 0.55, an offset of 122.30 μg/kg, a correlation of 0.78, an R^2 of 0.59 and an RMSEP of 518.95 μg/kg. The predictions needed fewer PCs for the cross-validated model, resulting in an optimum number of PCs of 10. In this case, two wavelengths that contained high variances were also determined, explaining the DON changes in the model. However, these two wavelengths were at the spectral extremes (941.7 nm and 1728 nm), where the 1stD spectral noise is enhanced (Agelet & Hurburgh, 2010). A third wavelength (1380 nm) also had significant weight on the model (local minimum), which matched with the characteristic wavelengths found in the models for the unground wheat. It led us to select unground samples as a more reliable choice for model development.

5.4.7. Classification of ground samples according to DON concentration by LDA

A total of 495 images were used for classification by LDA. Initially, all the spectra were classified by cross-validation, obtaining the performance parameters. Then,

they were divided into a training and test set, validating the model independently. The process for ground samples consisted only of a milling step, in which the product obtained was not refined, so the wheat bran was maintained. Thus, the classification threshold was the UE maximum limit of DON (1250 μg/kg), as for unprocessed cereals.

Table 10. LDA accuracies for training and validation sets (threshold 1250 μg/kg) in ground samples.

	Training set				**Validation set**			
		Predicte		Accuracy		Predicte		Accuracy
Raw spectra	Group	B	C	93.58	Group	B	C	82.53
	B	191	13		B	176	31	
	C	3	42		C	12	27	
ABS/BC	Group	B	C	83.14	Group	B	C	87.81
	B	168	36		B	180	27	
	C	6	39		C	3	36	
1stD	Group	B	C	99.2	Group	B	C	85.37
	B	203	1		B	188	19	
	C	1	44		C	7	22	

B = low-contaminated group of samples (< 1250 μg/kg); C = contaminated group of samples (≥ 1250 μg/kg). Grey cells indicate the number of correctly classified samples. White cells indicate the number of miss-classified samples.

Table 2 (annexe) shows the LDA accuracies for a cross-validated models in ground samples. For the milled sample analysis, the 1stD pre-treated spectra presented the highest classification accuracy (97.18%), beyond that obtained for the non-treated and ABS/BC spectral results (94.35% and 84.05%, respectively). The low number of over-limit samples misclassified as under-limit contaminated samples should be considered in all cases. For the 1stD model, only one sample highly-contaminated was classified incorrectly. Conversely, Table 10 gathers the LDA results for the training and validation sets. The highest accuracy for the training set (99.20%) was for the 1stD spectra. In addition, the accuracies obtained

for the validation set were similar for the ABS/BC spectra and the 1stD spectra (87.81% and 85.37%, respectively), although the 1stD model presented a higher overall accuracy. For the ABS/BC spectra, the obtained calibration accuracies were poorer than validation. It can occur when the validation sample set differs from the one used in the calibration. Nevertheless, the accuracies for the 1stD corrected spectra as a whole (training and validation) presented higher overall performance compared to the ABS/BC transformed data set efficiencies. As found for the cross-validated models, low percentage samples with concentrations over the legal limit were misclassified.

5.5. Discussion

5.5.1. Ergosterol quantification in wheat samples through HSI-NIR spectroscopy

Ergosterol was detected in all wheat samples, showing most of the samples medium-low ergosterol concentrations and a few presenting high ergosterol levels. It suggested that all samples presented fungal contamination. Our ergosterol results had higher ergosterol content than that found by Perkowski et al. (2008), whose range was 0.40-3.40 mg/kg for naturally infected wheat, but similar to the content range of 1.46 to 42.14 mg/kg reported by Lamper et al. (2000). It demonstrates that our samples covered a broader range of concentrations than other naturally infected samples, making them appropriate for HSI-NIR evaluation.

Interestingly, the HSI-NIR models obtained from unground samples performed better than those for ground samples. This point can attribute to the fact that ergosterol is normally present on the surface of the kernels as a result of fungi colonizing their surface; thus, grinding could reduce ergosterol detection. The regression coefficients with the highest values were determined to reduce the variables and model complexity. Two peak maxima (983.8 nm and 1701 nm) and

two peak minima (960.3 nm and 1380 nm) were considered for their high weights on the model, which can explain the ergosterol variability.

One of the first studies that quantified ergosterol in wheat samples by NIR was published by Dowell et al. (1999), who adjusted their model with an R^2 of 0.62 and an SEC of 108 mg/kg for ergosterol concentrations above 50 mg/kg. As in our study, they used all the spectral ranges between 500-1700 nm. The results have been improved recently (Berardo et al., 2005; Börjesson et al., 2007) on maize and barley samples, respectively. Berardo et al. (2005) reported the best regression models that showed an R^2 of 0.81 and a SEP of 1.74 mg/kg using the characteristics bands of 1430 nm, 1470 nm, 1820 nm, 2140 nm, and 2180 nm, and Börjesson et al. (2007) detected ergosterol by NIR reflectance with an R^2 of 0.83 and an RMSE of 4.5 mg/kg, considering the whole complex information from the NIR region to estimate ergosterol. Our best results (1^{st}D spectra for unground kernels) show lower errors (RMSEP = 1.17 mg/kg) and a higher R^2 (0.89). In our study, four wavelengths (960 nm, 983.8 nm, 1380 nm and 1701 nm) presented higher weights for the whole model, as they explained the variance of ergosterol compared to the other bands. Only the 1400 nm region of the spectra was used to detect ergosterol in previous studies. Furthermore, HSI-NIR spectroscopy may be more appropriate to describe ergosterol content based on the surface reflectance of unground samples, as our results for ground wheat presented weaker adjustment parameters (R^2 of 0.77) compared to the previous reports. In conclusion, HSI-NIR spectroscopy is a suitable method to assess grain quality in terms of fungal presence.

In our previous study (Femenias et al., 2020b), we assessed the correlation between kernel symptomatology and DON contamination using PCA and showed that, in general, DON contaminated kernels show visible symptoms, but that asymptomatic kernels with high DON can also appear. As grains were not individually analysed to build the PCA, the entire samples should be evaluated

to determine the contamination levels. In the present study, the same kernels were first scanned by HSI-NIR and analysed by the reference method, presenting advantages for model calibration. In addition, ergosterol is present at higher concentrations than DON; therefore, it would be an interesting compound for fungal spoilage detection before the apparition of visual symptoms, despite its low correlation with mycotoxins.

5.5.2. DON quantification in wheat samples through HSI-NIR

From the 165 original samples analysed by the reference method, 62 presented concentrations under the LOD. Ideally, the dataset should represent the broadest DON concentration range possible, having the maximum variability to build a solid prediction model. Our results showed a DON distribution with a high density of samples with low DON concentrations. Despite this, the interest of this study is that it used naturally contaminated samples, and, consequently, the results are directly applicable in real situations for DON prediction in wheat. In addition, the dataset was equally divided into calibration and validation groups, covering similar ranges of concentration. Balanced sets of data are required to obtain validation performance parameters that represent the maximum variance of the model calibration.

The models applied to unground and ground wheat samples presented the best performances for the 1stD pre-treatment. The unground grain model had a slope of 0.59, an R^2 of 0.61 and an RMSEP of 501 μg/kg. Alternatively, the milled grain model had a slope of 0.55, an R^2 of 0.59 and an RMSEP of 518 μg/kg. These results showed a slightly higher performance for unground samples than for ground samples. Avoiding the grinding step presents advantages to the method: faster and reduced complexity. The differences in the majority components of wheat, such as water, protein or starch, could influence DON prediction errors, which may interfere in the quantification; thus, it is more suitable to model such variables concerning DON for the classification of samples than for

quantification. However, multivariate analysis techniques allow us to model the spectral differences generated by the different sample components.

Some preliminary studies used pre-HSI technology for DON quantification, although most works used NIR and Fourier Transform Near Infrared (FT-NIR) spectroscopy. Although these technologies cannot recognize the spatial distribution of the cereals, some approximations for mycotoxin content prediction have been described. Dvořáček et al. (2012) estimated the DON content in intact wheat samples by FT-NIR; thus, we can discuss and compare their results with our outcomes for unground wheat. Their best PLS-DA result showed a high correlation of 0.92 and a high SEP of 2.35 mg/kg. Unlike in our study, they used ELISA as a reference method, and they worked on artificially contaminated samples at a higher DON range (0-90 mg/kg). In addition, they identified two spectral regions between 1390-1770 nm and 1880-2070 nm, using them to describe DON contamination. Our methodology focused on the NIR spectra, whose range went from 895 nm to 1728 nm; thus, only the first region is comparable to our results. The study of Peiris, Dong, Davis, Bockus, & Dowell (2017) obtained a SEP of 2400 μg/kg and an R^2 of 0.48, and, in this case, using the entire spectral range with a mean centring for the calibration of the FT-NIR. They scanned 65-70 g of non-milled wheat; thus, their model parameters are comparable to ours for unground samples. However, some spectral bands were related to the presence of DON because they can be correlated to the light interaction differences with DON vibrating bonds. Therefore, their regression coefficients showed spectral peaks at 1310 nm, 1400 nm, 1420 nm, 1920 nm and 1960 nm. The first three peaks are comparable to ours, obtained at the same spectral region (1380 nm), which led us to consider the region of maximum information for DON. Remarkably, the present study is the first one that uses naturally contaminated wheat samples for HSI-NIR technology.

HSI-NIR technologies have been used for DON quantification by a few authors. In our previous study (Femenias et al., 2020b), the PLS regression parameters for bulk samples were poorer than in the present study, using fewer samples and different kernels for both HSI and HPLC analyses. The R^2 has increased from 0.27 to 0.61, and the RMSEP has been reduced from 1174 μg/kg to 501 μg/kg. Moreover, the 1stD of the spectra, which was not the best spectral pre-treatment method for DON-contaminated single kernel discrimination by PCA in our previous work, presents the best results for bulk kernel analysis by PLS regression in the present work. However, comparing the ABS/BC spectral model results obtained from both studies, the PLS parameters are also improved (R^2 of 0.52 and RMSEP of 561 μg/kg). The characteristic peaks obtained in the previous work were local minima or maxima at 955 nm, 1287 nm, 1403 nm, 1455 nm, 1528 nm, 1671 nm and 1714 nm. The pre-treatment of the spectral data may introduce changes to our spectral behaviour, but our peaks are still comparable to those obtained in previously presented unground models (1220 nm and 1380 nm). However, the unground model for DON determination can avoid characteristic bands near the extremes that introduce noise to the ground wheat model (Agelet & Hurburgh, 2010; Yao & Lewis, 2010).

Our results were comparable to the ones of De Girolamo et al. (2009), who also worked with naturally contaminated ground wheat samples with a similar DON concentration range (50-3000 μg/kg); however, they used FT-NIR to scan milled and sieved wheat. For our ground model, we obtained a similar slope and R_{cv}^2 (0.72 and 0.69, respectively) than in their case (0.71 in both cases). Nevertheless, our RMSECV was better (403 μg/kg) than that obtained in the previous study (516 μg/kg). For the independent validation of the model for milled samples, the R^2 was slightly lower (0.59) than the compared study (0.63), and RMSEP was better (518 μg/kg) than the 868 μg/kg obtained by De Girolamo et al. (2009). Moreover, the high-influence peaks in this study were near the 1409 nm region

and the 1904 nm band. Our results also pointed out the spectral region near 1400 nm, which may be related to DON contamination. In addition, De Girolamo et al. (2014) used FT-NIR for DON evaluation of the ground naturally contaminated wheat samples. In this case, the range of concentrations increased to 16000 μg/kg. Their PLS results using ground and sieved wheat presented a reduced prediction capacity compared to our model (not sieved). They obtained an RMSEP of 1977 μg/kg and an R^2 of 0.63. Although their R^2 was similar to ours (0.69), their RMSEP was much higher than ours (403 μg/kg). This increase in the RMSEP can be due to the higher DON range, which depends on the original Y variable scale. In the last two studies, samples were sieved, obtaining a final sample size of < 500 μm. This step may reduce sample heterogeneity at the expense of losing DON, which is present with a higher probability at the external layer of the kernel. After milling, the larger particles correspond to the outer layer and the smaller particles to the endosperm. To avoid DON loss in our samples, we did not sieve because it increases the operation time and the analysis complexity.

5.5.3. Classification of wheat samples according to DON levels through HSI-NIR

As in the present study, De Girolamo et al. (2014, 2009) classified milled wheat samples by LDA. In the first study, they obtained discrimination of 69% of the samples below and above the cut-off (300 μg/kg). A high prediction accuracy, ranging from 75-90%, was achieved for 3 classes of discrimination (< 1000 μg/kg; 1000-2500 μg/kg; > 2500 μg/kg) by De Girolamo et al. (2014) using FT-NIR, which is comparable to our results of more than 82% correctly classified samples. Although the high accuracy of classification from the 495 spectra obtained in this work, only 84 samples were above the UE maximum limit. Future studies should evaluate the introduction of similar frequencies of DON between groups above and under the threshold to obtain the same weight in models.

Peiris et al. (2017) also employed an FT-NIR device for DON classification at different thresholds. The contamination range varied between non-detectable levels to 58100 μg/kg. The closest cut-off they used (2000 μg/kg) is comparable to the one used in this work. Their overall classification accuracy for this cut-off was 87%, similar to ours. Nevertheless, their classification accuracy for the samples below the threshold (only 7.2% of the total samples) was 38.9%. In our case, we used a higher number of samples below the limit, with 96% correctly classified samples. It demonstrated that it is possible to manage naturally contaminated wheat batches, in which moderate concentrations are frequent. However, we need a more balanced dataset in which highly contaminated samples appear with similar frequency to low-contaminated.

Moreover, Barbedo et al. (2017) published a study evaluating DON by HSI in the NIR region. Although they did not consider it feasible to estimate the DON content, they focused on a classification method for wheat batches using two or three categories. The two categories model followed the EU legal limit for unprocessed cereals (1250 μg/kg) as the cut-off. They achieved a correct sorting ratio of 81%, slightly lower than our (83%) for the two split groups. Our study presents differences in the sampling conditions, in which the sample weights 14 g (approximately 400 kernels), unlike the 30-50 kernels used by Barbedo et al. (2017) for each image. Consequently, our sample volume is more representative of the whole batch than previous studies to classify wheat samples.

Complex statistical research was published by Liang et al. (2018), assembling spectral pre-processing and novel algorithms to determine different DON levels in bulk wheat samples. A PLS-DA model classified samples between classes divided into three mean categories (< 250 μg/kg, 1162 μg/kg and 2665 μg/kg). Samples contained a DON concentration ranging from 250 μg/kg to 5000 μg/kg and were analysed by HSI-Vis/NIR. The wavelength range varied between 250-1000 nm, so only one peak (980 nm) is comparable to our spectra (895-1731 nm).

Consequently, the characteristic wavelengths obtained by Liang et al. cannot be compared with the present study, as they worked in a different spectral range. Even though the computation involved in their models was complex, they obtained high classification accuracies, achieving their best result for the MSC-SPA-SVM combination, which classified correctly 97.75% of the test set samples.

5.6. Conclusions

Food and feed industries need urgently to have rapid methods that allow the analysis and rejection of mycotoxin-contaminated batches in a short time. With HSI-NIR application for fungal growth and DON inspection, traditional screening analysis, such as ELISA and LFD, could be replaced by rapid and non-destructive screening methods. The results demonstrated that despite the low correlation between ergosterol and DON, successful outcomes for ergosterol quantification with high performance can be achieved by HSI-NIR. In addition, our findings establish that it is possible to quantify DON in naturally contaminated bulk wheat samples with an error of prediction of 501.36 μg/kg. With such an error, the device can be implemented to screen DON-contaminated samples. Moreover, the classification model to accept or reject according to the EU maximum limit presented remarkable accuracies (> 80%), which can be applied to prevent highly contaminated batches from entering the food chain. In addition, further studies for single kernel screening via individual kernel sorting are required, avoiding the entire batch exclusion and improving DON reduction and production yield.

5.7. Acknowledgements

The authors are grateful to the University of Lleida (predoctoral grant), and to the Spanish Ministry of Science, Innovation and Universities (Project AGL2017-87755-R) for funding this work.

5.8. References

Agelet, L. E., & Hurburgh, C. R. (2010). A tutorial on near infrared spectroscopy and its calibration. *Critical Reviews in Analytical Chemistry*, *40*, 246–260.

Alisaac, E., Behmann, J., Rathgeb, A., Karlovsky, P., Dehne, H. W., & Mahlein, A. K. (2019). Assessment of *Fusarium* infection and mycotoxin contamination of wheat kernels and flour using hyperspectral imaging. *Toxins*, *11*, 1–18.

AOAC. (2005). Official Methods of Analysis. *Official Methods of Analysis of AOAC International*, *18*, 20877–22417.

Barbedo, J. G. A., Tibola, C. S., & Fernandes, J. M. C. (2015). Detecting Fusarium head blight in wheat kernels using hyperspectral imaging. *Biosystems Engineering*, *131*, 65–76.

Barbedo, J. G. A., Tibola, C. S., & Lima, M. I. P. (2017). Deoxynivalenol screening in wheat kernels using hyperspectral imaging. *Biosystems Engineering*, *155*, 24–32.

Berardo, N., Pisacane, V., Battilani, P., Scandolara, A., Pietri, A., & Marocco, A. (2005). Rapid detection of kernel rots and mycotoxins in maize by near-infrared reflectance spectroscopy. *Journal of Agricultural and Food Chemistry*, *53*, 8128–8134.

Beyer, M., Pogoda, F., Ronellen, F. K., Hoffmann, L., & Udelhoven, T. (2010). Estimating deoxynivalenol contents of wheat samples containing different levels of *Fusarium*-damaged kernels by diffuse reflectance spectrometry and partial least square regression. *International Journal of Food Microbiology*, *142*, 370–374.

Boldrini, B., Kessler, W., Rebnera, K., & Kessler, R. W. (2012). Hyperspectral imaging: A review of best practice, performance and pitfalls for in-line and on-line applications. *Journal of Near Infrared Spectroscopy*, *20*, 483–508.

Börjesson, T., Stenberg, B., & Schnürer, J. (2007). Near-infrared spectroscopy for estimation of ergosterol content in barley: A comparison between reflectance and transmittance techniques. *Cereal Chemistry*, *84*, 231–236.

Caporaso, N., Whitworth, M. B., & Fisk, I. D. (2018). Near-Infrared spectroscopy and hyperspectral imaging for non-destructive quality assessment of cereal grains. *Applied Spectroscopy Reviews*, *53*, 667–687.

De Girolamo, A., Cervellieri, S., Visconti, A., & Pascale, M. (2014). Rapid analysis of deoxynivalenol in durum wheat by FT-NIR spectroscopy. *Toxins*, *6*, 3129–3143.

De Girolamo, A., Lippolis, V., Nordkvist, E., & Visconti, A. (2009). Rapid and non-invasive analysis of deoxynivalenol in durum and common wheat by Fourier-Transform Near Infrared (FT-NIR) spectroscopy. *Food Additives & Contaminants: Part A*, *26*, 907–917.

Delwiche, S. R., Kim, M. S., & Dong, Y. (2011). *Fusarium* damage assessment in wheat kernels by Vis/NIR hyperspectral imaging. *Sensing and Instrumentation for Food Quality and Safety*, *5*, 63–71.

Delwiche, S. R., Rodriguez, I. T., Rausch, S. R., & Graybosch, R. A. (2019). Estimating percentages of *Fusarium*-damaged kernels in hard wheat by near-infrared hyperspectral imaging. *Journal of Cereal Science*, *87*, 18–24.

Dowell, F. E., Ram, M. S., & Seitz, L. M. (1999). Predicting scab, vomitoxin, and ergosterol in single wheat kernels using near-infrared spectroscopy. *Cereal Chemistry*, *76*, 573–576.

Dvořáček, V., Prohasková, A., Chrpová, J., & Štočková, L. (2012). Near infrared spectroscopy for deoxynivalenol content estimation in intact wheat grain. *Plant, Soil and Environment*, *58*, 196–203.

Esbensen, K. H., Swarbrick, B., Westad, F., Whitcombe, P., & Anderson, M. J. (2018). *Multivariate Data Analysis: An introduction to Multivariate Analysis, Process Analytical Technology and Quality by Design*. CAMO.

Femenias, A., Gatius, F., Ramos, A. J., Sanchis, V., & Marín, S. (2020b). Standardisation of near infrared hyperspectral imaging for quantification and classification of DON contaminated wheat samples, *111*, 107074.

Fox, G., & Manley, M. (2014). Applications of single kernel conventional and hyperspectral imaging near infrared spectroscopy in cereals. *Journal of the Science of Food and Agriculture*, *94*, 174–179.

Jin, F., Bai, G., Zhang, D., Dong, Y., Ma, L., Bockus, W., & Dowell, F. (2014). *Fusarium*-damaged kernels and deoxynivalenol in *Fusarium*-infected U.S. winter wheat. *Phytopathology*, *104*, 472–478.

Lamper, C., Téren, J., Bartók, T., Komorowski, R., Mesterházy, Á., & Sági, F. (2000). Predicting DON contamination in *Fusarium*-infected wheat grains via determination of the ergosterol content. *Cereal Reserach Communications*, *28*, 2000.

Liang, K., Liu, Q. X., Xu, J. H., Wang, Y. Q., Okinda, C. S., & Shena, M. X. (2018). Determination and visualization of different levels of deoxynivalenol in bulk wheat kernels by hyperspectral imaging. *Journal of Applied Spectroscopy*, *85*, 953–961.

Magan, N. (1993). Early detection of fungi in stored grain. *International Biodeterioration and Biodegradation*, *32*, 145–160.

Mancinelli, G., Costantini, M. L., & Rossi, L. (2014). Predicting ergosterol in leaf litter by near-infrared spectroradiometry: A preliminary assessment. *European Journal of Soil Biology*, *63*, 49–54.

Pandey, P., Srivastava, S., & Mishra, H. N. (2018). Comparison of FT-NIR and NIR for evaluation of phyisco-chemical properties of stored wheat grains. *Food Quality and Safety*, *2*, 165–172.

Peiris, K. H. S., Dong, Y., Davis, M. A., Bockus, W. W., & Dowell, F. E. (2017). Estimation of the deoxynivalenol and moisture contents of bulk wheat grain samples by FT-NIR spectroscopy. *Cereal Chemistry Journal*, *94*, 677–682.

Peiris, K. H. S., Pumphrey, M. O., Dong, Y., Maghirang, E. B., Berzonsky, W., & Dowell, F. E. (2010). Near-infrared spectroscopic method for identification of Fusarium head blight damage and prediction of deoxynivalenol in single wheat kernels. *Cereal Chemistry*, *87*(6), 511–517.

Peiris, K. H. S., Pumphrey, M. O., & Dowell, F. E. (2009). NIR Absorbance characteristics of deoxynivalenol and of sound and *Fusarium*-damaged wheat kernels. *Journal of Near Infrared Spectroscopy*, *17*, 213–221.

Perkowski, J., Bu, M., Stuper, K., Kostecki, M., Matysiak, A., & Szwajkowska-michalek, L. (2008). Concentration of ergosterol in small-grained naturally contaminated and inoculated cereals. *Biologia*, *63*, 542–547.

Pestka, J. J. (2010). Deoxynivalenol: Mechanisms of action, human exposure, and toxicological relevance. *Archives of Toxicology*, *84*, 663–679.

Ropelewska, E., & Zapotoczny, P. (2018). Classification of *Fusarium*-infected and healthy wheat kernels based on features from hyperspectral images and flatbed scanner images: a comparative analysis. *European Food Research and Technology*, *244*, 1453–1462.

Seitz, L. M. (1979). Ergosterol as a measure of fungal growth. *Phytopathology*, *69*, 1202.

Serranti, S., Cesare, D., & Bonifazi, G. (2013). The development of a hyperspectral imaging method for the detection of *Fusarium*-damaged, yellow berry and vitreous Italian durum wheat kernels. *Biosystems Engineering*, *115*, 20–30.

Stanisz, E., Zgola-Grezeskowiak, A., Stepien, L., & Beszterda, M. (2015). Can ergosterol be an indicator of *Fusarium* fungi and mycotoxins in cereals products? *Journal of Braz. Chem. Soc.*, *26*, 705–712.

Tekle, S., Mage, I., Segtnan, V. H., & Bjornstad, A. (2015). Near-infrared hyperspectral imaging of *Fusarium*-damaged oats (*Avena sativa* L.). *Cereal Chemistry*, *92*, 73–80.

Vidal, A., Sanchis, V., Ramos, A. J., & Marín, S. (2018). Stability of DON and DON-3-glucoside during baking as affected by the presence of food additives. *Food Additives and Contaminants - Part A Chemistry, Analysis, Control, Exposure and Risk Assessment*, *35*, 529–537.

Yao, H., & Lewis, D. (2010). Spectral Preprocessing and Calibration Techniques. *Hyperspectral Imaging for Food Quality Analysis and Control*, 45-78.

Chapter 6. Standardization of near-infrared hyperspectral imaging for wheat single kernel sorting according to deoxynivalenol level

Antoni Femenias, Maria Belén Bainotti, Ferran Gatius, Antonio J. Ramos & Sonia Marín

Food Research International 139 (2021) 109925

6.1. Abstract

The spatial recognition feature of HSI-NIR makes it suitable for *Fusarium* and DON management in single kernels in order to break the contamination heterogeneity in wheat batches and to replace commonly used time-consuming and destructive techniques. This study aimed to standardize HSI-NIR to predict the level of DON contamination and classify grains according to the DON EU maximum limit (1250 μg/kg) and *Fusarium* damage. The reference methods were visual inspection on *Fusarium* symptoms and HPLC analysis for DON determination. The kernels were positioned in crease-up and crease-down faces and scanned in different images. The spectra were pre-treated by MSC, SNV, 1stD and 2ndD, and normalisation. The differences of removing spectral tails also were evaluated. The best fitted predictive model was on SNV pre-treated data (R^2 0.88 and RMSECV 4.8 mg/kg), using 7 characteristic wavelengths. LDA, Naïve Bayes and K-nearest Neighbours (K-NN) models classified 100 % of the 1stD and SNV pre-treated spectra according to symptomatology and 98.9 and 98.4 % of the 1stD and SNV spectra, respectively. The starting point results encourage future investigations on HSI-NIR technique application to *Fusarium* and DON management in single wheat kernels to overcome their contamination heterogeneity.

Keywords: Hyperspectral imaging; Deoxynivalenol; Single Kernel; Near-infrared; Cereal sorting.

6.2. Introduction

DON, also known as vomitoxin, is a *Fusarium*-produced mycotoxin that presents a high incidence in wheat. DON ingestion includes a wide range of harmful effects, in which gastroenteritis and potential chronic diseases are the most frequent (Eriksen & Pettersson, 2004; Pestka & Smolinski, 2005). A significant cereal consumption in occidental countries associated with an increased incidence of mycotoxins due to global climatic change, in which high temperatures promote their production, is an issue of especial concern for human and livestock health (Nesic, Milicevic, Nesic, & Ivanovic, 2015; Uhlig et al., 2013). Due to this exposure, the European Commission established DON maximum limits for unprocessed durum wheat (1750 μg/kg), unprocessed wheat other than durum wheat (1250 μg/kg) for human foodstuffs (European Commission, 2006b) and recommended limits for animal feed (5 mg/kg) (European Comission, 2006a). As its presence is not reduced sufficiently in the pre-harvest stages, food producers demand post-harvest strategies to reduce mycotoxins in the food industry. Recent studies demonstrated that part of DON contamination remains after food processing (Vidal et al., 2016). Consequently, it should be reduced before entering the food industry.

To date, several analytical methods are accessible for DON detection in wheat batches, including HPLC, ELISA and MS. These techniques are time-consuming, expensive and, associated with low representability in sample collection in food industry entrance and increase batch rejections. DON heterogeneity causes the refusal of entire wheat lots. The methods of cereal sampling established by the European Commission (2006a) lay down that an aggregate sample weight of 10 kg, obtained from 100 incremental samples, is analysed for larger batches than 50 tonnes. Consequently, some highly contaminated kernels can disrupt the whole batch admission in the food industry according to UE legal limit, with a high impact on food chain sustainability. Rapid analyses could avoid the over-

contaminated grains, discarding them from the whole batch. As a result, a sub-batch with kernels not exceeding the DON established limits could be obtained.

HSI-NIR has been proposed as a rapid, low cost and eco-friendly technique, which permits the analysis of chemicals in a specific sample position. This method combines the spectral features of each pixel location in the image acquired. Thus, the spatial skill of HSI allows the discernment of an individual kernel light spectrum (Fox & Manley, 2014). This information is used to calibrate models to quantify DON and discard over-contaminated kernels from whole batches.

Revision articles compiled several studies referring to similar purposes attempting effective systems for cereal sorting according to fungal and DON contamination (Femenias et al., 2020a; Fox & Manley, 2014). The authors used SK-NIR to assess FDK and DON contamination. Some studies with the same aim used NIR technology recording single grain reflectance (Jin et al., 2014; Peiris, Bockus, & Dowell, 2016; Peiris et al., 2010).

However, the HSI development introduced spatial features to spectroscopic measurements, which permitted single kernel recognition in a whole image. Several authors have used HSI-NIR for *Fusarium* damage detection and classification in a wheat single-grain. Singh, Jayas, Paliwal, & White (2009) and Delwiche et al. (2010, 2011) built a DA by selecting wavelengths in NIR and Vis/NIR region spectra, respectively. All these studies used visual inspection as a reference method to discern as a sprout, midge or *Fusarium* damaged and healthy kernel. Moreover, Shahin & Symons (2011) used the same method, classifying healthy and FDK by LDA based on PCA scores. In addition, the whole Vis/NIR spectrum (450-950 nm) and six selected wavebands defined the most accurate model, also based on visual inspection.

Both studies from Barbedo et al. (2015) and Ropelewska & Zapotoczny (2018) used HSI-Vis/NIR technology for FHB and *F. graminearum* infection in individual

wheat kernels, respectively. The first study used a complex system based on the FI, which reveals the grain likelihood of being infected, to build a probability distribution function discerning between FHB and sound kernels and correlate it with DON. Based on these results, Barbedo et al. (2017) built a CM algorithm based on k values to classify kernels in two and three categories below 500 μg DON/kg, between 500 and 1250 μg DON/kg and above 1250 μg DON/kg (legal EU limit). In both cases, they used direct competitive LC-MS obtaining the reference DON concentrations of 30-50 kernel lots instead of single kernels. The second research selected three characteristic wavelengths to compare LDA, Logistic Model Tree (LMT), Partial Decision Tree (PART), Naïve Bayes and K star classifications from artificially infected and visually examined kernels. Delwiche et al. (2019) used the potential of HSI-NIR to classify sound and FDK by PLS-DA and LDA. The first classifier obtained the best results for two wavelengths selection and the second model obtained the best accuracies selecting four wavelengths between 1000-1400 nm. Single kernels also were visually checked, which introduced the inspector subjectivity to the analysis. In addition, Alisaac et al. (2019) investigated FHB in artificially inoculated wheat kernels and flour by HSI-Vis/NIR by comparing the spectral signature reflectance. Spectral profiles of FDK presented higher reflectances than non-infected ones. HSI-NIR could also be used to recognize early FHB in the field by spikelet's analysis. Alternatively, Zhang, Pan, Feng, & Zhao (2019) targeted *Fusarium* damage by the FHB classification index, calculated by, first, an extraction of four sensitive wavelengths. Then, they used PLS to determine the broadest differences in the spectral index (two bands extraction) to calculate both best combinations and detect and classify healthy and damaged wheat kernels according to the index.

Despite the studies applying HSI-NIR on single wheat kernels to detect and classify DON, batch heterogeneity remains an issue in the so-far published studies. The present work aims to overcome the kernel diversity by

standardization of HSI-NIR to screen kernels by DON level. To reach this purpose, spectral pre-treatments, wavelength selection and model calibrations were performed, mainly using PLS for single kernel DON quantification and LDA for individual kernel classification.

6.3. Materials and methods

6.3.1. Wheat samples

A feed producing agricultural cooperative supplied the wheat samples during 2018-2019. Their origin was the plain area of Lleida province. They were from the quality control programme from each incoming truck. A subsample (200–500 g), arising from the whole homogenized batch, was given to our laboratory. A total of 18 kernels from a non-contaminated sample were selected to validate the UHPLC analytical method and 50 grains from a highly-contaminated for the experimental analysis.

6.3.2. Visual symptoms assessment

The 50 kernels used for the experimental study were selected manually and divided into three levels (symptomatic, mildly-symptomatic and asymptomatic) according to visual symptoms of fungal infection. Discoloured, shrivelled and wrinkled kernels were considered symptomatic (S). The grains with part of these symptoms were considered mildly symptomatic (M), and the ones not presenting visible signs as asymptomatic (A). The grains were selected trying to cover, as wide as possible, all the visual kernels characteristics. Consequently, the percentage of kernels with symptoms in our working sample set was higher than in the original sample.

6.3.3. HSI-NIR experimental work

6.3.3.1. Instrumentation and data acquisition by HSI-NIR

A Pika NIR-320 camera assembled in RESONON Inc. (Bozeman, MA, USA) was used in this study, scanning with push-broom mode to obtain the hyperspectral images. The device consists of an InGaAs sensor line scan camera with 320 × 256-pixel resolution, a 30 × 30 μm pixel size and a 14-bit resolution A/D spectrograph (Goldeye G-008 SWIR TEC1, Allied Vision Technologies GmbH, Germany). The framerate was 520 fps, combining the spectral resolution of 4.9 nm (164 spectral bands from 900 to 1700 nm) and a spatial resolution of 320 pixels. The objective lens was positioned 220 mm above the scanning surface and had 24 mm of focal length (F/1.4 SWIR, 0.9–1.7 μm, 21 mm image format, c-mount). The illumination device consisted of four halogen lamps lighting systems with Lambertian filters fixed on an adjustable tower. The lights were turned on at least 20 minutes before taking the images to ensure the stability of light beams. Samplexpower® power converter (SEC-1223CE, Burnaby, BC, V5A 0C6, Canada) powered the illumination system, which provides a highly regulated output DC voltage of 13.8 V at 23 Amps with an AC input of 230 V, 50 Hz. Lastly, the fixed optical devices could register entire samples due to a motor-powered linear translation stage of 600 mm.

The Spectronon PRO software permitted the Resonon's benchtop control before and after the image acquisition. The captured intensities of each sample data array were transformed automatically to reflectance by dividing the dark current by the dark subtracted white standard at each of the corresponding wavelengths (1). A dark correction image was obtained before samples' scanning, removing the dark noise by the camera lens cover. Likewise, the intensity from a 99% reflectance standard, made of polytetrafluoroethylene (PTFE) (Spectralon™, SRT-99-120, Labsphere, North Sutton, NH, USA) to correct lighting effects, was

registered immediately after the dark image. These two images were applied to the subsequent sample intensities as the equation 1:

$$I = \frac{I_0 - I_b}{I_w - I_b} \qquad (1)$$

where I_0 is the raw hyperspectral image obtained, I_w is the white reference and I_b is the dark current reference. Apart from the dark and absolute reflectance response, the camera controls also were used to correct the pixel illumination saturation. Framerate and integration times were set, ensuring that no pixel on the image was saturated.

The 50 wheat kernels were first scanned in triplicate individually for both positions (crease-up and crease-down). The kernel location was adjusted on the scanning plate, recording all the grains spectra at the same image position. The Spectronon PRO software provided the mean raw and the mean 1stD spectrum of each kernel. Subsequently, the same 50 grains were placed on the scanning tray shifting positions, repeating the process in triplicate for both kernel faces. Images adjusted to 350 bands for the horizontal axis and approximately 90 mm for the vertical. The pixels were selected with the mean and mean 1stD reflectance's of similar spectrum pixels by Euclidian distance best adjusted to the ROI to remove the background signal. Both spectra for each kernel, saved as a text file, were subsequently exported to the spectral analysis software

6.3.4. Determination of DON concentration in wheat kernels by UHPLC

6.3.4.1. Reagents and chemicals

Milli-Q® SP Reagent water system from Millipore Corp. (Brussels, Belgium) gave the water. Methanol (HPLC grade) was from Scharlab (Sentmenat, Spain) and the DON standards from Romer Labs (Tulln, Austria). Finally, IAC for DON (DONPREP®) came from R-Biopharm (Rhone LTD Glasgow, UK).

6.3.4.2. Preparation of DON solutions

DON concentration in the stock solution, checked by UV spectroscopy according to AOAC Official Methods of Analysis, Chapter 49 (AOAC, 2005), had a concentration of 962 μg/mL. Standard solutions of DON were prepared in methanol at a concentration of 10 μg/mL and stored at 4 °C. Calibration curves were prepared appropriately by diluting known volumes of the stock solution with the mobile phase.

6.3.4.3. IAC extraction of DON from wheat kernels for analytical method validation

The 9 kernels from a non-contaminated sample used in this section were previously analysed twice by UHPLC (< LOD). Individual grains were spiked at different contamination levels before DON extraction with specific IAC (DONPREP®) following the manufacturer's instructions. A single wheat kernel previously crushed and pulverized with a small mortar and pestle was mixed with 1.5 mL of MiliQ water in a 1.5 mL Eppendorf tube, followed by 10 min stirring. Then, samples were centrifugated for 10 min at 1780×g, repeating this process three times to obtain a supernatant extract with a final volume of 4.5 mL. The filtrate, passed through the IAC and washed with 10 mL of bi-distilled water, contained the toxins, eluted with 3 mL of methanol HPLC-grade (the first 1.5 mL performing back-flushing). Samples were evaporated under a low nitrogen steam at 40 °C and resuspended in 0.3 mL of mobile phase (methanol:water, 10:90, v/v). All the resuspended extracts passed through a nylon filter (0.4 μm) before being injected into the UHPLC-DAD system.

6.3.4.4. Direct extraction of DON from wheat kernels for analytical method validation

The other 9 kernels from the same sample, used in the previous section, were also spiked at two different levels before their direct extraction. Concisely, individual wheat kernels, previously ground with a small laboratory mortar and pestle, were mixed with 0.3 mL of MiliQ water in 1.5 mL Eppendorf tubes, followed by

a 10 min vortexing. Then, samples were centrifugated for 10 min at 1780×g. The supernatant passed through a nylon filter (0.4 μm) before being injected into the UHPLC-DAD system.

6.3.5. Performance of the UHPLC analytical method

Selectivity was checked by injecting 50 μL of standard solution at least three times (150 μg/L) and comparing retention time and peak resolution between injections. For linearity check, a calibration curve, using eight concentration levels for DON solutions (20, 30, 50, 100, 250, 500, 1000, 3000 μg/L solutions), was prepared and injected into the system, generating a linear regression plotting solutions' concentration versus peak area according to the methodology used by (Wall-Martínez et al., 2019). The method performance, obtained according to Commission Regulation (EC) 401/2006 (European Commission, 2006c), gave the curve ability to predict DON concentrations. Precision was determined by preparing blank kernels, and kernels spiked with DON at several levels and obtaining the recovery percentages: 64–105% (direct extraction), 68–125% (IAC extraction) (Table 11).

Table 11. Performance of methods for the determination of DON from wheat kernels.

Mycotoxin	Extraction	[a]LOD (μg/kg)	[b]LOQ (μg/kg)	n	Spiking level (μg/kg)	[c]Recovery (%)	[d]RSDr (%)
DON	Direct	100	300	5	1000	87 ± 10	12
	IAC	100	300	4	1500	93± 17	19
				5	700	111 ± 9	8.2
				4	1250	80 ± 17	21

[a] LOD = limit of detection. [b] LOQ = limit of quantification. [c] Mean value ± standard deviation. [d] RSDr = relative standard deviation.

The recovery rates obtained for DON in single kernels for direct and IAC extraction were similar. Still, the direct extraction seems to be more suitable for small samples to avoid more steps, which could lose the toxin. Furthermore, this study used direct extraction due to its effectiveness, quickness and low costs (European Commission, 2006c).

6.3.5.1. Direct DON extraction from wheat kernels for experimental work

A highly-contaminated sample was selected, previously analysed twice by UHPLC (2682.8 and 2403.5 μg/kg). A total of 50 wheat kernels, arising from this sample, were selected, presenting a mean weight of 33 mg in a range between 11.3 to 53.4 mg per kernel. DON was extracted from every grain with Mili-Q water following the same methodology used in the direct DON extraction to validate the analytical method.

6.3.5.2. UHPLC system

DON was determined using an Agilent Technologies 1260 Infinity UHPLC system (California, USA) coupled with an Agilent 1260 Infinity II DAD. The device had a Gemini® C18 column from Phenomenex 150 × 4.6 mm (California, USA) with a particle size of 5 μm and a pore size of 110 Å. The absorption wavelength was 220 nm. The mobile phase was methanol:water (10:90, v/v) and had a flow rate of 1 mL/min. The column temperature was 40 °C, the injection volume was 50 μL, and the total run time was 15 min for mycotoxin analyses. The performance of the quantification method for DON in wheat was determined, considering the limit of detection (LOD) as three times the signal of the noise (100 μg/kg). Once quantified, the kernels were categorised as contaminated above the EU legal limit (C) and below (B) for subsequent classifications.

6.3.6. Hyperspectral data modelling for quantification and classification of DON contaminated kernels

Spectral data were processed using The Unscrambler software (version 7.6 SR1, CAMO, Oslo, Norway, 2001). First, to compare the spectral differences between high-contaminated (≥ 1250 μg/kg) and low-contaminated kernels (< 1250 μg/kg), a linear representation of the mean spectral profile was performed. Once established the reflectance differences, the DON predictive models were calibrated by using the single kernel spectral information. The calibration was performed by recording mean reflectances of the pixels from the kernel as the explanatory variables (X) and the DON concentrations (from <LOD to 79.7 mg/kg) obtained by UHPLC as the dependent variables (Y). A total of 150 images (arising from 50 kernels) were obtained to develop a leave-one-out cross-validated prediction and classification models by leaving out a single sample of the training set for each iteration and using it to validate the corresponding model. This validation is considered the most realistic to obtain the closest prediction parameters to the independent set validation. However, it is used when a large sample size, separated between calibration and validation sets that can guarantee the representativeness of the population of samples, is not available. In our case, our sample size is small (150 images from 50 kernels), so we used leave-one-out cross-validation, removing a single sample from the training set for each iteration. The spectra were recorded with Spectronon PRO, testing the mean spectra of the kernel pixel's for crease-up and crease-down positioned kernels for single kernel and fifty-kernel images.

First, the spectral data were pre-processed by applying different pre-treatments apart from the raw and 1stD ones obtained directly from the Spectronon PRO software. The spectral array was imported to The Unscrambler software, and scatter correction pre-treatments were applied to minimise the non-linear effect of light scatter due to particle size differences among samples, as MSC and SNV.

The first and second derivatives were applied to remove noise, multiplicative and additive effects, selecting 5-point Savitzky-Golay derivates. There is no standard optimum pre-treatment for a specific type of data, as it depends on the signal (reflectance, absorbance or transmittance), sample features, instrument configuration or trial (prediction or discrimination). Consequently, its selection needs a trial and error process followed by experience.

Delwiche (1998) reported possible nonlinearities between reflectances at spectral extremes and the single kernel components. Thus, we aimed to check if there was a substantial enhancement in the model when removing the extremes. Moreover, Agelet, Armstrong, Romagosa-Clariana, & Hurburgh (2012) also improved their model performance by removing the noisy extremes of the NIR range in a single kernel analysis. Consequently, we also subtracted the spectral tails, leaving a short wavelength range of 1000-1650 nm.

The prediction models, which used short and large spectral ranges and each pre-treatment by PLS regression, were calibrated. The models were refined to obtain the lower RMSECV. The RMSECV is defined as:

$$RMSECV = \sqrt{\frac{\Sigma\,(\hat{y}_i - y_i)^2}{n}} \qquad (2)$$

In which $\hat{y}_i$ = ith validation sample predicted value; y_i = ith validation measured values; $\bar{y}$ = mean of the n values (measured or predicted), n = number of samples.

For model depuration, data points that differed significantly from the other samples were considered outliers. The criteria followed for outlier exclusion was to represent the residual influence plot, representing the residual Y variance versus the leverage. Those samples that presented high values of both parameters were removed one by one, and the models recalculated for each rejection. The outlier detection removed less than 10 % of the original spectra. In addition, the overriding criterion for the optimal PC of the model selection was the first PC which presented a minimum on the RMSECV curve. Finally, the

regression coefficients of the PCA representation, able to separate high (≥ 1250 µg/kg) and low (< 1250 µg/kg) contaminated DON kernel groups (marked as (B) and (C) in the previous section), gave the characteristic wavelengths (the spectral band which had the highest weight on the model). The performance parameters determined the fitness of the models, which consisted in the slope and offset, correlation (R), R_{cv}^2, RMSEC, RMSECV, Standard Error of Cross-Validation (SECV) and bias. Finally, the ratio of prediction to deviation (RPD), which is the ratio between the laboratory-measured data standard deviation to the RMSE of cross-validation, was estimated (3) according to Rossel, Mcglynn, & Mcbratney (2006):

$$\mathrm{RPD} = \frac{\mathrm{Sdev}}{\mathrm{RMSE}} \qquad (3)$$

The RPD distinguish between five levels: excellent predictions (RPD > 2.5); good (RPD of 2.0 to 2.5); approximate quantitative predictions (RPD of 1.8 to 2.0); possibility to distinguish high and low values (RPD of 1.4 to 1.8); and unsuccessful (RPD < 1.40). The best-fitted models were ones combining the closest to 1 for slope and R^2, the highest RPD and the lowest RMSECV and the number of PC. Most of the models presented excellent predictions as they achieved RPD > 2.5 due to low errors of predictions in models and a high standard deviation in reference values.

For the best models, characteristic wavelengths were the ones that presented high positive or negative regression coefficients. They were recalibrated only with the spectral bands contributing substantially to explaining DON variance within the model.

The same 50 kernels previously used were classified according to visual symptoms and DON. Statistical analysis was performed with JMP PRO 14.1.0 (SAS Institute Inc., 2018) software using LDA, Naïve Bayes Confusion, K-NN and Neural Networks. Classification models were also cross-validated by a leave-

one-out method. The concentration threshold was 1250 μg/kg. As stated before, spectra from kernels above this limit formed the group (C) and from below the limit formed the group (B). The classification accuracies and the false-negative percentages provided the model performances. Neural networks tended to over-fit data for such a reduced data set. Thus, it was discarded from the results, although future testing on a broader sample set will be essential to develop robust neural network models. Figure 20 represents, in a schematic way, the steps mentioned in the previous sections to bring an overview of the methodology

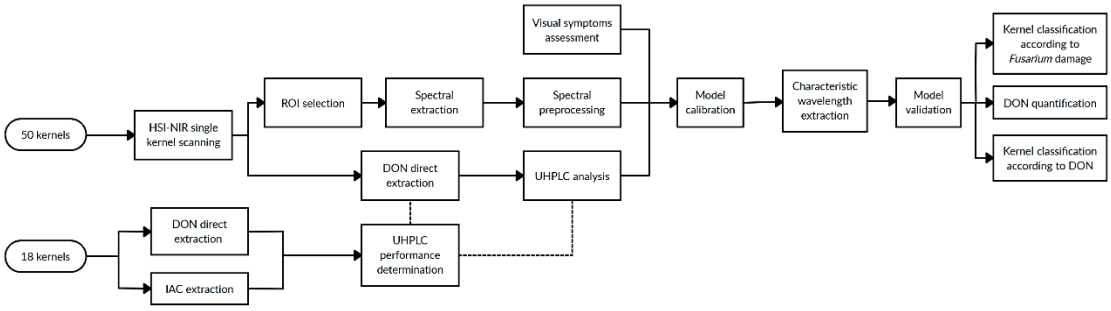

Figure 20. Schematic representation of the methodology for SK-HSI analysis.

used in the study.

6.4. Results

6.4.1. Comparison of spectral profiles

The mean spectral profiles of crease-down and crease-up positioned kernels for single kernel images and crease-down located for one picture containing the fifty grains are represented in Figure 21. The blue-coloured spectral profiles belong to the high-contaminated kernels (≥ 1250 μg/kg), and the red-coloured profile refers to the low contaminated grains (< 1250 μg/kg). The contaminated ones presented higher reflectances than low-contaminated, although kernels spectral shapes remained visually similar in all the cases. Consequently, as we cannot attribute any change in a specific spectral band associated with DON concentration,

multivariate analysis methods are needed to explain the spectral variability and associate them with DON contamination.

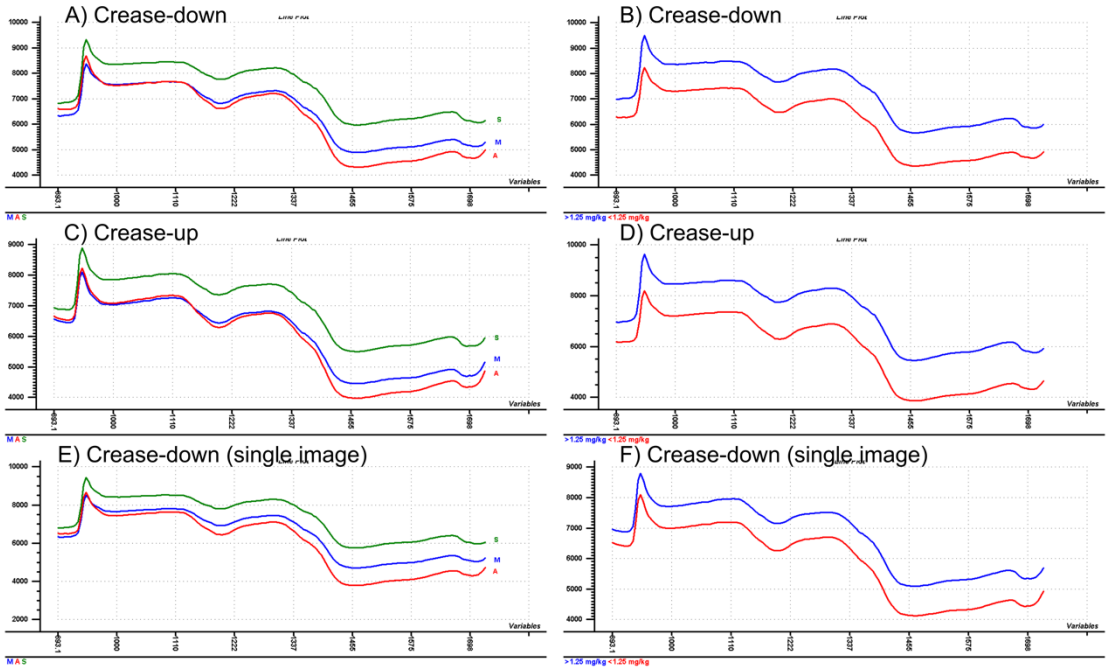

Figure 21. Symptomatology and DON effect on spectral profiles depending on kernel position and image acquisition (raw reflectance's). A) Mean spectra of crease-down positioned kernels for each symptomatology category (one image per kernel). B) Mean spectra of crease-up positioned kernels for each symptomatology category (one image per kernel). C) Mean spectra of crease-down positioned kernels for each symptomatology category (one image for the 50 kernels). Categories: A = Asymptomatic (red); M = Mildly-symptomatic (blue); S = Symptomatic (green). D) Mean spectra of crease-down positioned kernels DON level (one image per kernel). E) Mean spectra of crease-up positioned kernels DON level (one image per kernel). F) Mean spectra of crease-down positioned kernels DON level (one image for 50 kernels). DON levels: ≥ 1.25 mg/kg (blue); < 1.25 mg/kg (red).

6.4.2. Single kernel DON variability

Table 12 includes the descriptive statistics of the kernels used in the experimental work. As indicated before, the results correspond to the direct DON extraction methodology. The parameters reported are the DON content and single kernel weight. The minimum DON content of a single kernel was below the LOD, while

the maximum was 78.7 mg/kg. The mean concentration of the dataset was 12.9 mg/kg. It is interesting to suggest that the differences between this mean and the original sample concentration analysed twice (2682.8 and 2403.5 μg/kg) could be explained by the manual selection of the broader symptomatology range. In addition, the single kernel weight range includes loads from 11.3 mg to 53.4 mg. Figure 22 shows the frequency and distribution of single kernel DON content measured by the UHPLC system used in this study. Figure 22a describes the frequency and distribution of samples regarding DON contents. A 68 % of the kernels had a DON content from below the LOD to 10 mg/kg, including the maximum UE legal limit (1.25 mg/kg). The rest of the kernels presented lower frequencies for higher intervals, as higher concentrations of DON are rarer in naturally contaminated wheat. The distribution of the reference DON content in the single kernels is asymmetric under the mean, as 40% of the sample set had DON concentrations below the LOD. Thus, it does not follow a Gaussian distribution due to many environmental and harvest causes. Figure 22b shows the highest frequency in kernels between 20-25 mg, which corresponds to 20% of the entire sample set. Kernel weight could vary due to fungal infection, as its weight loss is a characteristic symptom of fungal growth.

Table 12. Descriptive statistics for the variables used in the present work.

		Mean	**Range**	**SDev**	**CV (%)**
Data set	DON content (mg/kg)	12.9	< 0.1 – 79.7	21.3	163.2
	Kernel weight (mg)	33.0	11.3 – 53.4	11.4	34.6

SDev = standard deviation; CV = coefficient of variation.

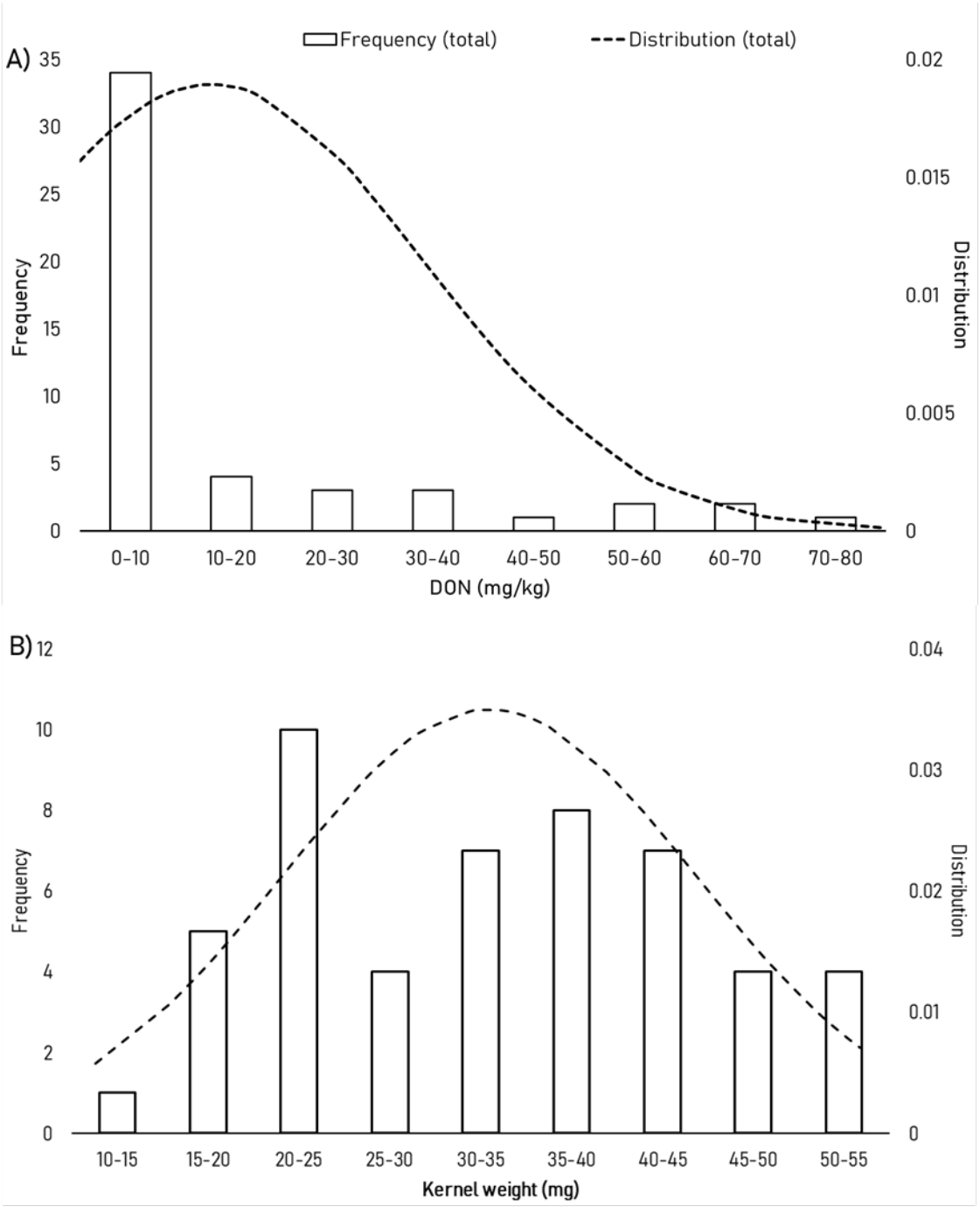

Figure 22. Distribution of DON content and kernel weight in single wheat kernels on the full dataset. A) Total kernel DON frequency and distribution. B) Total kernel weight frequency and distribution.

6.4.3. Quantification of DON concentration in single wheat kernels based on spectral data

The quantifications considered the effect of several conditions (pre-treatment, spectral region, kernel position and number of images). Table 3 (annexe) collects all the regression performance parameters for cross-validated models. Although the crease-up or crease-down positions had no notable performance differences, individual kernel images or 50 kernel images presented some differences. Also, the effect of the kernel position and removing spectral bands from the extremes were estimated, leaving a wavelength range from 1000-1650 nm.

Different spectral pre-treatments to quantify DON were tested before PLS regression, showing a substantial effect on the model performances. However, four models were selected for their high-performances and positive adjustments, representing their regression plots in Figure 23. The two best pre-treatments were SNV and 1stD, or the combination of both.

Table 13. Performance parameters of PLS regressions from selected optimal wavelengths.

Model	Optimal wavelengths (nm)	Slope	RMSECV (mg/kg)	R^2	SEP (mg/kg)	PC	RPD
SNV	1198, 1322, 1353, 1428, 1445, 1497, 1549	0.88	4.8	0.88	4.8	6	4.4
1stD	1112, 1205, 1345, 1401, 1452, 1499, 1525, 1541	0.79	8.1	0.78	8.1	6	2.6
1stD + SNV	1325, 1396, 1406, 1421	0.81	6.1	0.81	6.1	3	3.4

Table 13 includes the bands and the performance parameters of the models. Model A presented enhanced results, with a higher R^2 (0.88) and lower RMSECV (4.8 m/kg) with only 6 PC and 7 bands. In addition, model C presented slightly

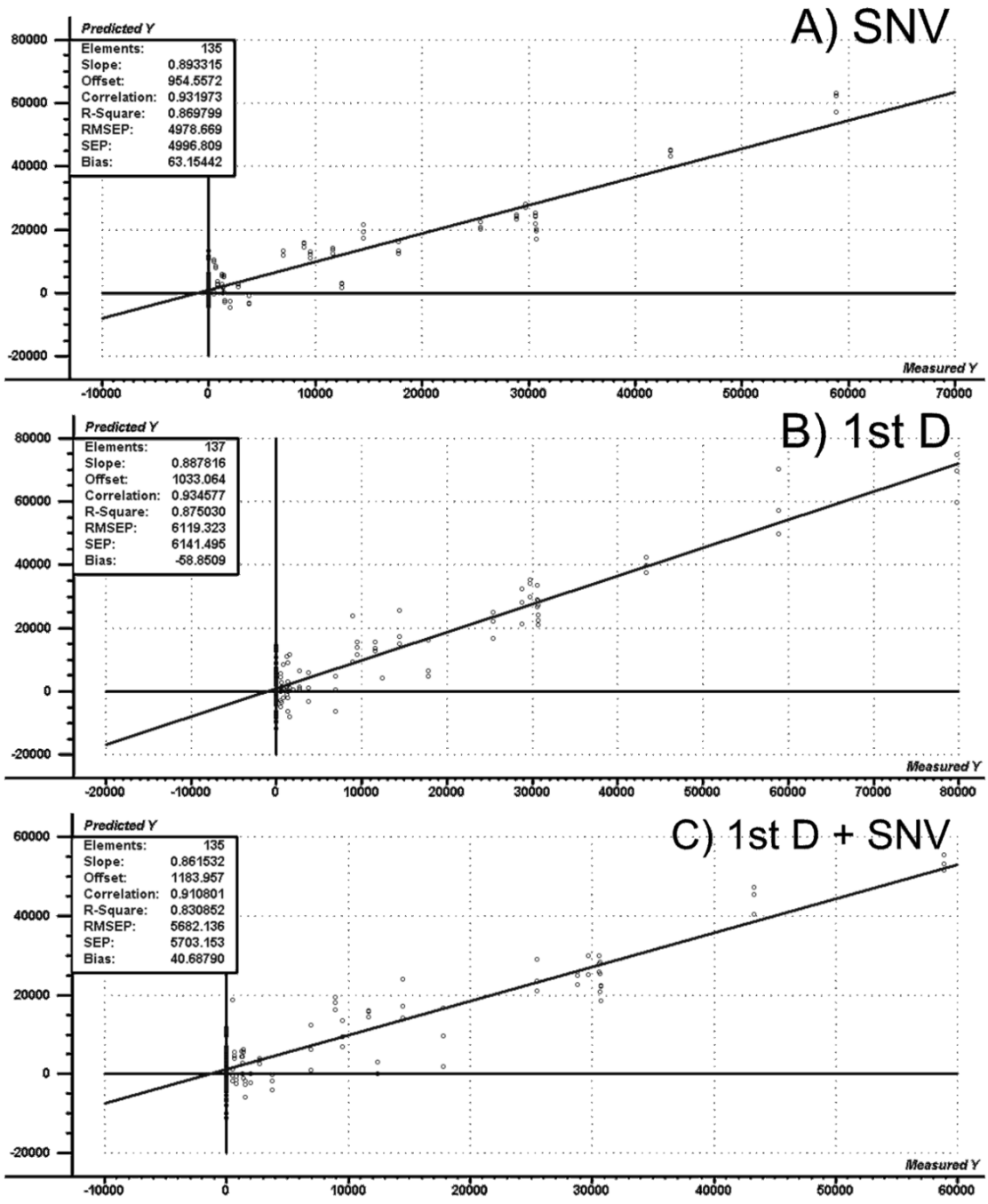

Figure 23. Predicted vs measured plots of cross-validated models. Spectral range: 1000-1650 nm. A) SNV pre-treated model for crease-up kernel position; n = 135; optimum PCs = 10. B) 1st derivative pre.treated model for crease-up kernel position; n = 137; optimum PCs = 13. C) 1st derivative + SNV pre-treated model for crease-up kernel position; n =135; optimum PCs = 8.

under-fitted results compared to the whole spectra model. Thus, a well-fitted model is obtained with a reduced wavelength number (4). As the model complexities are reduced to multispectral dimension by optimal wavelengths selection, they are closer to online DON detection.

6.4.4. Classification of single kernels according to visual symptoms by LDA

PCA was used for a first screening to discern between symptomatology, estimating the ability of HSI-NIR to discriminate between levels of symptomatology (asymptomatic, mildly-symptomatic and severe-symptomatic). Almost all the models showed a tendency to differentiate between those groups, as shown in Figure 24. However, 1stD seemed to be the pre-treatment that presented the best separation into three groups. Consequently, classification models, such as LDA, Naïve Bayes and K-NN, were performed, discriminating samples according to typical visual symptoms (shrivelling, discolouration and wrinkling) in fungal-contaminated wheat. The classifications contemplated the effect of the pre-treatments used in the DON quantification section.

The results do not show differences for those conditions, except for spectral pre-processing. Table 14 shows the mean accuracies for each analysis type and pre-treatment. Naïve Bayes algorithms presented inefficient classifications because the conditional probabilities of class membership are assumed, independent. Classifications were above the 88.8 % to 97.6% of accuracy for K-NN predictions, although they correspond only to its calibration. Thus, those results would be overestimated compared to a validated model. The highest accuracies were for LDA cross-validated models, 1stD spectra, and the combination of 1stD and SNV

pre-treatments, presenting correctness of 100%. The classification results, including all the conditions independently, are represented in Table 14.

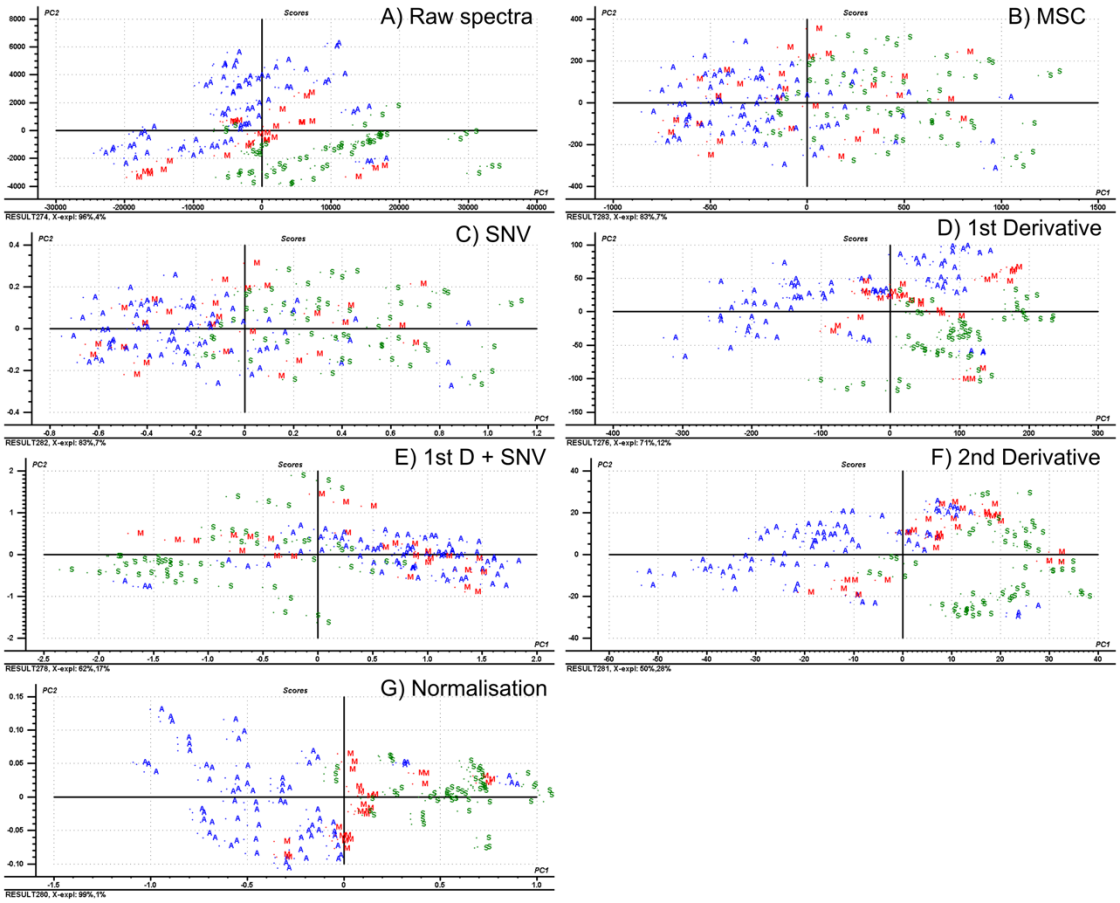

Figure 24. PCA scores for visual symptoms screening. A = asymptomatic; M = mildly-symptomatic; S = symptomatic. A) Raw spectra, X-exp: 96%, 4%. B) Multiplicative Scatter Corrected spectra, X-exp:83%, 7%. C) SNV corrected spectra, X-exp: 83%, 7%. D) 1st Derivative spectra, X-exp: 71%, 12%. E) 1st Derivative + SNV corrected spectra, X-exp: 62%, 17%. F) 2nd Derivative spectra, X- exp: 50%, 28%. G) Normalised spectra, X-exp: 99%, 1%.

Table 14. Classification accuracies (mean values) for single kernel classification according to symptomatology. A = asymptomatic; M = mildly-symptomatic; S = symptomatic. Correctly-classified kernels correspond to grey cells numbers.

		Pre-treatment																				
		Raw spectra			**MSC**			**SNV**			**1st D**			**2nd D**			**1st D + SNV**			**Normalisation**		
	Symptomatology	A	M	S	A	M	S	A	M	S	A	M	S	A	M	S	A	M	S	A	M	S
LDA	A	56.2	4.7	0.3	63.2	3.5	0.3	62.5	4.3	0	69	0	0	58.3	3	5.8	69	0	0	59.7	4	0
	M	9.3	17.8	10	3.3	22	3.7	3.5	20.5	5.5	0	27	0	4	21	2.2	0	27	0	7.7	19.8	6.3
	S	3.5	4.5	43.7	2.5	1.5	50	3	2.2	48.5	0	0	54	6.7	3	46	0	0	54	1.7	3.2	47.7
	Accuracy (%)		78.4			90.1			87.7			100			83.6			100			84.8	
Naïve Bayes	A	55.5	15.3	10.2	54.5	11.8	8	31.7	6.8	5.2	46.5	3.5	0.5	53.2	5	1.3	55	7.5	2.8	50.5	3.2	0
	M	3.5	3	12	7.5	10	10.2	29.8	14.8	15.7	19.5	20	5.5	12.2	18.5	6.5	6.2	13.2	7	14.5	18.8	11.7
	S	10	8.7	31.8	7	5.2	35.8	7.5	5.3	33.2	3	3.5	48	3.7	3.5	46.2	7.8	6.3	44.2	4	5.0	42.3
	Accuracy (%)		60.2			66.9			53.1			76.3			78.6			74.9			74.4	
K-NN	A	64	4.3	0.7	62.7	4.8	2.2	62.7	4.7	2.8	66.3	3.8	1.8	65	3	3.2	66.2	3.3	3.3	68	1.5	0.3
	M	3	20.2	3.2	4.5	20.2	1.5	4	20.5	1.3	1.7	21.3	1.3	3.3	21.7	1.7	1.8	22.2	1.2	1	24.8	0.2
	S	2	2.5	50.2	1.8	2	50.3	2.3	1.8	49.8	1	1.8	50.8	0.7	2.3	49.2	1	1.5	49.5	0	0.7	53.5
	Accuracy (%)		89.6			88.8			88.7			92.3			90.6			91.9			97.6	

6.4.5. Classification of single kernels according to DON levels by LDA

The 68.3% of the kernels were symptomatic and contaminated over the EU limit and asymptomatic and below the limit. Thus, the remaining 31.7% were the grains that, although they had no symptoms, were heavily contaminated or even presented fungal changes, did not have DON. In addition, the DON content regarding other components of the sample, e.g. starch, protein and moisture, makes the ability to discern between levels challenging.

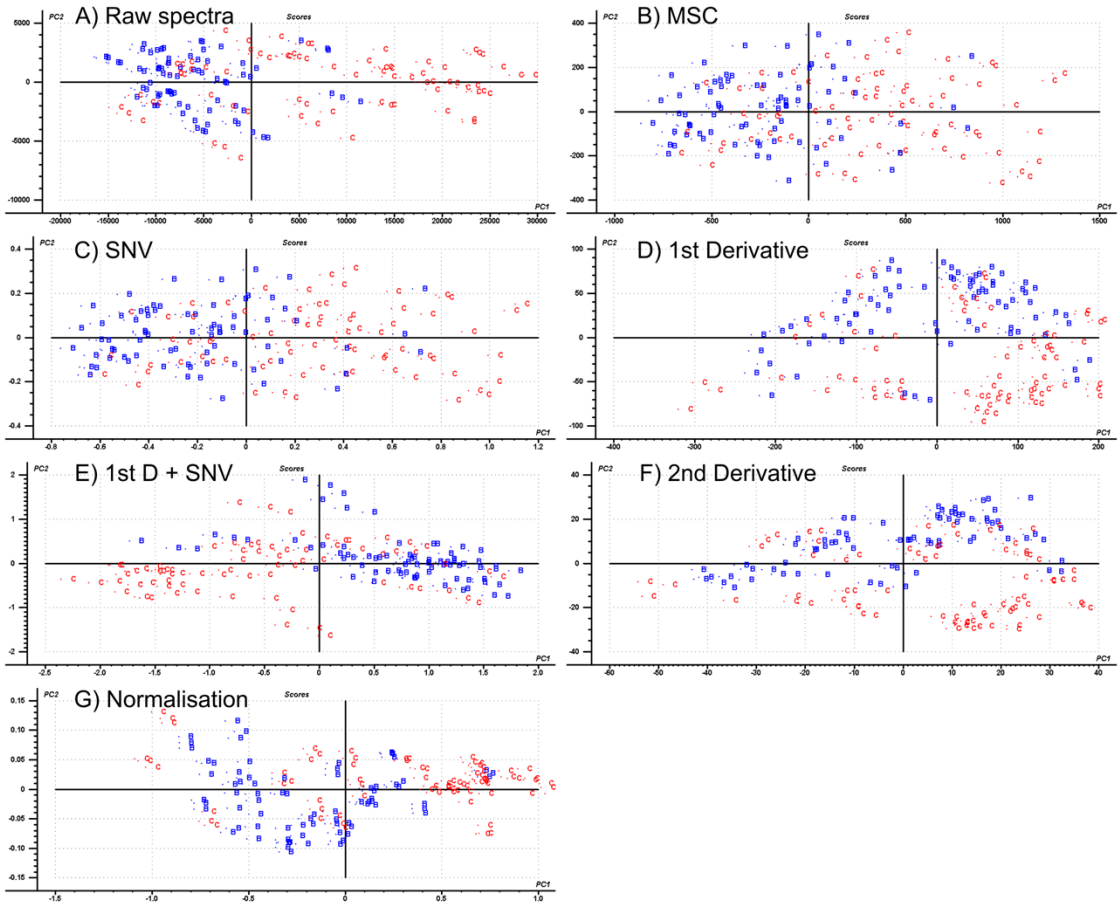

Figure. 25. PCA scores for visual DON screening. B = < 1250 µg/kg kernels; C = ≥ 1250 µg/kg kernels. A) Raw spectra, X-exp: 96%, 4%. B) Multiplicative Scatter Corrected spectra, X-exp:83%, 7%. C) SNV corrected spectra, X-exp: 83%, 7%. D) 1st Derivative spectra, X-exp: 77%, 14%. E) 1st Derivative + SNV corrected spectra, X-exp: 62%, 17%. F) 2nd Derivative spectra, X- exp: 50%, 28%. G) Normalised spectra, X-exp: 99%, 1%.

A prior PCA analysis was performed to assess the ability of the NIR spectra to distinguish between samples contaminated above and below the UE maximum limit of DON (1250 μg/kg) (Figure 25). The classifications of kernels according to the 1250 μg/kg threshold presented results similar to symptomatology.

discrimination, although the match between symptomatology and DON levels was low. The highest discrimination accuracies were obtained for the cross-validated LDA models with a mean of 98.9 % for the 1stD spectra and 98.4 % for the combination of 1stD and SNV, represented in Table 15. For Naïve Bayes and K-NN algorithms, the classifications were from 73.4 to 81.9 % and 85.2 to 96.4 %, respectively. The compilation of the results for each condition is presented in Table 15.

Table 15. Classification accuracies (mean values) for single kernel classification according to DON levels. B = < 1250 µg/kg; C = ≥ 1250 µg/kg. Correctly-classified kernels correspond to grey cells numbers.

		Pre-treatment													
		Raw spectra		**MSC**		**SNV**		**1st D**		**2nd D**		**1st D + SNV**		**Normalisation**	
	DON levels	B	C	B	C	B	C	B	C	B	C	B	C	B	C
LDA	B	65.5	24.3	74.2	10.7	72.8	12.7	74.5	1.2	62.8	11.8	73.7	1	64.5	22
	C	9.5	50.7	0.8	64.3	2.2	62.3	0.5	73.8	12.2	63.2	1.3	74	10.5	53
	Accuracy (%)	77.4		92.3		90.1		98.9		84		98.4		78.3	
Naïve Bayes	B	63.7	28.5	68.3	20.5	66.2	28.3	61	18.2	63.5	21.7	62	21.5	58.7	23.5
	C	11.3	46.5	6.7	54.5	8.8	46.7	14	56.8	11.5	53.3	13	53.5	16.3	51.5
	Accuracy (%)	73.4		81.9		75.2		78.6		77.9		77		73.4	
K-NN	B	64.2	11.3	70.8	7	69.5	7.7	69.5	6.7	67.7	7.3	70.2	6.3	72.3	2.7
	C	10.8	63.7	4.2	68	5.5	67.3	5.5	68.3	7.3	67.7	4.8	68.7	2.7	72.3
	Accuracy (%)	85.2		92.6		91.2		91.9		90.2		92.6		96.4	

6.5. Discussion

DON heterogeneity from a single batch is demonstrated in this irregular distribution, as its kernels can be infected from extremely high concentrations up to 79.7 mg/kg to undetectable levels. In addition, kernel weight could also affect NIR images acquisition, so its management is crucial to avoid measurement interferences. FDK and DON contaminated kernels had higher spectral intensities than healthy and uncontaminated ones. To summarize the results, the standardization of the methodology, quantifying DON and classifying grains according to their visual symptoms and DON levels, presented positive results for a reduced sample set. The results demonstrated that 1stD pre-treatment, SNV or both combined had the best PLS regressions performances and LDA accuracies. In addition, the outcomes confirmed that the kernel position and the image acquisition (one image for each kernel or one image for all) did not affect the results, selecting the single image for dorsally positioned grains for its low operation complexity. In addition, the re-calibration of models using only the optimal wavelengths reduced the complexity of the regression and maintained their adjustment. Consequently, this methodology will offer a rapid scanning of lots of kernels for its possible adaptation to industry, as most of the applied online detection models in the industry use multispectral analysis.

The present study achieved lower errors of prediction for DON than one of the first studies trying to quantify DON concentrations in single wheat kernels (Dowell et al., 1999), for which SEC was 44 mg/kg and R_c^2 of 0.64. To validate, they used 20% of kernels from the original 88, obtaining an SEP of 52 mg/kg and an R^2 of 0.66. Even though our research was cross-validated, not being entirely comparable with their validation results, their calibration results were weaker than the R_{cv}^2 of 0.88 and 4.8 mg/kg RMSECV obtained in our work. Jin et al. (2014) and Peiris et al. (2010) evaluated the SK-NIR reflectance for FDK and DON estimation. The results were different from ours since they worked with DON

contamination ranges from 0.49 to 29.5 mg/kg and 0.2 to 1008.4 mg/kg, respectively. However, the correlations obtained for Visual-FDK/SK-NIR FDK and GC-MS-DON/SK-NIR-DON were weak (0.72 and 0.49). Peiris et al. (2010) obtained an R_{cv}^2 of 0.72 and an SECV of 154.2 mg/kg for DON quantification, a 98.8 and 99.9% of correct classification of sound and damaged kernels and a 95.7 and 96.7% of the correctness of DON contamination above and below 60 mg/kg, respectively. Thus, our results presented higher DON prediction and classification accuracies, despite the different range of contamination and classification threshold. Polder et al. (2005) measured in transmittance mode instead of reflectance, not only the surface of the kernels but also the inner part, detecting *Fusarium*.

The spatial ability of hyperspectromics permitted the analysis of a single kernel as the ROI from a whole image. As in our previous study (Femenias et al., 2020b), PCA evaluated the data before LDA classification to show differences in kernels symptomatology and DON contamination. The results confirmed the tendency to discriminate between classes extracting the most relevant information and compressing it into new orthogonal variables, although evaluations require LDA to overcome the covariance in the data matrix. Singh et al. (2009), Delwiche et al. (2011) and Shahin & Symons (2011) established a DA by selecting specific wavelengths of the NIR and the Vis/NIR spectra. The first research accomplished an LDA classification of 100% between healthy and damaged kernels with only three wavelengths (1101.7, 1132.2 and 1305.1 nm). Our studies also achieved the same accuracy using the whole spectra but using the 1^{st}D or combined 1^{st}D + SNV spectra pre-treatment, and our characteristic bands only can be comparable in the 1100-1200 nm region. Moreover, Delwiche et al. (2011) LDA results achieved a mean accuracy of 95%, for which the 1200 nm region (related with ergosterol absorption) was a remarkable wavelength for damage determination. Finally, Shahin & Symons (2011) classified FDK kernels by a combined LDA-PCA

method, achieving an accuracy of 92% for the validation set. Even though we cross-validated the LDA, our accuracies are higher than the calibration results obtained by these authors (93%).

A method based on FI, which is the likelihood of a kernel of being infected by *Fusarium*, was used by Barbedo et al. (2015) to assess FHB in 50 individual grains by HSI-NIR screening. It is essential to state that visual inspection is subjective for fungal contamination perception. In some cases, the damage is not appreciable when an early stage fungal infection, making the detection by humans and devices remain indiscernible. However, the direct detection of FHB was 91 %, obtaining a FI correlation with DON contamination of 0.84. Moreover, Ropelewska & Zapotoczny (2018) also classified *Fusarium* infected kernels using HSI-Vis/NIR. They used some of the same discrimination models we employed (LDA and Naïve Bayes), even though they used a single selected wavelength. Their higher accuracies were using the ventral side for 550 and 710 nm bands, which were not in our spectral range, for which the correctness was from 90-100% for LDA and Naïve Bayes. In our work, the classifications accuracies for LDA are higher than for the Naïve Bayes models, which are in discordance with their results for which both models were similar. Data scarcity and continuous variables in Naïve models can be responsible, resulting in numerical instabilities and higher misclassification rates compared to a single band used in the discussed study.

Delwiche et al. (2019) and Zhang et al. (2019) evaluated FHB by HSI in individual kernels. The first study used LDA to evaluate kernel health status, for which they granted a value of 0 and 1 for sound and damaged, respectively, from 200 randomly orientated scanned kernels. Only mean centring (except for one test using SNV) was applied as spectral data pre-treatment, developing a cross-validated model with selected wavelengths (1100, 1197, 1308 and 1394 nm). It was able to classify 97.1% of FDK and 96.4% of healthy ones. Their results were

close to the obtained in this study, although they achieved slightly lower accuracies, probably due to the higher number of kernels (556). As our results determined that no considerable differences are present between crease-up and crease-down positions, it would be interesting to test randomly individual grains as in the study discussed. Alternatively, Zhang et al. (2019) build a FHB classification index to determine its damage on spikelets using hyperspectral microscopy imaging. They extracted four characteristic wavelengths, employing two (417 and 668 nm) for FHB classification index calculation. Even though the technique was quite different from HSI-NIR, they obtained an FDK overall classification accuracy of 89.9%. It was similar to Alisaac et al. (2019) findings, for which HSI-Vis/NIR spectral signatures showed correlations between fungal DNA and DON in wheat kernels.

Some studies tried to classify wheat by HSI-NIR according to DON contamination levels. The first study which reached this purpose was that of Barbedo et al. (2017), in which a two and three categories CM was developed (< 1250 μg/kg; > 1250 μg/kg and < 500; 500-1250; > 1250 μg/kg) for which they classified wheat batches with an 81 and 72 % of correctness, respectively. Even though they used naturally-contaminated wheat according to DON, remarkable differences with sampling conditions are noticeable, as they scanned 30-50 kernels instead of single kernel analysis and analysed all the kernels together by ELISA as the reference method. Recently, Liang et al. (2020, 2018) also investigated DON detection, but they used 70 wheat kernel samples instead of single kernels. Consequently, this research had a different aim from ours, as they assessed bulk wheat samples. Nevertheless, in their last publication, the SNV was assigned as the best spectral pre-treatment for HSI-NIR (1000-2500 nm) classifications which, according to the present paper, it is appropriate for wheat classification according to DON levels.

6.6. Conclusion

Preliminary analysis demonstrated that 16 of the 50 kernels were FDK and DON uncontaminated or vice versa. We accomplished that reflectances of DON contaminated kernels were higher than kernels with DON levels above the UE limit. In addition, this study revealed by the PCA analysis that all the spectral pre-treatments showed a tendency in FDK and DON separation. This research proposed quantification and sorting according to DON of single grains, demonstrating that, despite the RMSEP (4.8 mg/kg) being higher than the EU maximum limit, a simplified model (7 WL and 6 PC) can identify the high contaminations. Moreover, the LDA cross-validated classifications presented promising results, achieving a 100 % accuracy for symptomatology prediction and 98.9 % for DON (according to EU maximum). Thus, based on these findings, HSI-NIR has a potential application as an accurate kernel sorting technique. Once standardized the single kernel analysis, further research will require to build better-fitted prediction models and increase the sample size to obtain robust classifications.

6.7. Acknowledgements

The authors are grateful to the University of Lleida (predoctoral grant), and to the Spanish Ministry of Science, Innovation and Universities (Project AGL2017-87755-R) for funding this work.

6.8. References

Alisaac, E., Behmann, J., Rathgeb, A., Karlovsky, P., Dehne, H. W., & Mahlein, A. K. (2019). Assessment of *Fusarium* infection and mycotoxin contamination of wheat kernels and flour using hyperspectral imaging. *Toxins*, *11*, 1–18.

AOAC. (2005). Official Methods of Analysis. *Official Methods of Ananlysis of AOAC International*, *18*, 20877–22417.

Barbedo, J. G. A., Tibola, C. S., & Fernandes, J. M. C. (2015). Detecting Fusarium head blight in wheat kernels using hyperspectral imaging. *Biosystems Engineering*, *131*, 65–76.

Barbedo, J. G. A., Tibola, C. S., & Lima, M. I. P. (2017). Deoxynivalenol screening in wheat kernels using hyperspectral imaging. *Biosystems Engineering*, *155*, 24–32.

Delwiche, S. R. (1998). Protein content of single kernels of wheat by near-infrared reflectance spectroscopy. *Journal of Cereal Science*, *27*, 241–254.

Delwiche, S. R., Kim, M. S., & Dong, Y. (2010). Damage and quality assessment in wheat by NIR hyperspectral imaging. *Sensing for Agriculture and Food Quality and Safety II*, *7676*, 1–8.

Delwiche, S. R., Kim, M. S., & Dong, Y. (2011). *Fusarium* damage assessment in wheat kernels by Vis/NIR hyperspectral imaging. *Sensing and Instrumentation for Food Quality and Safety*, *5*, 63–71.

Delwiche, S. R., Rodriguez, I. T., Rausch, S. R., & Graybosch, R. A. (2019). Estimating percentages of *Fusarium*-damaged kernels in hard wheat by near-infrared hyperspectral imaging. *Journal of Cereal Science*, *87*, 18–24.

Dowell, F. E., Ram, M. S., & Seitz, L. M. (1999). Predicting scab, vomitoxin, and ergosterol in single wheat kernels using near-infrared spectroscopy. *Cereal Chemistry*, *76*, 573–576.

Eriksen, G. S., & Pettersson, H. (2004). Toxicological evaluation of trichothecenes in animal feed. *Animal Feed Science and Technology*, *114*, 205–239.

Agelet, L. E., Armstrong, P. R., Romagosa Clariana, I., & Hurburgh, C. R. (2012). Measurement of single soybean seed attributes by near-infrared technologies. A comparative study. *Journal of Agricultural and Food Chemistry*, *60*, 8314–8322.

European Comission. (2006a). Comission recomendation of 17 August 2006 on the presence of deoxynivalenol, zearalenone, ochratoxin A, T-2 and HT-2 and fumonisins in products intended for animal feeding. *Official Journal of the European Union*, *229*, 2297–2299.

European Commission. (2006b). Commission Regulation (EC) Nº 1881/2006 of 19 December 2006. Setting maximum levels for certain contaminants in foodstuffs. *Official Journal of the European Communities*, *364*, 5–24.

European Commission. (2006c). Commission regulation (EC) Nº 401/2006 of 23 February 2006. Laying down the methods of sampling and analysis for the official control of the levels of mycotoxins in foodstuffs. *Official Journal of the European Union*, *70*, 12–34.

Femenias, A., Gatius, F., Ramos, A. J., Sanchis, V., & Marín, S. (2020a). Use of hyperspectral imaging as a tool for *Fusarium* and deoxynivalenol risk management in cereals: A review. *Food Control*, *108*, 106819.

Femenias, A., Gatius, F., Ramos, A. J., Sanchis, V., & Marín, S. (2020b). Standardisation of near infrared hyperspectral imaging for quantification and classification of DON contaminated wheat samples. *Food Control*, *111*, 107074.

Fox, G., & Manley, M. (2014). Applications of single kernel conventional and hyperspectral imaging near infrared spectroscopy in cereals. *Journal of the Science of Food and Agriculture*, *94*, 174–179.

Jin, F., Bai, G., Zhang, D., Dong, Y., Ma, L., Bockus, W., & Dowell, F. (2014). *Fusarium*-damaged kernels and deoxynivalenol in *Fusarium*-infected U.S. winter wheat. *Phytopathology*, *104*, 472–478.

Liang, K., Huang, J., He, R., Wang, Q., Chai, Y., & Shen, M. (2020). Comparison of Vis-NIR and SWIR hyperspectral imaging for the non-destructive

detection of DON levels in *Fusarium* head blight wheat kernels and wheat flour. *Infrared Physics & Technology*, *106*, 103281.

Liang, Kun, Liu, Q. X., Xu, J. H., Wang, Y. Q., Okinda, C. S., & Shena, M. X. (2018). Determination and visualization of different levels of deoxynivalenol in bulk wheat kernels by hyperspectral imaging. *Journal of Applied Spectroscopy*, *85*, 953–961.

Nesic, K., Milicevic, D., Nesic, V., & Ivanovic, S. (2015). Mycotoxins as one of the foodborne risks most susceptible to climatic change. *Italian Oral Surgery*, *5*, 207–210.

Peiris, K. H. S., Bockus, W. W., & Dowell, F. E. (2016). Near-infrared spectroscopic evaluation of single-kernel deoxynivalenol accumulation and Fusarium Head Blight resistance components in wheat. *Cereal Chemistry Journal*, *93*, 25–31.

Peiris, K. H. S., Pumphrey, M. O., Dong, Y., Maghirang, E. B., Berzonsky, W., & Dowell, F. E. (2010). Near-infrared spectroscopic method for identification of Fusarium head blight damage and prediction of deoxynivalenol in single wheat kernels. *Cereal Chemistry*, *87*, 511–517.

Pestka, J. J., & Smolinski, A. T. (2005). Deoxynivalenol: Toxicology and potential effects on humans. *Journal of Toxicology and Environmental Health - Part B: Critical Reviews*, *8*, 39–69.

Polder, G., Van Der Heijden, G. W. A. M., Waalwijk, C., & Young, I. T. (2005). Detection of *Fusarium* in single wheat kernels using spectral imaging. *Seed Science and Technology*, *33*(3), 655–668.

Ropelewska, E., & Zapotoczny, P. (2018). Classification of *Fusarium*-infected and healthy wheat kernels based on features from hyperspectral images and flatbed scanner images: a comparative analysis. *European Food Research and Technology*, *244*, 1453–1462.

Rossel, R. A. V., Mcglynn, R. N., & Mcbratney, A. B. (2006). Determining the composition of mineral-organic mixes using UV – vis – NIR diffuse reflectance spectroscopy. *Geoderma*, *137*, 70–82.

Shahin, M. A., & Symons, S. J. (2011). Detection of *Fusarium* damaged kernels in Canada Western Red Spring wheat using visible/near-infrared hyperspectral imaging and principal component analysis. *Computers and Electronics in Agriculture*, *75*, 107–112.

Singh, C. B., Jayas, D. S., Paliwal, J., & White, N. D. G. (2009). Detection of sprouted and midge-damaged wheat kernels using near-infrared hyperspectral imaging. *Cereal Chemistry Journal*, *86*, 256–260.

Uhlig, S., Eriksen, G. S., Hofgaard, I. S., Krska, R., Beltrán, E., & Sulyok, M. (2013). Faces of a changing climate: Semi-quantitative multi-mycotoxin analysis of grain grown in exceptional climatic conditions in Norway. *Toxins*, *5*, 1682–1697.

Vidal, A., Sanchis, V., Ramos, A. J., & Marín, S. (2016). The fate of deoxynivalenol through wheat processing to food products. *Current Opinion in Food Science*, *11*, 34–39.

Wall-Martínez, H. A., Pascari, X., Bigordà, A., Ramos, A. J., Marín, S., & Sanchis, V. (2019). The fate of *Fusarium* mycotoxins (deoxynivalenol and zearalenone) through wort fermenting by Saccharomyces yeasts (S. cerevisiae and S. pastorianus). *Food Research International*, *126*, 108587.

Zhang, N., Pan, Y., Feng, H., & Zhao, X. (2019). Development of Fusarium head blight classification index using hyperspectral microscopy images of winter wheat spikelets. *Biosystems Engineering*, *186*, 83–99.

Chapter 7. Near-infrared hyperspectral imaging evaluation of *Fusarium* damage and DON in single wheat kernels

Antoni Femenias, Enric Llorens-Serentill, Antonio J. Ramos, Vicente Sanchis, Sonia Marín

Manuscript in submission

7.1. Abstract

Fusarium is a DON producing filamentous fungi which commonly infects small grain cereals. HSI-NIR is considered for its potential to manage this contamination, as it uses spatial recognition, which may be able to deal with the heterogeneity inside the batches for cereal sorting implementation. The focus of this study was the application of HSI-NIR for FDK detection and DON prediction and discrimination of wheat kernels over EU limits. After the HSI scanning of 300 individual grains, the reference values were obtained attributing categories for typical fungal symptoms and analysing DON from individual grains by HPLC. Several spectral pre-processing methods selected valuable information before model calibration. Externally validated PLS predictions showed RMSEP of 6.66 mg/kg, an R^2 of 0.88 and an RPD of 3.21. However, the classification models managed wheat contaminations more appropriately, obtaining discrimination accuracies of 85.8% and 76.9% for fungal symptoms and DON at the EU limit, respectively. These findings suggest that HSI-NIR can be a suitable tool for sorting DON contaminated kernels at EU limits.

Keywords: Single-Kernel; Hyperspectral imaging; Deoxynivalenol; Fungal damage; Cereal sorting

7.2. Introduction

Fusarium is a well-known plant-pathogen fungus associated with small grain cereal diseases, such as FHB, which grows in favourable moist and warm conditions. Its infection is related to yield and grain quality reduction with the appearance of FDK. The main changes produced in FDK are shrivelling, weight loss, and discolouration. From a food safety perspective, *F. graminearum* and *F. culmorum* can produce mycotoxins, in which DON is the most common. This secondary metabolite is associated with human and livestock health problems. Acute and chronic disorders are attributed to DON through cereal consumption (Sudakin, 2003), thus exposure to a cereal-based diet, and the increased incidence of mycotoxins due to climatic change (Marroquín-Cardona, Johnson, Phillips, & Hayes, 2014) can increase the risk of developing an associated disease. Consequently, food safety authorities have established a maximum limit of DON for unprocessed wheat in 1750 μg/kg for durum wheat and 1250 μg/kg for cereals other than durum wheat, oats, and maize (European Commission, 2006a).

Conventional analysis techniques, such as ELISA, HPLC, and High-Performance Liquid Chromatography-Mass Spectrometry (HPLC-MS) and immunochromatographic strips, for DON detection, have been frequently applied before cereal entrance in the food industry. The official controls of mycotoxins levels (European Commission, 2006b) attempts to represent, as far as possible, the contamination of the entire batch. Nevertheless, even if a suitable sampling protocol is applied, enough representation of the lot is not reached, and few extremely-contaminated kernels can disrupt the admission of the whole batch associated with a loss in the production yield and a negative economic impact. The heterogeneous distribution of the contaminated grains is an issue in the cereal batches. Some kernels suffer fungal infection (with or without associated DON presence) inside the sample, while the rest can remain healthy (Champeil, Fourbet, & Doré, 2004; Delwiche, Pearson, & Brabec, 2007). Besides,

the abovementioned traditional techniques are expensive, time-consuming, and sample destroying. Companies require new methods able to sort mycotoxin contaminated kernels overcoming batch heterogeneities.

In some studies, authors used FDK as DON presence indicators (Delwiche et al., 2011; Dowell et al., 1999; Jin et al., 2014). However, Paul et al. (2005) obtained a correlation of 0.73 between FDK and DON. Moreover, Barbedo et al. (2015) used an algorithm based on a FI (probability of a kernel of being infected with FHB based on visual inspection) that presented a correlation of 84% with DON. It also demonstrated that correlations found for high DON levels were substantially higher than for low DON concentrations. Although they reached positive correlations, the indirect determination of DON using FDK would drag consecutive errors that would affect the reliability of the results.

SK-NIR has been used for *Fusarium* detection in wheat by Polder et al. (2005), which used NIR technology linked to RT-PCR to predict the amount of *Fusarium.* However, most studies with the same objective used the visual inspection of kernel symptoms to typify them as FDK or healthy by NIR (Delwiche et al., 2011). Some of them also analysed DON in single kernels (Peiris et al., 2010 & 2016) by SK-NIR technology. However, in both studies, artificial inoculation of wheat spikes was performed before GC-MS analysis, achieving kernel discrimination with a DON threshold of 60 mg/kg. Dowell et al. (1999) analysed by SK-NIR using HPLC as the reference method for DON. In their calibration, they removed kernels with contamination > 5 mg/kg, for which most of them presented a DON concentration between 50-500 mg/kg, a level which differs from those commonly found in naturally contaminated samples. Jaillais, Roumet, Pinson-gadais, & Bertrand (2015) developed SK-NIR multivariate imaging method to detect FHB in wheat kernels. They analysed different trichothecenes-producing fungi with RT-PCR. Then, they calibrated PCA models for contaminated grains detection

and PLS to map the contaminated regions within the kernels using selected spectral bands.

Researchers used HSI to combine the whole spectra and the spatial resolution, making it appropriate to apply it to single kernel screening. All the studies except one focused on detection of *Fusarium* in wheat single kernels. In most of the works, an inspector examined manually the grains, which added subjectivity to the study. On the other hand, Singh et al. (2012) artificially inoculated kernels with fungi before scanning them by HSI-NIR and digital colour imaging. Although the artificial contamination avoided the subjectivity from visual inspection, the controlled inoculation presents differences from natural contamination. Delwiche et al. (2011) calibrated a FHB classification model based on LDA using HSI-Vis/NIR on four characteristic wavelengths (502, 678, 1198 and 1496 nm). A second attempt was done (Delwiche et al., 2019) but using HSI-NIR (938-1654 nm). They selected four spectral bands (1000, 1197, 1308 and 1394 nm) as the optimum for LDA calibration, although they built an alternative PLS-DA model. In addition, Ropelewska & Zapotoczny (2018) classified FHB damaged kernels by testing different mathematical classifiers (Bayes net, LDA, K-Star, Rules PART and LMT for hyperspectral and colour images. Barbedo et al. (2015) also evaluated FHB in SK, which used HSI-Vis/NIR technology to build an algorithm based on the FI. The probability density function based on FI, identifying sound and diseased kernels, was correlated with DON concentration to attempt an indirect estimation of the DON levels. Liang et al. (2018) focused exclusively on the determination of different levels of DON using a complex algorithm. Although they did not analyse single kernels, they built a distribution map discerning heavily infected regions within the bulk samples corresponding to the highly contaminated grains.

This study focused on DON prediction in single wheat kernels by an optimized algorithm and to classify them according to typical visual symptoms caused by

Fusarium infection and different DON levels according to EU maximum limit. This study is a starting point for HSI-NIR calibration that could at real-time identify and reject damaged or DON contaminated kernels at food industry entrance.

7.3. Material and methods

7.3.1. Wheat kernels

A feed-producing agricultural cooperative supplied wheat samples harvested during 2018-2019. The origin of the wheat was the plain area of Lleida province. A highly contaminated sample was selected, previously analysed twice by UHPLC (2682.8 and 2403.5 μg/kg of DON). Three hundred wheat kernels from the sample were selected, including all the typical characteristics of sound and diseased wheat kernels. The kernels had a mean weight of 30.2 mg, ranging from 6.2 to 58.1 mg, and were used for DON prediction and classification according to fungal symptomatology and DON levels.

7.3.2. HSI-NIR instrumentation and data acquisition

The HSI system consisted of a Pika NIR-320 camera assembled by RESONON Inc. (Bozeman, MA, USA). The device consists of an InGaAs sensor line scan camera with a 320×256-pixel resolution, 30×30 μm pixel size, and 14-bit resolution A/D spectrograph (Goldeye G-008 SWIR TEC1, Allied Vision Technologies GmbH, Germany). The spectral resolution was 4.9 nm (167 spectral bands from 895 nm to 1700 nm), with a spatial resolution of 320 pixels and a frame rate of 520 fps. The objective lens had a focal length of 25 mm (F/1.4 SWIR, 0.9-1.7 μm, 21 mm image format, c-mount) and was positioned 220 mm above the image surface. The illumination unit was composed of a four halogen lamp lighting system with Lambertian filters fixed onto an adjustable tower that was turned on at least 20 min before image acquisition. Samplexpower® converter (SEC-1223CE, Burnaby, BC, V5A 0C6, Canada) supplied the illumination unit power,

which provides a highly regulated output DC voltage of 13.8 Volts at 23 Amps with an AC input of 230 Volts, 50 Hz. Finally, a motorized linear translation stage with a range of 600 mm was also used, which permitted scanning of the whole sample with the optical systems remaining in a fixed position.

Spectronon PRO software performed the image processing controlled by Resonon's benchtop. The raw reflectance readings for each test sample data array were corrected by dividing the dark current-subtracted reflectance by the dark current subtracted white standard reflectance at each of the corresponding wavelengths (Equation 1). A dark current intensity image, taken with the covered camera's lens, removed the dark noise. Likewise, a reflectance standard with a 99% intensity made of polytetrafluoroethylene (Spectralon™, SRT-99-120, Labsphere, North Sutton, NH, USA) corrected the illumination effects. These two images were applied to subsequent sample intensity images.

$$I = \frac{I_0 - I_b}{I_w - I_b} \qquad (1)$$

where the I is the corrected reflectance intensity, I_0 the raw hyperspectral image intensity, I_w the white reference intensity and I_b the dark current reference intensity. In addition to the dark current, the camera controls permitted the adjustment of the pixel illumination saturation. The configuration of the framerate and the integration time avoided pixel saturation.

The hyperspectral system acquired data for 300 kernels to calibrate the predictive and classification models. According to our previous studies (Femenias, Bainotti, Gatius, Ramos, & Marín, 2021), the analysis was performed for the crease-down side of the kernel, which is more rapid and easily manipulated and did not show significant differences in results with the crease-up position.

In all cases, the black tray reduced the background noise in the image to obtain an accurate pixel selection. The image scan had 350 bands on the horizontal size and approximately 90 mm on the vertical. Kernel's pixels data were collected by

the mean reflectance and mean 1stD values of similar spectrum pixels calculated by Euclidian distance, which is best adjusted to the ROI to remove the background signal. Individual kernel raw and 1stD spectra were saved as a text file for subsequent exporting to the spectral analysis software.

7.3.3. DON analysis of wheat kernels by UHPLC

7.3.3.1. Reagents and chemicals

A Milli-Q® SP Reagent water system from Millipore Corp. (Brussels, Belgium) produced the water used. Methanol and acetonitrile (HPLC grade) were purchased from Scharlab (Sentmenat, Spain). DON standards were obtained from Romer Labs (Tulln, Austria).

7.3.3.2. Preparation of DON solutions

The DON concentration was checked in the stock solution by UV spectroscopy following the AOAC Official Methods of Analysis, Chapter 49 (AOAC, 2005). The concentration obtained was 7530 μg/mL for the stock solution. Standard solutions of DON were prepared in acetonitrile at a concentration of 10 μg/mL and stored at 4 °C. The calibration curves were prepared by the appropriate dilutions of known volumes of the stock solution with the mobile phase.

7.3.3.3. DON extraction in wheat kernels

The kernels already analysed by spectroscopy were quantified for DON by UHPLC. The extraction followed the methodology used by Femenias et al. (2021). Concisely, each grain was individually and manually ground with a small laboratory mortar and pestle and mixed with 0.5 mL of MiliQ water in a 1.5 mL Eppendorf tube, followed by 10 min vortexing and 10 minutes of sonication. Then, samples were centrifuged for 10 min at 1780×g. The supernatant was filtered through a nylon filter (0.4 μm) and was evaporated. Finally, the sample was resuspended with 150 μL of mobile phase before being injected into the UHPLC-DAD system.

7.3.3.4. UHPLC system

DON concentrations were obtained using an Agilent Technologies 1260 Infinity UHPLC system (California, USA) coupled with an Agilent 1260 Infinity II DAD. A Gemini® C18 column from Phenomenex 150 × 4.6 mm (California, USA) with a particle size of 5 μm and a pore size of 110 Å was used. The absorption wavelength was set at 220 nm. The mobile phase was composed of methanol:water (10:90, v/v/v) and set at a flow rate of 1 mL/min. The column temperature was 40 °C, the injection volume was 100 μL and the total run time was 15 min for mycotoxin analyses. The performance of the method for the quantification of DON in wheat was tested, in which the limit of detection (LOD: 100 μg/kg) was considered to be three times the signal of the blank.

7.3.4. Prediction and classification modelling of DON for individual kernel analysis

Selectivity was checked by injecting 5 μL of standard solution at least three times (150 μg/L) and comparing retention time and peak resolution between injections. For linearity check, a calibration curve of eight concentration levels for DON solutions (20, 30, 50, 100, 250, 500, 1000, 3000 μg/L solutions) was prepared and injected into the system, generating a linear regression plotting solutions' concentration versus peak area. The method performance was assessed according to Commission Regulation (EC) 401/2006 (European Commission, 2006b).

7.3.4.1. Quantification modelling of DON contamination

Hyperspectral data were modelled with The Unscrambler software (version 7.6 SR1, CAMO, Oslo, Norway, 2001) for DON level prediction. The reflectance data were used as raw data for the calibration of the regression models. Each kernel was scanned three times, recording intensities from 900 hyperspectral images. Once the grains were optically analyzed, the DON concentration was determined

from each kernel by UHPLC. The contamination of the 300-kernels set ranged from <LOD to 135.73 mg/kg and the mean concentration was 9.02 mg/kg. The mean reflectance intensities of the pixels from each kernel corresponded to the explanatory variables (X) and the DON concentration obtained by UHPLC was the dependent variable (Y). A first modelling screening was performed by the regression of the hyperspectral data versus the reference method by a leave-one-out cross-validation. This approach allowed an overall perspective of the data adjustment by a single sample leaves out of the training set for each *n* iterations. The leave-one-out cross-validation demonstrated the most realistic approximations to the independent set validation. The data size used in this study is sufficiently large to validate the predictive models independently. The data was divided into a calibration set, which consisted of 540 hyperspectral images (3 images of 180 kernels), and a validation set, which included 360 images (3 images of 120 kernels).

Before the predictive models' calibration, spectral pre-processing tools were applied to the raw data to enhance the remarkable information. The transformations applied in The Unscrambler software were first and second 3 and 5-point Savitzky-Golay and Norris Gap derivatives which reduce noise, additive and multiplicative effects. Alternatively, MSC and SNV were applied to overcome the non-linearity of light scattering due to the differences in kernels size. Other pre-treatments, such as Normalization and Baseline Correction, were also used to obtain balanced variances and to remove baseline noise, respectively. The optimum pre-treatment is not the same for all data sets, as it depends on the raw reflectances, absorbances and transmittances, instrument configuration and calibration, goal and sample characteristics. Thus, several spectral pre-treatments had been tested followed by the statistical experience. Otherwise, the improvements tested in previous investigations demonstrated

non-linearities and noisy regions in the extremes of the spectra. Thus, models on the 1000-1600 nm range were also calibrated.

The information obtained was used to build the predictive model. We considered PLS regression as the most suitable chemometric tool to be used for NIR data calibration, as it is focused on the Y information to obtain better-adjusted models. The performance of the PLS models depended on the parameters obtained in the model calibration steps. The parameters which determine the most suitable model for DON quantifications are the slope, the offset, the R^2, the RMSEP, the optimum number of PC and the RPD.

Table 16. Performance statistic parameters of the PLS regression.

Validation set parameters		
R_p^2	Coefficient of determination of prediction	$R_p^2 = \frac{\Sigma\,(\hat{y}_i - \bar{y})^2}{\Sigma\,(y_i - \bar{y})^2}$
RMSEP	Root Mean Square Error of Prediction	$RMSEP = \sqrt{\frac{\Sigma\,(\hat{y}_i - y_i)^2}{n}}$
RPD	Ratio of Performance to Deviation	$RPD = \frac{Sdev}{RMSE}$

Depending on the RPD values, the models can be categorized as excellent predictions (RPD > 2.5); good (RPD of 2.0-2.5); approximate quantitative predictions (RPD of 1.8-2.0); possibility to distinguish high and low values (RPD of 1.4-1.8); and unsuccessful (RPD < 1.40) (Agelet & Hurburgh, 2010). The combination of the RPD values with high slopes and R^2 and low RMSEP and number of PC indicates a high predictive power of the model. These parameters were calculated following the mathematical expressions included in Table 16.

The calibration models were performed for full spectral range (893.1-1731 nm) and extremes removed spectra (1000-1600 nm). A characteristic wavelength extraction for the best-fitted models was performed, to simplify the

computational complexity of the models. The optimum bands were higher regression coefficients wavelengths, whose selection reduced data dimensionality with the minimum loss of information. Thus, band selection reduced the model complexity, the computational time and noise. Despite the reduction in data dimensionality, it explained most of DON variability.

7.3.4.2. Classification modelling of fungal symptomatology and DON contamination

Hyperspectral data from 300 kernels were modelled to discriminate fungal and DON contaminated kernels. Previous to the hyperspectral acquisition, the kernels were visually inspected and categorized as symptomatic (S) (discolouration, weight loss and shrivelled), medium-symptomatic (part of the symptoms) (M) and asymptomatic (A) (no visible symptoms). Then, based on the DON analysis of kernels by UHPLC, they were also categorized as contaminated (C) and non-contaminated (B) according to the threshold established (1250 µg/kg) corresponding to the legal limit of the EU. JMP PRO 15.2 software was used to calibrate the classification LDA, Naïve Bayes, K-NN and Artificial Neural Networks (ANN) models. The model performances were evaluated by the classification accuracy, expressed in percentage, and the ratio of false negatives, which indicated the introduction of contaminated kernels into the food chain.

7.4. Results

7.4.1. DON and weight variability in single kernels

Kernels from the same batch presented broad differences in DON content. DON contamination covered a range from < LOD and 135.7 mg/kg with a mean concentration of 9.02 mg/kg. From the kernel set, 82 were contaminated under the LOD, which represented the 27.3 % of the entire set. In addition, 204 grains had a concentration below the EU legal limit (1.25 mg/kg), and 59 kernels over 10 mg/kg, which indicated that the rejection of a wheat batch could be due to a reduced percentage of highly contaminated kernels. The kernels were manually

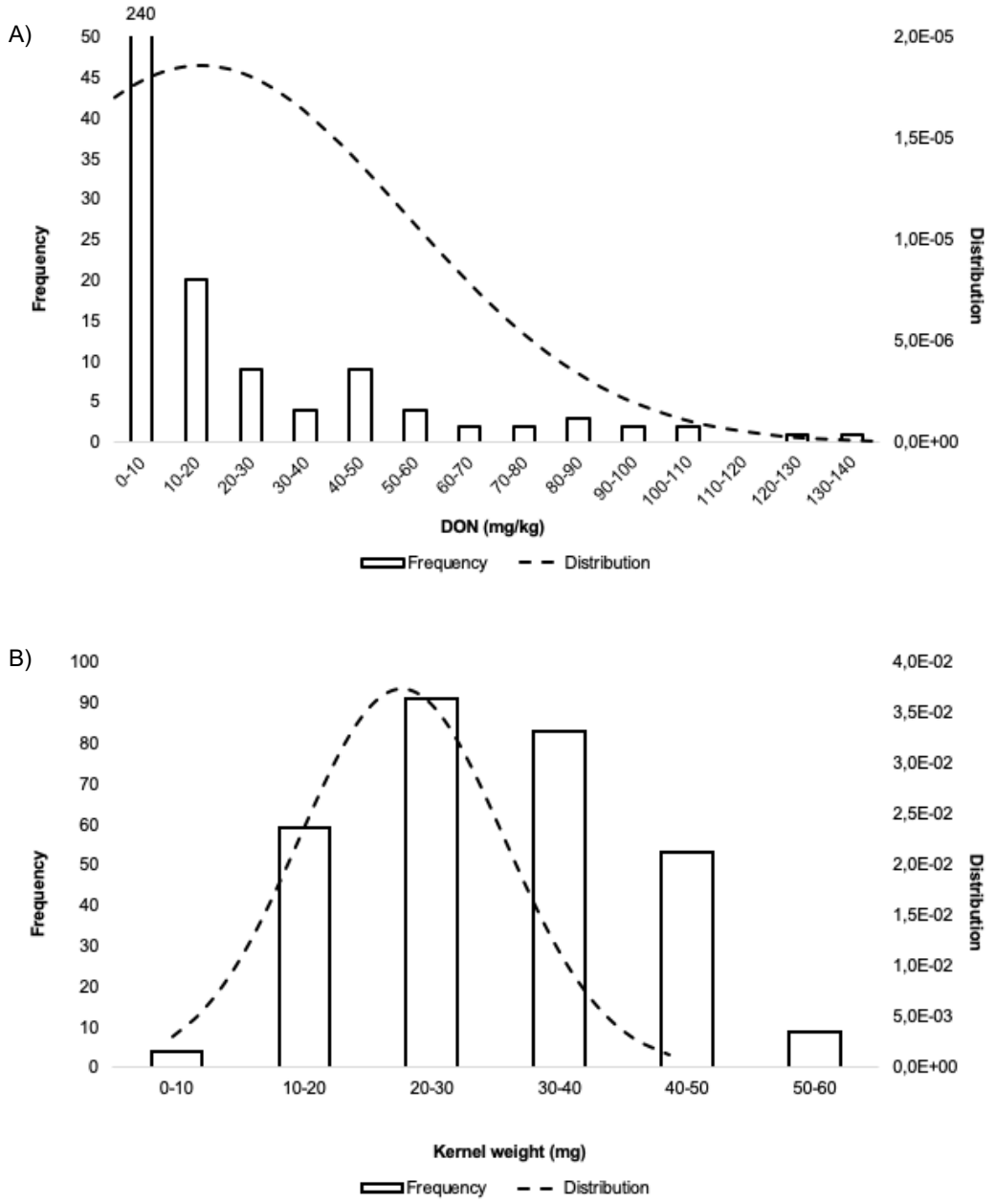

Figure 26. Distribution of DON content and kernel weight in 300 single wheat kernels dataset. (A) Total kernel DON frequency (in number of kernels) and distribution. (B) Total kernel weight frequency (in number of kernels) and distribution.

selected to cover the maximum symptomatology range possible. For that reason, wide variability in DON concentration was observed.

Kernel minimum weight was 6.2 mg, while the maximum observed was 58.1 mg. The differences in the kernel weight could be due to changes produced by fungal

growth on the kernel. DON concentrations for kernels lighter or heavier than 30 mg demonstrated that the differences in kernel weight are associated with DON, presenting the light a mean concentration of 15.5 mg/kg and the heavy 2.4 mg/kg. The weights with higher frequencies were the kernels between 20-30 mg, as is reported in Figure 26.

7.4.2. Spectral profile comparison of FDK and DON affected kernels

The 1stD spectra in the NIR region were compared to detect differences in bands caused by *Fusarium* growth and mycotoxin contamination. From the spectral region used (895-1728 nm), the predominant changes were in the range between 1100-1450 nm, which could be due to the differences produced by the fungal primary or secondary metabolism. Figure 27 shows the differences in the 1stD mean spectral profile of the (A) sound, mildly symptomatic and FDK and (B) DON kernel contamination above and below 1.25 mg/kg. The spectral bands around 1146 nm, 1220 nm, 1350 nm and 1406 nm showed differences between the mean of FDK and healthy kernels and DON high and low contaminated seeds. The use of differences in characteristic spectral peaks for contamination detection was not possible due to the high amount of data to be managed and the overlapping in specific bands. Therefore, the applied chemometric tools resolved the overlapping problems of NIR spectra. In addition, they highlighted the valuable information to build predictive and classification models presented in the following sections.

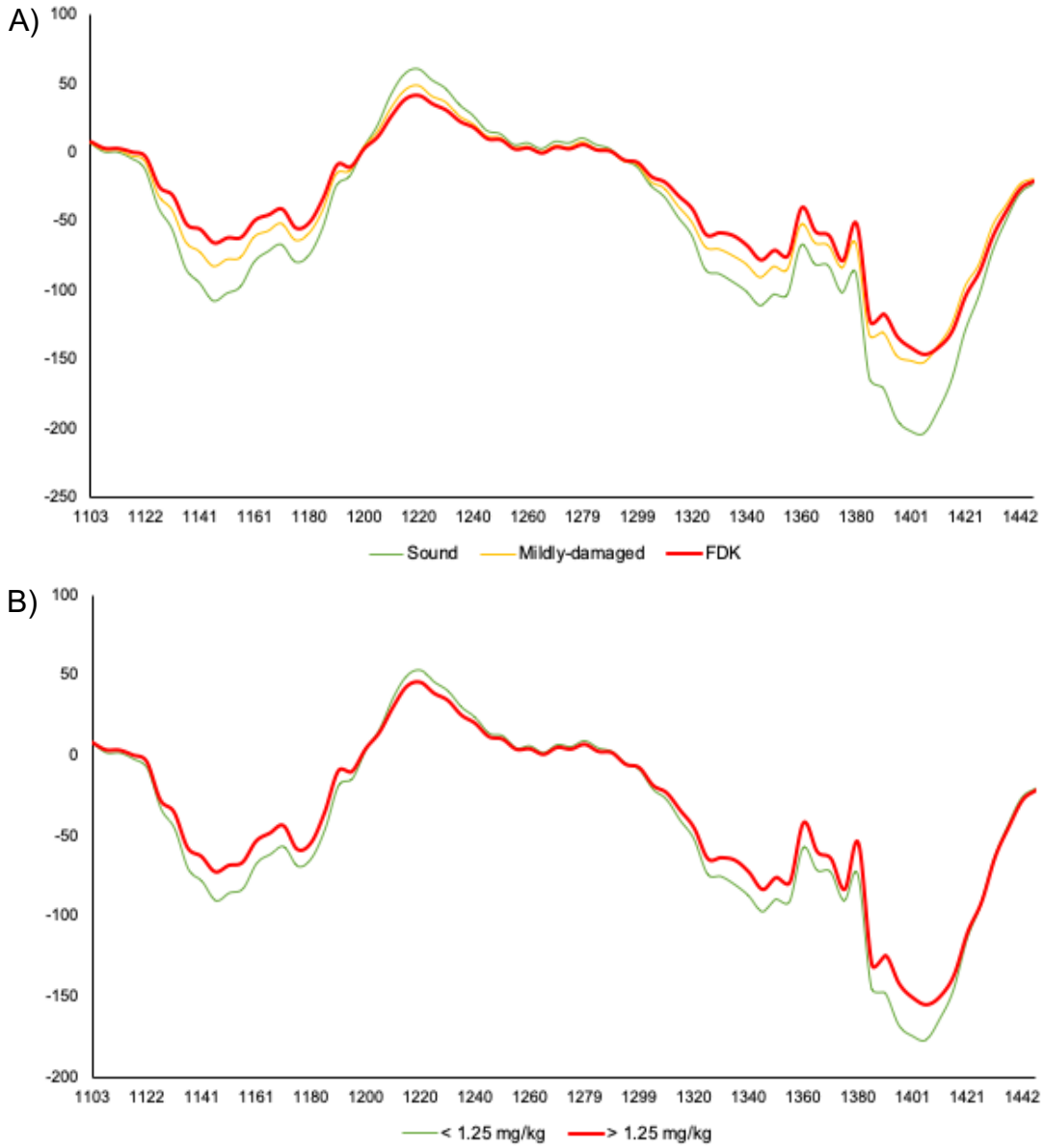

Figure 27. Mean 1st derivated spectral profile of the (A) difference between FDK (red/bold), mildly-damaged (yellow/semi-bold) and healthy kernels (green/light) and (B) DON contaminated above (red/bold) and below (green/light) 1250 µg/kg.

7.4.3. DON quantification of SK by HSI-NIR

For DON quantification, data pre-processing improved the model performances. The results presented correspond to the different spectral pre-treatments and entire or extreme-reduced spectra. Despite the models calibrated presented similar results, some of them obtained better adjustments due to the spectral pre-treatment. SNV and MSC pre-treated models had the highest performance in

cross-validation and external validation procedures. Nevertheless, the models calibrated on SNV transformed spectra presented slightly better adjustment with an RMSEP of 6.66 mg/kg, an R^2 of 0.88 and an RPD of 3.21 by 14 PC calibration, as indicated in Figure 28. Table 4 (Annexe) collects the performance parameters of all the models with the different spectral pre-treatments used.

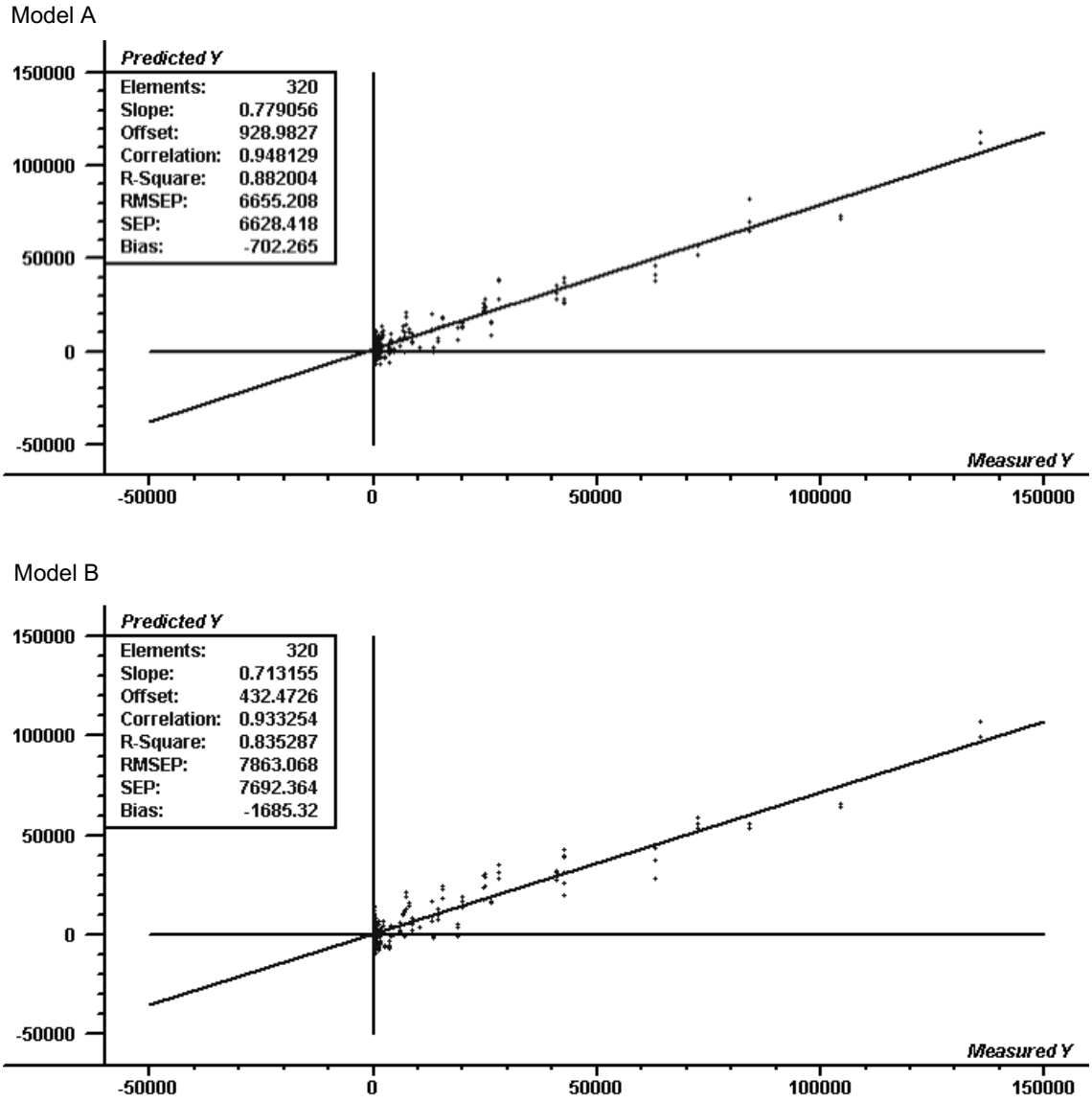

Figure 28. PLS regression predicted vs. measured plot for independent set validation. Model A: SNV pretreated 1000-1600 nm spectra; optimum number of PC = 14. Model B: SNV pre-treated 11 characteristic wavelengths; optimum number of PC = 10.

For the model selected (Figure 28, Model B), 11 characteristic wavelengths were the spectral bands with higher regression coefficients. Thus, the model is reduced

from the hyperspectral dimension to multispectral to reduce model complexity. The bands were 1067, 1159, 1193, 1222, 1252, 1343, 1363, 1378, 1399, 1497, 1554 nm. The model calibrated with those variables was adjusted with an R^2 of 0.84, an RMSEP of 7.86 mg/kg and an RPD of 2.72 with 10 PC. For both models, RPD was higher than 2.5, which indicated that the models could predict DON concentrations adequately.

7.4.4. Classification of SK according to symptomatology by HSI-NIR

HSI was used to discriminate kernels according to the symptoms of fungal infection. The grains were categorized as symptomatic, mildly-symptomatic and asymptomatic depending on the visual inspection of symptoms. The classifiers used to discern between classes were LDA, Naïve-Bayes, K-NN and ANN. The percentage of correctly classified kernels evaluated the discrimination accuracy of the models among the three categories. Table 17 indicates the classification accuracies for each pre-treatment and classifier; the overall results ranged from 57.2 to 85.8 %. The pre-treatment which led to better discrimination was the normalization with a mean overall accuracy of 82.4%. However, the classifier that obtained the best accuracy in kernel separation was the ANN, with a percentage of 82.2 %.

The classification model that showed the maximum accuracy was the ANN using the spectra transformed to absorbance (85.8 %). However, normalized spectra modelled with ANN and ABS/BC spectra with LDA also presented high-accurate results, obtaining 85.3 % and 82.8% of accuracy, respectively. The differences between the results for the whole spectral range and the extreme-reduced spectra were not remarkable. Nevertheless, in some cases, the entire spectral range accuracies were higher.

7.4.5. Classification of SK according to DON by HSI-NIR

In some cases, changes produced on the kernel due to fungal growth do not imply an increased level of mycotoxins in the product. The classification according to DON levels was challenging due to batch contamination heterogeneity and the discordance between the fungal growth and the mycotoxin contamination. DON was over the legal limit in symptomatic kernels (excluding mildly symptomatic ones) or under the legal limit in asymptomatic or mildly symptomatic ones in 70.7% of the cases. For the remaining 29.3 %, DON was present between LOD and the legal limit in symptomatic kernels (20.7 %), while the 8.6% had high DON concentrations without presenting visual symptoms.

Table 18 contains the discrimination accuracy of single wheat kernels according to the level of contamination (above and below 1250 μg/kg). For DON discrimination, classification accuracies ranged between 65.0 % and 76.9 %. The most accurate model was the ANN classifier, with a 73.2 % of mean correctness. In addition, the results for the MSC and SNV pre-treated spectra had the highest mean accuracies compared with the other pre-treatments. The most accurate model obtained was the ANN classification with SNV, with an accuracy of 76.9 %. However, other models also achieved discriminations above the 76.0 %, as Naïve Bayes model with SNV application (76.4 %), Naïve Bayes and ANN from the MSC transformed spectra (both 76.1 %), ANN for MSC transformed full spectral range (76.4 %), and ANN calibration with SNV and 1stD application (76.1 %). In this case, the differences between the entire spectral range and the extreme reduced spectra calibrations were not significant. Nevertheless, most of the best results obtained in this section are using the spectra with the extremes removed.

Table 17. External validation accuracies of single wheat kernels discrimination according to symptomatology.

Pre-treatment	Spectral range	LDA	Naïve Bayes	K-NN	ANN	Mean
Raw spectra	895-1731	76.1	60.6	83.3	84.8	76.3
	1000-1600	77.5	60.3	84.2	83.6	
1stD	895-1731	75.8	78.1	76.9	83.3	78.2
	1000-1600	78.3	74.4	78.1	80.6	
SG 1stD 3-2	895-1731	76.4	77.2	79.2	83.1	78.5
	1000-1600	77.5	74.7	78.3	81.4	
SG 1stD 5-3	895-1731	75.8	76.9	79.4	81.1	78.6
	1000-1600	78.6	74.7	79.4	82.5	
SG 2ndD 3-2	895-1731	75.8	68.1	71.4	80.0	74.0
	1000-1600	75.0	71.4	71.1	78.9	
SG 2ndD 5-3	895-1731	75.8	79.2	76.9	83.3	78.8
	1000-1600	76.4	77.5	77.8	83.6	
NG 1stD 21	895-1731	80.6	76.9	79.2	83.9	79.2
	1000-1600	79.7	71.9	79.7	81.7	
NG 1stD 5	895-1731	78.9	77.8	79.2	83.6	79.1
	1000-1600	77.5	74.7	78.1	83.1	
SNV	895-1731	80.6	68.1	75.6	80.6	74.7
	1000-1600	79.4	58.6	73.9	80.8	
SNV + 1stD	895-1731	74.7	77.8	71.7	82.2	75.3
	1000-1600	77.2	63.9	72.5	82.2	
MSC	895-1731	71.1	70.6	76.9	78.9	72.3
	1000-1600	70.0	57.2	75.0	78.9	
MSC +1stD	895-1731	76.4	78.3	71.9	80.8	74.8
	1000-1600	75.6	63.6	71.9	80.0	
Normalization	895-1731	81.4	83.1	82.2	85.3	82.4
	1000-1600	81.4	82.5	80.0	83.6	
Absorbance	895-1731	83.3	60.3	83.6	85.8	77.7
	1000-1600	80.0	60.8	83.9	83.6	
ABS/BC	895-1731	85.3	76.4	80.6	82.5	80.8
	1000-1600	82.8	78.3	78.1	82.8	
Mean		77.8	71.8	77.7	82.2	

Table 18. Validation accuracies of single wheat kernels discrimination according to DON.

Pre-treatment	Spectral range	LDA	Naïve Bayes	KNN	ANN	Mean
Raw spectra	895-1731	67.8	72.2	70.8	69.3	71.7
	1000-1600	75.0	72.8	70.8	75.0	
1stD	895-1731	69.4	69.2	69.4	71.4	70.4
	1000-1600	70.6	66.4	72.5	74.2	
SG 1stD 3-2	895-1731	70.8	68.9	72.8	73.1	71.1
	1000-1600	70.3	65.3	73.6	73.9	
SG 1stD 5-3	895-1731	70.3	69.2	72.5	75.3	71.2
	1000-1600	70.8	66.4	72.5	72.8	
SG 2ndD 3-2	895-1731	68.9	70.3	71.4	73.3	71.4
	1000-1600	68.9	72.8	72.8	72.5	
SG 2ndD 5-3	895-1731	70.6	71.7	72.8	68.1	71.3
	1000-1600	71.4	71.9	72.2	71.4	
NG 1stD 21	895-1731	74.2	67.2	72.8	73.3	71.9
	1000-1600	74.4	65.0	72.2	76.1	
NG 1stD 5	895-1731	71.4	67.5	71.9	67.2	69.9
	1000-1600	71.7	65.3	73.3	71.1	
SNV	895-1731	71.7	74.2	71.4	73.9	73.3
	1000-1600	71.1	76.4	71.1	76.9	
SNV + 1stD	895-1731	68.1	71.9	72.5	76.1	72.7
	1000-1600	73.1	75.0	74.7	70.6	
MSC	895-1731	69.7	75.3	71.9	76.4	73.5
	1000-1600	70.8	76.1	71.9	76.1	
MSC + 1stD	895-1731	68.6	71.9	71.9	74.4	73.1
	1000-1600	73.1	75.3	75.6	73.9	
Normalisation	895-1731	73.9	71.7	72.2	73.1	72.3
	1000-1600	73.1	71.7	69.4	73.1	
Absorbance	895-1731	72.5	72.8	71.4	74.7	72.8
	1000-1600	75.6	72.8	69.4	73.1	
ABS/BC	895-1731	71.7	71.7	71.9	73.6	71.8
	1000-1600	75.6	73.6	65.6	70.8	
Mean		71.5	71.1	71.9	73.2	

7.5. Discussion

The analysis of DON content from individual kernels revealed the heterogeneity of the wheat batches. An 80 % of the 300-kernel set used in this study had a level of contamination below 10 mg/kg. Moreover, 204 kernels (68 %) had a concentration below the legal limit set by the EU (1.25 mg/kg). It indicates that a considerable part of the set (20 %), with extreme high contaminations up to 135.7 mg/kg, are responsible for entire batch rejections. Thus, removing the percentage of high-contaminated kernels would mitigate DON presence to avoid whole batches refusal and ensure low DON levels accepted fraction to reduce harmful health effects and economic losses to producers.

The weight of the grain is also a considerable parameter in the discrimination of the high-contaminated percentage. The mean DON concentration of kernels weighing more than 30 mg was 2.4 mg/kg, while the level in tiny grains lower than 30 mg was 15.5 mg/kg. These differences suggest that weight is correlated with fungal symptomatology and DON production, as the common fungal infection effects include weight loss and shrivelling caused by moisture decrease. NIR data contains the physicochemical changes produced on the sample and can manage kernel size variations to obtain also an effect on the analytical information correlated, in part, by fungal and DON contaminations.

The low correlation between kernels with characteristic visual symptoms and its DON contamination does not avoid the characterization of DON content considering the physical characteristics of the grains. As DON is synthesized as a product of the secondary metabolism of fungi, the amount of fungal growth does not match with the level of contamination. However, even if there are no visible physical changes on the kernels, DON contamination could be modelled by the chemical and nutritional modifications produced by fungal growth on the surface or inner parts of the grains. It includes sugar and free fatty acids content reduction, protein modifications and new fungal metabolites as chitin, ergosterol

and antibiotics (Sauer, 1988). Then, NIR spectra include all the chemical information of the ROI, which has to be modelled to extract the information required.

The predictive models can be calibrated for more than one chemical compound. The reference values of the compound of interest are required to obtain predictive models to quantify chemicals by spectroscopic analysis. Consequently, authors use multivariate regression methods deal with the complexity of the NIR data to build well-fitted predictive models. Several published studies aimed to quantify mycotoxins in wheat batches, but only a few tried to use the spatial ability of HSI for the same purpose in individual kernels. First, conventional NIR techniques attempted DON detection in single grains.

One of the first studies regarding DON prediction in single wheat kernels published by Dowell et al. (1999) obtained a prediction error for external validation of 54 mg/kg, including a weak adjustment of data (R^2 of 0.66). The performance was far away from the common DON contamination as they only used scab-damaged kernels with a DON range between 0-400 mg/kg. Despite Dowell et al. (1999) worked on 114 single grains for DON assessment, they used only highly contaminated above 5 mg/kg. Even using high contaminations, which ideally would obtain the best adjustments than working on low contaminated samples, the R^2 was 0.66 and the SEP 52 mg/kg. Thus, they concluded that NIR spectrometry is unsuitable for this aim. As demonstrated in the study of Peiris et al. (2010), the results improved while working on high levels of contamination from artificially inoculated kernels (> 60 mg/kg), obtaining an R^2 of 0.87 and a SEP of 60.8 mg/kg. Their results would be far from naturally-contaminated DON concentrations found in the field and, thus, the application of their model would not fit with the legislation demands. Although we obtained similar adjustments (R^2 = 0.88), we focused on naturally found levels of

contamination (<LOD to 135.7 mg/kg) that would be able to accurately detect high-DON contaminated kernels in terms of RMSEP (6.66 mg/kg).

Otherwise, Jin et al. (2014) estimated the correlation between the visual FDK and SK-NIR DON data obtaining a correlation of 0.68. As expected, their results were similar to our percentage of kernels which, even though they presented symptoms of fungal growth, did not contain DON and vice versa. On the other hand, Peiris et al. (2009) studied DON absorbance NIR spectra. The different spectral profiles from DON in acetonitrile, sound and FDK were subtracted and compared. It allowed to attributing the changes produced by fungi and DON contamination to the differences in peak intensities in specific bands. They used log (1/T) and 2nd derivative pre-processing to detect differences in the spectral peaks. For FDK, broad differences were observed at 1205 nm and around 1400 nm for 1/T and 1195 and 1425 nm for the 2nd derivative. These peaks are found in similar regions to our characteristic peaks, as 1220 and 1406 nm. Peiris et al. (2009) related the spectral peak at 1363 nm with FDK, close to the 1350 nm we obtained. Nevertheless, we should consider that their analysis was on kernels contaminated in a broader range (33-1008 mg/kg) than the one we used (<LOD-135.7 mg/kg), in which they used artificial contamination that can cause differences in position and peak intensities.

Although previous studies did not reach accurate DON predictions in single kernels, the emerging of HSI technology may permit a fast analysis of specific regions from the image, as a single kernel or even a portion, for the contamination levels. On the other hand, Tekle et al. (2015) also evaluated DON contamination, although they used single oat kernels. They also worked with a spectrum for each reference value regarding an individual grain, using PLS regression to model them. Otherwise, they applied logarithmic functions to avoid non-linearities. The performance of their model reached an R^2 of 0.81 and an RMSECV of 39.8 mg/kg. Due to the high RMSE obtained, the authors considered HSI-NIR suitable for

FDK detection in oats. On the other hand, recently published works attempted the quantification of DON using HSI but in barley or corn (Parrag et al., 2020; Su et al., 2021). However, Parrag et al. (2020) predicted the level of DON in corn homogenized samples using a ROI of 20 x 100 pixels instead of single kernels. The model performance had an RMSEP of 11.95 mg/kg using 20 PC. Despite the results showing the difficulty to predict DON, we obtained better efficiencies for SK predictions (RMSEP = 6.65 mg/kg), even using naturally contaminated samples and a broader range of contaminations. Shi, Liu, Zhao, Liu, & Zheng (2020) studies focused on the Multispectral Imaging (MSI) analysis of 105 samples of 20 wheat grains instead of individual kernels with HSI. As they were working with the mean spectra of 20 wheat kernels, reference values presented fewer deviations than for SK analysis, in which the DON differences between grains are high. Thus, they obtained accurate predictions and classifications for wheat batches. MSI has been proposed as a potential technique for DON spectral analysis that could reduce data dimension and enhance analysis speed. Thus, characteristic wavelengths selection from HSI would be a considerable strategy to reduce data dimension. Despite the recent advances in DON detection by HSI-NIR, the correctness in toxin levels prediction need to improve. Consequently, discriminant strategies won popularity for DON management with HSI strategies.

The correlation between *Fusarium* and DON presence with the physical and chemical changes of the cereal kernels remains a goal for cereal sorting strategies. *Fusarium* and DON analysis by NIR spectroscopy usually presents sensitivity issues that should be monitored to detect contaminated grains. However, Jin et al. (2014) correlated the visually labelled FDK and SK-NIR data, obtaining a correlation of 0.72. In addition, the higher correlation between visual symptoms and DON suggested the use of both techniques for the indirect estimation of DON in wheat (0.74). However, the correlation of SK-NIR for FDK estimation

with DON falls to 0.49, which shows the difficulty of indirect detection of DON levels. Thus, classification strategies by NIR spectroscopy are more suitable than studying the correlation between fungal damage and DON.

Several authors focused on the NIR detection and classification of contamination on kernels. Singh et al. (2012) detected fungal damage on wheat kernels using NIR and colour imaging technologies. Although colour imaging obtained enhanced performances, NIR technology also gave good results, showing accuracies above 88.7%, especially in LDA models. From the full NIR spectra used by Pearson & Wicklow (2006), some wavelengths (580, 790 and 1405 nm) could describe the features of healthy and fungal infected maize with 85% and 98%, respectively. The authors also used kernels with advanced fungal symptomatology, and obtained a correct discrimination of 96.6%. Tallada, Wicklow, Pearson, & Armstrong (2011) categorized four levels depending on their stage of infection with LDA and multi-layer perception neural network (MLP). The reference criteria used was also according to the visual symptoms. The models could classify correctly the 89% and 79% of the control and infected kernels, respectively, which are comparable to ours (86%). All the authors cited in this section artificially inoculated fungi to their samples before NIR analysis. Consequently, the symptoms observed are sometimes more severe than using naturally contaminated samples and have to be considered when comparing the results.

In some studies, authors used different reference methods than visual inspection and artificial to detect fungi. Polder et al. (2005) quantified *Fusarium* amount on the kernel by quantitative Polymerase Chain Reaction (qPCR) analysis, avoiding the subjectivity of visual inspection, as it is specific on the fungal species of interest. The authors could correlate the spectral information with *Fusarium* DNA levels above 100 pg with an R^2 of 0.8.

HSI and MSI -NIRs discriminated wheat kernels according to DON levels. Chemometric methods modelled the spectral information extracted from single wheat kernels to discriminate them according to certain DON limits. There are not many studies available on the classification of wheat kernels according to DON levels. However, some authors also tried to classify cereal kernels according to different mycotoxins. Yao et al. (2013) used HSI to discriminate corn kernels according to AFs levels. The spectral ranges used were the Vis and the NIR, irradiating the sample with fluorescence light. Two classification models, different from the one applied in the present study and based on pixel discrimination, were implemented (maximum likelihood and binary encoding). Nevertheless, the binary encoding presented higher performance results with 87% correct classification for a 20 μg/kg threshold. The single-pixel analysis compares with the analysis of DON in oat kernels done by Tekle et al. (2015). They used PLS-DA to classify pixels according to DON with a correlation between predicted and measured values of 0.79. Following similar goals to those in the present study, some authors focused on the discrimination of DON contaminated kernels. Barbedo et al. (2017) developed an algorithm based on probability functions able to discriminate the images in three different groups (≤ 0.5 mg/kg; 0.5 - 1.25 mg/kg: > 1.25 mg/kg). Algorithms classified wheat batches (not individual kernels) with 72% accuracy for three classes. With the cut-off fixed at 1.25 mg/kg for the discrimination into two groups, the classification accuracy rose to 81%. The results were comparable with ours, as we obtained correctness above 76%, although we used individual kernels instead of groups of around 30-50 kernels.

Instead of building classification algorithms, Alisaac et al. (2019) compared spectral signatures of kernels with different DON concentrations. They obtained correlations of > 0.80 between the NIR spectra and DON. These high correlations in the NIR range suggest that our classifications models focused on the

information contained in specific regions, which account for the changes produced by fungi when DON is present. Several studies tried the detection of mycotoxins using HSI technologies. Nevertheless, most of them analysed bulk samples or grain groups instead of single kernels. Liang et al. (2020) and Shi et al. (2020) achieved the classification of bulk wheat and groups of wheat kernels, respectively, according to DON levels. Shi et al. (2020) focused on MSI for the calibration of the PLS-DA model with an accuracy precision of 94.29%. Although wheat grains were scanned individually in the crease-up and down position, they used 20 kernel batches for calibration and validation. Conversely, Liang et al. (2020) analysed 70 grains in each sample in the NIR range. The combination of SNV, GA and SAE showed their best performance, similar to the previous commented study.

7.6. Conclusions

HSI-NIR analysis of wheat individual kernels presented differences in the spectral profile from fungal and DON contaminated and non-contaminated grains. The differences in spectral intensities, especially between the 1100-1400 nm, could be correlated to the symptomatology caused by *Fusarium* growth on wheat kernels, and consequently, with an indirect DON prediction. However, the changes produced in the cereal chemical composition due to fungal growth, like proteins, carbohydrates and lipids, have more effects on the spectra than DON. DON quantification results show too high prediction errors to quantify DON at EU legal limits. Consequently, the authors focused on the discrimination of infected kernels as a more convenient mitigation approach. According to the results, it was proven that the classification strategies are more suitable for fungi and DON management in cereals than for their quantification, obtaining discrimination accuracies according to the EU cut-off around 86% and 77%, respectively. Thus, the detection of the low percentage of highly contaminated

kernels inside a batch would be a key mitigation strategy for contaminated cereals.

7.7. Acknowledgements

This work was supported by Project AGL2017-87755-R funded by MCIN/ AEI /10.13039/501100011033/ FEDER "Una manera de hacer Europa" and project PID2020-114836RB-I00 funded by MCIN/ AEI /10.13039/501100011033. The authors are grateful to the University of Lleida (predoctoral grant).

7.8. References

Agelet, L. E., & Hurburgh, C. R. (2010). A tutorial on near infrared spectroscopy and its calibration. *Critical Reviews in Analytical Chemistry*, *40*, 246–260.

Alisaac, E., Behmann, J., Rathgeb, A., Karlovsky, P., Dehne, H. W., & Mahlein, A. K. (2019). Assessment of *Fusarium* infection and mycotoxin contamination of wheat kernels and flour using hyperspectral imaging. *Toxins*, *11*, 1–18.

AOAC. (2005). Official Methods of Analysis. *Official Methods of Ananlysis of AOAC International*, *18*, 20877–22417.

Barbedo, J. G. A., Tibola, C. S., & Fernandes, J. M. C. (2015). Detecting Fusarium head blight in wheat kernels using hyperspectral imaging. *Biosystems Engineering*, *131*, 65–76.

Barbedo, J. G. A., Tibola, C. S., & Lima, M. I. P. (2017). Deoxynivalenol screening in wheat kernels using hyperspectral imaging. *Biosystems Engineering*, *155*, 24–32.

Champeil, A., Fourbet, J. F., & Doré, T. (2004). Effects of grain sampling procedures on *Fusarium* mycotoxin assays in wheat grains. *Journal of Agricultural and Food Chemistry*, *52*, 6049–6054.

Delwiche, S. R., Kim, M. S., & Dong, Y. (2011). *Fusarium* damage assessment in wheat kernels by Vis/NIR hyperspectral imaging. *Sensing and Instrumentation for Food Quality and Safety*, *5*, 63–71.

Delwiche, S. R., Pearson, T. C., & Brabec, D. L. (2007). High-Speed Optical Sorting of Soft Wheat for Reduction of Deoxynivalenol. *Plant Disease*, *89*, 1214–1219.

Delwiche, S. R., Rodriguez, I. T., Rausch, S. R., & Graybosch, R. A. (2019). Estimating percentages of *Fusarium*-damaged kernels in hard wheat by near-infrared hyperspectral imaging. *Journal of Cereal Science*, *87*, 18–24.

Dowell, F. E., Ram, M. S., & Seitz, L. M. (1999). Predicting scab, vomitoxin, and ergosterol in single wheat kernels using near-infrared spectroscopy. *Cereal Chemistry*, *76*, 573–576.

European Commission. (2006a). Commission Regulation (EC) Nº 1881/2006 of 19 December 2006. Setting maximum levels for certain contaminants in foodstuffs. *Official Journal of the European Communities*, *364*, 5–24.

European Commission. (2006b). Commission regulation (EC) Nº 401/2006 of 23 February 2006. Laying down the methods of sampling and analysis for the official control of the levels of mycotoxins in foodstuffs. *Official Journal of the European Union*, *70*, 12–34.

Femenias, A., Belén Bainotti, M., Gatius, F., Ramos, A. J., & Marín, S. (2021). Standardization of near infrared hyperspectral imaging for wheat single kernel sorting according to deoxynivalenol level. *Food Research International*, *139*, 109925.

Jaillais, B., Roumet, P., Pinson-gadais, L., & Bertrand, D. (2015). Detection of Fusarium head blight contamination in wheat kernels by multivariate imaging. *Food Control*, *54*, 250–258.

Jin, F., Bai, G., Zhang, D., Dong, Y., Ma, L., Bockus, W., & Dowell, F. (2014). *Fusarium*-damaged kernels and deoxynivalenol in *Fusarium*-infected U.S. winter wheat. *Phytopathology*, *104*, 472–478.

Liang, K., Huang, J., He, R., Wang, Q., Chai, Y., & Shen, M. (2020). Comparison of Vis-NIR and SWIR hyperspectral imaging for the non-destructive detection of DON levels in Fusarium head blight wheat kernels and wheat flour. *Infrared Physics & Technology*, *106*, 103281.

Liang, Kun, Liu, Q. X., Xu, J. H., Wang, Y. Q., Okinda, C. S., & Shena, M. X. (2018). Determination and visualization of different levels of deoxynivalenol in bulk wheat kernels by hyperspectral imaging. *Journal of Applied Spectroscopy*, *85*, 953–961.

Marroquín-Cardona, A. G., Johnson, N. M., Phillips, T. D., & Hayes, A. W. (2014). Mycotoxins in a changing global environment - A review. *Food and Chemical Toxicology*, *69*, 220–230.

Parrag, V., Gillay, Z., Kovács, Z., Zitek, A., Böhm, K., Hinterstoisser, B., … Baranyai, L. (2020). Application of hyperspectral imaging to detect toxigenic *Fusarium* infection on cornmeal. *Progress in Agricultural Engineering Sciences*, *16*, 51–60.

Paul, P. A., Lipps, P. E., & Madden, L. V. (2005). Relationship between visual estimates of Fusarium Head Blight intensity and deoxynivalenol accumulation in harvested wheat grain: A meta-analysis. *Phytopathology*, *95*, 1225–1236.

Pearson, T. C., & Wicklow, D. T. (2006). Detection of corn kernels infected by fungi. *Transactions of the ASABE*, *49*, 1235–1245.

Peiris, K. H. S., Bockus, W. W., & Dowell, F. E. (2016). Near-infrared spectroscopic evaluation of single-kernel deoxynivalenol accumulation and Fusarium

Head Blight resistance components in wheat. *Cereal Chemistry Journal*, *93*, 25–31.

Peiris, K. H. S., Pumphrey, M. O., Dong, Y., Maghirang, E. B., Berzonsky, W., & Dowell, F. E. (2010). Near-infrared spectroscopic method for identification of Fusarium head blight damage and prediction of deoxynivalenol in single wheat kernels. *Cereal Chemistry*, *87*, 511–517.

Peiris, K. H. S., Pumphrey, M. O., & Dowell, F. E. (2009). NIR Absorbance characteristics of deoxynivalenol and of sound and *Fusarium*-damaged wheat kernels. *Journal of Near Infrared Spectroscopy*, *17*, 213–221.

Polder, G., Van Der Heijden, G. W. A. M., Waalwijk, C., & Young, I. T. (2005). Detection of *Fusarium* in single wheat kernels using spectral imaging. *Seed Science and Technology*, *33*, 655–668.

Ropelewska, E., & Zapotoczny, P. (2018). Classification of *Fusarium*-infected and healthy wheat kernels based on features from hyperspectral images and flatbed scanner images: a comparative analysis. *European Food Research and Technology*, *244*, 1453–1462.

Sauer, D. B. (1988). Effects of fungal deterioration on grain: nutritional value, toxicity, germination. *International Journal of Food Microbiology*, *7*, 267–275.

Shi, Y., Liu, W., Zhao, P., Liu, C., & Zheng, L. (2020). Rapid and nondestructive determination of deoxynivalenol (DON) content in wheat using multispectral imaging (MSI) technology with chemometric methods. *Analytical Methods*, *12*, 3390–3396.

Singh, C. B., Jayas, D. S., Paliwal, J., & White, N. D. G. (2012). Fungal damage detection in wheat using short-wave near-infrared hyperspectral and digital colour imaging. *International Journal of Food Properties*, *15*, 11–24.

Su, W. H., Yang, C., Dong, Y., Johnson, R., Page, R., Szinyei, T., … Steffenson, B. J. (2021). Hyperspectral imaging and improved feature variable selection for

automated determination of deoxynivalenol in various genetic lines of barley kernels for resistance screening. *Food Chemistry*, *343*, 128507.

Sudakin, D. L. (2003). Trichothecenes in the environment: Relevance to human health. *Toxicology Letters*, *143*, 97–107.

Tallada, J. G., Wicklow, D. T., Pearson, T. C., & Armstrong, P. R. (2011). Detection of fungus-infected corn kernels using near-infrared reflectance spectroscopy and color imaging. *Transactions of the ASABE*, *54*, 1151–1158.

Tekle, S., Mage, I., Segtnan, V. H., & Bjornstad, A. (2015). Near-infrared hyperspectral imaging of *Fusarium*-damaged oats (*Avena sativa L.*). *Cereal Chemistry*, *92*, 73–80.

Yao, H., Hruska, Z., Kincaid, R., Brown, R. L., Bhatnagar, D., & Cleveland, T. E. (2013). Hyperspectral image classification and development of fluorescence index for single corn kernels infected with *Aspergillus flavus*. *Transactions of the ASABE*, *56*, 1977–1988.

Chapter 8. Determination of the best solvent for deoxynivalenol (DON) extraction from the maize for the subsequent Fourier transform infrared spectroscopic analysis with attenuated total reflection (ATR-FTIR) using advanced chemometric methods

Antoni Femenias, Polina Fomina, Valeria Tafintseva, Stephan Freitag, Volha Shapaval, Boris Zimmerman, Sonia Marín, Achim Kohler & Boris Mizaikoff

Preparing for submission

8.1. Abstract

Farmers, cereal suppliers and processors still demand rapid techniques for the assessment of mould-associated contamination. DON is one of the most produced *Fusarium* toxins, which is related to human and animal diseases and economic yield reductions. The regulatory routine analysis is based on chromatographic techniques, inconvenient for their high cost, time-consumption and use of pollutant chemicals. The present study evaluates the feasibility of FTIR on different extraction solvents to separate maize samples in contamination groups divided by the EU regulatory limit (1750 μg/kg). In this study, the liquid solvent was deposited on the diamond ATR-crystal, recording the MIR absorption spectrum. Reference DON concentrations were determined by LC-MS/MS. The studied maize varieties are naturally infected or have been artificially inoculated in the field with *F. graminearum*, *F. culmorum* or *F. verticillioides*. PCA exploratory analysis demonstrated that water and methanol (70%) were the solvents presenting fungal-related clusters over the rest. The supervised SPLS-DA results presented significant classification accuracies of 86.7% and 90.8% for water and methanol extracts, respectively. Fungal infection and DON contamination groups exhibited positive correlations with IR spectra variables associated with carbohydrates, proteins and lipid content changes in cereal.

Keywords: FTIR; Deoxynivalenol; Cereals; MIR; Chemometrics

8.2. Introduction

F. graminearum and *F. culmorum* are plant-pathogen fungal species commonly found on cereals that have several associated negative effects. In preharvest stages and during storage, these fungal species can grow on cereal ears and cause associated diseases. Maize ear rot is a severe disease caused by the growth of these species during flowering and before kernel development. Corn susceptibility to infection can trigger root, stalk and ear rot. Its most common effects are discolouration of ears, mycelial red or pink growth and drying of husks associated with weight loss. Thus, symptomatic ear affects cereal quality and it is also related to a decreased crop yield and economic loses (Logrieco, Mulè, Moretti, & Bottalico, 2002; Pascale, Visconti, & Chelkowski, 2002).

Under suitable conditions, these species can produce mycotoxins derived from their secondary metabolism. One of the most commonly produced mycotoxins by these fungal species is DON, which is a well-known mycotoxin generally found in cereals. Fungal secondary metabolism can be activated under favourable environmental conditions or due to inadequate storage, but DON is frequently produced and accumulated on grain during preharvest stages (Pestka, 2007). Furthermore, even the asymptomatic growth of *Fusarium* on maize ears can accumulate high amounts of DON, as well as FBs and other mycotoxins. Consequently, symptom inspection cannot be used as an indicator of mycotoxin presence (Gromadzka, Błaszczyk, Chełkowski, & Waśkiewicz, 2019). Recent studies confirmed that climatic change effects, as warmer weather, humidity, and extreme climate, have induced fungal growth with an increase of DON incidence (Uhlig et al., 2013).

On the other side, its presence is considered threatening to humans and livestock due to the associated diseases experienced by mycotoxin contaminated products consumers. The main health effects of DON intoxication are related to acute and

chronic toxicity. Acute response to DON poisoning can derive from emesis, diarrhoea, headache and gastrointestinal irritation, and it can derive to death if a high dose is consumed in a short period. On the other side, chronic exposure is related to nutritional and immunological disorders, teratogenicity, and carcinogenesis. Anorexia is a frequently detected problem in livestock that causes weight loss and derived economic impact (Pestka, 2010). In addition, due to its high stability, DON is not completely removed by commonly used food processing methods, such as milling, baking, boiling, etc. (Bullerman & Bianchini, 2007; Vidal et al., 2016). Consequently, to fight against *Fusarium* toxins contamination, many countries have established maximum levels for foodstuffs, in particular for DON. The maximum level set by the European Commission (2006) for DON in unprocessed maize is 1750 μg/kg and milled maize with a particle size larger than 500 μm has a limited value for DON of 750 μg/kg. Finally, for fractions with a particle size lower than 500 μm, the limit established is 1250 μg/kg.

The most commonly used methods for analysis of mycotoxins are conventional wet chemistry techniques, including LC and ELISA. Despite the high sensitivity and specificity for mycotoxin detection and quantification, they also present some shortcomings. The main drawbacks of these methods are the complexity in sample preparation, time-consumption, cost, sample-destruction and pollution (Turner et al., 2009). Other main disadvantages are the need for specialized personnel and expensive devices to detect mycotoxin contamination. Thus, new technologies are required for the rapid and cost-effective detection and quantification of mycotoxins in cereals.

Within optical methods, ATR-FTIR has been proposed as effective for its potential in mycotoxin detection in cereals. The implementation of FTIR, as it requires a minimum sample preparation, could reduce time dependence of the

analysis (Krska & Molinelli, 2007). Additionally, the amount of solvent needed for mycotoxin extraction is also notably reduced, thus it is considered an eco-friendly technique. FTIR has other associated advantages, such as the simultaneous compound analysis, reliability, robustness and potential to be miniaturized (Öner et al., 2019). FTIR is ideally suggested for a rapid in-field screening before laboratory confirmation with a reference analysis (e.g. LC-MS) if the levels are close to the legally established limits.

FTIR screens the stretching and bending vibrations of molecules to obtain a chemical outline of the sample. The region between 2500-25000 nm (MIR range) is a sufficiently reproducible area of the electromagnetic spectrum in which little variations of sample composition can be consistently detected (Subramanian & Rodriguez-Saona, 2009). Changes in protein, lipids and polysaccharides caused by fungal growth are translated into small changes in the spectral IR profile. The stretching vibrations of cereal samples are usually from carbonyl groups (CO) and amide, which correspond to polysaccharides and proteins, respectively. Nevertheless, for the interpretation of these changes in the IR spectrum it is not adequate to use a single spectral band. Thus, multivariate methods, such as PCA, PLS regression and DA (Kumar et al., 2014), are required to deal with numerous spectral features and overlapping absorption bands to obtain accurate and robust classification and quantification results (Öner et al., 2019).

This study describes the application of ATR-FTIR for DON detection in maize, thus a review of the most significant studies has been included. A method for FTIR analysis of *Fusarium* fungi was established, in which changes in spectra due to lipid, protein and carbohydrate content variations were measured. DON and ergosterol were taken as reference and classification of up to 75% were successfully performed (Kos et al., 2002). The classification was upgraded up to 100 % while sieving samples to similar particle size (Kos et al., 2003). The method

was optimized by the analysis of several particles for which 100-250 μm showed the best reproducibility. A decreased relative standard deviation of spectral measurements was obtained, thus classification results on DON analysis were successful (Kos, Lohninger, Mizaikoff, & Krska, 2007). Classifications on maize at DON regulatory limits were completed by Kos et al. (2016). FTIR was successful to discriminate samples with DON at 1750 and 500 μg/kg threshold with minimum sample pre-treatment for which it is proposed as a suitable method for rapid measurements at industrial entry or storage points. Other mycotoxins have been also evaluated by ATR-FTIR in cereal commodities. The application of the method to FBs analysis has not shown positive results for concentrations lower than 10 mg/kg and it was only possible to distinguish between extremely contaminated samples (190 mg/kg) and samples below 10 mg/kg (Jaksic et al., 2017). However, the application of machine learning algorithms to ATR-FTIR data showed exceptional results for DON contaminated samples classification (Öner et al., 2019).

ATR-FTIR has been applied to grinded cereal samples (Abramović et al., 2007; De Girolamo et al., 2019; Jaksic et al., 2017). IR-spectroscopy gathers molecular information of solid, liquid and gas samples. Hence, liquid extraction of cereal components for a subsequent analysis would be a promising approach to highlight soluble substances, especially DON. For that purpose, a study of the most suitable solvent which permits suitable discrimination between high and low contaminated samples is required. Thus, the main objective of this work was the determination of the most appropriate solvent for DON contaminated samples classification at the regulatory threshold. In the present study different organic solvents and mixtures of them with water have been tested. Afterwards, the results were analysed by PCA and SPLS-DA to determine the ability of the solvent to extract sample components to discern between groups.

8.3. Material and methods

8.3.1. Sample preparation

Maize samples were supplied by Saatbau Linz (SBL; Linz, Austria) and by the Cereal Research Center (CRC; Szeged, Hungary). The samples consisted of maize hybrids used for field production which included dent or flint kernels types. Besides, two types of contamination were performed. Low contaminated samples were obtained by natural contamination in the field. Conversely, contaminations were generated with artificial infection by silk injection or toothpick inoculation of *F. graminearum*, *F. verticillioides* or *F. culmorum*, each specie separately. The artificial infections were performed during preharvest. Silk channel infection was performed 5 days after 50% of silking and toothpick 10 days after 50% silking. Maize ears were injected in the silk channel with 2 ml of *Fusarium* suspension at a concentration of 5×10^5 conidia ml^{-1}. According to the method performed by Mesterházy (1977), in which a bubble breeding method in mung bean broth was used, the suspensions were obtained. Frozen aliquots (-80°C) were brought rapidly to 35°C before use. Alternatively, the toothpick method consisted in drilling a hole to the centre of the ear and inserting a toothpick with *Fusarium* isolate. Harvested samples were milled (Romer, Union, MO, USA) before the extraction with several solvents. The samples were labelled according to the inoculation method: injection of *F. graminearum* in the silk channel (IG); toothpick inoculation with *F. culmorum* (ZC); injection of *F. verticillioides* in the silk channel (IV); toothpick inoculation with *F. verticillioides* (ZV); and natural infection unknown strains (NA).

Before weighting, the obtained maize powder was shaken to homogenize the mycotoxin content. Then, 200 mg of powder were weighted at the precision balance (Sartorius Gmbh, Gottingen, Germany) and were transferred to a 1.5 ml tube (Eppendorf AG, Hamburg, Germany). 800 µl of solvent was added to the

tube. In the first part of the study, the tested solvents were: Water (100), Methanol:Water (70:30), Acetonitrile:Water (70:30), Ethanol:Water (70:30), Methanol:Water (30:70) and Methanol (100). The tubes were shaken horizontally on the VWR Rocking platform for 30 minutes at 70 rpm. Then, the extracts were centrifuged at the VWR Clinical 100 centrifuge for twice 2 minutes at 5800 rpm obtaining the liquid phase in each step. In the second part of the work, a deep evaluation of a green solvent (Water) and a non-green solvent Methanol:Water (70:30) was performed, increasing the number of samples in both datasets.

For the spectroscopic analysis, an aliquot of each extraction solution (10 μl) were poured on the ATR crystal so that it remained completely covered. In all cases, enough time was allowed for solvents to evaporate before analysing. The times used were 15 minutes for Water (100) and Methanol:Water (70:30); 5 minutes for Acetonitrile:Water (70:30), Ethanol:Water (70:30), Methanol:Water (30:70); and 2 minutes for Methanol (100). Once the solvent was evaporated, the thin film on the ATR crystal formed from the solution was analysed by FTIR spectroscopy. Between each analysis, the crystal was cleaned with isopropanol and the background was registered to avoid atmospheric effects. In the first part of the study, a reduced sample set was used to select, from the six solvents used, one green and one non-green solvent for further investigations. Once selected, additional samples were extracted following the same procedure to increase the dataset in order to attempt the calibration of robust classification models.

8.3.2. Infrared spectroscopy

All infrared spectra were registered using FTIR spectrometer ALPHA II with the platinum ATR unit and DLaTGS (L-alanine doped triglycine sulfate) detector (Bruker, Germany). The ATR unit is equipped with one reflection – diamond crystal as an ATR element. Opus 8.1. software (Bruker, Germany) was used to record the spectra. 128 scans with the resolution 2 cm^{-1} formed the spectrum of each sample. The spectral range of the MIR region (2500 – 25000 nm) was chosen for the analysis. However, the ranges 3225 – 3571 nm and 5555 – 12500 nm were significant for the chemometric evaluation, since all relevant bands for the analysis are in this region (Table 19), as was found out in the previous studies (Kos et al., 2016). Each extract was measured three times.

Table 19. Bands in the IR spectrum of maize in the MIR region.

Vibrations	Wavelength (nm)
C-H	3448
C-O ester stretching	5730
C-O fatty acid	5847
Amide I	6060
Amide II	6493
-C-H stretching, fatty acid	6711-7017
-C-H symmetric bending, methyl groups	7042-7518
Ring vibrations of carbohydrates	9708

Beyond the maize bonds, characteristic bonds of DON belong to the range of 5555 – 12500 nm: e.g. bond at 5952 nm, which corresponds to C-O vibrations.

EssentialFTIR Spectroscopy Software Toolbox (Operant LLC, USA) was used to convert the spectra to multifile for further convenient data evaluation. All data pre-processing was done during the chemometric analysis later on.

8.3.3. Reference method

Homogenised samples of 5 g were extracted with 20 ml of extraction solvent (acetonitrile/water/acetic acid 79:20:1, v/v/v) for 90 min on a rotary shaker (GFL 3017, Burgwedel, Germany). After a 1 + 1 (v/v) dilution using dilution solvent (acetonitrile/water/acetic acid 79:20:1, v/v/v), the diluted extracts were injected without further pre-treatment.

The analytical technique of Liquid Chromatography – Tandem Mass spectrometry (LC-MS/MS) with a QTrap 550 LC-MS/MS System (Applied Biosystems, USA) equipped with TurboIonSpray electrospray ionization (ESI) source and 1290 Series HPLC Systems (Agilent, Germany) has been applied as a reference method. The detailed parameters of the reference measurements are described by Kos et al. (2016). The accuracy of the method is verified on a routine basis by regular participation in proficiency testing schemes. This approach quantifies the exact concentrations of DON in the maize samples. The LODs for DON was 1.2 μg/kg.

8.3.4. Data analysis

Spectral quality test and outlier detection was done prior to analysis (Tafintseva, Shapaval, Smirnova, & Kohler, 2020). Thus, spectra of one sample from water dataset, one from acetone, one from ethanol, four from methanol 30%, three from methanol 100% were removed from the analysis. Spectral pre-processing was applied prior to data analysis and modelling. The following was done: (1) spectra of each sample were averaged; (2) second derivative was calculated using Savitzky-Golay algorithm (Savitzky & Golay, 1964; Zimmermann & Kohler, 2013) with second order polynomial and window size 13; (3) the spectral ranges 3225 to 3571 nm and 5555 to 12500 nm were chosen and used for the analysis; (4) extended multivariate signal correction (EMSC) was applied using linear and quadratic terms (Kohler, Solheim, Tafintseva, Zimmermann, & Shapaval, 2020;

Martens & Stark, 1991). The same pre-processing was applied to each dataset and the pre-processed spectra were used in all subsequent analysis.

PCA was applied in order to discover patterns in the data in an unsupervised manner. Further supervised analysis was done using SPLS-DA. SPSL-DA is a variable selection technique which is used to establish robust models which are much easier to interpret (Karaman et al., 2013; Lê Cao, Rossouw, Robert-Granié, & Besse, 2008). In SPLS-DA loading weights are penalized using soft thresholding resulting in sparse loadings. Sparse PLSR algorithm penalizes the loading weight vectors according to a parameter called degree of sparsity which defines a number of zeros in a given loading (Shen & Huang, 2008; Tafintseva et al., 2018). For each PLS component, we selected the degree of sparsity to be 99%. This means that for each PLS component 99% of variables were penalized and thus put to zero and only 1% of variables were used for model building.

The models established in the analysis were discriminative models for low vs high DON samples. The threshold was selected to be 1750 μg/kg according to the EU standard (European Commission, 2006). Thus, samples with DON < 1750 μg/kg were considered uncontaminated, while samples with DON ≥ 1750 μg/kg were considered contaminated with DON. The modelling was only possible for the samples extracted by water and methanol 70% since there were enough samples in each group whereas in other datasets obtained by other extraction methods there were not enough samples to perform classification.

SPLS-DA models were established using leave-one-out cross-validation. Such an approach is fully justified since no replicates were present in the dataset, all of them were averaged prior the analysis. The optimal number of LVs (A_{opt}) was selected based on the classification accuracy of the groups. The number was optimized to maximize the accuracy of the group with the lowest classification accuracy (Tafintseva et al., 2022). This approach helps avoiding biased

classification of one of the groups especially when the groups are unbalanced. Regression coefficients, scatter plots and correlation loading plots were used to learn about models and patterns in the data.

8.4. Results

8.4.1. DON variability within the maize samples

This study investigated a set of DON contaminated maize samples of known concentrations. DON concentration distribution is displayed to represent the number of samples within each contamination level for the two inoculation types used (Figure 29). It provides individually the DON concentrations distribution histogram for naturally contaminated and artificially inoculated samples. Comprehensibly, the concentration range for naturally contaminated samples was narrower (96 – 6528 μg/kg) than for inoculated ones (81.6 – 73840 μg/kg). Despite the range differences, both inoculation groups had balanced number of samples above and below the EU regulatory limit. Naturally contaminated sample set was composed of 11 samples at the low contamination group and 8 at the high contaminated one, while the inoculated set had 24 samples below the threshold and 32 above. The balanced contamination sets are crucial to build robust classification models at the established threshold.

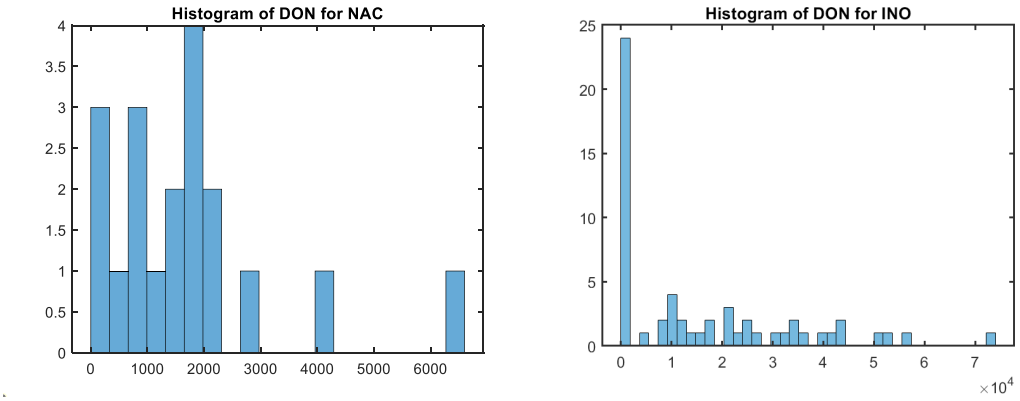

Figure 29. Histogram of DON concentrations of naturally contaminated (NAC) and artificially inoculated (INO) maize samples.

8.4.2. Spectral comparison of DON-contaminated and uncontaminated maize samples

The solid residue of 10 µl drops on the ~ 3 mm ATR crystal had enough homogeneous material to obtain 3 repeated sample measurements with adequate signals. The spectra obtained showed differences depending on the solvent used and their regions were identified according to the band assignments for MIR spectrum vibration assignments. Then, the range of interest was selected, avoiding solvent differences and regarding sample features differences, and it was fixed on 3225 – 3571 nm and 5555 – 12500 nm. This reduction in spectral range ensured the good representation of the sample and reduced noise and non-useful information on models. To obtain a first overview over the differences caused by fungal-related contaminations, the raw spectral differences of two maize extracts for each solvent were studied. Figure 9 (annex) shows the chemical differences at the fingerprint region between a high DON- contaminated sample (52.3 mg/kg) and an uncontaminated one (0.2 mg/kg) for the selected solvents. Water and methanol extract spectra presented more variations in absorbance intensities than acetonitrile and ethanol ones. Although the differences should be estimated with a larger sample set and using chemometric tools able to model the spectral variations, the representation is an initial approximation to determine the most suitable solvent for DON extraction. A deeper statistical analysis was obtained for a larger sample set by projecting their spectra with PCA.

8.4.3. Determination of the most suitable solvent to extract DON for FTIR spectra by PCA.

PCA analysis was done using FTIR spectra to determine which solvent better extracted fungi or DON-related components from the sample. The samples were

labelled as contaminated and uncontaminated depending on the DON concentration, previously analysed by LC-MS/MS. As we focused on the extraction power comparison of the different solvents, we established a 1750 μg/kg threshold, to evaluate the potential of FTIR to detect contamination at regulatory limits.

The differences between groups are presented in PCA score plots (see Figure 10, annex), where samples corresponding to the type of inoculation are differentiated by colour: naturally contaminated in blue and inoculated in red, while level of contamination is labelled by 0 representing uncontaminated samples and 1 representing contaminated samples, respectively. The PCA analysis shows that none of the solvents allow clear separation according to the contamination level, although some of them (e.g. ethanol) allow clearer separation of inoculated samples from naturally contaminated, more efficiently than acetonitrile. From the polar solvents tested, one of the green solvents (between water and ethanol) recommended for the solvent selection guides (Byrne et al., 2016) and one non-green solvent (methanol and acetonitrile), which can present environmental issues, were selected for the subsequent supervised modelling. The PCA score plots display a clustering tendency for the water extracts, although ethanol PCA showed an overlapping of uncontaminated samples (specified by 0 in plots) on the contaminated (specified by 1 in plots). In addition, the separation of water extracts was predominantly influenced by DON contamination, while ethanol extracts exhibited a separation according to the inoculation type (natural vs inoculation in blue and red colours, respectively). Regarding the nature of both compounds, despite both of them are non-toxic and bio-based, ethanol presents disadvantages, such as the flammability and production cost. Consequently, from the green solvents water was selected for its applications and preference.

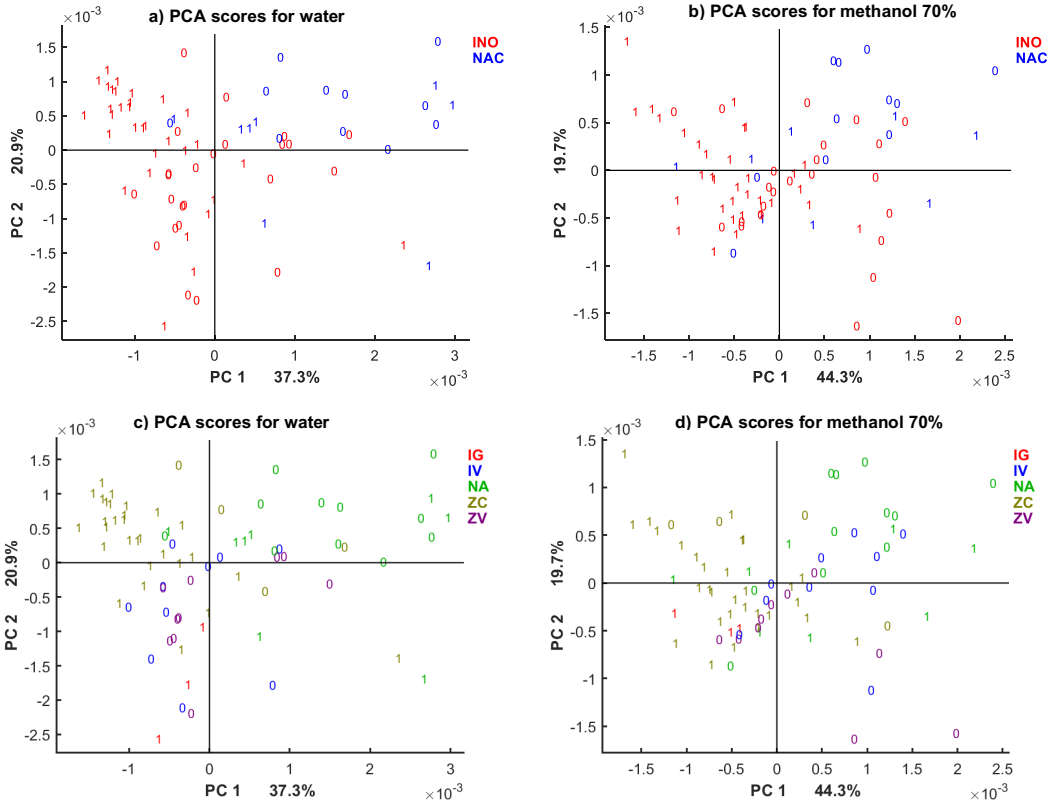

Figure 30. PCA score plot for the first two PCs of different solvents (a), (c) water, (b), (d) methanol 70% where colours of labels correspond to (a), (b) inoculation type: inoculated (INO) in red and naturally contaminated (NAC) in blue, (c), (d) fungal strain and inoculation method used (IG: *F. graminearum* in the silk channel; ZC: toothpick inoculation with *F. culmorum*; IV: injection of *F. verticillioides* in the silk channel; ZV: toothpick inoculation with *F. verticillioides* and; NA: natural infection, unknown strains), while labels correspond to DON levels where 0: DON < 1750 µg/kg, 1: DON ≥ 1750 µg/kg obtained by the reference method. The PCA plots (a), (c) and (b), (d) represent the same models, with different colour coding used.

From the non-green solvents, acetonitrile and methanol (100%) did not show clustering tendency in the PCA scores for the inoculation type neither for DON levels. Whereas for methanol (30%), we can see mostly clear clustering of the samples according to the inoculation type, for methanol (70%) the cluster tendency follows again the separation into DON groups according to the threshold without any observable impact of the inoculation type. In addition, methanol (30%) is almost a water-based solvent, for that reason, methanol (70%)

was selected as the non-green solvent for the further supervised analysis. Once water and methanol (70%) were selected, the datasets for each one were enlarged with new samples extraction.

Also, it was of interest to check whether clustering according to the inoculated species can be observed. The PCA score plot in Figure 30 provides this information and the inoculation type described in the previous section using the enlarged datasets. The samples are labelled by the fungal species inoculated by a given method: injection of *F. graminearum* in the silk channel (IG); toothpick inoculation with *F. culmorum* (ZC); injection of *F. verticillioides* in the silk channel (IV); toothpick inoculation with *F. verticillioides* (ZV); and natural infection unknown strains (NA). The PCA score plot show clear clustering according to the fungal species. Clustering was more well-defined for methanol (70%) extracts than for water. In methanol extracts, PC1 and PC2 divided more prominently between samples infected with *F. culmorum* (DON producer, samples in brown colour) from *F. verticillioides* (predominantly FBs producer, in blue and purple) and naturally contaminated (in green). Although the set only included three samples infected with *F. graminearum*, the samples were clustering in between two groups of inoculated samples. The results of unsupervised data analysis by PCA indicate that the fungal species produce different changes on the cereal matrix causing differences in MIR spectra. The PCA suggests that DON-producer species cause different compositional changes than the FBs-producer, providing broader separation from the naturally contaminated samples. Further, supervised multivariate analysis was used to obtain more information.

8.4.4. Determination of the best solvent to extract DON for FTIR analysis by supervised modelling based on SPLS-DA.

Classification of maize samples into contaminated and non-contaminated was done using SPLS- DA method. The threshold for was set at DON = 1750 μg/kg

and the two datasets evaluated were water extracts and methanol 70% extracts. Figure 31 presents the results of classification while Figure 32 provides scatter plots of the model to show the clustering patterns in the SPLS-DA model. We can observe that the difference between the two models accuracy is 4.1%, with higher accuracy in methanol 70% (90.8%) than water (86.7%). The models have the same number of LVs: A_{opt} = 11 which indicated moderate complexity. The overall number of samples incorrectly classified were 10 for water and 7 for methanol 70%. Among the total samples with contaminations ≥ 1750 µg/kg (40), 15% (7 samples) were incorrectly classified in water extracts, while 10% (4 samples) for methanol 70%, indicating that the percentage of false negatives is also higher for water extractions, while the number of false positives was equal (3 samples by both models). From the incorrectly classified samples, three were common in both models, with DON concentrations equal to 1904, 2024 and 6528 µg/kg. As can be seen, two of these samples have contamination close to the threshold 1750µg/kg. The most discriminant variables obtained from the regression models were 3418 & 3505 nm, 5730 – 6493 nm, 8695 – 10822 nm (highest peaks at 9523

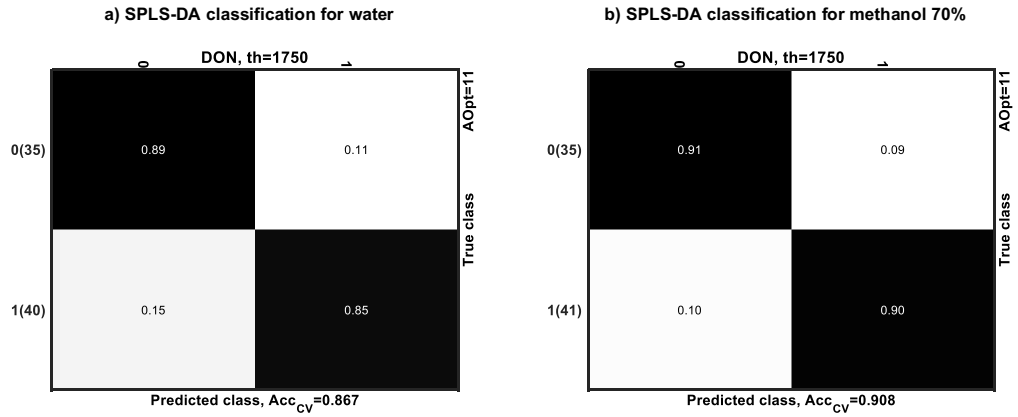

Figure 31. SPLS-DA classification results for maize samples into two groups: non-contaminated labelled as (0) DON < 1750 µg/kg and contaminated labelled as (1) DON ≥ 1750 µg/kg (a) in water and (b) methanol 70% extracts. The results are provided as accuracy of cross-validation, the number of latent variables are A_{opt} = 11 for both models, the number of samples are indicated in parenthesis next to groups' labels 1 and 0.

and 9842 nm) and 12195 nm for water, and 3428 – 3503 nm, 5770 nm, 6042 nm (amide I), 6410 nm (amide II), 7147 nm, 8695 – 10204 nm and 12195 nm for methanol 70%.

The scatter plots shown on Figure 32 represent patterns in the samples space of the SPLS-DA models. There are clear clusters of contaminated vs non-contaminated samples represented by labels 1 and 0, respectively, with a small cluster of overlapping samples. The clustering is also characterized by the type of inoculation: natural and inoculation represented by colours. Thus, both types of information are detected in spectra: inoculation type and contamination level. SPLS – DA model for methanol 70% did not present such clear clusters for the inoculation type (presented in colours), although a much clear clustering is observed according to DON contamination.

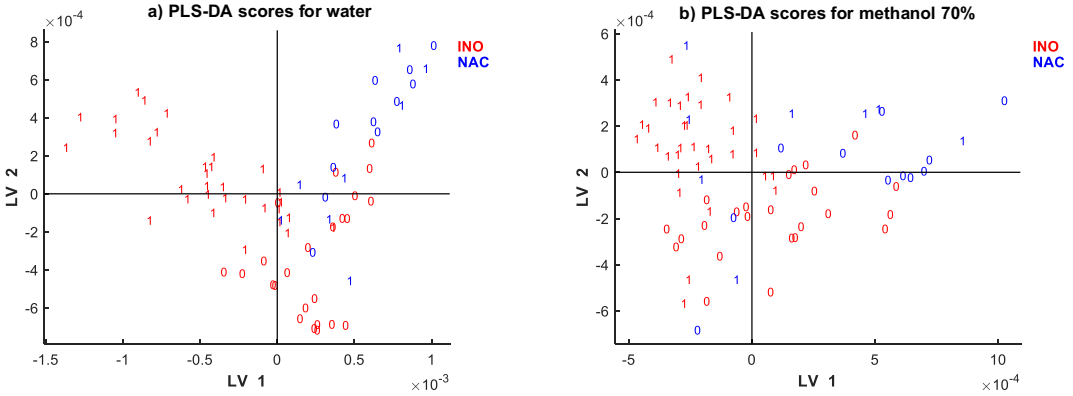

Figure 32. SPLS-DA score plot of different solvents (a) water and (b) methanol 70%. The colour corresponds to inoculation type: inoculated (INO) in red and naturally contaminated (NAC) in blue, and labels represent DON concentration (0: < 1750 μg/kg, 1: ≥ 1750 μg/kg).

To observe the influence of the samples clustering by different fungal species the same SPLS- DA models scatter plots are shown in Figure 33 labelled by the DON contamination level (0 or 1) but coloured by inoculated fungal species. Naturally contaminated samples form a separate group in green. The score plot showed clear clustering according to the fungal species. For water extracts, there is a clear

separation in LV1 of the samples infected by *F. graminearum* and *F. culmorum* (red circle) from the naturally infected samples in green. LV2 is separating these two clusters from a third cluster (showed in blue circle) represented by the samples infected with *F. vericilloides* by two types of inoculation: the injection into the silk channel (labelled by IV) and took pick inoculated samples (labelled by ZV), indicating that the clustering according to DON (0, 1) depends also on the fungal species infecting the sample and its ability to produce DON. In addition, injected and toothpick inoculated *F. verticilloides* are clustered together, suggesting that the type of inoculation does not affect the classification performance. There is a linear trend of fungal species shown by arrow in the LV1 and LV2 plane. There

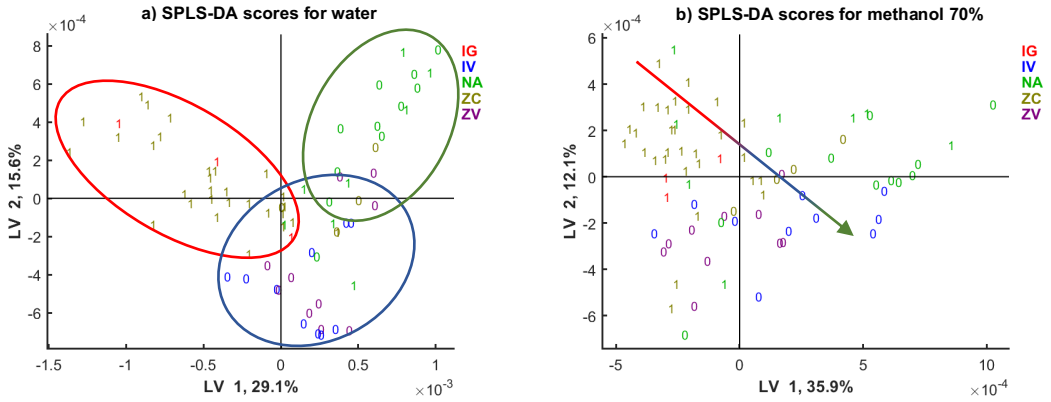

Figure 33. SPLS-DA score plot of (a) water and (b) methanol 70% extracts. Colours represent fungal strains and method of inoculation used (IG: *F. graminearum* in the silk channel; ZC: toothpick inoculation with *F. culmorum*; IV: injection of *F. verticillioides* in the silk channel; ZV: toothpick inoculation with *F. verticillioides* and; NA: natural infection, unknown strains) and labels represent DON concentration (0: < 1750 µg/kg, 1: ≥ 1750 µg/kg).

is a bit less of a separation of the naturally infected samples of maize in green.

To learn about pattern in the sample's space and variables space representing different spectral bands correlation loading plots were investigated. Such analysis allows easy visualization of the correlations between spectral variables, design parameters and any metadata available in the experiment. To obtain a

correlation loading plot, scores of the corresponding model are used and the variables of interest are projected onto the scores. Figures 34 (a) and (b) represent the correlation analysis for the water extracts and methanol 70% extracts, respectively. Based on the distances between variables in the correlation loading plot, variables clustering together are strongly correlated to each other. Points closer to the outer circles are highly important and well explained by the model, while those close to the centre do not have any importance. Points far along the LV1 and LV2 axes present no correlation.

In the correlation loading plots for both solvents, the origin of the samples (labelled by CRC and SBL) did not have importance for the model in LV 1 and 2, appearing in the centre of the plot. However, the inoculation type (inoculated or naturally infected, labelled by INO and NAC in purple) are negatively correlated

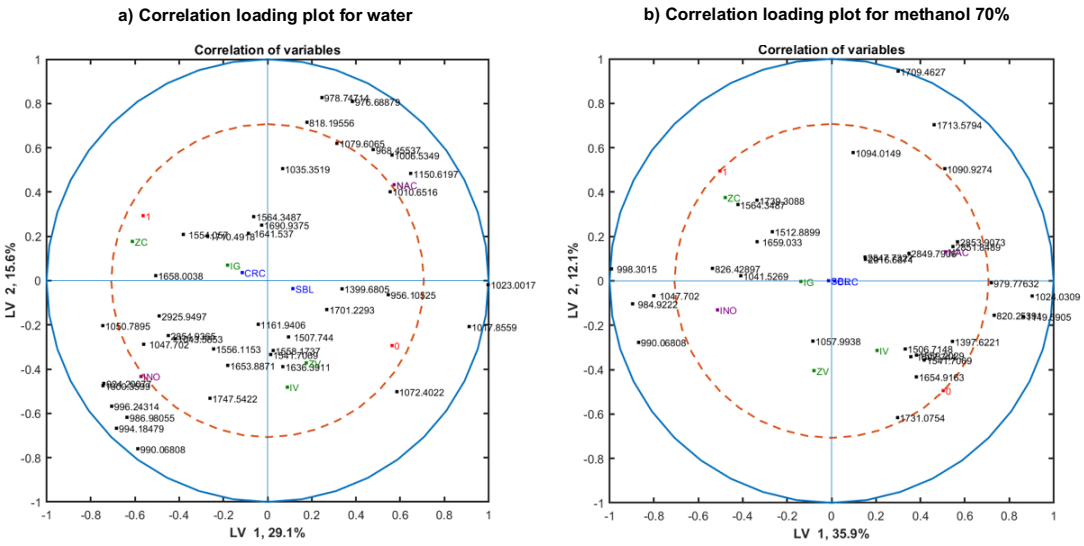

Figure 34. Correlation loading plots using SPLS-DA models' scores for (a) water and (b) methanol 70% showing correlations of the major spectral variables and design parameters such as maize origin, type of inoculation, fungal species and DON levels for the first two LVs. The labels are: *F. graminearum* in the silk channel (IG); toothpick inoculation with *F. culmorum* (ZC); injection of *F. verticillioides* in the silk channel (IV); toothpick inoculation with *F. verticillioides* (ZV); natural infection (NAC), inoculated (INO); Saatbau Linz (SBL); and Cereal Research Center (CRC).

with high importance on the model for both solvents, despite that the importance of them being slightly lower in methanol 70% extracted samples. Contrarily, the groups of samples with DON above and below the limit (labelled by 0 and 1 in red) for methanol 70% extraction presented higher importance than in water. However, for both solvents, they correlated negatively in the plot. It is important to underline that *F. culmorum* infected group positively correlated with DON contaminated samples. On the opposite side of the plot, *F. verticillioides* correlate negatively with the other fungal species and positively with DON contaminations below the threshold. It is also remarkable that both *F. verticillioides* inoculation methods (injection and toothpick inoculation) are highly correlated, demonstrating that the inoculation type does not matter as much as the fungal specie.

The spectral features with high influence in the models are similar for water and methanol 70% extracts in the inoculated (INO) group, represented mostly by the carbohydrate peaks in the region 9523 – 10101 nm. However, the correlation is completely different for naturally infected samples, showing a strong correlation of the carbohydrate peaks in the region 8695 – 10000 nm for water extracts, while fatty acids peaks of the region 3428 – 3512 nm were observed the for methanol 70%. The majority of peaks with high importance in the correlation loading plot of the water extracts are carbohydrate peaks and they are mostly correlated to the inoculation type. This means that water solvent extracts mostly sugars. Correlation loading plot of the methanol 70% extracts show a lot of different peaks, such as lipid peaks (5747 and 5777 nm), fatty acid peaks (3428 – 3512 nm), protein peaks (6027, 6045, 6393 and 6489 nm) in addition to carbohydrate peaks (9551, 10101 and 10162 nm). Those bands have also high importance on the model and correlate to the DON levels (below and above the threshold).

8.5. Discussion

In this study, a variety of contaminated samples with different fungal species and DON levels around the EU regulatory cut-off were used to prove the feasibility of FTIR to discriminate the class of contaminated maize samples (DON ≥ 1750 µg/kg) from non-contaminated ones (DON < 1750 µg/kg). In the first instance, the selection of the maximum valuable spectral region is fundamental to remove the non-informative variables. The lipid-water (3225 – 3571 nm) and the fingerprint region (5555-12500 nm) used in the analysis proved to contain enough information to discriminate between DON contaminated and uncontaminated samples (Figure 9, annex, shows the fingerprint region). Due to DON polarity, several polar solvents were selected to test their ability to extract DON from maize samples. However, the other polar matrix compounds extracted by those solvents should be considered as associated with DON produced by fungal infections. Further studies including nonpolar solvents to determine fungal growth associations with nonpolar compounds, such as lipids, should be considered. DON contamination in maize samples was broadly distributed on equitable parts for edible and unfit for consumption. Understandably, the number of inoculated samples with high DON was higher than in naturally-contaminated ones. However, the number of naturally contaminated samples above the DON threshold and inoculated below it was enough to ensure the representation of both groups and, at the same time, the variability was full on each class. In addition, this study used a larger sample set than previously published investigations with similar aims (Abramović et al., 2007; Sieger et al., 2017). A considerable number of samples with concentrations close to the limit was used to obtain a robust model (see Figure 29). The DON concentration distribution at cut-off concentrations ensured the representability of

contaminations at field common levels as the studies of Kos et al. (2016) and Öner et al. (2019).

Considering the unsupervised modelling and the recommendations in solvent selections, acetonitrile and ethanol exhibited disadvantages against the other solvents tested. Contrarily, methanol 70% and water PCA plots displayed a tendency in separation depending on the artificial and natural contamination, reinforced by the fungal species clustering. PCA results proved the extracts' ability to form clusters on contamination and indicated that the clustering depended on the fungal components and their compositional changes produced in the cereal matrix extracted by the polar solvents. The supervised results provided a more in-depth explanation of the clustering behaviour and the related IR variations.

SPLS-DA classifications exhibited high accuracies in water (86.7%) and methanol 70% (90.8%) for the chosen threshold (DON = 1750 µg/kg). From the incorrectly classified, four and three samples for each solvent, respectively, presented DON levels close to the cut-off, two of them in common in both models. Some deviations between FTIR and reference analysis could be caused by the different subsample analysis. In addition, the reference analysis error must be considered, which is approximately 5% with a tendency to overestimate DON concentration. The error depends on the extraction recovery, the matrix effect and the apparent recovery. Literature displayed RSD_r for DON in maize, reporting recovery errors between 10-20% (De Santis et al., 2017; Santini, Ferracane, Somma, Aragón, & Ritieni, 2009). Thus, the 5% error would be optimistic and could reach higher deviations in DON measurements. It is important to notice that, if uncertainties of 20% were considered, the accuracies could increase to 90.7% for water and 93.4% for methanol, remaining two samples close to the threshold value (1708.9 and 1747.2 µg/kg). Although samples with concentrations near the threshold

induce error, it is important to point out that are required to train the algorithms at cut-off concentrations, modelling the small differences that decide whether samples are rejected or accepted.

DON cannot be directly determined in maize by IR technques because of the overlapping of the DON signals with the matrix features, displaying a convoluted spectrum. Extensive approaches were used to identify the source of variations induced by different experimental parameters such as inoculation type and fungal species. SPLS-DA scores exhibited defined clusters for classes of the above and below the DON threshold in both solvents and similar tendency in grouping samples by the inoculation type (artificial or natural). However, not only the inoculation type was investigated but also the influence of the diverse fungal species on the model ability to discriminate DON classes, which demonstrated a correlation between the fungal species and DON classes. The results match those of Kos et al. (2016), whose classification could more precisely discriminate DON contaminated maize samples from blank samples when using only *F. graminearum* and *F. culmorum* inoculated samples (79%) than using additionally *F. verticillioides* inoculated samples, which impact negatively on the accuracy (73%). Despite we did not work with maize powder, our SPLS-DA score plots could prove that DON-producer species separate well from the naturally infected but at the same time *F. verticillioides* (producing in majority FBs) forms a cluster in between, which could reduce the model performance. Despite the tendency of forming clusters for the inoculation type (natural or artificial), the SPLS-DA results reveal that the clustering is more important due to the different fungal species used. Thus, the clustering tendency according to inoculation type could be attributed to the differences caused by the fungal species.

The correlation loadings plot showed that variations in IR spectra that were important for the classification of DON groups were associated with the

proteolytic fungal activity causing the degradation of cereal reserve proteins and of proteins from plant cell walls (affecting mainly the 6060 nm and at 6451 nm bands) (Alconada, Moure, & Ortega, 2019). We observed that *F. culmorum* infected samples positively correlated with high DON in both solvents. The most relevant spectra signatures for the DON groups are encompassed between the 5747 – 6622 nm region corresponding to the double bond region (carbonyl, carboxylic acids and amide groups), which can be related to the lipid and protein content. These signatures were much stronger represented when methanol 70% was used. It has been reported that *F. culmorum* inoculation reduces the overall lipid content in cereals due to the predominant reduction of oleic acid (Havrlentová et al., 2021). *F. graminearum* infection had a minor influence on the correlation loading plot. Also, it has been described that its infection reduces the lipid content but to a lesser extent than for *F. culmorum* infection. The lipid variations influence also naturally contaminated samples, with characteristic peaks predominantly in the 3389 – 3508 nm region. But for the naturally contaminated samples the fungal species are unknown. This region is primarily related to absorptions in alkyl groups, which could be methyl alcohols or methyl ketones as a product of the β-oxidation of lipids and fatty acids.

Characteristic peaks correlated positively to *F. culmorum* and DON are 6435 nm in water and 6393 nm in methanol 70% related to N–H absorptions (functional groups found in proteins). Literature reported alterations in proteins depending on the fungal species infecting the cereal. It is reported that during pathogenic instigation, plant cells increase structural protein content on cell wall as a defensive function to avoid the pathogen penetration (Houston, Tucker, Chowdhury, Shirley, & Little, 2016). Cereal quality is reduced in fungal infection episodes caused by the deterioration of proteins and carbohydrates. Apart from the amide bands, a strong correlation between the inoculation type (natural or artificial) the alcohol functional group (C–O) was reported, primarily for natural

infections in water extracts (9267, 9900, 9940 and 10330 nm) but also for inoculated samples extracted with methanol 70% (9551, 10101 and 10162 nm), mostly due to polysaccharide absorption. Also, *F. verticillioides* and naturally infected samples exhibited a positive correlation with carbohydrates characteristic peaks (9460 and 9661 nm, respectively). Hettiarachchy & Boyacioğlu (1995) reported that the total amount of reducing and nonreducing sugars increases during *Fusarium* growth caused by the destruction of starch and cellulose.

The general results indicated that the classification of samples according to the DON regulatory threshold depends on the inherent food biomolecules alterations, such as lipids, proteins and carbohydrates. Those variations are reported to be correlated to the fungal species infecting the cereal. Methanol and water-based extracts presented similar performances, despite methanol- based models were slightly more accurate. However, special consideration has to be taken to water as an environmentally friendly solvent. Non-polar solvents should also be tested, due to the reported influence of the lipid regions related to the fungal species and DON contamination. Some issues still need to be addressed, such as bigger sample set where more infected samples by each fungal species should be a included. In addition, the naturally contaminated samples are required to build a classification model able to manage the common field DON concentrations. In addition, including more samples with DON concentrations close to the threshold would be also convenient to build robust classifiers able to detect the small variations at cut-off levels and improve the discrimination around those levels.

8.6. Conclusions

The unsupervised and supervised analysis used in this study demonstrated the feasibility of water and methanol (70%) over other polar solvents to extract DON

associated components from maize samples and discriminate them into groups of contaminated vs non-contaminated with DON regulatory threshold of 1750 μg/kg with an accuracy of 86.7% and 90.8%, respectively. The results demonstrated the correlation of the maize extracts from the DON-producer fungal species (*F. culmorum* and *F. graminearum*) with DON contaminated extracts (DON ≥ 1750 μg/kg), both negatively correlated with the maize extracts from FBs-producer (*F. verticillioides*) and the non-contaminated group (DON < 1750 μg/kg). The biomolecular changes in cereal matrix and fungal specie infecting the samples appear to be the resulting factors for the high accuracy of classification of the maize samples contaminated by DON and non-contaminated samples, overcoming the low sensibility of IR to detect DON molecules in food. Therefore, the extraction of DON associated components and their detection by FTIR analysis is feasible and could be used in routine analysis. A rapid sample preparation and a data analysis automatization makes this approach practical for its implementation in cereal industry during processing and storing stages. Moreover, the suitability of water as the extraction solvent offers a non-pollutant sorting tool before LC-MS positive confirmation. Further developments must be focused on the optimization of the FTIR measurement set up, reinforcing the fungal species and DON variability, building a robust model to monitor the recently increased DON occurrences caused by climate change.

8.7. Acknowledgements

The authors thank Robert Taucher at Saatbau Linz, Austria, and Professor Akos Mesterhazy at the Cereal Research Centre, Szeged, Hungary, for providing the hybrids used in this study.

This work was supported by PHOTONFOOD project.

8.8. References

Abramović, B., Jajić, I., Abramović, B., Ćosić, J., & Jurić, V. (2007). Detection of deoxynivalenol in wheat by fourier transform infrared spectroscopy. *Acta Chimica Slovenica*, 54, 859–867.

Alconada, T. M., Moure, M. C., & Ortega, L. M. (2019). *Fusarium* infection in wheat, aggressiveness and changes in grain quality: a review. *Vegetos*, *32*, 441–449.

Bullerman, L. B., & Bianchini, A. (2007). Stability of mycotoxins during food processing. *International Journal of Food Microbiology*, *119*, 140–146.

Byrne, F. P., Jin, S., Paggiola, G., Petchey, T. H. M., Clark, J. H., Farmer, T. J., … Sherwood, J. (2016). Tools and techniques for solvent selection: green solvent selection guides. *Sustainable Chemical Processes*, *4*, 1–24.

De Girolamo, A., Cervellieri, S., Cortese, M., Porricelli, A. C. R., Pascale, M., Longobardi, F., … Lippolis, V. (2019). Fourier transform near-infrared and mid-infrared spectroscopy as efficient tools for rapid screening of deoxynivalenol contamination in wheat bran. *Journal of the Science of Food and Agriculture*, *99*, 1946–1953.

De Santis, B., Debegnach, F., Gregori, E., Russo, S., Marchegiani, F., Moracci, G., & Brera, C. (2017). Development of a LC-MS/MS method for the multi-mycotoxin determination in composite cereal-based samples. *Toxins*, *9*, 169.

European Commission. (2006). Commission Regulation (EC) N° 1881/2006 of 19 December 2006. Setting maximum levels for certain contaminants in foodstuffs. *Official Journal of the European Communities*, *364*, 5–24.

Gromadzka, K., Błaszczyk, L., Chełkowski, J., & Waśkiewicz, A. (2019). Occurrence of mycotoxigenic *Fusarium* species and competitive fungi on preharvest maize ear rot in poland. *Toxins*, *11*, 224.

Havrlentová, M., Šliková, S., Gregusová, V., Kovácsová, B., Lančaričová, A.,

Nemeček, P., … Hozlár, P. (2021). The influence of artificial *Fusarium* infection on oat grain quality. *Microorganisms*, *9*, 1–13.

Hettiarachchy, N. S., & Boyacioğlu, D. (1995). Changes in some biochemical components of wheat grain that was infected with *Fusarium graminearum*. *Journal of Cereal Science*, *21*(1), 57–62.

Houston, K., Tucker, M. R., Chowdhury, J., Shirley, N., & Little, A. (2016). The plant cell wall: A complex and dynamic structure as revealed by the responses of genes under stress conditions. *Frontiers in Plant Science*, *7*, 1–18.

Jaksic, S., Jajic, I., Despotovic, V., Zivkov-Balos, M., Stojanov, I., Krstovic, S., … Abramović, B. (2017). Application of ATR-FTIR analysis for determination of fumonisins in corn. *Zbornik Matice Srpske Za Prirodne Nauke*, *133*, 47–56.

Karaman, I., Qannari, E. M., Martens, H., Hedemann, M. S., Knudsen, K. E. B., & Kohler, A. (2013). Comparison of Sparse and Jack-knife partial least squares regression methods for variable selection. *Chemometrics and Intelligent Laboratory Systems*, *122*, 65–77.

Kohler, A., Solheim, J. H., Tafintseva, V., Zimmermann, B., & Shapaval, V. (2020). Model-Based Pre-Processing in Vibrational Spectroscopy. In *Comprehensive Chemometrics*, 83–100.

Kos, G., Lohninger, H., & Krska, R. (2002). Fourier transform mid-infrared spectroscopy with attenuated total reflection (FT-IR/ATR) as a tool for the detection of *Fusarium* fungi on maize. *Vibrational Spectroscopy*, *29*, 115–119.

Kos, G., Lohninger, H., & Krska, R. (2003). Development of a Method for the Determination of *Fusarium* fungi on corn using Mid-Infrared spectroscopy with Attenuated Total Reflection and chemometrics. *Analytical Chemistry*, *75*, 1211–1217.

Kos, G., Lohninger, H., Mizaikoff, B., & Krska, R. (2007). Optimisation of a sample preparation procedure for the screening of fungal infection and assessment of deoxynivalenol content in maize using mid-infrared attenuated total

reflection spectroscopy. *Food Additives and Contaminants*, *24*, 721–729.

Kos, G., Sieger, M., McMullin, D., Zahradnik, C., Sulyok, M., Öner, T., … Krska, R. (2016). A novel chemometric classification for FTIR spectra of mycotoxin-contaminated maize and peanuts at regulatory limits. *Food Additives & Contaminants: Part A*, *33*, 1596–1607.

Krska, R., & Molinelli, A. (2007). Mycotoxin analysis: State-of-the-art and future trends. *Analytical and Bioanalytical Chemistry*, *387*, 145–148.

Kumar, N., Bansal, A., Sarma, G. S., & Rawal, R. K. (2014). Chemometrics tools used in analytical chemistry: an overview. *Talanta*, *123*, 186–199.

Lê Cao, K.-A., Rossouw, D., Robert-Granié, C., & Besse, P. (2008). A Sparse PLS for Variable Selection when Integrating Omics Data. *Statistical Applications in Genetics and Molecular Biology*, *7*, Article 35.

Logrieco, A., Mulè, G., Moretti, A., & Bottalico, A. (2002). Toxigenic *Fusarium* species and mycotoxins associated with maize ear rot in Europe. *European Journal of Plant Pathology*, *108*, 597–609.

Martens, H., & Stark, E. (1991). Extended multiplicative signal correction and spectral interference subtraction: New preprocessing methods for near infrared spectroscopy. *Journal of Pharmaceutical and Biomedical Analysis*, *9*, 625–635.

Mesterházy, Ák. (1977). Reaction of winter wheat varieties to four *Fusarium* species. *Journal of Phytopathology*, *90*, 104–112.

Öner, T., Thiam, P., Kos, G., Krska, R., Schwenker, F., & Mizaikoff, B. (2019). Machine learning algorithms for the automated classification of contaminated maize at regulatory limits via infrared attenuated total reflection spectroscopy. *World Mycotoxin Journal*, *12*, 113–122.

Pascale, M., Visconti, A., & Chelkowski, J. (2002). Ear rot susceptibility and mycotoxin contamination of maize hybrids inoculated with *Fusarium* species under field conditions. In *European Journal of Plant Pathology*, *108*, 645–651.

Pestka, J. J. (2007). Deoxynivalenol : Toxicity, mechanisms and animal health risks. *Animal Feed Science and Technology*, *137*, 283–298.

Pestka, J. J. (2010). Deoxynivalenol: Mechanisms of action, human exposure, and toxicological relevance. *Archives of Toxicology*, *84*, 663–679.

Santini, A., Ferracane, R., Somma, M. C., Aragón, A., & Ritieni, A. (2009). Multitoxin extraction and detection of trichothecenes in cereals: an improved LC-MS/MS approach. *Journal of the Science of Food and Agriculture*, *89*, 1145–1153.

Savitzky, A., & Golay, M. J. E. (1964). Smoothing and differentiation of data by simplified least squares procedures. *Analytical Chemistry*, *36*, 1627–1639.

Shen, H., & Huang, J. Z. (2008). Sparse principal component analysis via regularized low rank matrix approximation. *Journal of Multivariate Analysis*, *99*, 1015–1034.

Sieger, M., Kos, G., Sulyok, M., Godejohann, M., Krska, R., & Mizaikoff, B. (2017). Portable infrared laser spectroscopy for on-site mycotoxin analysis. *Scientific Reports*, *7*, 44028.

Subramanian, A., & Rodriguez-Saona, L. (2009). Fourier Transform Infrared (FTIR) Spectroscopy. *Infrared Spectroscopy for Food Quality Analysis and Control*, 145–178).

Tafintseva, V., Lintvedt, T. A., Solheim, J. H., Zimmermann, B., Rehman, H. U., Virtanen, V., … Kohler, A. (2022). Preprocessing strategies for sparse infrared spectroscopy: A case study on cartilage diagnostics. *Molecules*, *27*, 1–15.

Tafintseva, V., Shapaval, V., Smirnova, M., & Kohler, A. (2020). Extended multiplicative signal correction for FTIR spectral quality test and pre-processing of infrared imaging data. *Journal of Biophotonics*, *13*, 1–15.

Tafintseva, V., Vigneau, E., Shapaval, V., Cariou, V., Qannari, E. M., & Kohler, A. (2018). Hierarchical classification of microorganisms based on high-

dimensional phenotypic data. *Journal of Biophotonics*, *11*, 1–10.

Turner, N. W., Subrahmanyam, S., & Piletsky, S. A. (2009). Analytical methods for determination of mycotoxins: A review. *Analytica Chimica Acta*, *632*, 168–180.

Uhlig, S., Eriksen, G. S., Hofgaard, I. S., Krska, R., Beltrán, E., & Sulyok, M. (2013). Faces of a changing climate: Semi-quantitative multi-mycotoxin analysis of grain grown in exceptional climatic conditions in Norway. *Toxins*, *5*, 1682–1697.

Vidal, A., Sanchis, V., Ramos, A. J., & Marín, S. (2016). The fate of deoxynivalenol through wheat processing to food products. *Current Opinion in Food Science*, *11*, 34–39.

Zimmermann, B., & Kohler, A. (2013). Optimizing Savitzky–Golay Parameters for improving spectral resolution and quantification in infrared spectroscopy. *Applied Spectroscopy*, *67*, 892–902.

Chapter 9. General discussion

Mycotoxins are secondary fungal metabolites that accumulate in plants during growing or in post-harvest stages and are a risk for human and animal health. Fungal and mycotoxin presence in the food industry remains a frequent problem. Their management in field is especially difficult for cereal producers, thus mycotoxin contaminated grains, especially produced by *Fusarium*, arrive to industry entrance and cause production yield reduction and associated economic losses. Mycotoxins removal from cereals is complex due to their stability during food processing. Consequently, the surveillance and prevention of fungal infections in pre-harvest and post-harvest stages are crucial to avoid mycotoxins entering the food chain. The main step between harvest and cereal processing is the product reception in the cereal industries. Cereal receptors analyse the material using several methods to check that suppliers provide uncontaminated products. Some official sampling methods are available to overcome the frequent heterogeneity of cereal contamination before the analysis. They focus on enough sample size collection and its homogenisation to obtain an overall representative contamination level from the batch.

The AOAC (2005) proposed analytical chemistry operations for sampling from bulk or packaged goods. Samples from three separated regions of the bulk content or three packs should be collected. For bulk cereals, the three gross samples are aggregated to form a composite. Then, a subsample is collected from the gross, and divided into different laboratory samples, grinding them before the analysis. Packages are divided first into primary samples and then separated twice into aggregates and subsamples. The three subsamples are joined and ground before laboratory analysis. The European Commission (2006) laid down the official control sampling methods for mycotoxins in cereals. Lots > 50 tonnes must be divided either into three sub lots or several sub lots of either 100 or 500 tonnes (depending on their weight). At least 100 incremental samples must be collected from each sub lot. The aggregate sample weight (100 incremental

samples of at least 100 grams samples) must be 10 kg. For lots < 50 tonnes, 3-100 incremental samples must be taken, depending on the lot weight. In this case, the aggregate sample weight must be 1-10 kg. The sampling method shows that from a lot weighing several tonnes, only a few kilograms from each lot reach the laboratory, from where a portion is analysed. Consequently, although those strategies intend to represent as much as possible the entire batch contamination, it remains a problem for mycotoxins mitigation, which would still put consumers and livestock at risk.

The European Comission (2006) does not suggest the methods of analysis for mycotoxins in food, despite they propose several criteria that they should accomplish, such as repeatability, reproducibility and recovery. Following the standards, chromatographic and immunologic methods are the most frequently used for mycotoxin analysis in cereals. However, although they accomplish the EU recommendations, they present drawbacks predominantly related to the operation time, the analysis costs, the sample destruction and the green relation with the environment. In addition, the previously discussed sampling methods also demonstrate the complexity of working with heterogeneous contaminations, which may cause deviations in the results. Thus, future studies should focus on emergent technologies to overcome the problems presented by traditional wet chemistry, immunological and sampling methods.

In recent times, sensors have been currently implemented in the food industry to detect chemical or biological compounds, determine adulterations or monitor food processes (El-Mesery, Mao, & Abomohra, 2019). Such technologies attempt the online monitoring of food quality. Therefore, they must have short operation time to obtain the results while screening. In addition, the food industry demands pocket-sized and portable technologies to be carried into the field to analyse preharvest products in situ. Although some advances are available in online monitoring of several quality parameters applied in the cereal fields,

fungal infections and mycotoxins detection methods are still unavailable (Huang, Liu, & Ngadi, 2014).

Spectroscopic methods are applied broadly as an alternative to chromatographic methods in food analysis for their potential for the fast determination of multiple food compounds. Food producers demand NIR devices due to their cost-effectiveness, stability to environmental factors and spectral information. NIR spectrometers are found commonly in the food chain to determine the compositional parameters of products. Despite NIR's application remaining popular for food analysis, the interest has increased in MIR spectroscopy for its reproducibility, simple qualitative analysis and strong signals. In some studies, both spectral regions are combined to obtain more information about the sample, increasing the analytical power (Bureau et al., 2019; Caporaso et al., 2018).

HSI has drawn the attention of food suppliers and industry for the benefits of its application to cereal analysis. The space vision of the HSI devices introduces various advantages to the conventional spectrometers. Unlike those methods that require an extraction or grinding step, HSI analysis does not demand sample destruction or solvents, so the analysed cereals can remain in the further processing steps. Spectroscopy could be extremely useful in cereal analysis as a rapid complementary technique to chromatography. Moreover, HSI opens a broad range of possibilities for cereal analysis, which has to be fixed depending on the requirements of the food industry. The present work has two main targets: the first for sample analysis as a complement to the conventional methods used at cereal reception in the food industry; the second for online sorting purposes, analysing cereal kernels individually to discriminate the high-contaminated ones. A third complementary target focused on the most suitable solvent selection for cereal analysis by FTIR. The following sections discuss the most relevant results, providing a global vision of the calibration and applications.

9.1. Preliminary work for wheat samples HSI analysis

9.1.1. Region of interest selection

The ROI selection is a crucial step for cereal analysis. The sample delimitation from the surroundings is required to obtain the desired information, avoiding background or noise deviations. Several ROI selection methods have been applied, segmenting cereal samples before HSI analysis. The present work selected in triplicate the similar spectrum pixels by Euclidian distance as the most suitable ROI delimitation method, which is a fast-manual selection. However, other authors used diverse segmentation techniques to remove the contributions from the background. The most frequent approach for removing the non-desired surrounding noise was to establish an intensity threshold between one or more spectral bands. The intensities of the pixels above and below the threshold correspond to the kernel and the background, respectively. Typically, the spectral band that presents more variations between the cereal pixels and the surroundings is selected by normalising intensities to values between 0 – 1 and establishing the threshold between 0.1 – 0.25. The pixel spectrum is removed if the selected wavelength intensity value is below the threshold. This ROI selection processing is the most frequent in the studies aiming the fungal and mycotoxins analysis (Delwiche & Kim, 2000; Delwiche et al., 2010, 2011; Delwiche et al., 2019; Liang et al., 2020; Polder et al., 2005; Shahin & Symons, 2011, 2012). Although it is simple, it presents some drawbacks, as the kernels reflectance differences caused their deformities, noise influence from the background and the specular reflection. Some authors attempted to solve this problem using the variations of four bands instead of a single band (Barbedo et al., 2015; Barbedo et al., 2017). However, they proposed using manual selection when some crucial wavelengths are not available to discern the delimitation region.

9.1.2. Chemometric tools applied to ROI segmentation

Numerous studies used multivariate imaging (MVI) based on PCA to group the image pixels between kernels and background, edge or shadowed pixels (Chu et al., 2020; Serranti et al., 2013; Williams et al., 2010). Depending on the image obtained, pixels cluster in the score plot divided into interest and background pixels. In some cases, the differences are interpreted in the score image, detecting simply the separation of both groups. Although the performances in background segmentation using multivariate analysis are accurate, sometimes it requires iterations to obtain the desired results. Consequently, the computational time can be an obstacle in threshold segmentation optimisation.

Instead of manually selecting the pixels from the image to obtain the ROI information, a different manual segmentation is also available, inspecting the spectra directly. Tekle et al. (2015) removed the background pixels manually, observing and comparing all raw spectra. The ones with lower intensity than the threshold were removed from the overall data, keeping just the cereal pixels spectra. Finally, the watershed segmentation was applied in kernel segmentation, consisting of the representation of the image as a topographic landscape, which differentiates between water basins and watershed boundaries (Chu et al., 2020). The water basins are a group of pixels surrounding a grayscale minimum. Then, the regions between the kernels were determined as water basins, while the grains corresponded to the watershed boundaries, permitting a kernel-level segmentation.

The ROI selection at PW level is more frequent than at object-wise (OW). The PW selection considers the pixel spectrum as the sample, while the OW considers the mean spectrum. The present study uses OW delimitations for wheat bulk samples and individual kernels selection. Although Chu et al. (2020) study obtained better classifications for PW segmentation with visual maps, OW presents advantages in data handling. The mean spectrum selection from the

entire kernel reduces the data dimension and improves the computational time. In addition, we understand that determining the contamination at pixel-level does not have any applicability for decontamination purposes, as a kernel section cannot be removed. Future work will be focused on cereal samples or individual kernels spectra selection, programming an automated selection system to obtain the ROI information.

9.1.3. Kernel orientation effect

NIR spectra do not contain only the chemical information of the samples but also the physical features, such as shape, size, deformities, etc. Wheat kernels present different aspects depending on their position. The dorsal side (or crease-down) has smoothed and regular curved shape, while de ventral side (or crease-up) has a dash sunken, which can present differences in the light interaction with the kernel. Before determining the effect of kernel orientation, the authors inspected the fungal damage or mycelial growth in the grain using microscopic techniques. Abramson, Gan, Clear, Gilbert, & Marquardt (1998) affirmed that, besides the common fungal effects (shrivelling, chalk, decolouration, etc.), FDK have pink/white fibrous growth at the crease. Tekle et al. (2015) supported the previous findings, observing *F. graminearum* mycelial growth in oat high-contaminated kernels crease. In addition, Shahin & Symons (2011) affirmed that mycelia were not exclusively in the crease and its surroundings but also at the germ.

As in our methods, most studies aiming at fungal or associated contamination detection used crease-down positioned kernels to build classification models (Delwiche, 1998; Delwiche & Kim, 2000; Delwiche et al., 2010, 2011; Shahin & Symons, 2011). Although the previously mentioned studies affirmed that mycelial growth was predominantly at the crease, the crease part has a more non-uniform shape that can present shadowing or scattering light effects. However, Caporaso et al. (2018) calibrated PLS models for protein prediction in wheat

kernels, obtaining slightly lower R^2 for the crease-down side. Unlike the R^2, the PLS performances were similar in random and crease-down positions, which indicated that kernels orientation does not affect protein prediction. In addition, Caporaso et al. (2017) affirmed that kernels could orientate randomly for baking quality determination (Hagberg falling number). For corn kernels, Williams, Geladi, Britz, & Manley (2012) found differences depending on germ orientation, attributing those discrepancies to the lipid content of the germ. As we have already discussed, they attributed non-germ side shadow and deformity differences of corn, in which the indent (similar to the crease shape of wheat) vary in depth or size from kernel to kernel. In transmission mode, kernel orientation does not affect the result because the light can fully penetrate inside the kernel, obtaining the information of both sides. In reflectance mode, the beam partially penetrates inside the grain and is reflected in the detector. Consequently, the amount or direction of light reflected is inevitably affected by the surface attributes, affecting the results (Wang et al., 2015).

In our PCA results, kernels showed a slight tendency to cluster in crease-up and crease-down position groups. Comparing orientation and contamination PCA results, they showed that contamination clustering was more prominent than the orientation, determining that the orientation effects did not influence the results on DON analysis. Then, the comparison of the PLS performances did not show notable performance differences according to the kernel orientation. However, the random position showed weaker results than a defined orientation, selecting the crease-down for its handling advantages. As the kernel has a round (non-crease) and a flat (crease) part, the grains tend to orientate with the flat face in contact with the scanning tray (crease-down). Consequently, it would be interesting for further investigations to find an approach that locates the kernels in a crease-down position (e.g. vibration).

Concerning bulk sample analysis, the kernel both sides representation effect must be studied, avoiding deviations and ensuring repeatability. In our study, bulk wheat samples were analysed in triplicate, shaking between each scanning to change the kernels randomly and increase sample repeatability. The scanned cereals presented contact between the grains, being an OW measurement. The spectra did not have wide deviations between repetitions, although the position and orientation of kernels changed. It demonstrated that the NIR spectra contained the general information about the sample, and it was suitable to model the changes of different samples caused by fungal-related contaminations. For wheat analysis, Barbedo et al. (2015) and Delwiche et al. (2019) positioned randomly and separately the kernels over the scanning tray for one face analysis, which were then inspected visually for fungal damage. Liang et al. (2020) analysed 25 g samples, where the average pixels intensities of all the randomly-positioned kernels were extracted and processed. Finally, Su et al. (2021) used the same strategy, analysing 10 g of bulk barley, presenting the grains randomly to the HSI system, and having contact between the kernels. However, they did a single measurement, representing only one kernel face. The positive results in bulk sample analysis, scanning random-positioned kernels on the tray, suggested that the kernel orientation does not affect the overall spectral intensity. It was concluded that scanning the averaged spectra of a high kernel number in different positions and subsequently analyse them by the reference method altogether led to good results. Our studies reduce even more the orientation effect, triplicating the number of scans.

9.2. Fungal inoculated vs naturally infected wheat

When fungi infect wheat plants naturally in the field, two main processes may occur. The first is related to the primary metabolism, intrinsic to fungal growth. *Fusarium* can grow at a wide temperature and water activity range, changing the optimum depending on the strain. Concretely, *F. graminearum* optimum

conditions are 24-28 °C and -10 to -14 bars, while for *F. culmorum* are 20-25 °C and -8 to -14 bars. Fungal development changes the cereal composition while using the plant reserves (carbohydrates, proteins and lipids) to sprout. The second is associated with secondary metabolism activation when the optimum conditions are available. In those conditions, fungi produce mycotoxins which accumulate in the cereal plant tissues. *F. graminearum* and *F. culmorum* produce DON in cereals at temperatures between 25-28 °C and a_w 0.97 (Doohan, Brennan, & Cooke, 2003).

Natural infection in wheat depends on several parameters. *Fusarium* infection incidence correlates with the climatic conditions of the geographical region (temperature and rainfall). Those climatic parameters affect the production and propagation of the *Fusarium* fungi. The fungi reproduce sexually or asexually depending on the environmental conditions which influence the dissemination. Other parameters which influence natural proliferation are nutrient availability, pH, competition between *Fusaria* and light (Magan, Medina, & Aldred, 2011). Artificial inoculation involves the fungal suspensions inoculation either preharvest, directly to the plant in the field, or in cereal kernels in the laboratory. Propagation parameters do not influence artificial inoculation because the plant is inoculated with fungal suspensions. For laboratory inoculation, the dissemination, nutrient accessibility or environmental conditions are controlled, obtaining an optimum fungal growth on the cereal.

For HSI detection of *Fusarium* and DON in cereals, most studies used artificially inoculated kernels or samples with fungal suspensions (Alisaac et al., 2019; Dvořáček et al., 2012; Su et al., 2021; Tekle et al., 2015). Fungal inoculation ensures the presence of the fungi in the field or the optimum growth at the laboratory, which translates to a high fungal presence and DON levels in samples. Spectroscopic data do not contain only the fungal and mycotoxins information but also the variations of the physical and chemical components. Our results

allow us to conclude, as the first instance, that NIR and MIR present convoluted peaks for molecules in low concentrations in complex matrixes, such as DON. Consequently, DON detection involves modelling the compositional changes related to fungal primary and secondary metabolism. As we already explained, artificial inoculation produces dramatic changes in cereal matrixes compared to natural infection. The studies using artificially inoculated samples present higher accuracies, although they used higher fungal and DON levels than those common in the field. Thus, further studies using natural contamination are required to build robust calibrations with common field contaminations and higher applicability to the industry (Barbedo et al., 2017; De Girolamo et al., 2014; Peiris et al., 2017).

9.3. Correlation between ergosterol and DON contents

Ergosterol is a common fungal cell wall component not present in plant tissues (Seitz, 1979). We used ergosterol to determine the fungal presence in wheat samples. Its analysis revealed that all the analysed samples presented ergosterol and showed that fungal infections are a current problem in the field. Ergosterol is produced on the cereal surface due to the fungi predominantly growing and accumulating on the outer parts of the cereal, being suitable for diffuse reflectance NIR analysis. We tried to correlate ergosterol and DON to determine if ergosterol indirect HSI-NIR analysis could be useful to predict DON contamination. However, our hypothesis presented some drawbacks, mainly that ergosterol is not exclusively in *Fusarium* genera compound but also of other fungi, and the low correlation between the fungal first metabolism (fungal growth) and secondary metabolism (DON production). Ergosterol content showed a correlation with DON of 0.61, not being possible to predict DON content indirectly. Studies with similar purposes reinforced our findings, affirming that ergosterol does not correlate with mycotoxins (Stanisz & Beszterda, 2015). However, one of the first authors who tried to predict DON

using ergosterol content (Lamper et al., 2000) supported the indirect prediction. Although they did not use spectroscopic techniques, ergosterol strongly correlated with DON (R = 0.87) and with visual evaluation (R = 0.89). They reported that most samples with severe symptomatology presented high ergosterol and DON levels. Thus, it is expected to obtain high correlations at high contaminations and weaker correlations at lower correlations. In addition, Snijders & Krechting (1992) found a positive correlation of ergosterol and DON with coefficients between 0.71 and 0.85 in wheat kernels. Several studies confirmed that ergosterol levels are in all cases higher than DON (Abramson et al., 1998; Dowell et al., 1999); in addition, they did not find any correlation between ergosterol and DON, while *Fusarium* damage or exoantigens (soluble extracellular components) correlated positively with DON. Polisenska et al. (2008) studied the ergosterol correlation with DON in corn contaminated kernels, showing a correlation coefficient of 0.38, although the coefficient was higher between ergosterol and maize ear rot damage (0.47). The overall findings confirm that, although ergosterol and DON correlate, the correlation is not sufficient to predict DON via ergosterol. They also demonstrated that fungi may grow in high amounts on cereals without producing significant DON levels. Additionally, as ergosterol is not exclusively present in *Fusarium*, their levels can be high due to other fungi growing on cereals, although they are not producing DON.

Although the DON indirect detection was not possible, studies revealed that ergosterol is suitable to determine fungal biomass and correlate it with cereal diseases. Ergosterol content prediction through HSI was interesting regarding the fungal biomass presence in wheat samples, which correlates directly with cereal quality due to changes produced on cereal composition while fungi are growing.

9.4. Correlation between visual damage and DON content

Fusarium diseases, predominantly FHB, produce changes in kernels appearance, such as shrivelling, discolouration, weight loss, etc. Kernel visual inspection can recognize all these symptoms, characterizing them according to the disease severity. Fungal damage has been proposed as a mycotoxin presence indicator. Comparing our results of visual inspection and DON concentrations, we obtained that the 68.3% of the grains presented symptoms and DON levels over the EU limit (1250 μg/kg) or were visually healthy and had DON levels below the limit. The remaining 31.7% of the kernels showed no correlation between symptomatology and DON, presenting symptomatic condition and contaminations below the EU regulations or appeared healthy but contained DON above the cut-off. Without considering the mildly-symptomatic kernels, only the 3.7% of the kernels were fully asymptomatic and contaminated over the limit, and the 20.7% were uncontaminated and symptomatic. As for ergosterol, visual symptoms are indicators of the fungal presence and cereal spoilage and are one of the most used reference methods to calibrate HSI-NIR models because visual inspection is fast and cost-effective. Despite its advantages, visual inspection cannot determine the fungal species or even the genera infecting the cereal, as the symptoms can be similar in some other diseases. In addition, the visual observation of the samples requires a trained expert that determines the typical symptoms. Often, the human-eye inspected symptoms induce subjectivity, having different results depending on the inspector. Broad correlation diversity has been published regarding the association of FHB symptoms and DON and presenting FDK-DON correlations that varied between studies or within the same one from -0.47 to 0.98 (Paul et al., 2005). Positive correlations between FDK-DON (0.73) were stronger than measuring the diseased spikelets per spike, the proportion of diseased spikes or the diseases-head severity. That suggests that the proportion of visibly scabby kernels at

harvest is the more suitable observation approach to correlate with DON accumulation. Additional studies reported that although relating kernels damage with DON is complex, the kernels with DON levels above 50 mg/kg (> 80%) presented FHB damages (Dowell et al., 1999). However, 60% of the healthy grains had detectable DON levels, suggesting that damage recognition do not indicate low DON levels presence. Moreover, it was concerning that a considerable percentage (> 70%) of kernels between 6-50 mg/kg of DON were sound. Thus, visual inspection at mid-high DON levels induces errors to correlate FHB damage and DON. In conclusion, considering the discussed results, *Fusarium* damage recognition presents variable correlations with DON that depends on many factors, such as harvesting time, DON producing ability of the fungal strains, optimum environmental conditions to produce DON, etc. Although both events present some correlation, FDK inspection is adequate to determine fungal infection and not reliable enough to determine DON presence in cereal products.

9.5. Sample milling prior HSI analysis

Cereal grinding is an additional step which allows samples homogenisation. Milled wheat HSI analysis presented lower prediction performances for ergosterol and DON than intact kernels. Sample grinding can affect NIR spectra differently, having advantages and drawbacks. Two advantages of grinding are the kernel size and shadowing effect elimination. Grains have a round surface, producing shadows in some kernel regions or over others within the sample and affecting the spectral quality. Although this effect can occur when analysing bulk samples, we ensured the correct separation between kernels and the sample region delimitation to reduce the shadowing effects. However, milling presents some limitations on sample presentation to the HSI-NIR. NIR spectra are strongly affected by the physical and structural appearance of the sample. The grinding process destroys the cereal tissues, changing the spectral shape. Two

main variations are produced regarding fungal and DON infection while grinding. First, milling destroys the *Fusarium* disease visible damages. We consider that chemical composition is not the only target to detect fungal damage and DON but also structural changes due to the limited sensibility of NIR to molecules present in low concentrations. When milling the samples, those FHB frequent symptoms (shrivelling, discolouration, pinkish colour, etc.) are eliminated, losing that fungal-related information in the spectra.

The second is related to the contamination distribution in the sample. Fungal presence and, therefore, DON production are frequent in cereal surfaces, as fungi deposit on the outer kernel layers and grow there. As we worked in diffuse reflectance mode, the light beam slightly penetrates the sample, and the information detected is predominantly from the cereal surface. Fungi and DON are homogenised and redistributed across the ground samples. Consequently, it produces a dilution effect of the target compounds, making the detection of fungal components and DON molecules in the NIR spectra difficult. An additional disadvantage is the time-dependence of the method. Even if a grinding step is included, the analysis time will be shorter than for traditional chemistry or immunological techniques. Nevertheless, unground samples analysis would require even less time. In addition, sieving the ground samples could be an option to analyse the largest parts, which correspond to the outer layers (kernels skin) that may contain higher fungal and mycotoxin content.

Some studies compared intact and milled cereal analysis with HSI-NIR. Liang et al. (2020) analysed wheat kernels and then reanalysed them after milling. Like in our results, the whole wheat kernels analysis was more accurate (100%) for sample classification than flour analysis (96%), also not presenting broad differences depending on milling. In addition, the Vis-NIR range was optimum for the intact sample analysis and SWIR for milled wheat. Instead of classifying samples, Alisaac et al. (2019) compared wheat kernels and flour spectral profiles

and correlated them with fungal infections. Their results were comparable to ours, obtaining correlations above 0.80 for fungal detection in intact kernel samples and, in some NIR regions, the correlations were above 0.90. For flour analysis, the correlations were poorer, even though the correlation were higher at the Vis range (0.80). They affirmed that flour spectral profile has more accentuated peaks in the Vis range caused by the *Fusarium* effect on the starch and protein amount, although no correlation was detected in the NIR range due to the kernel tissue destruction. Tyska, Mallmann, Gressler, & Mallmann (2021) compared NIR and FT-NIR to detect DON in wheat flour, obtaining similar PLS-DA and PC-LDA classification accuracies for FT-NIR spectra and for NIR, between 85% and 90%. These results demonstrated that both NIR and FT-NIR are suitable techniques for wheat flour fungal and mycotoxin analysis, as flour is ideal for covering the cell to analyse solid samples (Börjesson et al., 2007; De Girolamo et al., 2014; De Girolamo et al., 2009).

9.6. Spectral profiles comparison of fungal-infected and DON contaminated wheat samples and kernels

Before multivariate analysis, sample and kernel spectral profiles showed band intensities variations, which can be related to fungal and DON infection. The raw and 1stD spectral profiles were plotted to compare the samples and kernels variations regarding DON, and grains variances regarding symptomatology (severe damage, mild damage and healthy). Wheat samples results diverged in reflectances intensity between contaminated samples above and below the EU limit. The spectral representation showed that the uncontaminated samples had, in general, higher signals than contaminated ones. The spectral peaks that diverged depending on the contamination were, for the raw spectra, near 1120, 1200, 1300 and 1450 nm. Additionally, the first derivate spectra presented remarkable spectral differences near 1150, 1220, 1345, 1370 and 1405 nm.

Additional bands (1280 and 1500 nm) in the 1stD spectra also differed, but the variations were not as strong as the abovementioned.

Unlike wheat samples, individual kernels presented higher NIR reflectances for FDK and DON contaminated kernels. Although the intensities were different, it indicated that contamination variations were registered at specific peaks occurring at similar spectral regions to whole kernel samples for raw spectra, such as 1120, 1200, 1300 and 1450 nm. Also, the differences in the 1stD spectra, showing more pronounced peaks, were around 1146, 1220, 1350, 1370 and 1406. Understandably, wheat samples have similar spectra to kernels, as only the ROI changes from the mean of several wheat kernels that form the sample to the mean spectra of a single grain.

Fungal infection symptoms changes cause differences in reflectance intensities among wheat samples. One of the damages caused by *Fusarium* diseases is weight loss and withering. Weight loss is associated with structural changes in kernels, losing size and thickness. Those changes in kernels size affect different regions of the NIR spectra, as the thicker grains have higher absorbances caused by the deeper penetration of the light (Chu et al., 2020). Consequently, FDK kernels, which present reduced size, would increase the overall reflectance in the NIR spectra. In addition, water has a high absorbance at the NIR region, for this reason, it is used frequently for moisture analysis. FDK kernels present shrivelling due to water loss, reducing the water absorption in the NIR region and, therefore, the overall reflectance increase. This effect is not produced in samples because they are composed of several kernels. Although the intensities shifted comparing whole kernel samples and individual grains, the spectra of both conditions have variations at similar peaks, containing information regarding fungal infection. Shrink and brightness are not described only by the overall NIR spectra but also by specific band differences. Those physical features divergences produced by *Fusarium* infection differ at the 1425-1450 nm region

and shift between bands, for FDK at the 1445 nm and healthy kernels at 1430 nm. Although our spectra did not present shifting between peaks at that region, a considerable variation in the 1450 nm band was observed that could be correlated with kernel size diminution and, consequently, brighter kernels.

NIR spectra do not contain only the structural and physical information of wheat but also the fungal-growth related chemical variations in cereal matrix components, predominantly in proteins, lipids, and starch content. Although the NIR signals are overlapped due to their amount of information, some of the peaks can be correlated to overtone vibrations of specific molecules, which permit the determination of sample changes.

Concerning fungal infection, Dowell et al. (1999) attempted DON indirect detection by correlating the differences in the 1400 nm region with the variances in protein and starch caused by fungal infection. In our 1stD spectra, we also observe a region at the same frequencies differing from the fungal/DON contaminated and healthy wheat, which could be due to those changes. Additionally, as shrink and brightness, the region near the 1450 nm band was related to the 1st overtone of N–H related to protein variations, although changes were in the 1446-1502 nm region for corn (Chu et al., 2020). However, it can be related to two characteristic peaks from our studies, one around 1450 nm and the other around 1500 nm. Our second peak comprises differences between 1480-1530 nm that may be associated with the N–H stretching of the $CONH_2$ of proteins. In addition, they reported phenolic content alterations caused by fungal damage which cause differences in intensities in the 1415-1512 nm that correlate to our peak at that region. However, other variations produced in fatty acids related to fungal infection are not represented in our spectra because the 1666-1818 nm region correspond to our spectral extreme, which is affected commonly by light scattering and deviations. Liang et al. (2020) detected variations in the 2nd overtone of C–H stretching vibration related to the 1190-1212 nm and

attributed them to starch and lipid variations. We obtained a strong peak in the 1200 nm band that presents differences between FDK and healthy, related to the stretching vibration on those molecules.

Further characteristic band variations are reported due to fungal infection, although they are out of the spectral area used in the present study. Shortly, those changes have been associated with fungal infection variations on kernel brightness (620-706 nm), 1st overtone C–H vibrations of amylose molecules (starch majoritarian compound) (1733-1778 nm), and water molecules stretching and bending (1935-1952 nm) (Su et al., 2021).

Depending on DON concentration, NIR signals change at specific regions. DON molecule is complex, having different bonds that can absorb light energy and produce variations detected in the reflected beam. Peiris et al. (2009) demonstrated that the main variations were in two NIR regions depending on DON concentration (1390-1440 nm and 1880-1950 nm). Those regions presented peaks in 1414 nm related to DON 1st overtone of O–H bonds and 1906 nm for -C=O and R–OH. The characteristic peak near 1414 nm also appears in our NIR spectra, attributing it to DON variations in the sample. Those results are not comparable to ours because they used pure DON in acetonitrile instead of a complex matrix as cereals. Thus, they obtained a defined signal for DON because they avoided overlapping effects of the region in which DON appears with other cereal compounds, absorbing light at the same frequencies, such as protein and starch. However, Peiris et al. (2009) not only obtained DON spectra in acetonitrile but also FDK in wheat, obtaining characteristic absorption peaks at 1205 nm and 1400 nm.

In conclusion, the comparison of our results with other studies allow us to attribute variations in our target NIR region (895-1731 nm) to fungal growth changes in the physical appearance and the chemical composition of cereals caused by the cereal matrix consumption while growing. Nevertheless, direct

DON visualization in the NIR spectra is complex due to the low levels of this molecule compared with the main cereal compounds, such as starch, protein, water and lipid, and the reduced sensibility of NIR spectroscopy to detect such concentrations. Low sensibility and overlapping problems should be solved with multivariate analysis, enhancing the variances caused by DON presence or correlating the *Fusarium* main changes in the cereal composition with the DON production. Thus, the following sections discuss the quantification and classification of wheat samples according to fungal and DON contaminations.

9.7. Perspectives for DON quantification in wheat samples and kernels by HSI

Predictive chemometric tools are broadly applied to spectral or hyperspectral data to predict target compounds. As discussed in the previous section, regression tools are applied to the spectral matrixes, modelling the data with the reference method results and predicting DON concentration in future samples. PLS regression is the most frequent multivariate approach used to predict food compounds concentration. As it is explained in the results section, we applied PLS to the wheat samples mean spectra to build a predictive model from the HPLC measurements. The present study includes different wheat analyses (whole and ground grain samples, and single kernels) to determine the suitability of HSI-NIR to predict DON levels, such as wheat entire sample, ground sample and individual kernels. Prediction models displayed performances of R^2 of 0.61 and RMSEP of 501.4 μg/kg, respectively. Although models presented a weak fitting, the predictive error was lower than the DON EU limit for wheat. If the data fitting improved, the model could be applied for DON predictions at low concentrations and implemented as a complementary analysis of the established routine chemical methods.

The individual kernels prediction presented better performance than sample analysis, achieving an R^2 of 0.88. However, the RMSEP was much higher (6.66 mg/kg). The performance parameters are not comparable between the models using samples and single kernels, as they depend on the contamination standard deviation of the calibration and validation set. A valuable parameter to compare between both models is the RPD. Contamination deviation in wheat samples and kernels was 0.84 mg/kg and 21.4 mg/kg, respectively. Understandably, the DON levels in wheat samples present, in general, lower deviations than in individual kernels as the DON contamination corresponds to 14 g, which contain high and low contaminated grains, smoothing the concentration deviations. By contrast, contamination deviations within grains of the same sample are higher. The results suggest that a limited number of highly contaminated kernels increase sample contamination above the legal limits. In addition, almost all the sample grains contain low DON levels, decreasing the concentration deviations between samples. According to the standard deviations and the RMSEP, the several-kernel sample RPD was 1.64 (able to distinguish low and high concentrations) and 3.21 for individual kernels (excellent predictions), confirming that predicting DON in individual grains was more suitable than for samples, even though the RMSEP was higher. More studies have been published regarding DON prediction in wheat samples by HSI than for single kernel analysis, although there is still not much-published information. Otherwise, there are no available studies on DON prediction using naturally infected samples by HSI. Chen et al., (2020) and Shi, Liu, Zhao, Liu, & Zheng (2020) tried to predict DON in wheat, but they used MSI and wheat flour, respectively. Additional studies are accessible using FT-NIR or FTIR, although in all cases used artificially inoculated wheat samples (Abramović et al., 2007; De Girolamo et al., 2009; Dvořáček et al., 2012; Peiris et al., 2017).

In most instances, artificially fungi-inoculated wheat samples have higher DON concentrations than natural inoculated cereals, which also present dramatic changes produced by fungal growth. Parrag et al. (2020) used HSI-NIR in the same spectral range but broader DON concentration range than ours (0.09-73.8 mg/kg). Even though they obtained an adjusted PLS model with an R^2 of 0.98, the RMSEP was 11.95 mg/kg. Both parameters can be related to the wide contamination range, as it can increase the adjustment and present higher RMSEP. Su (2021) worked with HSI-Vis/NIR on barley samples with a narrower contamination range (0-10 mg/kg). Their HSI scanning method was similar to ours, as they distributed randomly 10 g of barley kernels in the scanning tray. Their PLS regression presented a slightly better adjustment than ours (0.73), although their predictive power was lower (RMSEP of 3.80 mg/kg). In that case, it is also complex to compare the results, as our DON concentration range is narrower (<LOD-3.57 mg/kg). Chen et al. (2020) predictive results are comparable to our PLS regressions for naturally infected ground wheat, obtaining similar performance parameters (R^2 of 0.69 and RMSEP 0.70 mg/kg) using samples with similar DON contaminations (LOD-6.23 mg/kg).

DON quantification in single wheat kernels is a recently opened field of study. Single kernel analysis was performed before but not analysing DON from each individual kernel as the reference method. This study is the first that quantifies DON concentration from single wheat grains to build DON predictive models from HSI-NIR data. Thus, the results obtained in the present report can only be compared with those in Shen et al. (2022) study, working with similar methodologies. Although the results are comparable, they used *F. graminearum* inoculated samples, which resulted in extremely highly contaminated kernels, with a range of 39.45 to 507.28 mg/kg. Comparing the PLS results for the dorsal side, they obtained a weaker regression adjustment (R^2 0.76) and a considerable RMSEP (55.26 mg/kg). Even though their results reflect a starting point for

SKHSI-NIR analysis, the contamination levels used are not comparable to the commonly found in naturally infected kernels (found in the present work). Consequently, the method applicability for online quantification purposes would have limitations.

To date, the so far published results regarding HSI predictive performances for DON detection presented insufficiently adjusted models to screen contaminated wheat samples, or there is still not enough information available for single kernels analysis. The reduced performance in quantification models and the complexity of the heterogeneity for DON contamination in cereal batches have led the authors to switch from predictive models to discrimination models, classifying samples or kernels according to the established maximum legal limits.

9.8. Perspectives of discrimination of DON contaminated wheat samples and kernels by HSI

The limited predictive power for DON quantification in wheat commodities at EU regulatory levels (1250 or 1750 μg/kg, depending on the unprocessed cereal) made researchers focus on the discrimination of contaminated batches, establishing the threshold on the legal limits or close to them. The classifications from the present study are encouraging to apply them as further discrimination models for routine analysis. Unlike the predictive results, the whole and milled wheat sample discrimination was more accurate than for individual kernels. Comparing the LDA models of the different wheat analyses (unground and ground samples and single kernels) at the same threshold (1250 μg/kg), the discrimination of unground and milled samples (83.3 and 85.4%, respectively) is more accurate than for single grains (75.6%). Not only the classification accuracies are better, but also the percentage of false negatives (contaminated classified as uncontaminated, which would be accepted in the food chain, introducing risk). Sample classification presented a low percentage of false

negatives with 3.25% and 2.96% in unground and milled samples, respectively. Conversely, the false-negative ratio for individual kernels classification is significantly higher (13.6%). This result reinforces the discrimination power of samples above single grains. In addition, spectral pre-processing does not make substantial differences in classification performances. The better sample classification accuracy could be due to the contamination distribution. Wheat samples used in our study presented mean contamination under the established threshold (0.48 mg/kg), while grains mean concentration was 9.02 mg/kg. Thus, individual kernels discrimination within low contamination levels can be challenging. In addition, selection of grains according to their symptomatology in groups of similar size led to a higher overall DON contamination than in a real batch. Although sample discrimination worked well at the EU level, kernels discrimination threshold could be increased in future works (e.g. 10 mg/kg) to sort the extremely highly contaminated kernels (19.7%), which are responsible for the entire batch rejection.

The discrimination models from the literature are, in general, more precise than the predictive to manage DON contaminations. Liang et al. (2018) analyses are similar to ours because they worked with HSI-NIR in wheat samples. They scanned 70 kernels on the scanning tray, determining the DON concentration of all of them as a single sample by LC-MS/MS. Samples were discriminated into three groups, depending on their mean DON content (< 250, 1162 and 2655 μg/kg). They achieved a high discrimination power (97.92%) working in similar contamination ranges (250-5000 μg/kg) using an SVM classifier, pre-processed with MSC and selecting optimal wavelengths with SPA. Gathering the results of the discussed studies, they suggest that, in future applications, the optimal wavelength selection is essential to highlight DON contamination spectral features, improving the discrimination power. Barbedo et al. (2017) used a similar procedure as Liang et al. (2018) by scanning 30-50 kernels per image,

working as a sample unit. Although we used a larger sample size and did not separate grains on the scanning tray, the results are comparable, as they established the limit at 1250 μg/kg. At this cut-off, the classification accuracy was 81%, similar to our (83.3%), while dividing the model into three classes (500 and 1250 μg/kg limits), the overall accuracy decreases to 72%. In general, the results for the entire sample classification indicate the potential of HSI to discriminate according to DON levels.

HSI technologies have been applied to discriminate milled cereal commodities according to DON contamination, such as wheat flour and cornmeal. Chen et al. (2020) classified naturally-infected flour samples with LDA, comparing the use of spectral and colour imaging to discriminate according to DON at 1 mg/kg limit. The combination of spectral and colour imaging was the most accurate model (96.62%), selecting some variables to reduce noise (23 LV and 12 colour parameters). Without selecting spectral variables, the classification ratio decreased to levels comparable levels to ours (70.8-84.6%). Also, these findings indicate that characteristic bands selection is fundamental in DON contamination classification and must be applied in future cereal sorting strategies. In addition, several publications used FT-NIR in ground sample classification. The application of FTIR requires sample milling to homogenize the sample and ensure contact with the crystal, as it is spatially limited. However, the overall classification results were similar to the HSI accuracies, ranging between 75-90% for thresholds between 1000-2500 μg/kg. In addition, some studies reported accuracies of 69% for low limits (300 μg/kg) and up to 93.4% for higher limits (10 mg/kg). The present study is the only one that discriminates individual naturally infected wheat kernels according to DON by HSI-NIR, using grain concentrations to calibrate the classifiers. However, Peiris et al. (2010) attempted the first approximation of individual kernels classification using NIR spectroscopy. As in our study, they analysed kernels individually by

chromatography. However, the contaminations were extremely high due to artificial inoculation on spikes. Consequently, they could distinguish contaminated grains above and below 60 mg/kg with an approximate accuracy of 96%, far from the regulatory limits established. The generally positive results for DON-contaminated wheat samples and grains demonstrate the suitability of HSI-NIR as a mycotoxin mitigation strategy.

9.9. Discrimination of fungal contaminated kernels

HSI-NIR feasibility has been tested for FDK recognition. Unlike for DON, HSI has been applied broadly for fungal detection, not only FDK but also *Fusarium* species, such as *F. graminearum*, *F. culmorum*, *F. poae*. However, this technology detected also other fungi in wheat (*Aspergillus niger*, *A. glaucus* and *Penicillium* spp.). The most frequent reference method for FDK determination is a visual inspection of the typical FHB symptoms. The discrimination of single kernels according to fungal damage was more accurate than for DON, with accuracies up to 85.8%. As already discussed in previous sections, fungal growth produces physical changes in kernels, such as shrivelling, size diminution and colour change. In addition, the compositional changes which cause fungal consumption while growing, affect the protein, carbohydrate, and lipid composition of the kernels. The NIR spectra contain these variations, which are the base for discrimination models building (LDA, SVM, PLS-DA, etc.). However, DON production is not directly correlated to those changes, as it is a secondary metabolite present, commonly, at low concentrations.

Several researchers studied naturally infected kernels to discriminate them according to fungal infection. Interestingly, Shahin & Symons (2012) used the same analysis conditions than ours, except for the spectral range (400-1000 nm). In the 620-706 nm region, which is out of our target, spectral differences related to fungal infection occur. Those changes are associated with fungal infection

effect on kernel brightness and 1st overtone of C–H of amylose molecules (majority compound of starch). Thus, the spectral information in the Vis range could improve the accuracy to 92%. Ropelewska & Zapotoczny (2018) and Serranti et al. (2012) studies are similar to Chapter 3 because they used 70 and 120 kernels, respectively, and cross-validated the discrimination models. In all the models, the accuracies were excellent, reaching values close to 100%. Delwiche et al. (2019) also determined the percentage of FDK by PLS-DA and LDA, obtaining in all cases precisions above 92%. However, they used cross-validation in a 556 kernels sample set (half healthy/half FDK). Cross-validated models are suitable as a first estimation of the classification power of the spectral data.

Studies are available reporting artificial infection of wheat. The work performed by Barbedo et al. (2015) inoculated *Fusarium* on kernels, using a set of 803 grains. The classification model externally validated had a FI (probability to have FHB) of 91%, similar to our results (85.8%). Singh et al. (2012) and Zhang et al. (2007) reports used other fungal species. *A. niger*, *A. glaucus* and *Penicillium* spp. previously inoculated, so the visual inspection was not required. Using SNV, the classification performance of inoculated and non-infected kernels was above 87% (Zhang et al., 2007). Nonetheless, LDA models for HSI-NIR analysis ranged from 88.7 to 98.0%, depending on the inoculated species (Singh et al., 2012). Although we used natural infection, the LDA correctness went from 71.1-85.3%, depending on the pre-processing.

In short, the percentage of fungal damaged kernels presented higher performances than DON. Fungal infection and related structural and compositional changes are dramatic compared to the mycotoxin levels variations. A common discrimination model could be proposed for fungal infection and DON discrimination, considering the correlation between fungal and DON presence. However, as sometimes the correlation is not accomplished,

independent classification models are more suitable. In conclusion, HSI is feasible for fungal damage detection of individual kernels, obtaining high discrimination percentages in all the studies reported to date (70-100%).

9.10. HSI-NIR as a cereal sorting tool

Cereal industry processes have an impact on mycotoxin content. Typical stages in the grain industry, such as cleaning, sorting and milling, affect DON content (Nagy, Korzenszky, & Sembery, 2016; Tibola, Fernandes, & Guarienti, 2016). The studies reported a significant reduction in DON content while removing light, broken, shrivelled, and damaged grains by density or colour (between 28-33% of discarded kernels). It suggests that FDK removal would reduce mycotoxin content notably, although more precise strategies than gravity separation are required. The results reported in the present work indicated that HSI-NIR is appropriate to sort kernels in industrial processing steps. Its calibration according to fungal damage or DON would improve the detection specificity of fungal related damages, improving the ratio between the percentage of discarded kernels and DON reduction. Therefore, DON could be reduced by removing fewer kernels, which would increase the economic yield. HSI-NIR has been proposed as an inline sorting tool (Gruna et al., 2010; Tatzer et al., 2005), overcoming the reduced sensibility of optical sorters based on colour. Considering the present study results and literature, the advances in HSI-NIR for cereal sorting should involve (i) calibration with a suitable sample set, including naturally contaminated kernels with a wide range of DON concentrations and damage features (ii) the selection of optimal variables to reduce the computation time for online analysis, (iii) the analysis automatization (ROI selection, spectral pre-processing, contaminated kernels removal, etc.). Despite reported advances, future studies are required to implement this technology as an inline industrial process.

9.11. Solvent selection to classify DON contaminated maize samples by ATR-FTIR

Polar solvents were selected due to their extraction power of DON molecules. The PCA plots demonstrated that the most suitable solvents for DON contaminated samples discrimination at EU regulatory limits were water and methanol (70%). The classification accuracies obtained in the SPLS-DA algorithm (86.7% and 90.8%) revealed the potential of the FTIR technology to manage DON-contaminated samples at low concentrations. The classification performances were higher for solvent-extract than for maize powder analysis (79%), obtained by Kos et al. (2016). Still, a larger sample set is required to build independently-validated models and to cover a broader DON variability. In addition, the application of machine learning approaches for the automatic detection of contaminated samples over the regulatory limit involves calibration sets with additional samples contaminated close to the threshold concentrations to avoid the common misclassifications at those levels.

As expected, IR present convoluted peaks that cannot be distinguished for DON variations. However, the approach exhibited ability to cluster samples according to the fungal species, especially grouping DON-producer species separately from the FBs-producers and naturally-contaminated samples. In addition, high correlations were displayed between *F. culmorum* infection and DON contamination above the limit samples, as well as between *F. verticillioides* and DON below 1750 μg/kg. Moreover, the inoculation method did not have impact on grouping. The clustering is noted be due to the variations in protein, lipids and carbohydrates associated to fungal growth, supporting the affirmations of Kos et al. (2003). IR characteristic regions of those biomacromolecules functional groups were associated to fungal infections and DON. The solvent should extract those compounds to model fungal presence and its association to DON production, showing water and methanol the best performances. Water extracted

more polysaccharides, exhibiting significant IR variation at the alcohol functional groups. The methanol (70%) extracts presented slightly higher performances, although water must be significantly considered for its non-pollutant nature. The water extraction prior to the FTIR analysis would be a rapid, eco-friendly and cost-effective approach for its automatic implementation in in cereal industrial stages for routine analysis techniques complementation.

9.12. References

Abramović, B., Jajić, I., Abramović, B., Ćosić, J., & Jurić, V. (2007). Detection of deoxynivalenol in wheat by fourier transform infrared spectroscopy. *Acta Chimica Slovenica*, 54, 859–867.

Abramson, D., Gan, Z., Clear, R. M., Gilbert, J., & Marquardt, R. R. (1998). Relationships among deoxynivalenol, ergosterol and *Fusarium* exoantigens in Canadian hard and soft wheat. *International Journal of Food Microbiology*, *45*, 217–224.

Alisaac, E., Behmann, J., Rathgeb, A., Karlovsky, P., Dehne, H. W., & Mahlein, A. K. (2019). Assessment of *Fusarium* infection and mycotoxin contamination of wheat kernels and flour using hyperspectral imaging. *Toxins*, *11*, 1–18.

AOAC. (2005). Official Methods of Analysis. *Official Methods of Ananlysis of AOAC International*, *18*, 20877–22417.

Barbedo, J. G. A., Guarienti, E. M., & Tibola, C. S. (2018). Detection of sprout damage in wheat kernels using NIR hyperspectral imaging. *Biosystems Engineering*, *175*, 124–132.

Barbedo, J. G. A., Tibola, C. S., & Fernandes, J. M. C. (2015). Detecting Fusarium head blight in wheat kernels using hyperspectral imaging. *Biosystems Engineering*, *131*, 65–76.

Barbedo, J. G. A., Tibola, C. S., & Lima, M. I. P. (2017). Deoxynivalenol screening

in wheat kernels using hyperspectral imaging. *Biosystems Engineering*, *155*, 24–32.

Börjesson, T., Stenberg, B., & Schnürer, J. (2007). Near-infrared spectroscopy for estimation of ergosterol content in barley: A comparison between reflectance and transmittance techniques. *Cereal Chemistry*, *84*, 231–236.

Bureau, S., Cozzolino, D., & Clark, C. J. (2019). Contributions of Fourier-transform mid infrared (FT-MIR) spectroscopy to the study of fruit and vegetables: A review. *Postharvest Biology and Technology*, *148*, 1–14.

Caporaso, N., Whitworth, M. B., & Fisk, I. D. (2017). Application of calibrations to hyperspectral images of food grains: example for wheat falling number. *Journal of Spectral Imaging*, *6*, 1–15.

Caporaso, N., Whitworth, M. B., & Fisk, I. D. (2018). Near-Infrared spectroscopy and hyperspectral imaging for non-destructive quality assessment of cereal grains. *Applied Spectroscopy Reviews*, *53*, 667–687.

Caporaso, N., Whitworth, M. B., & Fisk, I. D. (2018). Protein content prediction in single wheat kernels using hyperspectral imaging. *Food Chemistry*, *240*, 32–42.

Chen, M., Zhao, T., Jiang, X., Shen, F., He, X., Fang, Y., … Hu, Q. (2020). Integration of spectra and image features of Vis/NIR hyperspectral imaging for prediction of deoxynivalenol contamination in whole wheat flour. *Infrared Physics & Technology*, *109*, 103426.

Chu, X., Wang, W., Ni, X., Li, C., & Li, Y. (2020). Classifying maize kernels naturally infected by fungi using near-infrared hyperspectral imaging. *Infrared Physics and Technology*, *105*, 103242.

De Girolamo, A., Cervellieri, S., Visconti, A., & Pascale, M. (2014). Rapid analysis of deoxynivalenol in durum wheat by FT-NIR spectroscopy. *Toxins*, *6*, 3129–3143.

De Girolamo, A., Lippolis, V., Nordkvist, E., & Visconti, A. (2009). Rapid and non-invasive analysis of deoxynivalenol in durum and common wheat by Fourier-Transform Near Infrared (FT-NIR) spectroscopy. *Food Additives & Contaminants: Part A*, *26*, 907–917.

Delwiche, S. R. (1998). Protein content of single kernels of wheat by near-infrared reflectance spectroscopy. *Journal of Cereal Science*, *27*, 241–254.

Delwiche, S. R., & Kim, M. S. (2000). Hyperspectral imaging for detection of scab in wheat. *Biological Quality and Precision Agriculture II*, *4203*, 13–20.

Delwiche, S. R., Kim, M. S., & Dong, Y. (2010). Damage and quality assessment in wheat by NIR hyperspectral imaging. In M. S. Kim, S.-I. Tu, & K. Chao (Eds.), *Sensing for Agriculture and Food Quality and Safety II*, *7676*, 1–8.

Delwiche, S. R., Kim, M. S., & Dong, Y. (2011). *Fusarium* damage assessment in wheat kernels by Vis/NIR hyperspectral imaging. *Sensing and Instrumentation for Food Quality and Safety*, *5*, 63–71.

Delwiche, S. R., Rodriguez, I. T., Rausch, S. R., & Graybosch, R. A. (2019). Estimating percentages of *Fusarium*-damaged kernels in hard wheat by near-infrared hyperspectral imaging. *Journal of Cereal Science*, *87*, 18–24.

Doohan, F. M., Brennan, J., & Cooke, B. M. (2003). Influence of climatic factors on *Fusarium* species pathogenic to cereals. *European Journal of Plant Pathology*, *109*, 755–768.

Dowell, F. E., Ram, M. S., & Seitz, L. M. (1999). Predicting scab, vomitoxin, and ergosterol in single wheat kernels using near-infrared spectroscopy. *Cereal Chemistry*, *76*, 573–576.

Dvořáček, V., Prohasková, A., Chrpová, J., & Štočková, L. (2012). Near infrared spectroscopy for deoxynivalenol content estimation in intact wheat grain. *Plant, Soil and Environment*, *58*, 196–203.

El-Mesery, H. S., Mao, H., & Abomohra, A. E. F. (2019). Applications of non-destructive technologies for agricultural and food products quality inspection. *Sensors (Switzerland)*, *19*, 1–23.

European Commission. (2006). Commission regulation (EC) Nº 401/2006 of 23 February 2006. Laying down the methods of sampling and analysis for the official control of the levels of mycotoxins in foodstuffs. *Official Journal of the European Union*, *70*, 12–34.

Gruna, R., Vieth, K., Michelsburg, M., & Puente León, F. (2010). Hyperspectral imaging – from laboratory to in-line food sorting. *International Workshop on Image Analysis in Agriculture, 2,* 79-90.

Huang, H., Liu, L., & Ngadi, M. O. (2014). Recent developments in hyperspectral imaging for assessment of food quality and safety. *Sensors (Switzerland)*, *14*, 7248–7276.

Kos, G., Lohninger, H., & Krska, R. (2003). Development of a method for the determination of *Fusarium* fungi on corn using mid-infrared spectroscopy with attenuated total reflection and chemometrics. *Analytical Chemistry*, *75*, 1211–1217.

Kos, G., Sieger, M., McMullin, D., Zahradnik, C., Sulyok, M., Öner, T., … Krska, R. (2016). A novel chemometric classification for FTIR spectra of mycotoxin-contaminated maize and peanuts at regulatory limits. *Food Additives and Contaminants - Part A Chemistry, Analysis, Control, Exposure and Risk Assessment*, *33*, 1596–1607.

Lamper, C., Téren, J., Bartók, T., Komorowski, R., Mesterházy, Á., & Sági, F. (2000). Predicting DON contamination in *Fusarium*-infected wheat grains via determination of the ergosterol content. *Cereal Reserach Communications*, *28*, 2000.

Liang, K., Huang, J., He, R., Wang, Q., Chai, Y., & Shen, M. (2020). Comparison

of Vis-NIR and SWIR hyperspectral imaging for the non-destructive detection of DON levels in Fusarium head blight wheat kernels and wheat flour. *Infrared Physics & Technology*, *106*, 103281.

Liang, Kun, Liu, Q. X., Xu, J. H., Wang, Y. Q., Okinda, C. S., & Shena, M. X. (2018). Determination and Visualization of Different Levels of Deoxynivalenol in Bulk Wheat Kernels by Hyperspectral Imaging. *Journal of Applied Spectroscopy*, *85*, 953–961.

Magan, N., Medina, A., & Aldred, D. (2011). Possible climate-change effects on mycotoxin contamination of food crops pre- and postharvest. *Plant Pathology*, *60*, 150–163.

Nagy, E. K., Korzenszky, P., & Sembery, P. (2016). The role of color sorting machine in reducing food safety risks. *Potravinarstvo Scientific Journal for Food Industry*, *10*, 354–358.

Parrag, V., Gillay, Z., Kovács, Z., Zitek, A., Böhm, K., Hinterstoisser, B., … Baranyai, L. (2020). Application of hyperspectral imaging to detect toxigenic *Fusarium* infection on cornmeal. *Progress in Agricultural Engineering Sciences*, *16*, 51–60.

Paul, P. A., Lipps, P. E., & Madden, L. V. (2005). Relationship between visual estimates of Fusarium head blight intensity and deoxynivalenol accumulation in harvested wheat grain: A meta-analysis. *Phytopathology*, *95*, 1225–1236.

Peiris, K. H. S., Dong, Y., Davis, M. A., Bockus, W. W., & Dowell, F. E. (2017). Estimation of the deoxynivalenol and moisture contents of bulk wheat grain samples by FT-NIR spectroscopy. *Cereal Chemistry Journal*, *94*, 677–682.

Peiris, K. H. S., Pumphrey, M. O., Dong, Y., Maghirang, E. B., Berzonsky, W., & Dowell, F. E. (2010). Near-infrared spectroscopic method for identification of Fusarium head blight damage and prediction of deoxynivalenol in single

wheat kernels. *Cereal Chemistry*, *87*, 511–517.

Peiris, K. H. S., Pumphrey, M. O., & Dowell, F. E. (2009). NIR Absorbance characteristics of deoxynivalenol and of sound and *Fusarium*-damaged wheat kernels. *Journal of Near Infrared Spectroscopy*, *17*, 213–221.

Polder, G., Van Der Heijden, G. W. A. M., Waalwijk, C., & Young, I. T. (2005). Detection of *Fusarium* in single wheat kernels using spectral imaging. *Seed Science and Technology*, *33*, 655–668.

Polisenska, I., Kubicek, J., Dohnal, V., Jirsa, O., Jezkova, A., & Spitzer, T. (2008). Maize ear rot, *Fusarium* mycotoxins and ergosterol content in maize hybrids. *Cereal Research Communications*, *36*, 381–383.

Ropelewska, E., & Zapotoczny, P. (2018). Classification of *Fusarium*-infected and healthy wheat kernels based on features from hyperspectral images and flatbed scanner images: a comparative analysis. *European Food Research and Technology*, *244*, 1453–1462.

Seitz, L. M. (1979). Ergosterol as a measure of fungal growth. *Phytopathology*, *69*, 1202.

Serranti, S., Cesare, D., & Bonifazi, G. (2012). Hyperspectral-imaging-based techniques applied to wheat kernels characterization. *Sensing for Agriculture and Food Quality and Safety IV*, *8369*, 83690T.

Serranti, S., Cesare, D., Marini, F., & Bonifazi, G. (2013). Talanta classification of oat and groat kernels using NIR hyperspectral imaging. *Talanta*, *103*, 276–284.

Shahin, M. A., & Symons, S. J. (2011). Detection of *Fusarium* damaged kernels in Canada Western Red Spring wheat using visible/near-infrared hyperspectral imaging and principal component analysis. *Computers and Electronics in Agriculture*, *75*, 107–112.

Shahin, M. A., & Symons, S. J. (2012). Detection of *Fusarium* damage in Canadian wheat using visible/near-infrared hyperspectral imaging. *Journal of Food Measurement & Characterization*, *6*, 3–11.

Shen, G., Cao, Y., Yin, X., Dong, F., Xu, J., Shi, J., & Lee, Y. W. (2022). Rapid and nondestructive quantification of deoxynivalenol in individual wheat kernels using near-infrared hyperspectral imaging and chemometrics. *Food Control*, *131*, 108420.

Shi, Y., Liu, W., Zhao, P., Liu, C., & Zheng, L. (2020). Rapid and nondestructive determination of deoxynivalenol (DON) content in wheat using multispectral imaging (MSI) technology with chemometric methods. *Analytical Methods*, *12*, 3390–3396.

Singh, C. B., Jayas, D. S., Paliwal, J., & White, N. D. G. (2012). Fungal damage detection in wheat using short-wave near-infrared hyperspectral and digital colour imaging. *International Journal of Food Properties*, *15*, 11–24.

Snijders, C. H. A., & Krechting, C. F. (1992). Inhibition of deoxynivalenol translocation and fungal colonization in Fusarium head blight resistant wheat. *Canadian Journal of Botany*, *70*, 1570–1576.

Stanisz, E., & Beszterda, M. (2015). Can Ergosterol Be an Indicator of. *Journal of Braz. Chem. Soc.*, *26*, 705–712.

Su, W. H. (2021). Rapid Assessment of Deoxynivalenol Content in Barley Using Hyperspectral imaging. *ASABE Annual International Virtual Meeting*, *2100348*, 1–8.

Su, W. H., Yang, C., Dong, Y., Johnson, R., Page, R., Szinyei, T., … Steffenson, B. J. (2021). Hyperspectral imaging and improved feature variable selection for automated determination of deoxynivalenol in various genetic lines of barley kernels for resistance screening. *Food Chemistry*, *343*, 128507.

Tatzer, P., Wolf, M., & Panner, T. (2005). Industrial application for inline material

sorting using hyperspectral imaging in the NIR range. *Real-Time Imaging*, *11*, 99–107.

Tekle, S., Mage, I., Segtnan, V. H., & Bjornstad, A. (2015). Near-infrared hyperspectral imaging of *Fusarium*-damaged oats (*Avena sativa L.*). *Cereal Chemistry*, *92*, 73–80.

Tibola, C. S., Fernandes, J. M. C., & Guarienti, E. M. (2016). Effect of cleaning, sorting and milling processes in wheat mycotoxin content. *Food Control*, *60*, 174–179.

Tyska, D., Mallmann, A., Gressler, L. T., & Mallmann, C. A. (2021). Near-infrared spectroscopy as a tool for rapid screening of deoxynivalenol in wheat flour and its applicability in the industry. *Food Additives and Contaminants - Part A Chemistry, Analysis, Control, Exposure and Risk Assessment*, *38*, 1958–1968.

Wang, W., Ni, X., Lawrence, K. C., Yoon, S. C., Heitschmidt, G. W., & Feldner, P. (2015). Feasibility of detecting Aflatoxin B1 in single maize kernels using hyperspectral imaging. *Journal of Food Engineering*, *166*, 182–192.

Williams, P. J., Geladi, P., Britz, T. J., & Manley, M. (2012). Investigation of fungal development in maize kernels using NIR hyperspectral imaging and multivariate data analysis. *Journal of Cereal Science*, *55*, 272–278.

Williams, P., Manley, M., Fox, G., & Geladi, P. (2010). Indirect Detection of *Fusarium verticillioides* in Maize (Zea mays L.) Kernels by near Infrared Hyperspectral Imaging. *Journal of Near Infrared Spectroscopy*, *18*, 49–58.

Zhang, H., Paliwal, J., Jayas, D. S., & White, N. D. G. (2007). Classification of Fungal Infected Wheat Kernels Using Near-Infrared Reflectance Hyperspectral Imaging and Support Vector Machine. *Transactions of the ASABE*, *50*, 1779–1785.

Chapter 10. Conclusions and future development

10.1. Conclusions

The present work demonstrated the HSI-NIR potential detecting *Fusarium* and DON contamination in wheat kernels. The conclusions are grouped into sample analysis and single kernel analysis.

HSI-NIR standardization. The results indicated that sampling, scanning conditions and image processing are crucial to establishing an analytical method. PCA results proved the standardization parameters, obtaining: (i) good scanning repeatability between days and according to the ROI delimitation; (ii) the position of kernels on the scanning tray does not affect the spectra; (iii) a clustering tendency is observed due to the kernel orientation (crease-up or crease-down), although the clustering caused by DON contamination is stronger; and (iv) defined clustering delimitate kernels contaminated with DON and symptomatic from uncontaminated and asymptomatic, although two groupings are formed in the intermediate region regarding the asymptomatic and contaminated kernels and the symptomatic and uncontaminated ones.

10.1.1. HSI-NIR analysis of wheat samples

Ergosterol detection. Although ergosterol correlated with DON (0.61), its R^2 is not enough for DON indirect detection. However, ergosterol PLS models proved the HSI-NIR quantification power in wheat entire samples with high performance (R^2 0.89 and RMSECV 1.17 mg/kg). Nevertheless, ergosterol indicated fungal presence, not only *Fusarium*.

DON quantification of wheat samples. The predictive performances demonstrated that whole wheat analysis is more appropriate for DON quantification (R^2 0.61 and RMSECV 501.4 µg/kg) than milled (R^2 0.59 and RMSECV 519.0 µg/kg). Spectral 1stD pre-processing enhanced all the models' performances, including ergosterol prediction, and seems to be the most effective

pre-processing method for wheat samples analysis. Although a better fitting would be required, HSI quantifies DON at regulatory limit concentrations.

Discrimination of DON-contaminated wheat samples. Classification models have similar discriminant performances for entire and ground samples, with accuracies of 83.3 and 85.4%, respectively. Discrimination performance demonstrated that HSI could detect a high percentage of contaminated batches and establish it as a routine analysis before chromatography confirmation.

10.1.2. HSI-NIR analysis of single wheat kernels

***Fusarium* damage-DON correlation.** FHB effects on wheat kernels are not direct indicators of DON presence. Only 68.3% of the grains matched having visible symptoms and DON over the EU limits. The remaining 31.7% were visually healthy kernels with high-DON concentrations or DON-free but damaged. Particularly, these results reinforce that, although the fungal growth and DON production correlate, there are differences in primary and secondary metabolism that add complexity to DON spectral analysis.

Spectral features. The spectral profile demonstrated that the significant spectral information appears in the 1100-1400 nm region. The signal variations are related to physical (brightness, size and shrivelling) and chemical (carbohydrates, lipids, proteins and water) grain changes. Fungal growth can produce those structural and compositional variations on wheat caused by metabolism consumption.

DON quantification in wheat kernels. Single kernel predictive models presented higher coefficients of determination than for samples (0.88), although the RMSEP increased (6.66 mg/kg). The RPD indicated that single kernel models (3.21) have more predictive power than sample analysis (1.64), due to the DON variability in individual kernels. The prediction performances suggested that, although the precision is not enough to quantify DON at regulatory limits, it could be applied to quantify highly contaminated grains.

Discrimination of DON-contaminated wheat kernels. The results showed that discrimination accuracy decreased compared to wheat samples (76.9%). An increase in false-negative kernels (23.3%) was also concerning, indicating that the discrimination depends on DON levels, as they presented higher contaminations than samples. However, DON variability among grains proved that a reduced fraction of extremely high contaminated kernels removal would decrease the general batch contamination.

Discrimination of FDK. The proportion of correctly discarded kernels increased to 85.8% and false negatives reduced to 8.6 %, compared to DON, although three severity categories were used. Fungal growth changes on the cereal matrix affect the spectral signals, directly correlated with its presence. DON detection is more complex for its weak correlation with fungal infection and the NIR overlapped signals at field levels. This work proves the precision of HSI-NIR to replace physical and visual sorting methods.

10.1.3. Solvent selection for FTIR analysis of maize samples

Determination of the most suitable extraction solvent. The selection procedure considered the solvents technological applications and the clustering ability according to DON levels. The green solvent selected was water and the non-green solvent was methanol (70%), both exhibiting clustering tendency according to DON regulatory limit.

FTIR ability to classify the two selected extracts according EU DON limit: The classification results showed the potential of FTIR to classify samples at regulatory threshold, displaying an accuracy of 86.7% and 90.8% for water and methanol (70%), respectively. The SPLS-DA showed the impact of fungal species in the classification accuracy, obtaining well-defined clusters between samples inoculated with DON-producing species, FBs-producing species and naturally-infected.

10.2. Future development

i. The cereal industry requires rapid and non-destructive analytical techniques to manage fungal spoilage and associated mycotoxin contamination. Considering standardization results, automatization of the computational process, especially the ROI selection, spectral data management and pre-processing and model application is required for the batch rejection and online sorting of contaminated cereal commodities. Thus, future work should focus on software development for the real-time detection of contaminated grains.

ii. Several studies used HSI-NIR to detect fungal contaminations, although most with artificially inoculated cereals. Further investigations on larger naturally contaminated cereal sets at field levels are essential to calibrate models with application at the commonly found concentrations.

iii. Further studies must approach pixels spectra, applying the previous models to estimate the contaminated regions of the sample areas over the maximum limit in a simulated stream of wheat. It could manually withdraw the kernels located in those areas, determine the contamination in the safe and rejected fractions, as well as its weight percentage.

iv. Studies investigating the HSI-NIR analysis of other cereals different than wheat (maize, oat and barley), other mycotoxins (FBs, ZEA and trichothecenes), masked mycotoxins (3-ADON, 15-ADON and DON-3G) and multiple mycotoxins in diverse commodities would be required.

v. For FTIR, studies increasing the sample set, based on water and methanol 70% extracts, are required for robust classification model's calibration, with especial consideration to samples with concentrations close to the regulatory limit.

Annexes

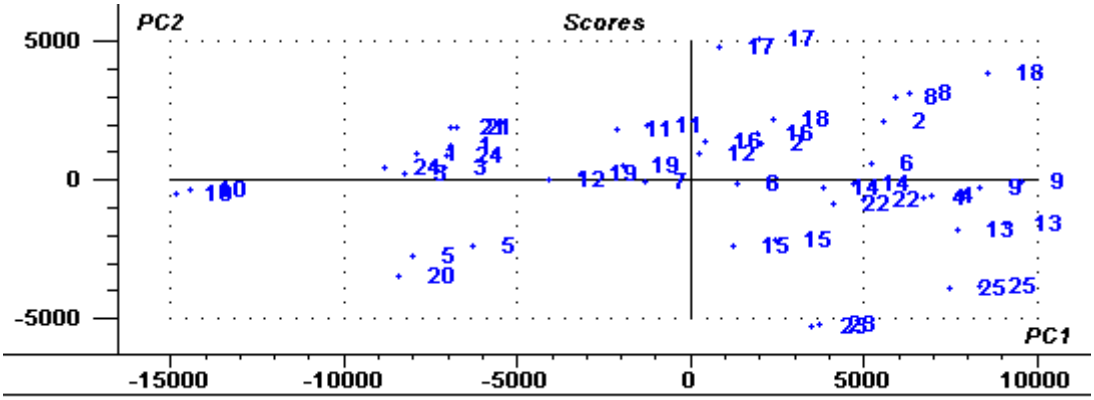

Figure 1. PCA score plot for the assessment of the repeatability of the pixel selection option. X-expl: 88%, 11%. N=50.

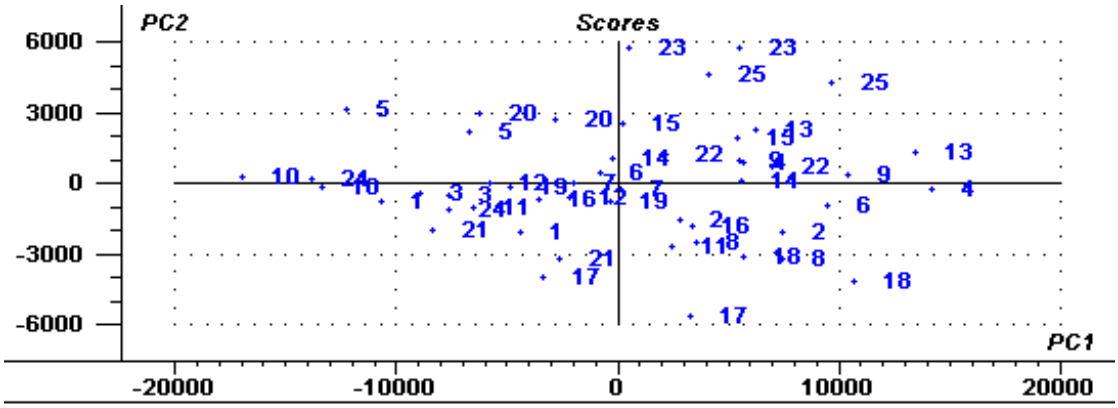

Figure 2. PCA score plot for the representation of the differences between narrow and wider pixel selection options. X-expl: 89%, 10%. N=50.

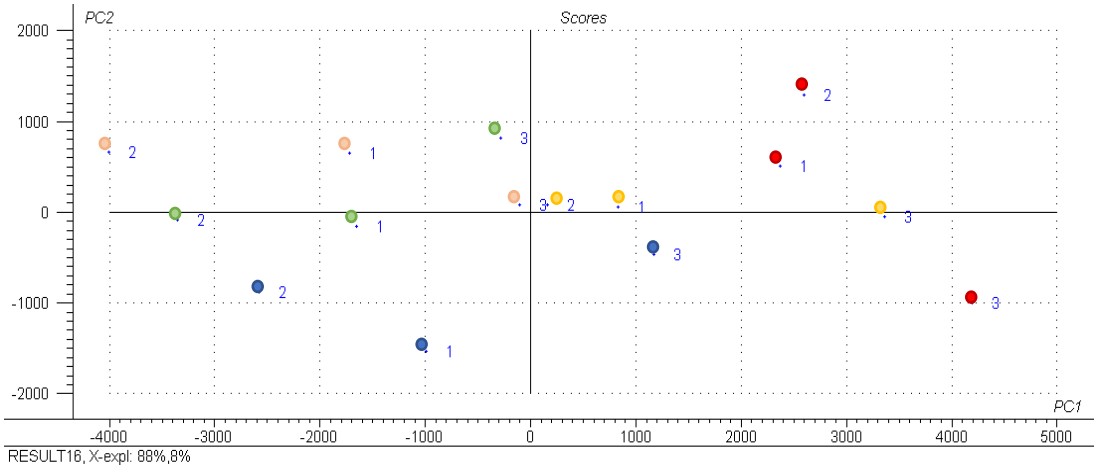

Figure 3. PCA score plot for the assessment of the interday repeatability. Five samples were scanned in three different days. Raw spectra. 1=1st day scan; 2=2nd day scan; 3=3rd day scan. X-expl: 88%, 8%. N=15.

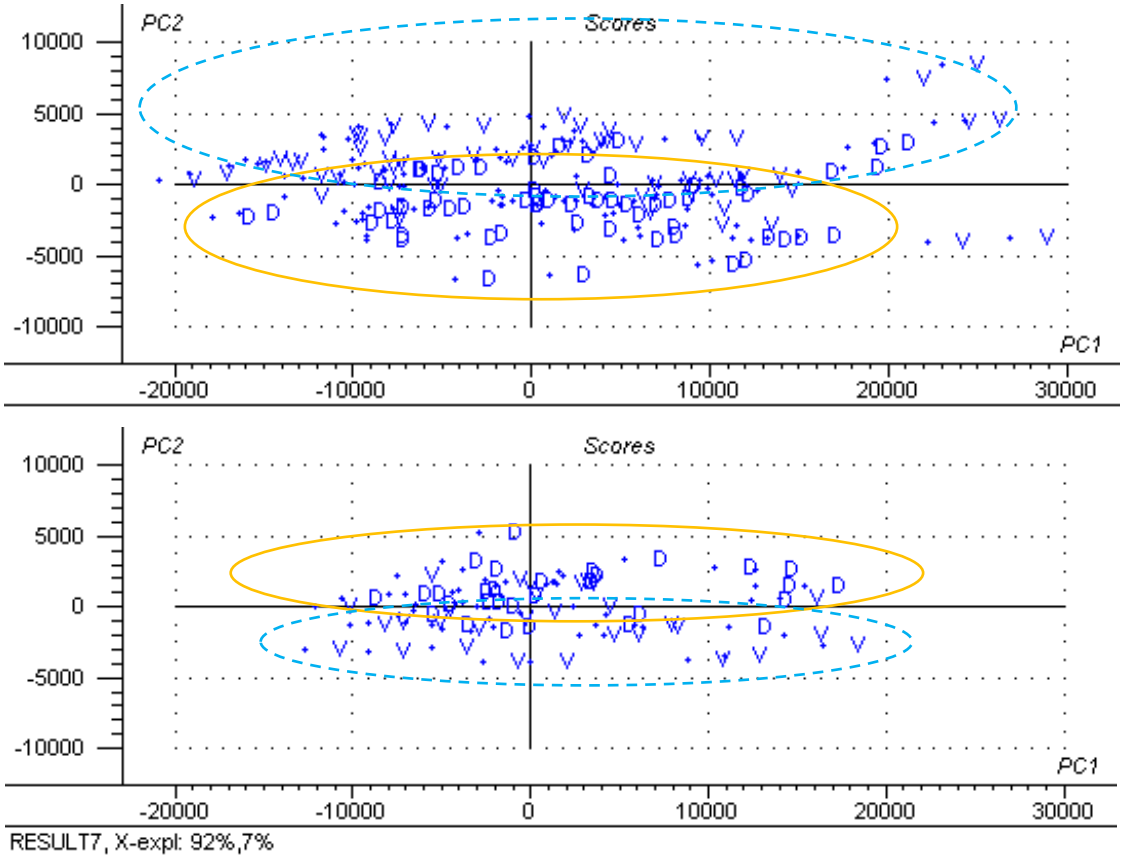

Figure 4. PCA score plot of the differences between crease-down/up kernel position for a DON-free sample (upper, X-expl: 93%, 7%. N=60) and a DON-contaminated sample (lower, X-expl: 92%, 7%. N=60). D = Crease down (Dorsal), V = Crease-up (Ventral).

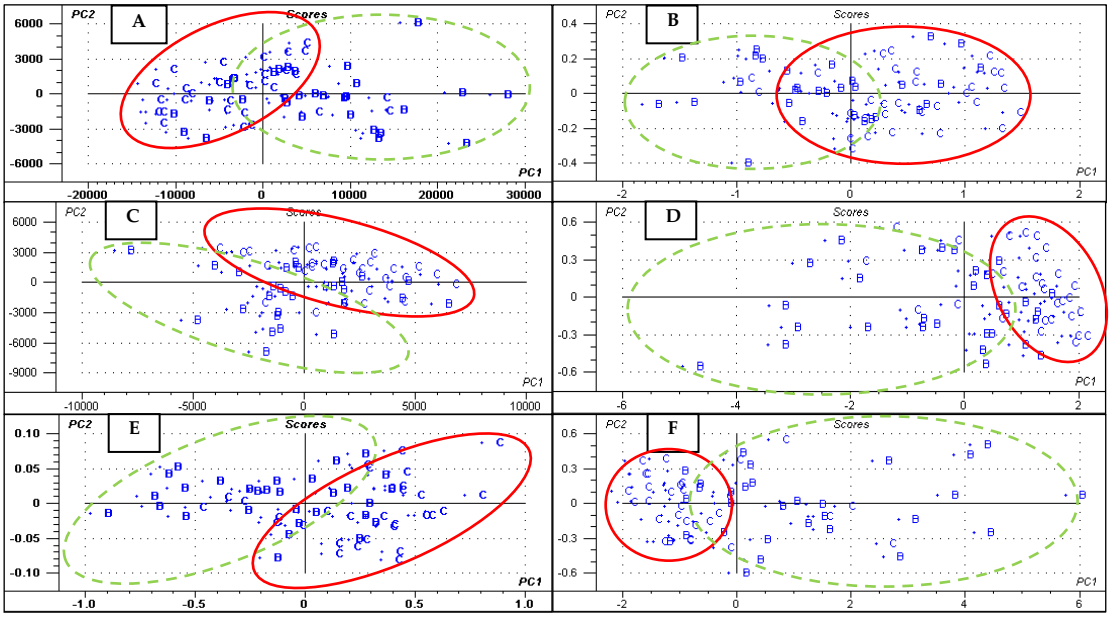

Figure 5. Comparison between spectral pre-treatments for crease-down positioned kernels. A = Raw spectra (reflectance) X-expl: 95%, 5%; B = Raw spectra (absorbance) X-expl: 95%, 4%; C = Reflectance + Baseline correction X-expl: 58%, 40%; D = Reflectance + SNV X-expl: 91%, 3%; E = Absorbance + Baseline correction X-expl: 98%, 1%; F = Absorbance + SNV X-expl: 94%, 2%. N = 60.

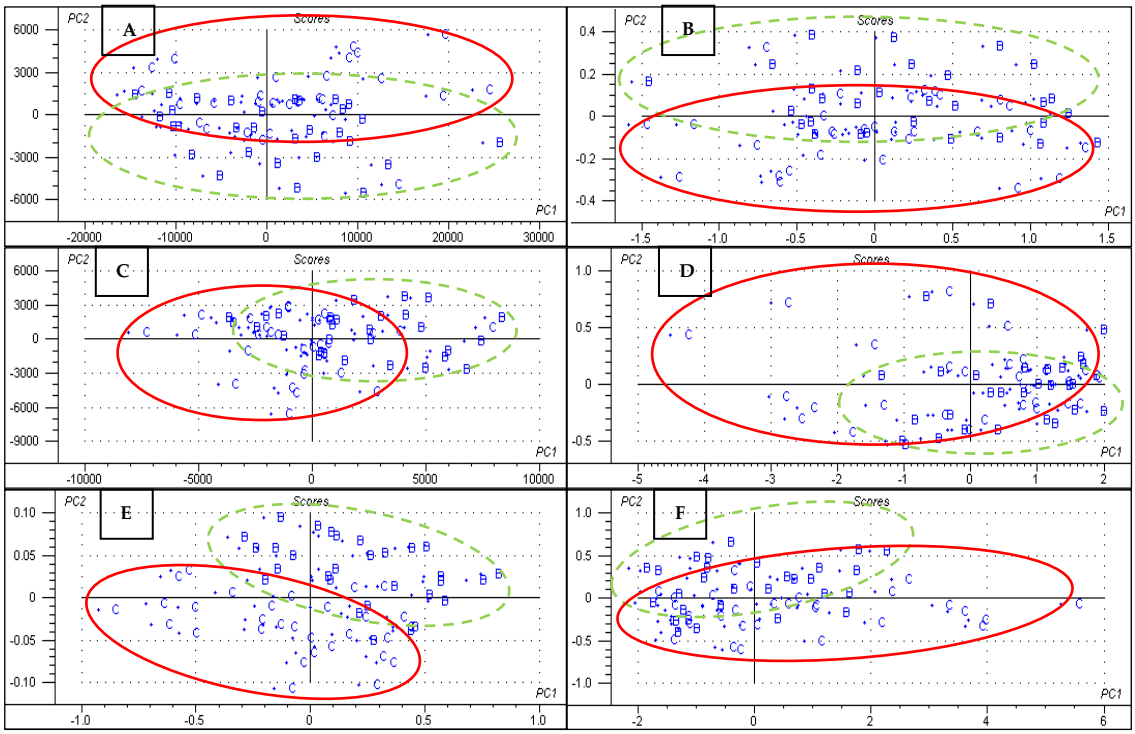

Figure 6. Comparison between spectral pre-treatments for crease-up positioned kernels. A = Raw spectra (reflectance) X-expl: 93%, 6%; B = Raw spectra (absorbance) X-expl: 94%, 5%; C = Reflectance + Baseline correction X-expl: 66%, 31%; D = Reflectance + SNV X-expl: 88%, 5%; E = Absorbance + Baseline correction X-expl: 97%, 2%; F = Absorbance + SNV X-expl: 91%, 3%. N = 60.

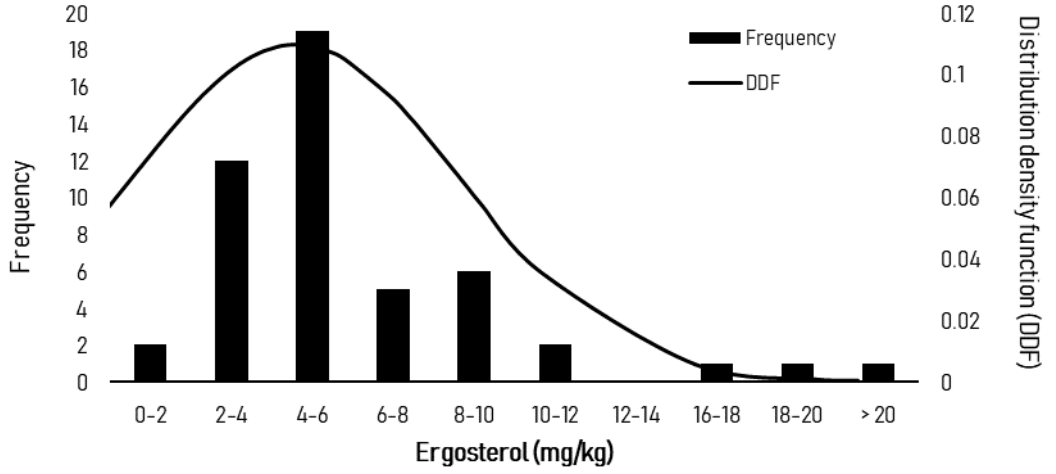

Figure 7. Distribution of total ergosterol content in single wheat kernels, on the full dataset used in the present experiments.

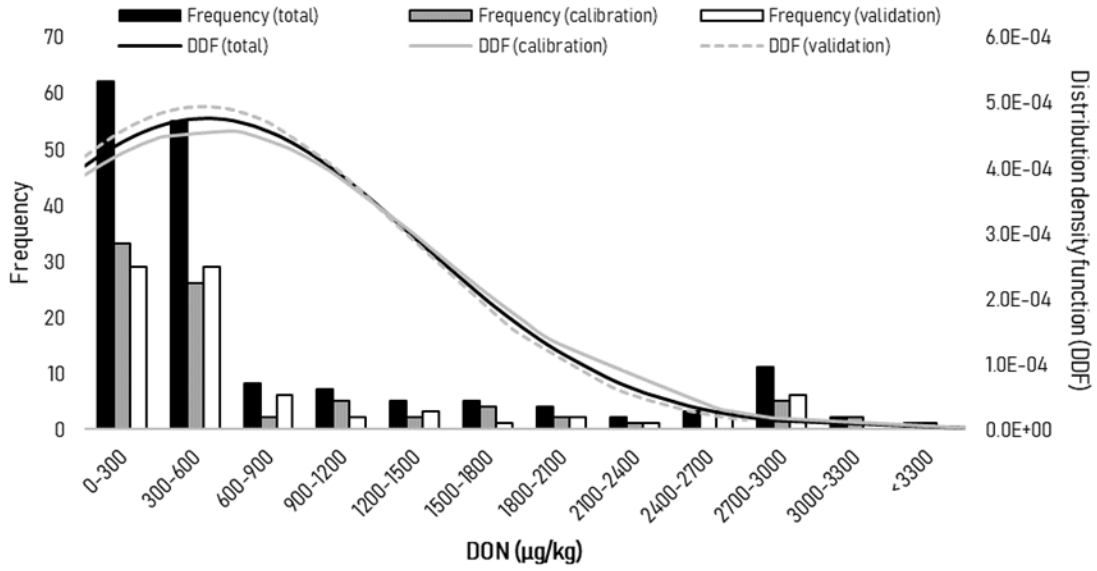

		No. of samples	Mean	Range	SDev	CV (%)
DON content (µg/kg)	**Calibration data set**	83	497.7	< 50 – 3537.0	873.7	175.5
	Validation data set	82	467.1	< 50 – 2628.5	807.8	172.9

Figure 8. Distribution of total DON content in wheat samples, on the full dataset used in the present experiments, and separately for the calibration and validation sets. Statistical analysis of the parameters of the samples used for DON models building, showing independently calibration and validation sets.

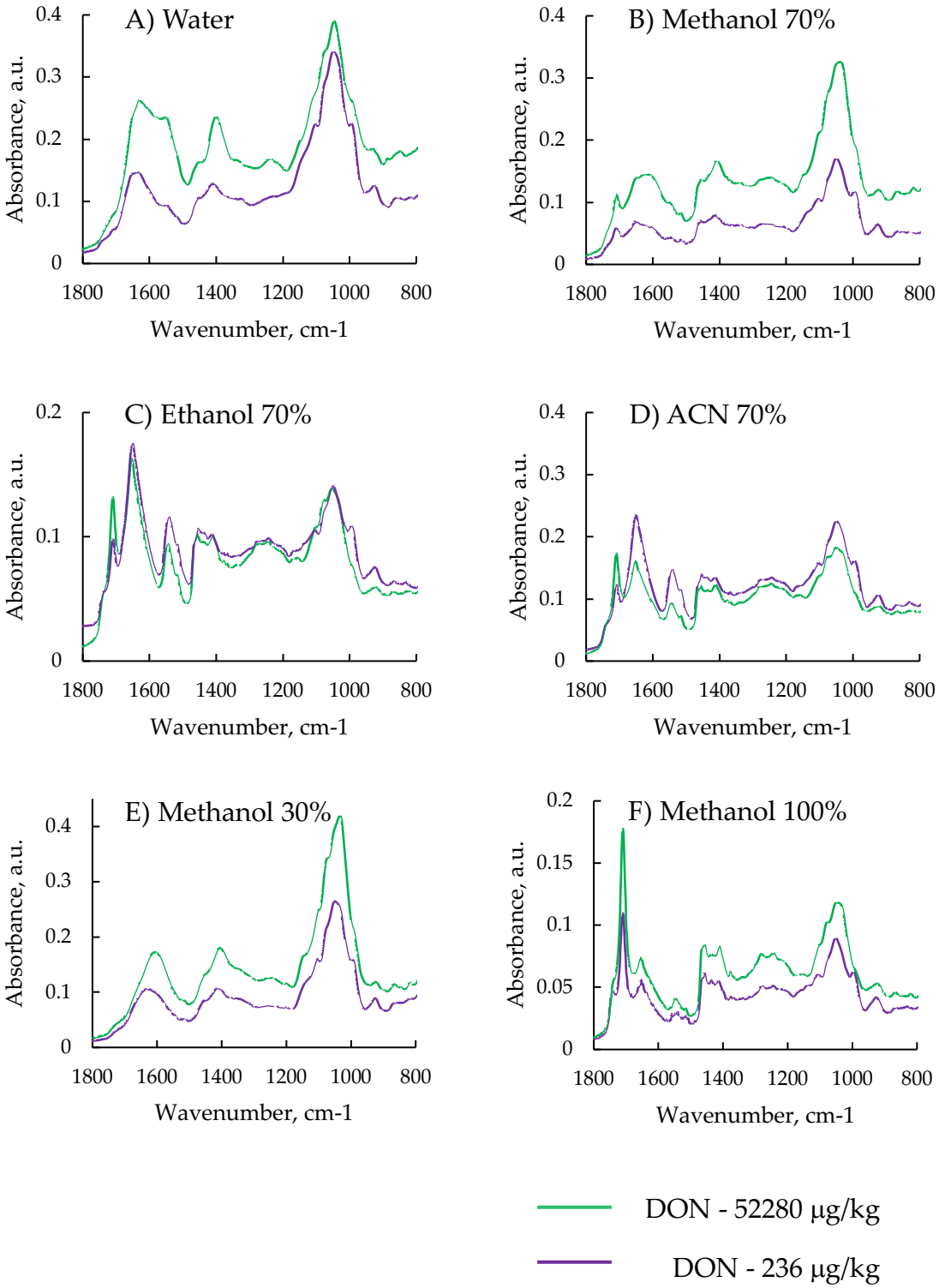

Figure 9. FTIR spectra of high and low DON-contaminated maize extracts in A) water, B) methanol 70%, C) ethanol 70%, D) acetonitrile 70%, E) Methanol 30%, F) Methanol 100%.

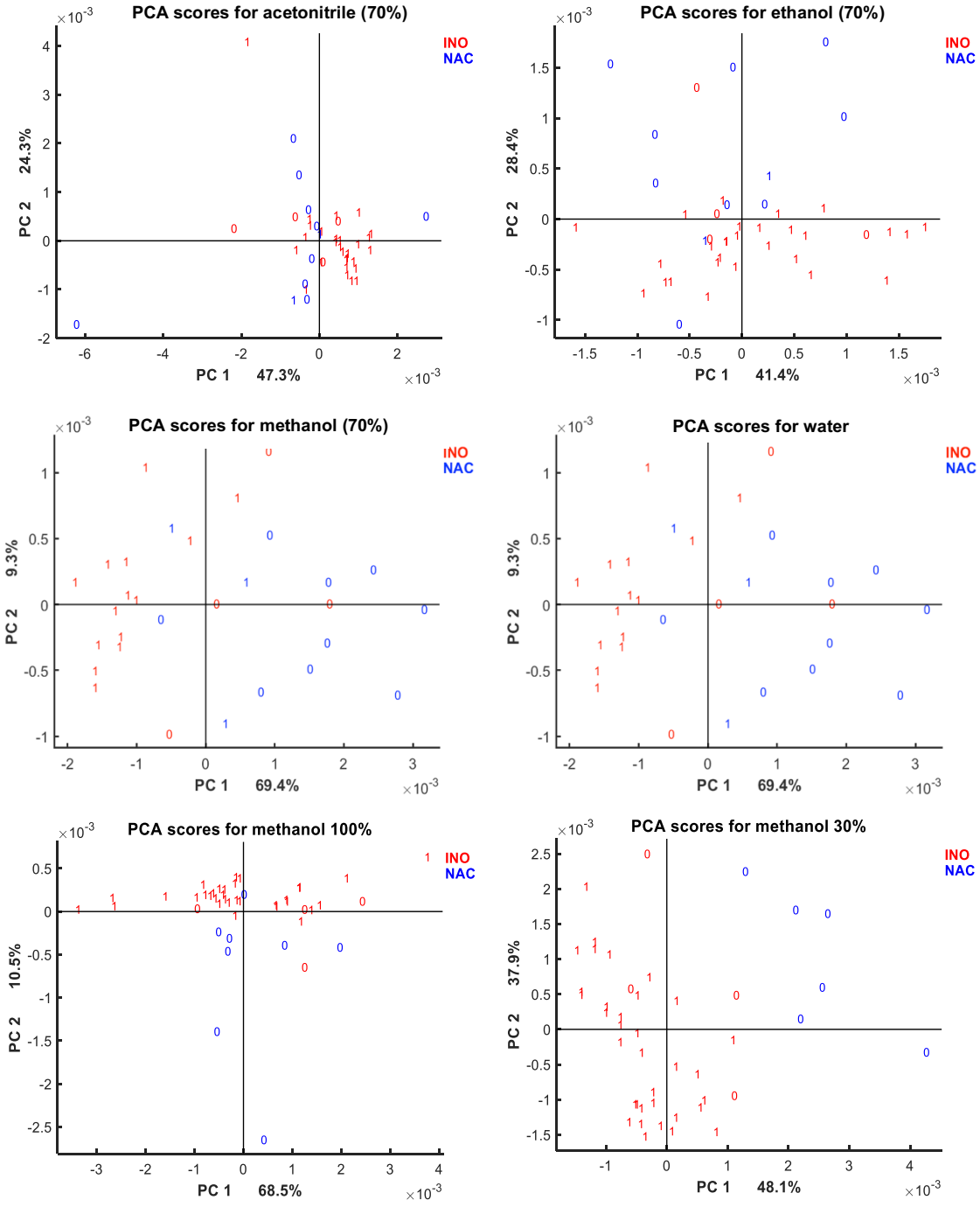

Figure 10. PCA score plot of acetonitrile (70%), ethanol (70%), methanol (70%) and water extracts where colours of labels correspond to inoculation type: inoculated in red and naturally contaminated in blue while labels correspond to DON levels where 0: DON < 1750 µg/kg, 1: DON ≥ 1750 µg/kg obtained by the reference method.

Table 1. LDA accuracies for the cross-validated model in unground samples.

Cross-validated set				
		Predicted		Accuracy (%)
Raw spectra	Groups	B	C	
	B	341	70	84.65
	C	6	78	
ABS/BC	Groups	B	C	
	B	336	75	83.64
	C	6	78	
1st D	Groups	B	C	
	B	393	18	95.66
	C	4	80	

B = low-contaminated group of samples (< 1250 μg/kg); C = high-contaminated group of samples (≥ 1250 μg/kg). Grey cells indicate the number of correctly-classified samples. White cells indicate the number of miss-classified samples.

Table 2. LDA accuracies for a cross-validated model (threshold 1250 μg/kg) in ground samples.

Cross-validated set				
		Predicted		Accuracy (%)
Raw spectra	Groups	B	C	94.35
	B	389	22	
	C	6	78	
ABS/BC	Groups	B	C	84.05
	B	341	70	
	C	9	75	
1^{st}D	Groups	B	C	97.18
	B	400	11	
	C	3	81	

B = low-contaminated group of samples (< 1250 μg/kg); C = contaminated group of samples (≥ 1250 μg/kg). Grey cells indicate the number of correctly-classified samples. White cells indicate the number of miss-classified samples.

Table 3. Performance parameters of PLS regression for different spectral pre-treatments.

DON									
Cross-validation (n = 150)									
Pre-processing	**Position**	**Spectral range (nm)**	**Slope**	**RMSECV**	**R^2**	**SEP**	**PC**	**Outliers**	**RPD**
Raw spectra	Crease-down	895 – 1731	0.85	7.6	0.80	7.6	13	6	2.8
		1000 – 1650	0.86	8.3	0.84	8.4	11	3	2.5
	Crease-up	895 – 1731	0.86	7.0	0.80	7.1	18	9	3.0
		1000 – 1650	0.83	9.0	0.82	9.0	10	5	2.3
	Crease-up (single image)	895 – 1731	0.89	7.2	0.85	7.2	16	7	2.9
		1000 – 1650	0.87	6.5	0.86	6.5	11	10	3.2
MSC	Crease-down	895 – 1731	0.86	6.1	0.85	6.2	9	9	3.4
		1000 – 1650	0.90	7.3	0.87	7.3	17	8	2.9
	Crease-up	895 – 1731	0.92	6.6	0.90	6.6	13	15	3.2
		1000 – 1650	0.90	6.5	0.90	6.5	16	12	3.2
	Crease-up (single image)	895 – 1731	0.81	7.7	0.80	7.7	7	7	2.7
		1000 – 1650	0.83	8.5	0.79	8.5	10	7	2.5
SNV	Crease-down	895 – 1731	0.87	5.9	0.86	5.9	6	9	3.6
		1000 – 1650	0.87	8.2	0.83	8.3	13	5	2.5
	Crease-up	895 – 1731	0.89	7.5	0.86	7.5	12	9	2.8
		1000 – 1650	0.88	7.9	0.84	7.9	15	6	2.7
	Crease-up (single image)	895 – 1731	0.86	5.2	0.85	5.3	6	12	4.0
		1000 – 1650	0.87	5.0	0.87	5.0	10	15	4.2
1stD	Crease-down	895 – 1731	0.87	7.7	0.85	7.7	17	14	2.7
		1000 – 1650	0.85	6.6	0.83	6.6	9	14	3.2
	Crease-up	895 – 1731	0.91	7.4	0.87	7.4	18	11	2.8
		1000 – 1650	0.86	7.7	0.84	7.7	8	9	2.7
	Crease-up (single image)	895 – 1731	0.89	6.1	0.87	6.2	16	13	3.4
		1000 – 1650	0.89	6.1	0.88	6.1	13	13	3.4
2ndD	Crease-down	895 – 1731	0.86	6.4	0.83	6.4	12	15	3.3
		1000 – 1650	0.83	7.2	0.82	7.2	9	15	2.9
	Crease-up	895 – 1731	0.87	6.8	0.84	6.8	12	14	3.1
		1000 – 1650	0.85	7.1	0.84	7.2	7	15	2.9
	Crease-up (single image)	895 – 1731	0.85	6.8	0.81	6.8	13	13	3.1
		1000 – 1650	0.78	6.7	0.76	6.8	7	15	3.1
1stD + SNV	Crease-down	895 – 1731	0.85	6.0	0.82	6.0	10	15	3.5
		1000 – 1650	0.92	6.0	0.90	6.0	16	15	3.5
	Crease-up	895 – 1731	0.87	7.5	0.83	7.5	13	10	2.8
		1000 – 1650	0.88	7.1	0.81	7.2	13	13	2.9
	Crease-up (single image)	895 – 1731	0.83	9.1	0.76	9.2	16	6	2.3
		1000 – 1650	0.86	5.7	0.83	5.7	8	15	3.7
Normalisation	Crease-down	895 – 1731	0.82	7.6	0.78	7.6	12	11	2.8
		1000 – 1650	0.88	7.3	0.83	7.3	18	14	2.9
	Crease-up	895 – 1731	0.82	7.7	0.80	7.8	11	15	2.7
		1000 – 1650	0.84	7.6	0.79	7.6	13	9	2.8
	Crease-up (single image)	895 – 1731	0.91	6.6	0.87	6.6	19	15	3.2
		1000 – 1650	0.77	7.3	0.71	7.4	11	13	2.8

Table 4. Performance parameters of externally-validated PLS models.

External validation PLS performance parameters								
Pre-treatment	**Spectral range**	**Slope**	**Offset**	**R^2**	**RMSEP**	**PC**	**Samples**	**% outliers**
Raw spectra	895-1731	0.69	0.92	0.72	8.53	13	847	5.9
	1000-1600	0.74	0.39	0.76	8.03	14	838	6.9
1stD	895-1731	0.69	0.71	0.74	8.24	14	849	5.7
	1000-1600	0.67	0.51	0.71	8.77	10	840	6.7
SG 1stD 5-SP 3-PO	895-1731	0.71	1.24	0.8	8.57	11	845	6.1
	1000-1600	0.65	1.32	0.7	8.92	7	850	5.6
SG 1stD 3-SP 2-PO	895-1731	0.73	0.79	0.81	8.33	14	829	7.9
	1000-1600	0.63	1.21	0.71	9.72	9	842	6.4
SG 2ndD 3-SP 2-PO	895-1731	0.57	1.04	0.69	10.77	17	838	6.9
	1000-1600	0.52	1.37	0.47	8.55	8	809	10.1
SG 2ndD 5-SP 3-PO	895-1731	0.65	1.02	0.78	9.15	19	820	8.9
	1000-1600	0.49	1.3	0.55	11.9	13	844	6.2
NG 1stD gap size 21	895-1731	0.72	1.28	0.82	8.08	11	811	9.9
	1000-1600	0.62	1.2	0.74	10.65	9	855	5.0
NG 1stD gap size 5	895-1731	0.74	0.84	0.83	8.02	16	815	9.4
	1000-1600	0.7	0.76	0.8	8.59	13	828	8.0
SNV	895-1731	0.79	0.34	0.87	7.04	18	826	8.2
	1000-1600	0.78	0.93	0.88	6.66	14	810	10.0
SNV + 1stD	895-1731	0.71	1.24	0.8	8.58	15	826	8.2
	1000-1600	0.71	1.76	0.81	8.53	10	812	9.8
MSC	895-1731	0.8	0.71	0.88	6.86	17	822	8.7
	1000-1600	0.78	0.92	0.88	7.43	12	825	8.3
MSC + 1stD	895-1731	0.8	1.31	0.8	7.15	11	811	9.9
	1000-1600	0.72	1.27	0.81	8.56	13	818	9.1
Normalisation	895-1731	0.7	0.61	0.79	8.9	18	808	10.2
	1000-1600	0.62	0.89	0.77	10.94	13	842	6.4
Absorbance	895-1731	0.75	1.19	0.72	7.7	10	811	9.9
	1000-1600	0.7	0.56	0.7	10.51	14	835	7.2
ABS/ttea	895-1731	0.66	1.65	0.69	8.1	7	814	9.6
	1000-1600	0.64	0.81	0.69	10.3	9	824	8.4

SG = Savitzky-Golay; 1stD = First derivative; SP = Smoothing Point; PO = Polynomial Order; SNV = Standard Normal Variate; MSC = Multiplicative Scatter Correction; BC = Baseline correction.